AD-A089 512 ATOMIC WEAPONS RESEARCH ESTABLISHMENT ALDERMASTON (EN--ETC F/G 8/11
THE 1976 EARTHQUAKE SEQUENCE IN UZBEKISTAN - FOCAL MECHANISMS D--ETC(U)
JUL 80 R G PEARCE, H BAINBRIDGE, P F KEY
UNCLASSIFIED AWRE-027/80 DRIC-BR-74998 NL

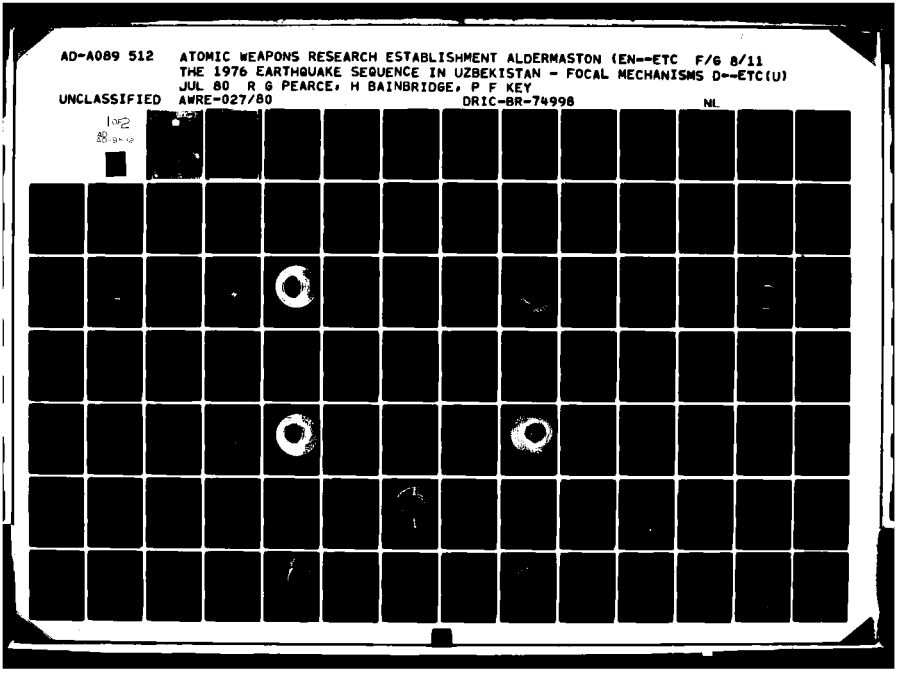

UK UNLIMITED

Procurement Executive - Ministry of Defence

AWRE, Aldermaston

AWRE [redacted] 027/80

Jul 80

The 1976 Earthquake Sequence in Uzbekistan - Focal Mechanisms Determined Using the Relative Amplitude Method

R.G. Pearce
Hilary Bainbridge
Pamela F. Key
J.B. Young

ISBN 0 85518140 0

CONTENTS

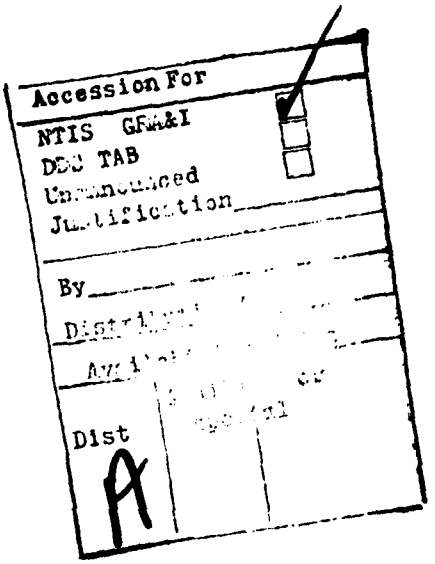

SUMMARY

The relative amplitude method of determining earthquake source orientations is applied to short period teleseismic array observations of the 1976 Uzbekistan earthquake sequence. Many of these events are shown to be consistent with a double couple source, and the method provides well determined orientations for most events with magnitude m_b between 4.0 and 5.6.

1. THE 1976 UZBEKISTAN SEQUENCE

This report concerns a sequence of earthquakes near the town of Gazli, in Uzbekistan, USSR (figure 1), which continued for several months from 8 April 1976. The sequence included three shocks with body wave magnitude (m_b) above 6, which are discussed by Pletnev et al. (1), and many large aftershocks, at least sixty of which were recorded at teleseismic distances. A list of all those earthquakes in this sequence which were reported by the USGS National Earthquake Information Service (NEIS), is given in table 1. Each event is given a reference number for the purpose of this report. Table 1 also shows their magnitudes as computed by NEIS. For the time period of interest, there were six additional earthquakes reported in the Bulletin of the International Seismological Centre (ISC) - these are shown at the end of table 1. Figure 2(a) shows the ISC hypocentres plotted on a map of the area. All but three of these lie in an area of 60 km square, but no spatial trend is apparent. In section 9 this question will be re-examined using epicentre relocation with the aid of focal depths determined from pP in this report.

This sequence of earthquakes is of considerable geophysical interest in that it occurred far from any major tectonic zone in an area of low seismic activity (2), with no previous teleseismically recorded earthquakes.

The sequence is also of interest in the context of earthquake/explosion discrimination; the wide range of magnitudes offers an ideal opportunity to discover how well focal mechanisms can be determined as a function of m_b for a large number of similar earthquakes in a structurally simple area. Our ability to compute focal mechanisms (ie, "fault plane solutions") from teleseismic observations has been extended to smaller magnitudes by the relative amplitude method, and the success of this method introduces the possibility that some events may be positively identified as earthquakes if observations are found to be compatible with a widely accepted earthquake source model. Such a positive identification could become particularly valuable at smaller magnitudes where alternative data (for example, long period surface waves) may not be available.

2. PURPOSE OF THIS REPORT

In this report, the relative amplitude method of Pearce (3-5) is applied to short period seismograms of the 1976 Uzbekistan earthquake sequence as recorded by the four short period medium aperture arrays at Eskdalemuir, Scotland (EKA), Gauribidanur, India (GBA), Warramunga, Australia (WRA) and

Yellowknife, Canada (YKA). Phased array sums are used throughout in order to exploit the improvement in signal to noise ratio which array records provide; we expect a maximum signal to noise ratio improvement of $\sqrt{n}$ where n is the number of seismometers included in the sum.

Application of the relative amplitude method to this earthquake sequence should provide the answers to two major questions. First, what is the practical capability of the method to positively identify these events as double couple sources (ie, earthquakes) given no more than four short period (array) stations at teleseismic distances? Second, how well can we constrain their focal mechanisms using the same stations? Of special importance in relation to both questions is the magnitude threshold below which the capability is lost, or is no longer reliable.

3. SOME COMMENTS ON THE RELATIVE AMPLITUDE METHOD

The relative amplitude method was introduced by, and is fully described by, Pearce (3,4). Extensions of the method and additional discussion is contained in reference (5).

Since for shallow earthquakes direct P and the surface reflections pP and sP are not well separated on long period seismograms, we use short period records, which in any case give us a lower detection threshold. It is important to note that this relative amplitude method (in contrast to methods which determine focal mechanisms from P first motions) is more suited to small than to large earthquakes, since small earthquakes are more likely to have direct and surface reflected phases which are observed as discrete pulses at short period. This we expect because small earthquakes tend to have a duration of source radiation which is within the short period bandwidth (ie, less than 1 s).

As used in this report, the relative amplitude method assumes that the source emits the P and S wave radiations of a double couple, and identifies those ranges, if any, of double couple source orientations which are compatible with a series of relative amplitude observations made at different stations, as explained in references (3) and (4). Hence, for an ideal double couple source with correct description of ray takeoff angles, source layer and surface layer velocities, and with the correct identification and measurement of each phase, we expect the method to yield at least one acceptable range of source orientations and we expect these acceptable range(s) to become smaller (but never to disappear) as more observations are incorporated into the computation. Conversely, for a non-double couple source, again with correct description of structural and ray information, we expect the acceptable regions to get smaller and to disappear as the number of observations is increased. Thus, we see that the number of acceptable orientations will always decrease as the number of observations is increased, but this tendency may mean either that the source is a double couple which is becoming more closely constrained, or that it is not a double couple and that the inclusion of additional observations will eventually eliminate all compatible orientations.

It may therefore appear that the potential of the method as a discriminant is very limited. However, experience has shown that, if there is any error in the representation of the seismograms, or if the source radiation deviates from that of a double couple, then all orientations are eliminated after only a small number of observations is included - say, two or three seismograms

of average quality - whereas compatibility persists to a far greater degree when the representation and the source model are basically correct.

There are two empirical results from previous work which are particularly relevant. First, a small deviation from ideal source radiation causes complete elimination of all orientations after only a small number of observations is included. Second, it has been found that, for an ideal double couple source, the region of acceptable orientations typically reduces to a small but finite range after only several observations have been included (3,5). In cases where all orientations are eliminated, we require to ascertain whether this has arisen through an error in the specification of structural or seismogram parameters, or whether the source genuinely does not radiate as a double couple. As explained in reference (4), the relative amplitude method has provisions to investigate such sources of anomaly.

4. OBSERVED SEISMOGRAMS

All available recordings at the stations EKA, GBA, WRA and YKA for the events in the NEIS section of table 1 were phased to obtain the optimum "best beam". Because the time code was absent on WRA tapes for several months from 17 May 1976, many of the seismograms could not be found at this station. Table 1 shows, for each earthquake, which array seismograms are available and whether or not the P-wave seismogram was detected. "Detections" include any cases where a phased arrival could be seen on the cross-correlogram of two semi-sums (filtered between 1 and 2 Hz) since this has a lower detection threshold than the phased array sum.

Examination of the seismograms revealed that, as expected, the three events with m_b greater than 6 (events 1, 2 and 32 of table 1 - figures 25 and 43) show highly complex short period seismograms, and so their mechanisms are not considered further in this report. Examination of the remainder revealed that most consist of one or more discrete arrivals which could be provisionally identified as P, pP and sP. (In most cases, the focal mechanism computations will add strength to these interpretations.) On the basis of this, the events were classified into five categories as follows:-

Category 1: Earthquakes with overloaded or extremely complex seismograms (the three large events already eliminated).

Category 2: Earthquakes with clear discrete phases identifiable on at least two (but generally three or four) seismograms, with consistent relative arrival times at each station.

Category 3: Earthquakes with at least two well-recorded seismograms but with complex waveforms or inconsistent phase arrival times between stations.

Category 4: Earthquakes with only one seismogram available with good signal to noise ratio, ie, a limitation is imposed by the unavailability of one or more arrays, rather than by signal amplitude.

Category 5: Low m_b earthquakes with low signal to noise ratio seismograms, or below the detection threshold.

Events are classified in this way in table 1, and in figure 3 which shows the relationship between magnitude, category and time. This figure gives a

preliminary indication of the magnitude threshold above which the relative amplitude method might give useful results; this will be discussed later.

Our criteria for classifying these earthquakes on the basis of their array waveform can be seen from examination of the seismograms. Those for Category 2 are shown in figures 5(b) to 23(b), and those for Categories 1, 3, 4 and 5 are shown in figures 25 to 67, together with correlograms filtered between 1 and 2 Hz. The correlograms indicate the arrival of phased energy which is useful in cases where the signal to noise ratio is low. Note that, for events in Category 1, some array seismograms were overloaded and are not shown.

For a given earthquake there are several factors which might make it impossible to apply the relative amplitude method, and the purpose of the above classification is to establish the relative importance of these. Thus, the Category 1 earthquakes are so large that their short period seismograms are highly complex and possibly overloaded, with no identifiable phases. Indeed we expect the duration of source radiation to be outside the pass band of the seismometer for m_b greater than about 6.0. Of the earthquakes below this limit, we are prevented from applying the method either because one or more seismograms are too complex (Category 3), or because some array stations were not operating (Category 4), or because the earthquakes were too small (Category 5). It is important to emphasise that of these categories, only Category 3 represents a fundamental limitation on the applicability of the method, whereas Category 4 requires only that recording gaps be reduced, and Category 5 requires that the signal to noise improvement be increased (ie, that the array instrumentation or processing be improved to lower the detection threshold). It is a remarkable feature of this suite of data that only four events are in Category 3.

5. SOURCE MECHANISM DETERMINATIONS

The relative amplitude method was applied to all the earthquakes in Category 2 of table 1; the assumed phase identifications and amplitude bounds are included in figures 5(b) to 23(b), and figures 80(b) and 81(b). We must always be aware of the possibility that the direct P wave is nodal, in which case care must be taken not to misidentify the second arrival (probably pP) as P. Although a large apparent travel time residual of two or three seconds would point towards this possibility, examination of the correlogram is more likely to reveal the presence of a small amplitude earlier arrival with the correct azimuth and phase velocity. Although correlograms and time codes are not shown in figures 5(b) to 23(b), they were in all cases examined carefully, and one example of a nodal P observation which was detected unambiguously from the correlogram is the EKA observation of Event 9 (figure 9(b)), which is discussed in reference (5). Other examples of nodal P observations are the GBA record of Event 41 (figure 18(b)); the EKA record of Event 8 (figure 8(b)), and the YKA records of Event 8 (figure 8(b)) and Event 36 (figure 46). We further note that the misidentification of phases must give rise to the incorrect specification of amplitude bounds, with consequent loss of compatibility with the double couple source model. An example of this is the GBA record of Event 34 (figures 17(b) and 24(b) - see later).

The width of the bounds on each sP phase is generally wider than those of P and pP, in order to allow for several extra uncertainties in sP amplitude (5). The most important of these is that the surface reflection

coefficient of sP is highly sensitive to the near-surface velocity structure; the specified sP bounds all include extra width to allow for this uncertainty, as it is assumed that we have no knowledge of shallow velocities.

The result of applying the relative amplitude method to each of these earthquakes is expressed graphically using a vectorplot which, for each earthquake, shows those source orientations which are compatible with a given set of relative amplitude observations. Interpretation of a vectorplot in terms of types of fault and angle of slip is aided by figure 4 (taken from reference (3)).

Each vectorplot presented here shows those ranges of orientations which are compatible with all the relative amplitude observations for one earthquake. An initial set of vectorplots was generated for all the Category 2 seismograms with the assumption that there was no energy loss suffered by pP or sP at discontinuities above the source, except at the free surface. A source layer velocity of 6.1 km/s was assumed for the purpose of calculating ray takeoff angles. These vectorplots are shown in figures 5(a) to 23(a), and 80(a) and 81(a), and represent realistic results for these shallow earthquakes if nothing is known about the overlying velocity structure.

Several general conclusions can be drawn from examination of these vectorplots. First, none of these earthquakes has failed to yield orientations which are compatible with a double couple source type. Second, the number of compatible orientations generally reflects the level of noise on the observed seismograms - the better quality recordings, with larger m_b, have orientations which are more closely constrained. Third, the fraction of orientations compatible with each set of seismograms is "small" in all cases except two, which are Events 27 and 49. These events give only a poor constraint in orientation, and are shown in figures 80 and 81. Table 3 shows the fraction of orientations compatible with each set of data - expressed as the fraction of incompatible orientations in real space, or "significance" (4). The values indicate that typically less than 1% of orientations are compatible with the three or four array seismograms used.

Although the above results exclude the effects of velocity structure, theoretical seismograms can be used to place constraints on the possible velocity structures above the source and when an appropriate velocity structure is allowed for in the relative amplitude calculations, the surface reflections are corrected for amplitude loss upon passage through shallow discontinuities. Table 2 shows a realistic velocity structure inferred partly from examination and modelling of the observed seismogram (details are given below), and the results obtained with the relative amplitude program using the same measurements as above are shown in figures 5(c) to 23(c), and 80(c) and 81(c), which are shown in addition to figures 5(a) to 23(a), etc, for comparison. Again the fraction of orientations compatible with each is shown in table 3.

For a given set of data we would expect the significance to decrease (ie, the fraction of orientations compatible to increase) as the representation of structural parameters becomes nearer the true values. Pearce (5) found this to be true for an earthquake in the Gulf of Suez. In the present sequence, 12 out of 22 earthquakes show a decrease in compatibility (table 3) which may indicate that the structure used is inaccurate. However, it is important to emphasise that the solutions are extremely stable under change of velocity structure; the fact that similar solutions are obtained in both cases, and that all the sets of data show

some compatible orientations, indicates that this matter is not crucial to the identification of the radiation patterns as double couples.

All the vectorplots presented allow a range of thrust mechanisms with a greater or lesser component of strike slip motion; in six of the less well constrained solutions a small population of very different orientations - either near-vertical strike slip or vertical dip slip - are also allowed. It is important to understand the significance of these different patterns of allowable orientations shown in each vectorplot, and to explain why these patterns occur. It is also important to interpret the angular bounds placed on the source orientations and to see in what sense the orientations are well constrained and in what sense they are poorly constrained. In order to assist in the qualitative interpretation of the vectorplots it would be helpful if each of them was reproduced by means of a conventional lower hemisphere equal area plot, on which the same set of acceptable orientations could be superposed. Such a composite lower hemisphere equal area plot has been produced which is equivalent to each of the vectorplots in figures 5(c) to 23(c) (ie, those with allowance for velocity structure). These are shown in figures 5(d) to 23(d). Because individual fault plane solutions cannot easily be distinguished when many are superposed, these composite plots have been produced at a 10^{o} rather than a 5^{o} angular increment; this reduces the number of plotted mechanisms by a factor of eight (but introduces the possibility that small acceptable ranges of orientations may be missed altogether). In order to enable each fault and auxiliary plane to be related, each pole is indicated by a small square.

Considering first the allowable thrust-type orientations, it is seen that some of the earthquakes (eg, Event 23 - figure 12) give a perfect thrust with no significant strike slip component and a well-constrained strike running north-west to south-east. Some other earthquakes (eg, Event 48 - figure 19) have a similar strike less well constrained, where all orientations have a similar and significant component of strike slip. (As usual, the two distinct acceptable regions in figure 19(c) denote the interchange of fault and auxiliary planes.) Still other earthquakes (eg, Event 9 - figure 9) allow orientations with almost any strike for certain well-defined slip angles, even though the fraction of orientations which is compatible is no larger. Here it is important to realize that it is the "shape" of the acceptable regions in orientation space which has changed - the separate bounds on the slip angle, dip and strike are not themselves indicators of the degree of constraint on the orientation, since the acceptable range may be of any shape. It is seen in figure 9(d) that the range of acceptable orientations represents a fault plane which is closely defined in dip and strike if it is assumed to be the north-west to south-east striking nodal plane.

All the above source orientations are fundamentally similar if we assume the north-west to south-east striking nodal plane is the fault plane, but there are six earthquakes which give near-vertical strike slip orientations as an entirely separate region of acceptable solutions in addition to the thrust type - on either or both of the vectorplots. This happens for Events 3, 8, 19, 22, 26 and 28 (figures 5, 8, 10, 11, 13 and 14 respectively). This is of importance since these two types of orientation are likely to have very different geophysical implications. A closer examination of the vectorplots shows that this is just an extreme case of other earthquakes where there is an "annulus" of acceptable orientations around the central thrust orientations, and in some cases where this second annulus is widely outside the central thrust area, it effectively cuts through the vertical strike slip or vertical dip slip parts of the vectorplot.

In order to explain this we first note that it is the thrust type faults which persist throughout all the sequence of earthquakes, and that, for most of the earthquakes, these other fault types are specifically excluded. A limitation of the present data is the azimuthal distribution of the four arrays (figure 1(b)) which sample two small ranges directly opposite each other. Hence, if most or all four arrays show positive first motion for P and a negative for pP, the first motion data alone do not allow only thrust solutions, but vertical strike slip solutions can also be oriented so that all four arrays lie in positive quadrants, and three of them can be arranged in positive quadrants for near-vertical dip slip if one or two pP polarities are allowed to be positive. For the larger earthquakes, bounds on the relative amplitudes are easily able to eliminate these alternatives, but for some of the smaller events, where the relative amplitude ranges are wide, or where not all first motions can be read, then some of these alternatives may remain.

The conclusion from this is that, if only four good stations are to be used, then it is vital to secure a good azimuthal coverage when looking near the detection threshold, where there may be little relative amplitude information available from each station.

There is one event (Event 34 - figure 17), where the GBA seismogram cannot be interpreted unambiguously, and the correlogram shows a possible nodal P pulse before the high amplitude pulse which is interpreted as P in figure 17(b). This ambiguity is not resolved by examination of the ISC predicted arrival time, which lies between the two possible P waves, so a second application of the relative amplitude method was attempted, with the assumption that the GBA P wave is nodal. This second interpretation also yielded compatible orientations, as shown in figure 24, where one orientation (figure 79) has been chosen to generate theoretical seismograms.

Sykes and Burdick (6) computed focal mechanisms for two of the large events (Events 1 and 32 of table 1) from first motions and modelling of long period P waves. It is interesting to note that their independently determined solutions for these two large earthquakes, shown in figure 87, give the same type of thrust mechanism as is obtained here for the smaller events using the relative amplitude method.

6. THEORETICAL SEISMOGRAMS

It is noted that, within the acceptable range of orientations, all orientations are equally probable, as all are compatible with the data to within the limits imposed by noise. In view of this, no attempt is made to select one orientation in preference to others. However, for the purpose of computing theoretical seismograms one compatible orientation is chosen from figures 5(c) to 23(c) for each earthquake, and the chosen orientation is in each case arrowed on the vectorplot. Theoretical seismograms are generated using the method of Hudson (7,8) and Douglas, Hudson and Blamey (9), with the velocity structure of table 2, and a focal depth which agrees with the relative times of P, pP and sP on the observed seismograms. These theoretical seismograms are shown in figures 5(b) to 23(b). All the earthquakes are assumed to be "small", in the sense that their pulse duration is less than 1 s, and a source radius of 1.0 km is used for each (table 2.)

The value of these theoretical seismograms is that they offer a means of investigating how well other features of the observed seismograms can be

reproduced, in addition to the relative amplitudes of P, pP and sP which are implicit in the source orientation. For each station we choose an anelastic attenuation factor of either t* = 0.2 s or 0.6 s - whichever yields a dominant period closer to that observed. (A more accurate matching of t* values would not be relevant to mechanism determinations.) Values of t* are shown in table 3. Generally speaking, there is little difference in the dominant periods either between the events or between the stations. Exceptions to this are Event 52 (figure 20(b)) which has a significantly longer period at YKA compared with EKA, and Event 31 (figure 16(b)) where an uncharacteristically long dominant period is observed at all four stations, together with a rather different pulse shape. We would expect these effects to be associated with larger sources, and indeed these two events are larger than most, with m_b of 5.3 and 5.1 respectively (table 2).

We note that, especially for the seismograms with high signal to noise ratios, we have succeeded in reproducing the pulse shapes of P and pP. In particular, the first half cycle of pP is typically suppressed; this is most apparent in the YKA seismograms and is reproduced in the theoretical equivalent. Reflection of P energy from the base of shallow sedimentary layers gives rise to small amplitude pP type arrivals which precede true pP by less than a second, thereby serving to increase the rise time of the pP pulse, with the observed effect on the narrow band seismogram. Furthermore, an arrival between P and pP is also modelled as a reflection from a sub-surface layer (see for example Event 9 (figure 9(b)).

Another general observation to be made is that, although seismograms observed at the same station for different earthquakes in this sequence in many cases have very different relative amplitudes between their phases, the source orientations are all of the same general type - with predominantly dip slip thrust motion. Thus, several EKA observations have a nodal direct P, while others show a high amplitude direct P wave. We conclude that apparently very different sets of seismograms can arise from very similar source orientations. The reason for this is that the amplitude of a phase may become large after only a few degrees of rotation from a nodal plane.

Figure 78 shows a composite lower hemisphere plot of the source orientations used in the models. Since each was chosen independently, it gives a general indication of the strong tendency towards north-west to south-east striking thrust mechanisms, although this tendency as shown in figure 78 is only qualitative in view of the fact that, for each event, one orientation was chosen from all those which were compatible.

In the cases where seismograms with low signal to noise ratio are used, the confidence limits on the source orientation must depend mainly upon the uncertainty imposed upon the signal amplitudes by the noise. This uncertainty can be estimated by the addition of noise with the observed frequency spectrum to a theoretical seismogram, in the way described by Pearce and Barley (10), who generated whole series of such noisy theoretical seismograms in order to establish the range of effects that a given character and amplitude of noise could have on the observed signal.

It is instructive to apply this method in the present situation, in order to check that the range of effects obtained is compatible with the amplitude bounds which have been placed on the phases. Figures 68 to 77 show ten cases; each shows the observed seismogram, followed by the theoretical seismogram and six randomly chosen noisy theoretical seismograms.

7. MAGNITUDE AND THE DETECTION THRESHOLD

Figure 3 showed the relation between m_b and "Category", when the earthquakes were classified as in section 4. The successful application of both the relative amplitude method and modelling to the Category 2 earthquakes has now confirmed the classification of these earthquakes in all but two cases (Events 27 and 49) which did not yield "well constrained" source orientations. Neglecting the four Category 3 earthquakes, we conclude that 16 out of 30 events with m_b between 4.5 and 6.0 have been successfully modelled as earthquakes, and a further one (Event 26) was unable to be processed only on account of data unavailability. Of two events with ISC m_b of 3.6, both were detected at YKA, and one was detected at all four arrays (see table 1.)

The four Category 3 earthquakes (ie, with complex seismograms) deserve special mention. They all occurred within two days (see table 1 and figure 3) which suggests that they are in some way related. Furthermore, the GBA and EKA seismograms for these earthquakes are complex, while the YKA records show the characteristic two-pulse waveform observed for all the other earthquakes, albeit with some superposed complexity. The four GBA records have similarities in their complexity, as do the EKA records. These four earthquakes therefore constitute a highly anomalous sub-set of this sequence, but their behaviour is unexplained.

8. EVENT LOCATIONS

In this section we ask whether there is any significant effect upon the distribution or scatter of the earthquake sequence when the whole suite is relocated using joint epicentre determination (JED) (11). For this purpose the depths of those earthquakes which are modelled are restrained to the values used in the model, which are effectively determined from the P to pP time. It must be remembered, however, that the identifications of pP have been supported by the success achieved in obtaining compatible orientations when the relative amplitude method was applied. In view of this, the same interpretations were placed upon those seismograms for earthquakes which were not modelled, so that many more events were given a restrained depth. In addition an origin time and hypocentre were restrained.

Figure 82 shows the result including all the ISC bulletin data (with Jeffreys weighting), with the starting approximation of the NEIS. Figure 83 shows the same data but with the starting approximation of the ISC. As we expect, the relocated epicentres are the same on each figure, to within the confidence ellipse of the location; figure 83 has some extra events to the south that were not reported in the NEIS bulletin.

It is of interest to learn how well these events can be located using only the four arrays, which offer relatively accurate arrival time measurements from phased sums. Lilwall (personal communication) has found that, for presumed nuclear explosions in East Kazakhstan, the four arrays give as good a location as is obtainable using the worldwide data contained in the ISC bulletin. Since no convergence can be obtained if the data are underdetermined, we can only use those earthquakes for which arrival times can be measured at three or four arrays - three arrival time observations and a restrained depth provide four measurements for the four degrees of freedom, namely latitude, longitude, depth and origin time.

Figure 84 shows these earthquakes relocated using the four arrays with the NEIS epicentres as starting approximation; the same epicentre is restrained as before. These relocated epicentres are compared in figure 85 with those obtained using the ISC bulletin data for the same earthquakes (figure 82). In most cases the array-relocated epicentres are within the confidence limits of those determined using the ISC data (see table 4), and a major part of the difference is made up of a systematic shift due to the restrained epicentre (figure 85).

It is interesting to note that the P to pP times give well determined depths which vary between 5 and 30 km for different events. This contrasts markedly with the ISC depths, many of which have gross errors, especially when the Quetta determinations have been used (see figure 2). We now ask whether the relocated epicentres exhibit any three-dimensional spatial trend when these depths are used. Figure 86 shows north-south and east-west sections for those epicentres computed in figure 83 for which pP-P depths were used. No significant spatial trend is apparent.

9. CONCLUSIONS

The observed seismograms presented in this report are remarkable in that the P waveforms comprise one or two discrete pulses, which have been identified as P and its surface reflections. Furthermore, this behaviour is maintained for upwards of fifty earthquakes.

Application of the relative amplitude method has confirmed that the phase identifications are compatible with the double couple radiation pattern for over half of these earthquakes between m_b 4.5 and 6.0 (details in figure 3), and for some of the earthquakes down to m_b 4.1. For 19 of these earthquakes well-constrained focal mechanism solutions have been obtained, indicating thrust faults with a predominance of south-west to south-east trending strikes. In a few cases a small number of near-vertical strike slips or vertical dip slip faults were also possible. The thrust type orientations agree with the mechanisms determined for two of the large shocks, which were computed independently by a different method (6).

The relative locations of these earthquakes have been determined almost as accurately using arrival times measured from phased sums at the four arrays, as is possible using ISC bulletin data at all stations.

The seismograms presented here constitute a remarkable sequence of simple P-wave signals which contain much valuable source mechanism information. Considerable success has been achieved in modelling these events using an earthquake source. Further studies will establish whether these array seismograms allow any of these events to be modelled using an explosion source.

REFERENCES

1. K G Pletnev, N V Shebalin, V V Shteinberg, V M Grayzer and P A Alexin: Seismic Engineering Program Report, US Geol Survey Circular 762-A, 28pp (January - April 1977)

2. S Crampin, C J Fyfe, D P Bickmore and R H W Linton: "Atlas of Seismic Activity 1909 to 1968". Institute of Geological Sciences Seismological Bulletin No. 5, HMSO (1976)

3. R G Pearce: "Fault Plane Solutions Using Relative Amplitudes of P and pP". Geophys J R Astr Soc, 50, 381-394 (1977)

4. R G Pearce: "Earthquake Focal Mechanisms from Relative Amplitudes of P, pP and sP: Method and Computer Program". AWRE Report No. O41/79 (1979)

5. R G Pearce: "Fault Plane Solutions Using Relative Amplitudes of P and Surface Reflections: Further Studies". Geophys J R Astr Soc, 60, 459-487 (1980)

6. L R Sykes and L Burdick: "Velocity and Q Structure". Annual Technical Report, Part 2, Lamont-Doherty Geological Observatory, Columbia University (1979)

7. J A Hudson: "A Quantitative Evaluation of Seismic Signals at Teleseismic Distances. I - Radiation from Point Sources". Geophys J R Astr Soc, 18, 233-249 (1969)

8. J A Hudson. "A Quantitative Evaluation of Seismic Signals at Teleseismic Distances. II - Body Waves and Surface Waves from an Extended Source". Geophys J R Astr Soc, 18, 353-370 (1969)

9. A Douglas, J A Hudson and C Blamey: "A Quantitative Evaluation of Seismic Signals at Teleseismic Distances. III - Computed P and Rayleigh Wave Seismograms". Geophys J R Astr Soc, 28, 385-410 (1972)

10. R G Pearce and B J Barley: "The Effect of Noise on Seismograms". Geophys J R Astr Soc, 48, 543-548 (1977)

11. A Douglas: "Joint Epicentre Determination". Nature, 215, 47-48 (1967)

12. W J Person (Ed): Seismological Notes. Bull Seism Soc Am, 68, 256-262 (1978)

13. J C Savage: "Radiation from a Realistic Model of Faulting". Bull Seism Soc Am, 56, 577-592 (1966)

TABLE 1

Uzbekistan Earthquakes in 1976 (NEIS Parameters)

Reference No.	Date (1976)	Origin Time	Latitude, °N	Longitude, °E	Depth,* km	m_b	Detection Information**				Category (See Text)	Figure Containing Observed Seismograms
							EKA	GBA	WRA	YKA		
1	8 April	02-40-27.0	40.31	63.77	33.0 N	6.5	✓	✓	✓	✓	1	25
2	8 April	02-59-05.5	40.17	63.81	33.0 N	6.2	✓	✓	✓	✓	1	-
3	8 April	03-15-21.7	40.17	63.92	33.0 N	4.5	✓	✓	✓	✓	2	5b
4	8 April	03-30-49.3	40.40	63.44	33.0 N	4.1	✓	✓	✓	✓	2	6b
5	8 April	04-46-08.9	40.43	63.32	33.0 N	4.2	✓	✓	✓	✓	5	26
6	8 April	04-58-53.9	40.40	63.69	33.0 N	4.8	✓	✓	✓	✓	5	27
7	8 April	06-16-50.0	40.23	63.84	33.0 N	4.7	✓	✓	✓	✓	2	7b
8	8 April	09-10-07.7	40.34	63.80	33.0 N	4.2	✓	✓	✓	✓	2	8b
9	8 April	12-03-41.1	40.20	64.06	33.0 N	5.1	✓	✓	✓	✓	2	9b
10	8 April	22-54-17.8	40.49	63.65	33.0 N	4.0	✓	×	✓	✓	5	28
11	9 April	02-46-23.9	40.35	63.54	33.0 N	4.5	✓	✓	✓	✓	5	29
12	12 April	06-35-23.5	40.43	63.71	33.0 N	3.8	×	×	×	✓	5	30
13	12 April	16-12-58.9	40.46	63.61	33.0 N	4.0	×	×	×	×	5	31
14	14 April	07-51-06.5	40.31	63.81	33.0 N	3.9	×	×	×	-	5	32
15	14 April	19-26-55.8	40.31	63.71	37.0	3.6	×	✓	×	✓	5	33
16	15 April	06-15-21.1	40.37	63.66	33.0 N	4.2	✓	✓	✓	×	5	34
17	15 April	16-35-15.7	40.40	63.38	33.0 N	3.9	×	×	×	✓	5	35
18	16 April	02-36-45.8	40.40	63.68	33.0 N	3.8	×	×	×	×	5	36
19	17 April	12-11-14.2	40.37	63.75	33.0 N	4.4	×	✓	×	✓	2	10b
20	17 April	13-47-55.1	40.30	63.64	32.0	4.0	×	×	×	✓	5	37
21	17 April	20-21-47.2	40.45	63.69	33.0 N	4.0	×	×	×	×	5	38
22	18 April	22-37-39.7	40.27	63.81	33.0 N	4.7	✓	✓	✓	✓	2	11b
23	21 April	14-41-34.6	40.26	63.80	33.0 N	5.0	×	✓	✓	×	2	12b
24	21 April	22-33-29.8	40.55	63.85	33.0 N	4.1	×	×	×	✓	5	39
25	21 April	23-18-33.9	40.45	63.57	33.0 N	4.0	✓	✓	✗	✓	5	40
26	23 April	01-56-48.3	40.30	63.77	33.0 N	4.7	×	-	-	✓	2	13b
27	23 April	20-55-31.7	40.33	63.61	33.0 N	4.4	✓	-	✓	✓	2	41,80b
28	24 April	13-57-01.0	40.36	63.72	33.0 N	4.7	-	-	✓	✓	2	14b
29	2 May	15-41-36.7	40.35	63.61	33.0 N	3.6	✗	-	-	✓	5	42
30	7 May	00-10-49.4	40.35	63.70	33.0 N	4.8	✓	✓	✓	✓	2	15b
31	9 May	07-51-16.7	40.34	63.93	18.0	5.1	✓	✓	✓	×	2	16b
32	17 May	02-58-40.6	40.38	63.47	10.0	6.3	✓	✓	-	✓	1	43
33	17 May	04-14-15.6	40.66	62.94	33.0 N	4.7	✓	-	-	✓	4	44
34	17 May	04-53-51.7	40.27	63.59	33.0 N	4.7	✓	✓	-	✓	2	17b,24b
35	17 May	11-01-26.3	40.48	63.24	33.0 N	4.1	-	-	-	×	5	45
36	17 May	17-46-17.2	40.28	63.28	30.0	4.9	✓	✓	-	×	3	46
37	18 May	04-16-25.9	40.27	63.69	33.0 N	4.7	✓	✓	-	✓	3	47
38	18 May	08-57-29.4	40.26	63.49	33.0 N	4.8	✓	✓	-	✓	3	48
39	18 May	13-54-23.9	40.23	63.34	33.0 N	4.7	✓	✓	-	✓	3	49
40	19 May	01-11-20.8	40.38	63.40	33.0 N	4.6	✓	×	-	✓	5	50
41	19 May	15-54-45.6	40.23	63.36	33.0 N	5.0	×	✓	-	×	2	18b
42	19 May	16-21-44.9	40.33	63.58	33.0 N	4.7	✓	✓	-	×	5	51
43	21 May	16-05-28.5	40.21	63.21	33.0 N	4.3	×	×	-	✓	5	52
44	21 May	18-28-57.3	40.41	63.58	33.0 N	3.9	×	-	-	✗	5	53
45	23 May	09-49-21.3	40.37	63.13	33.0 N	4.0	×	×	-	×	5	54
46	24 May	06-10-54.4	40.40	63.20	33.0 N	3.8	×	×	-	×	5	55
47	24 May	14-56-12.8	40.26	63.45	33.0 N	4.3	×	×	-	×	5	56
48	28 May	14-05-37.3	40.36	63.58	25.0	4.9	-	✓	-	✓	2	19b
49	1 June	07-31-59.2	40.32	63.52	35.0	-	✓	×	-	×	2	57,81b
50	6 June	04-19-09.7	40.40	63.31	33.0 N	4.5	✓	×	-	✓	5	58
51	11 June	13-42-37.1	40.26	63.62	33.0 N	4.5	-	×	-	×	5	59
52	20 June	23-33-48.8	40.40	63.74	12.0	5.3	×	-	-	✓	2	20b
53	23 June	09-49-32.8	40.37	63.63	33.0 N	4.8	×	✓	-	✓	2	21b
54	8 July	23-35-38.0	40.35	63.66	33.0 N	4.7	✓	✓	-	✓	2	22b
55	4 Aug.	02-23-44.1	40.34	63.32	33.0 N	3.7	×	×	-	×	5	60
56	18 Aug.	23-17-55.0	40.31	63.46	33.0 N	4.0	✓	-	-	×	5	61
57	21 Aug.	12-15-32.3	40.35	63.60	33.0 N	3.7	×	×	-	×	5	62
58	22 Sept.	21-49-42.6	40.49	63.41	33.0 N	4.7	✓	✓	-	✓	2	23b
59	9 Oct.	16-04-19.1	40.31	63.38	33.0 N	-	×	×	-	×	5	63
60	17 Oct.	03-25-33.1	40.38	63.70	33.0 N	5.1	✓	✓	-	✓	5	64
61	18 Oct.	21-01-48.2	40.24	63.39	33.0 N	4.8	✓	×	-	✓	5	65
62	2 Nov.	22-19-33.3	40.22	63.52	64.0	-	×	×	-	×	5	66
63	28 Nov.	20-39-39.0	40.19	63.81	33.0 N	4.6	-	✓	-	✓	5	67
Additional Events Reported to the ISC (ISC Parameters)												
	1976											
	23 April	19-55-30.0				-						
	17 May	03-21-54.0				4.4						
	17 May	03-57-42.0				-						
	17 May	05-53-14.3				-						
	13 June	20-49-34.5				-						

*N (normal) indicates that depth was constrained to 33.0 km in the NEIS computation.

**Using correlogram if necessary:-

✓ = P wave detected; ✗ = doubtful detection;
× = not detected; - = station not recording (later WRA seismograms could not be found because of absence of time code)

TABLE 2

Modelling Parameters

(a) Source region structure

The S-wave velocity in each layer is assumed to be $1/\sqrt{3}$ of the P-wave velocity.

Layer	v_p	Density, g/cm^3	Thickness, km
1	3.0	2.7	0.5
2	4.6	2.7	3.0
3	6.1	2.8	29.0
4	8.2	3.3	-

(b) Source mechanism (Savage (13) model with rupture amplitude falling off to edge of fault)

Fault radius: 1 km (circular)

Stress drop: 100 bars

Rupture velocity: 0.6 × S-wave velocity in source layer

TABLE 3

Focal Mechanisms and Anelastic Attenuation Factors

Event No.	Event		Source Orientation Used in Model			Anelastic Attenuation Factors Used in Model (t*, sec)				Depth Deduced from Modelling, km	Significance** (Without Structure)		Significance** (With Structure)
	Date (NEIS)	Time (NEIS)	Dip δ(deg)	Slip Angle ψ(deg)	Strike σ(deg)	YKA	EKA	GBA	WRA				
3	8 April	03-15-21.7	140	95	135	0.2	0.2	0.2	0.2	10.1	0.9935	<	0.9992
4	8 April	03-30-49.3	135	90	135	0.2	0.2	0.2	0.2	8.57	0.9746	>	0.9721
7	8 April	06-16-50.0	135	75	135	0.2	0.6	0.6	0.2	9.49	0.9920	<	0.9925
8	8 April	09-10-07.7	140	50	340	0.2	0.2	0.2	0.2	8.57	0.9909	<	0.9919
9	8 April	12-03-41.1	140	115	135	0.2	0.6	0.6	0.2	7.96	0.9979	>	0.9969
19	17 April	12-11-14.2	135	90	135	0.2	0.6	0.2	0.2	9.9	0.9967	>	0.9963
22	18 April	22-37-39.7	140	60	20	0.2	0.2	-	0.2	6.1	0.9961	<	0.9977
23	21 April	14-41-34.6	135	90	135	0.6	0.2	0.2	0.2	8.57	0.9967	<	0.9973
26	23 April	01-56-48.3	140	90	100	0.2	0.2	-	-	9.49	0.9638	>	0.9479
* 27	23 April	20-55-31.7									0.9575	>	0.9413
28	24 April	13-57-01.0	130	55	260	0.2	-	-	0.2	9.18	0.9697	<	0.9704
30	7 May	00-10-49.4	135	90	135	0.6	0.2	0.2	0.6	5.22	0.9970	<	0.9979
31	9 May	07-51-16.7	125	90	330	0.6	0.2	0.6	0.6	10.1	0.9998	<	0.9999
34	17 May	04-53-51.7	130	90	125	0.2	0.2	0.2	-	6.1	0.9946	>	0.9922
34	17 May	04-53-51.7	95	180	275	0.2	0.2	0.2	-	6.1	0.9825	<	0.9859
41	19 May	15-54-45.6	135	90	135	0.6	0.2	0.2	-	13.15	0.9969	>	0.9958
48	28 May	14-05-37.3	135	110	330	0.2	-	0.6	-	7.96	0.9983	>	0.9977
* 49	1 June	07-31-59.2									0.9679	>	0.9656
52	20 June	23-33-48.8	145	100	200	0.6	0.2	-	-	10.1	0.9903	<	0.9905
53	23 June	09-49-32.8	130	90	130	0.6	0.2	0.6	-	4.6	0.9975	>	0.9953
54	8 July	23-35-38.0	135	100	320	0.2	0.6	0.2	-	7.96	0.9992	>	0.9989
58	22 Sept.	21-49-42.6	130	90	130	0.2	0.2	0.2	-	12.84	0.9987	>	0.9976

*Not modelled

**See text

TABLE 4

Comparison of Relocated Epicentres Using Array Stations Only and Using all ISC Station Data

Event No.	Date (1976)	Origin Time	Original Epicentre (NEIS)		Relocated Epicentre Using Array Data				Relocated Epicentre Using ISC Data				Difference in Locations, km		
			Lat., °N	Long., °E	Lat., °N	Confidence Limit 95%, km	Long., °E	Confidence Limit 95%, km	Lat., °N	Confidence Limit 95%, km	Long., °E	Confidence Limit 95%, km	Lat.	Long.	Actual Distance
2	8 April	02-59-5.5	40.167	63.806	40.108	18.86	63.860	17.24	40.160	4.61	63.840	2.18	5.78	2.22	6.19
3	8 April	03-15-21.7	40.173	63.916	40.226	13.05	63.939	13.67	40.241	7.12	63.750	4.73	1.67*	21.0	21.06
6	8 April	04-48-53.9	40.40	63.693	40.366	20.41	63.965	15.07	40.397	4.64	63.705	2.86	3.44*	28.89	29.09
7	8 April	06-16-50.0	40.226	63.841	40.158	19.13	63.716	36.83	40.275	5.24	63.769	2.89	13.00	5.89	14.27
8	8 April	09-10-07.7	40.337	63.797	40.126	19.19	63.703	36.93	40.167	5.67	63.979	3.22	4.56*	30.67	31.00
19	17 April	12-11-14.2	40.370	63.754	40.276	18.18	64.112	35.58	40.294	4.65	63.780	2.59	2.00*	36.89	36.94
23	21 April	14-41-34.6	40.259	63.808	40.139	13.10	63.903	13.73	40.215	3.52	63.834	1.89	8.45	7.67	11.41
30	7 May	00-10-49.4	40.347	63.701	40.224	13.10	63.843	13.69	40.343	3.85	63.748	2.21	13.22	10.56	16.92
31	9 May	07-51-16.7	40.34	63.93	40.197	20.46	64.047	15.18	40.265	3.74	63.967	1.97	7.56	8.89	11.67
54	8 July	23-35-38.0	40.346	63.656	40.177	13.60	63.757	15.31	40.339	4.12	63.731	2.27	24.67	2.89	24.84
58	22 Sept.	21-49-42.6	40.486	63.411	40.412	13.54	63.681	15.15	40.449	4.11	63.379	2.14	4.11*	33.56	33.81

*Denotes that the difference lies within the confidence limits for both sets of data.

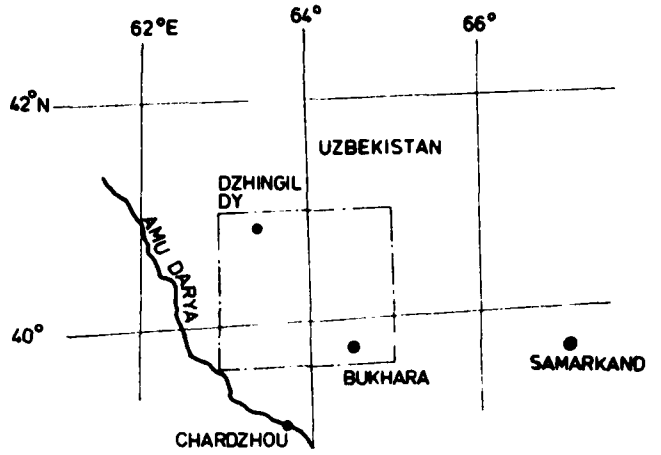

FIGURE 1a Location Map of Earthquake Region

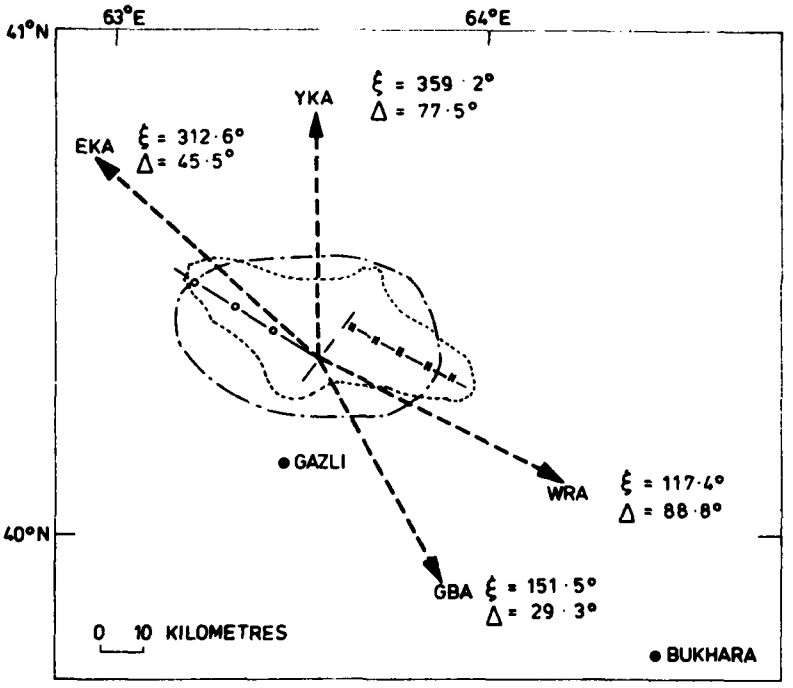

KEY

ξ AZIMUTH OF ARRAY

Δ EPICENTRAL DISTANCE TO ARRAY

DIRECTION OF ARRAY STATION FROM REGION OF EARTHQUAKE

INFORMATION FROM REFERENCE 12

FAULT PLANE OF APRIL 8 EARTHQUAKE

FAULT PLANE OF MAY 17 EARTHQUAKE

AFTERSHOCK AREA

INTENSITY IX ISOSEISMAL

FIGURE 1b Map showing Azimuths and Epicentral Distances to the Four Array Stations. Supposed Fault Planes and Aftershock Areas are from Reference 12

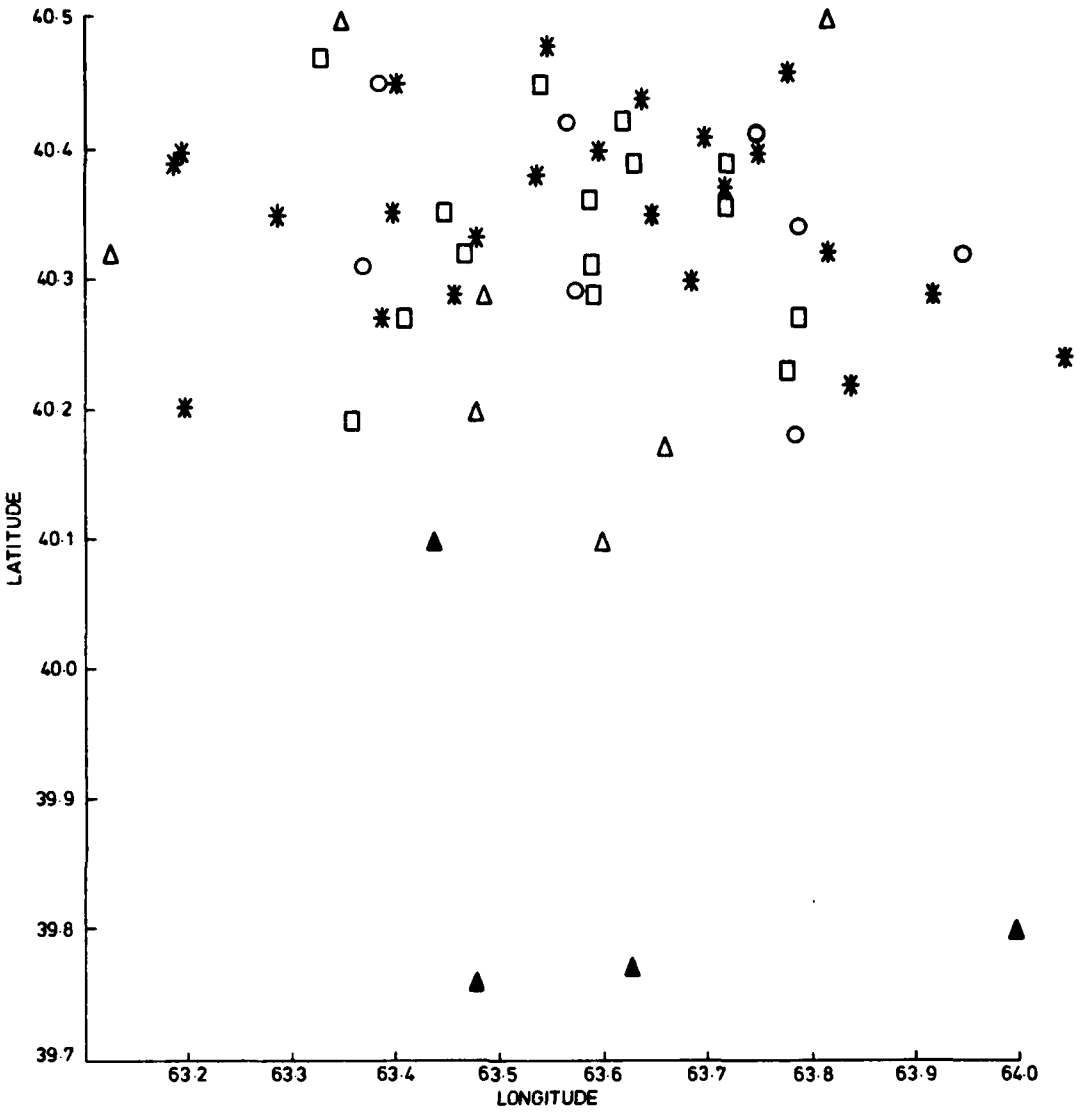

KEY

SYMBOL	ISC DETERMINED DEPTH
○	0 - 10 km
□	11 - 40 km
△	41 - 100 km
▲	> 100 km
✱	RESTRAINED TO 33 km

NOTES:
THOSE WITH DEPTH >100 km ARE CONSTRAINED ACCORDING TO THE QUETTA LOCAL DETERMINATION
pP-P TIMES GIVE ALL DEPTHS AS INTRACRUSTAL (SEE TEXT)
DEPTH RANGES ARE INDICATED BY DIFFERENT SYMBOLS AS SHOWN

FIGURE 2. Plot of Uzbekistan Hypocentres as Determined by the ISC

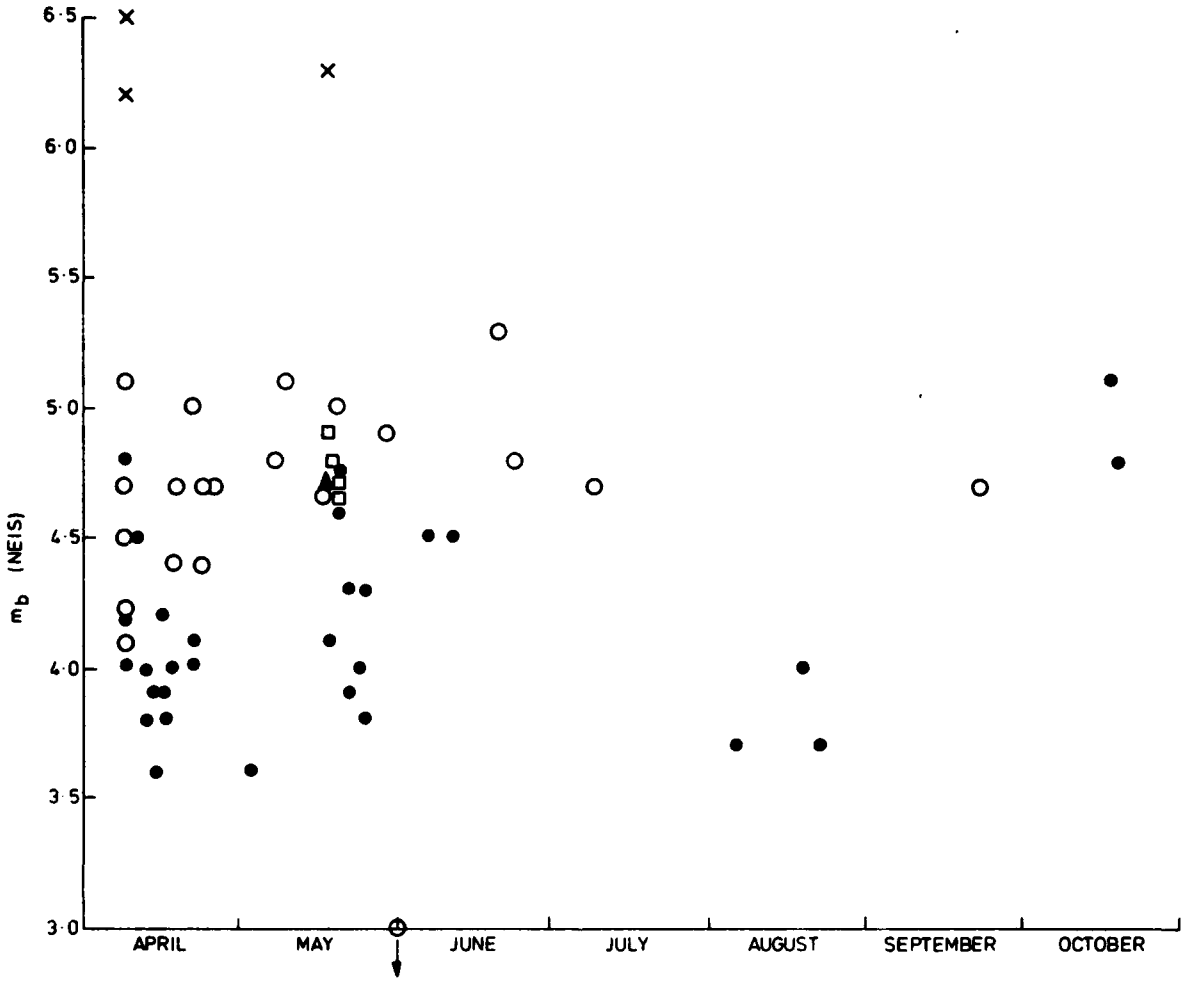

KEY TO CATEGORIES OF EARTHQUAKES (SEE TEXT)

×	CATEGORY 1	LARGE MAGNITUDE EARTHQUAKES WITH HIGHLY COMPLEX ARRAY SEISMOGRAMS
○	CATEGORY 2	AT LEAST TWO WELL-RECORDED ARRAY SEISMOGRAMS WITH CLEAR DISCRETE PHASES
□	CATEGORY 3	AT LEAST TWO WELL-RECORDED ARRAY SEIMOGRAMS WITH COMPLEX OR INCONSISTENT WAVEFORMS.
▲	CATEGORY 4	ONLY ONE GOOD QUALITY ARRAY SEISMOGRAM AVAILABLE
●	CATEGORY 5	SMALL MAGNITUDE EARTHQUAKES WITH DATA OF POOR SIGNAL TO NOISE RATIO

FIGURE 3 Relation beween m_b, Earthquake Category and Time

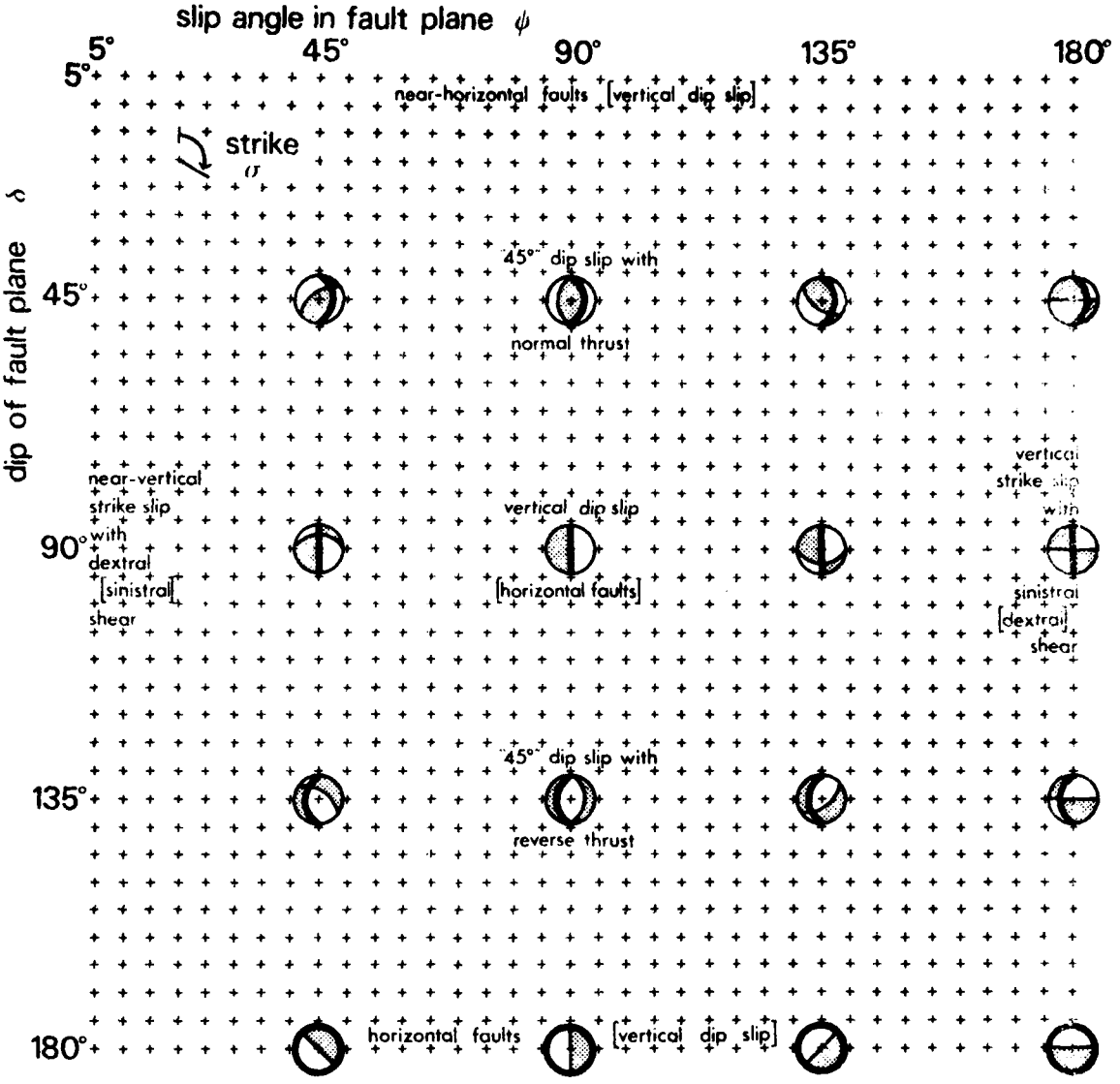

Acceptable orientations are plotted as vectors from the Cartesian point defining ψ and δ, in the direction of the strike σ. Lower hemisphere stereographic projections indicate the type of fault plane orientation represented by various combinations of ψ and δ, and are shown oriented for strike $\sigma = 360^{\circ}$ (northerly). In each case the fault plane is shown by a thick line ▬ and the auxiliary plane by a thin line ——. Shaded quadrants ◔ are negative. Different parts of the plot characterize various fault types, and some of these are shown. Where the interchange of fault and auxiliary planes yields a different fault type, this is shown in square brackets [ ].

FIGURE 4. METHOD OF REPRESENTING ACCEPTABLE FAULT PLANE ORIENTATIONS IN TERMS OF SLIP DIRECTION ψ, DIP δ AND STRIKE σ, AS DEFINED IN REFERENCE (3)

EVENT NO. 3: 8 April 1976 03-15-21.7
DEPTH DEDUCED BY MODELLING: 10.1 km
MAGNITUDE m_b (NEIS): 4.5
SOURCE ORIENTATION USED IN MODEL: Dip - 140°
Slip Angle - 95°
Strike - 135°

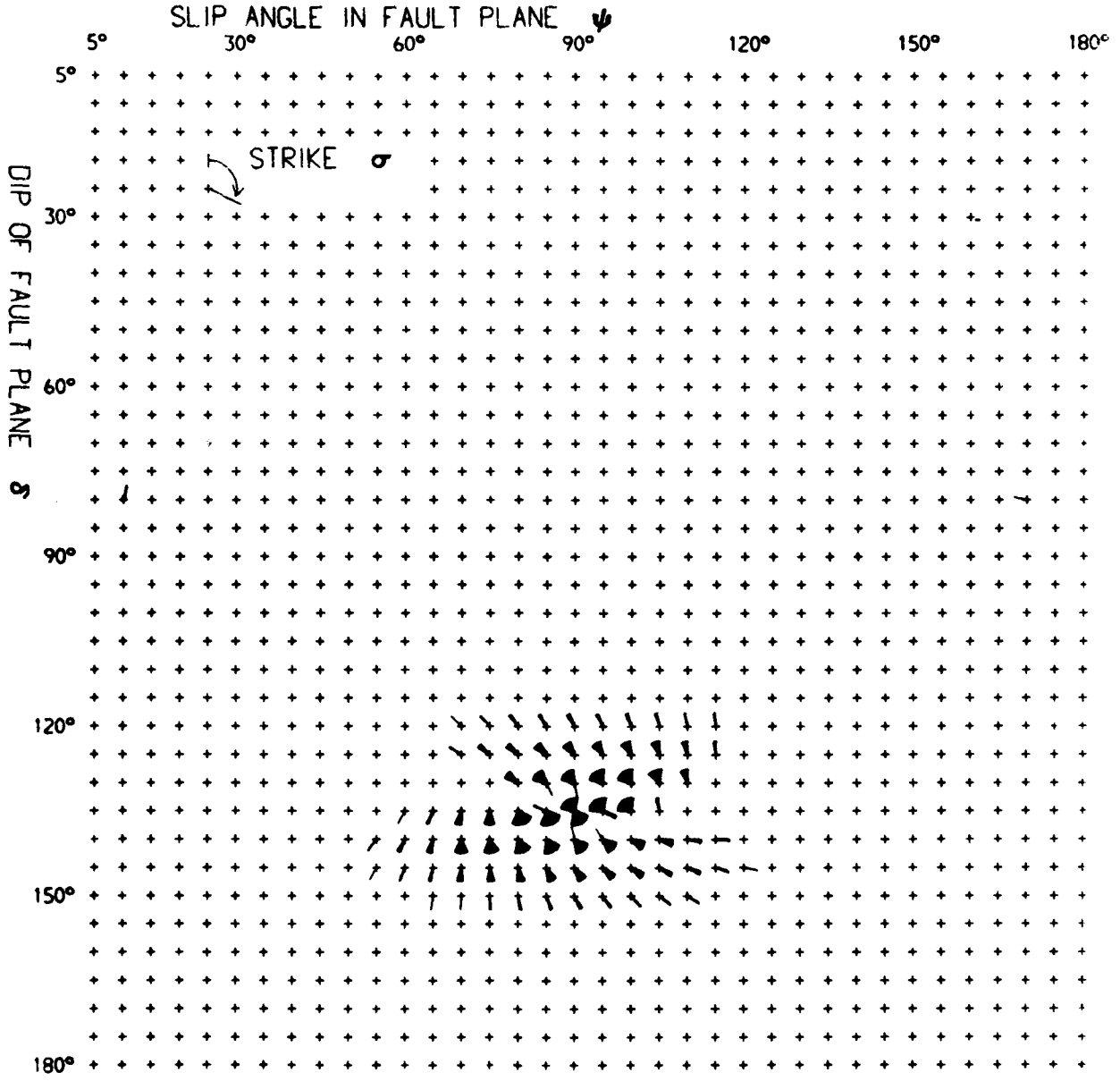

8 April 1976 03-15-21.7

(with no allowance for velocity structure)

Number of compatible orientations = 555

FIGURE 5(a)

EVENT NO. 3 (CATEGORY 2)

8 April 1976 03-15-21.7

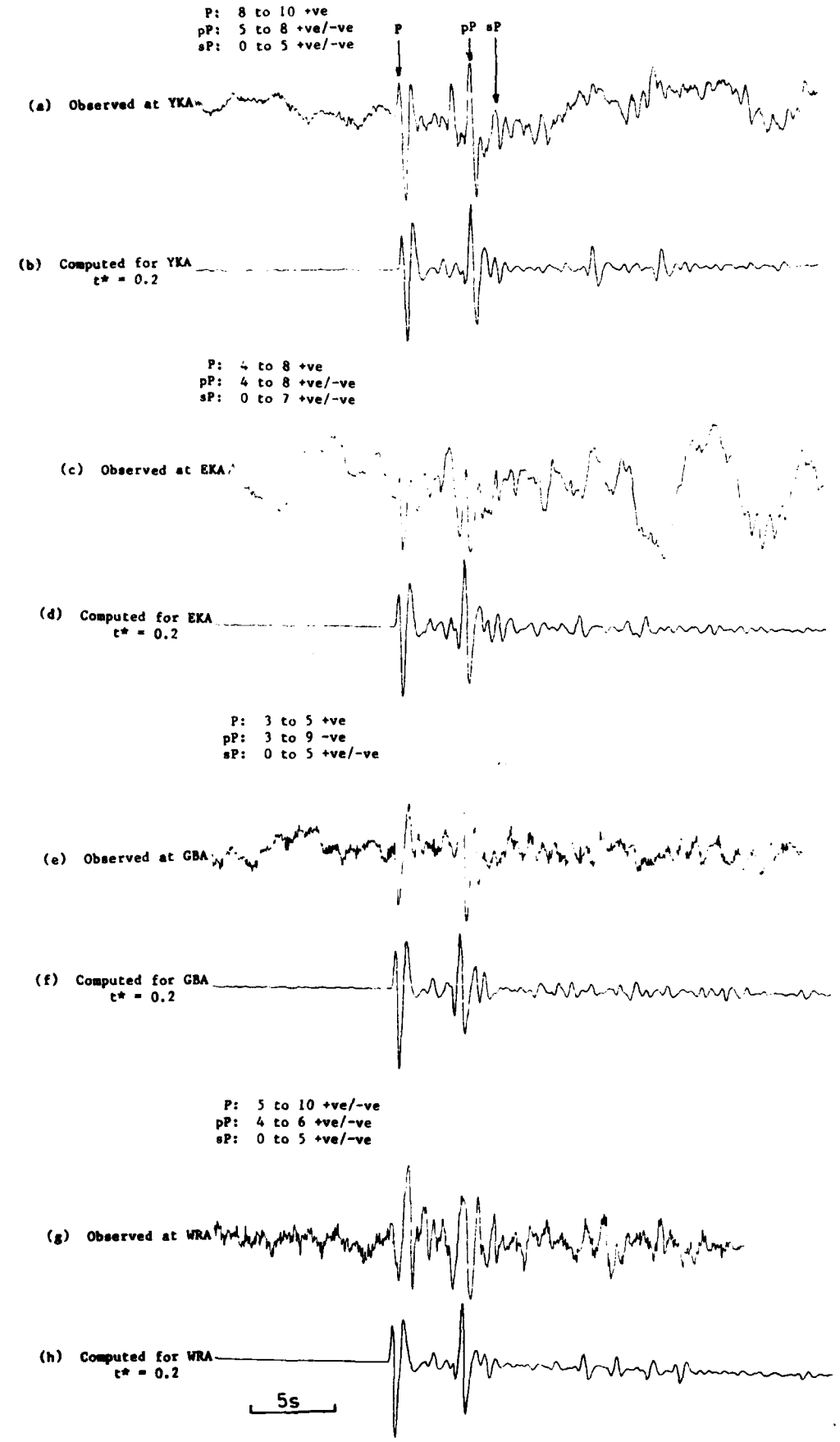

FIGURE 5(b)

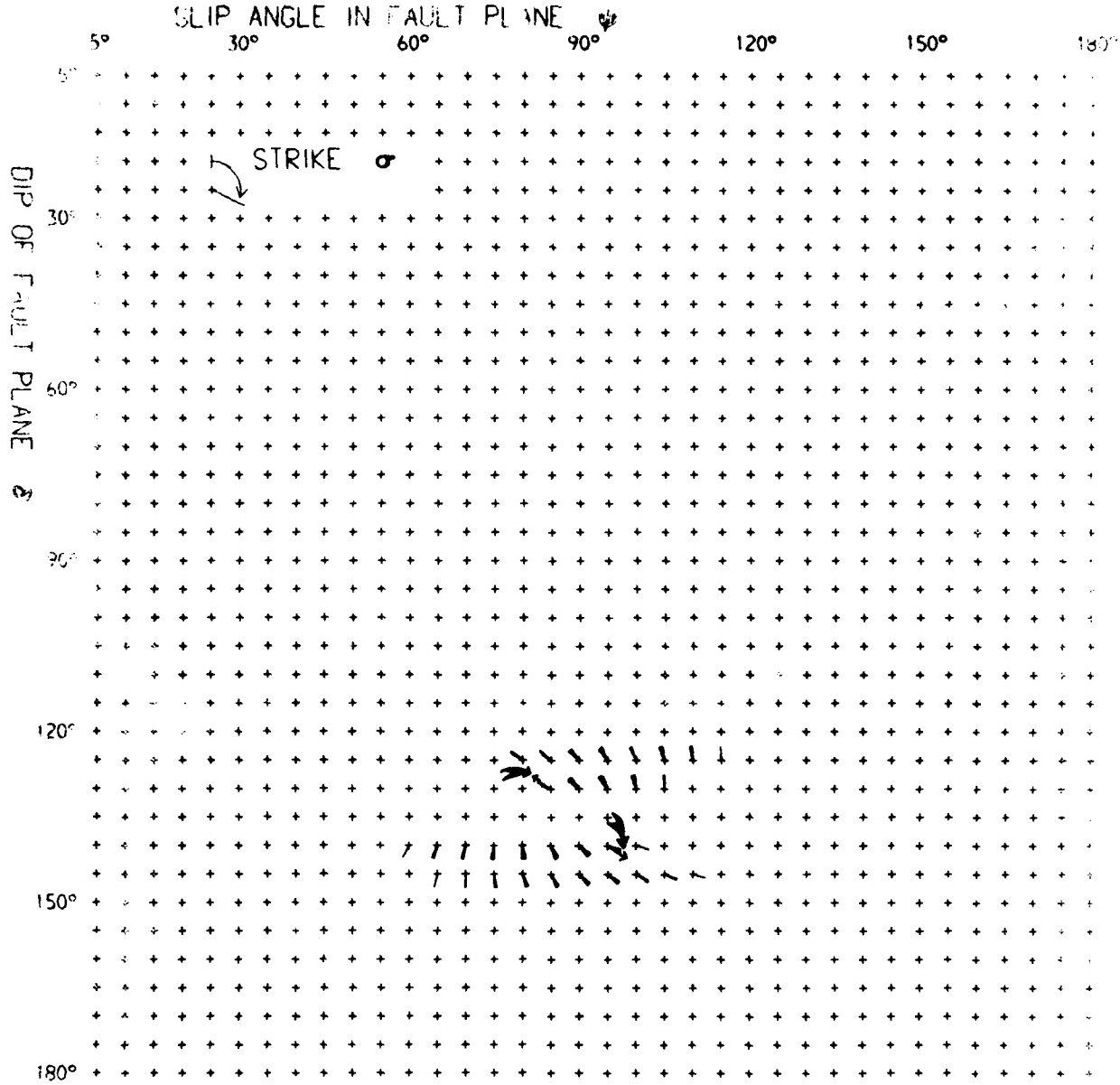

8 April 1976 03-15-21.7

(with allowance for velocity structure)

Number of compatible orientations = 105

FIGURE 5(c)

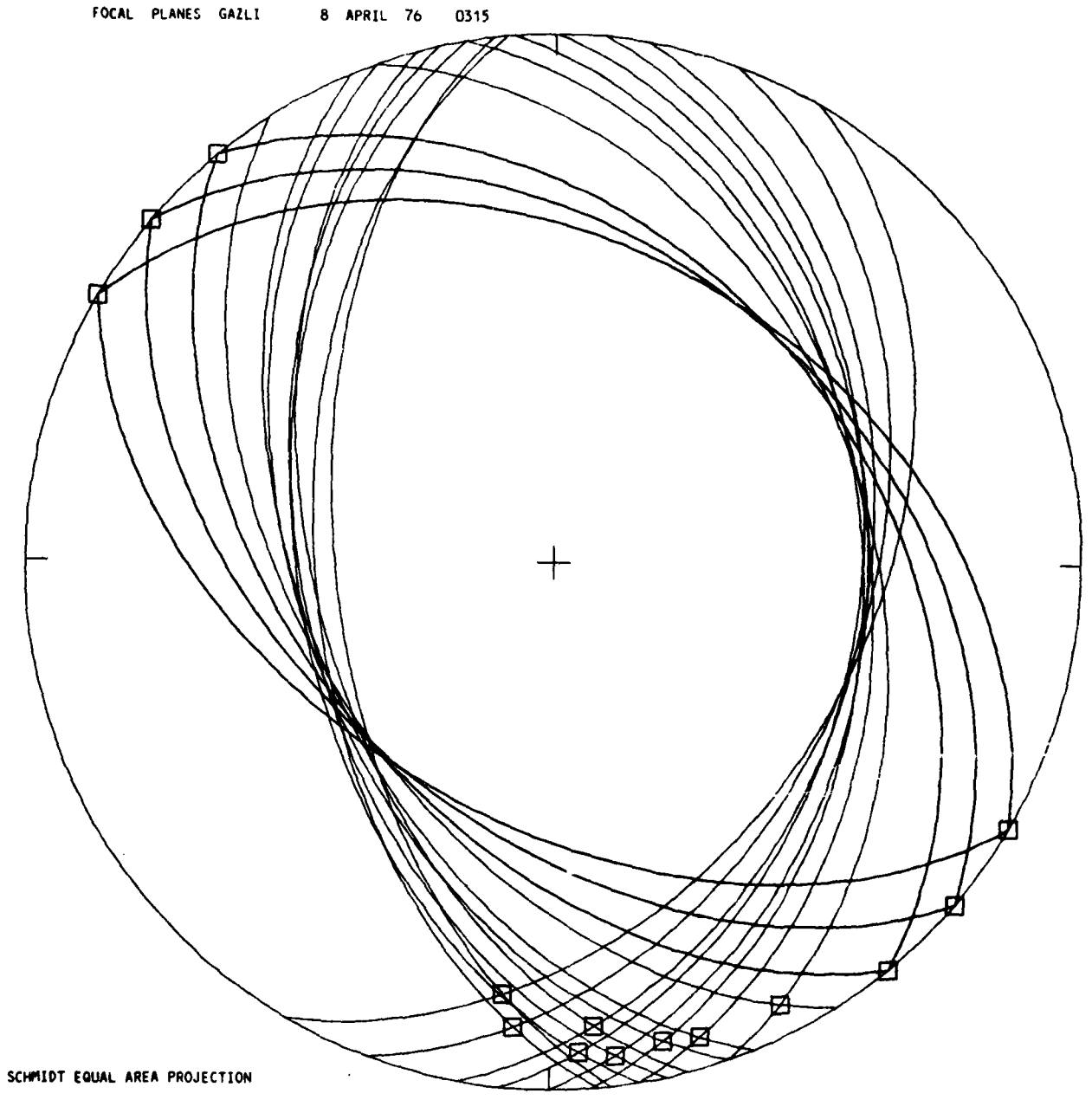

FIGURE 5(d)

(equivalent to figure 5(c))

EVENT NO. 4: 8 April 1976 03-30-49.3
DEPTH DEDUCED BY MODELLING: 8.57 km
MAGNITUDE m_b (NEIS): 4.1
SOURCE ORIENTATION USED IN MODEL: Dip - 135°
Slip Angle - 90°
Strike - 135°

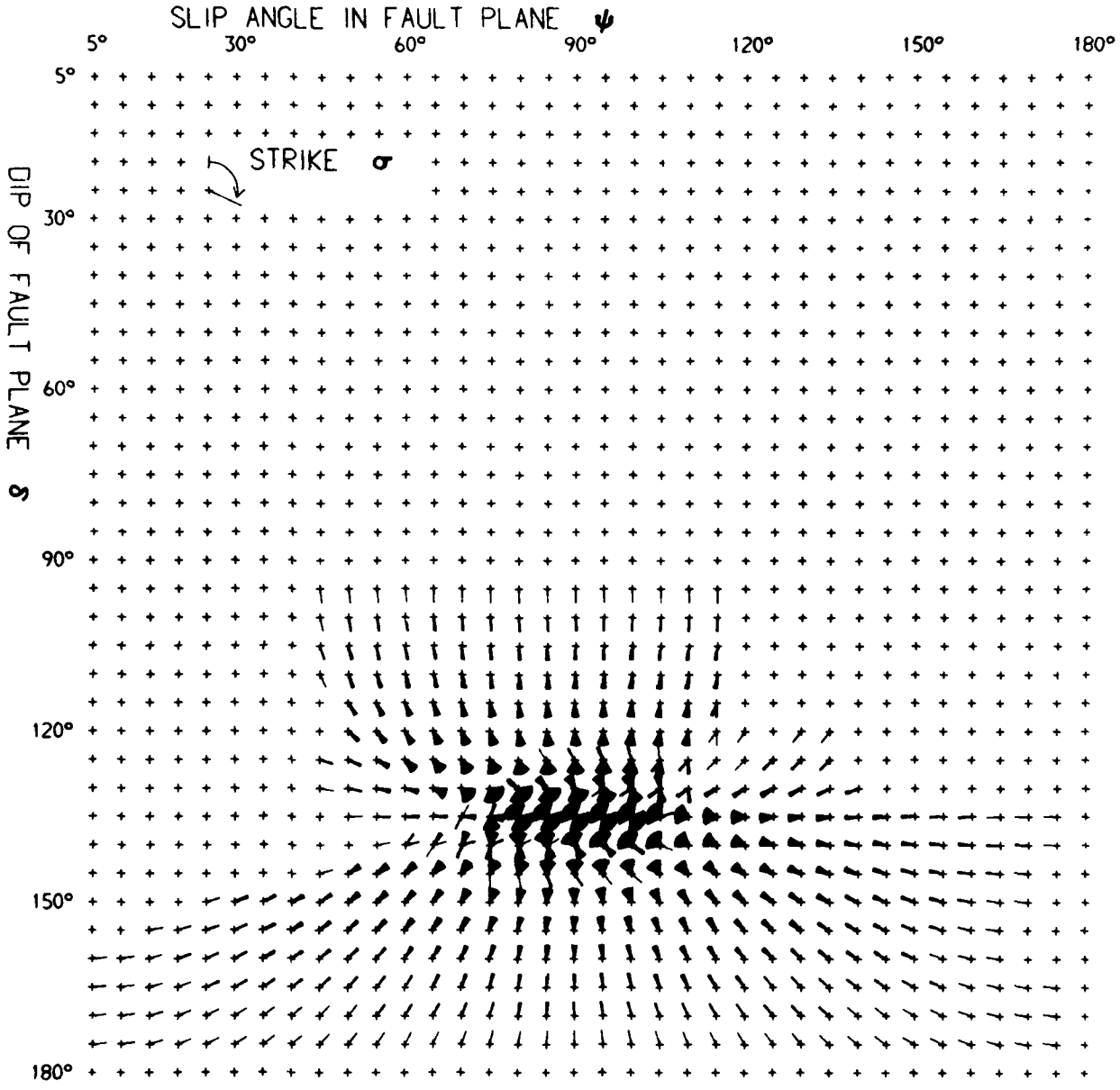

8 April 1976 03-30-49.3

(with no allowance for velocity structure)

Number of compatible orientations = 2332

FIGURE 6(a)

EVENT NO. 4 (CATEGORY 2)

8 April 1976 03-30-49.3

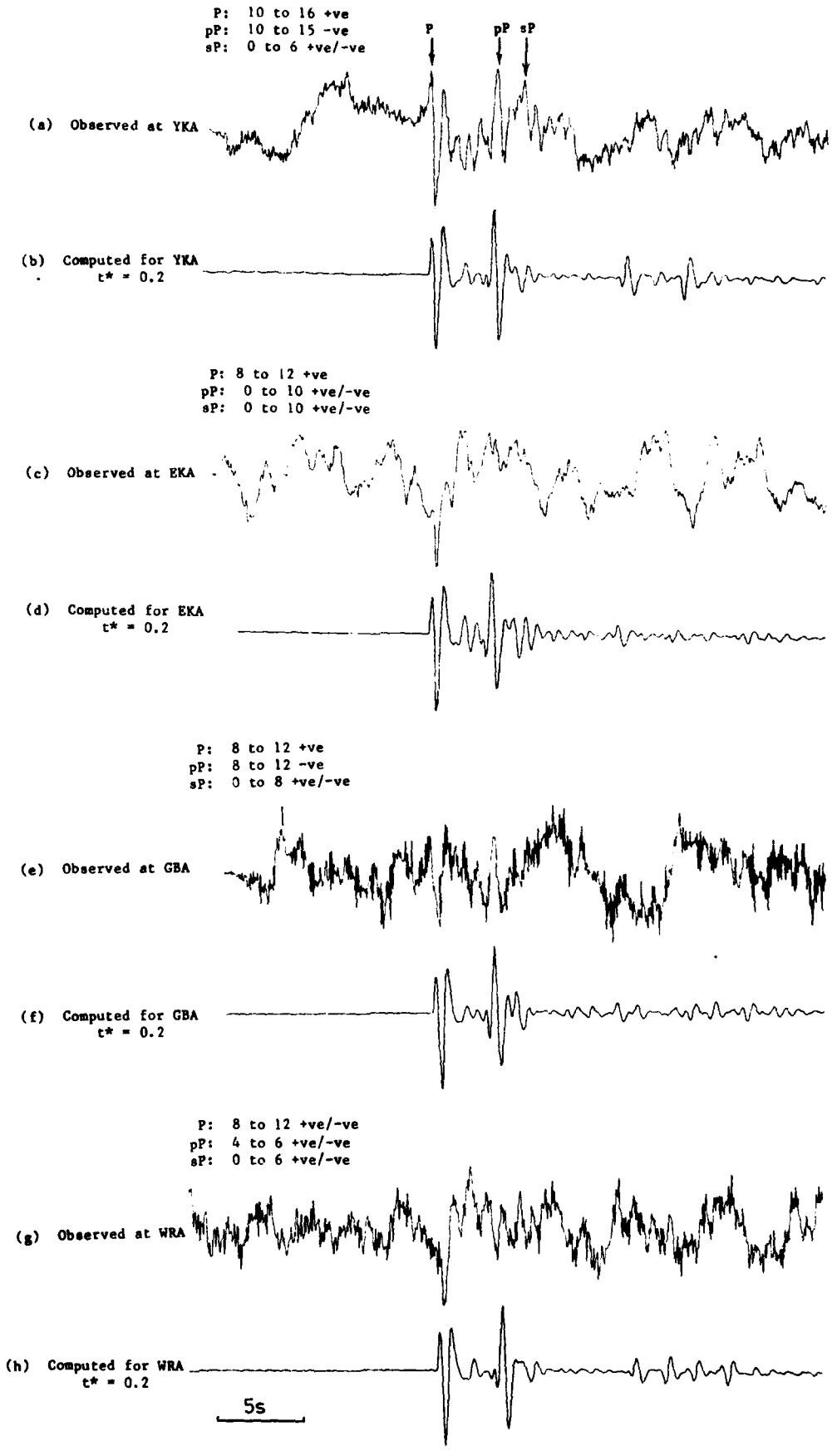

FIGURE 6(b)

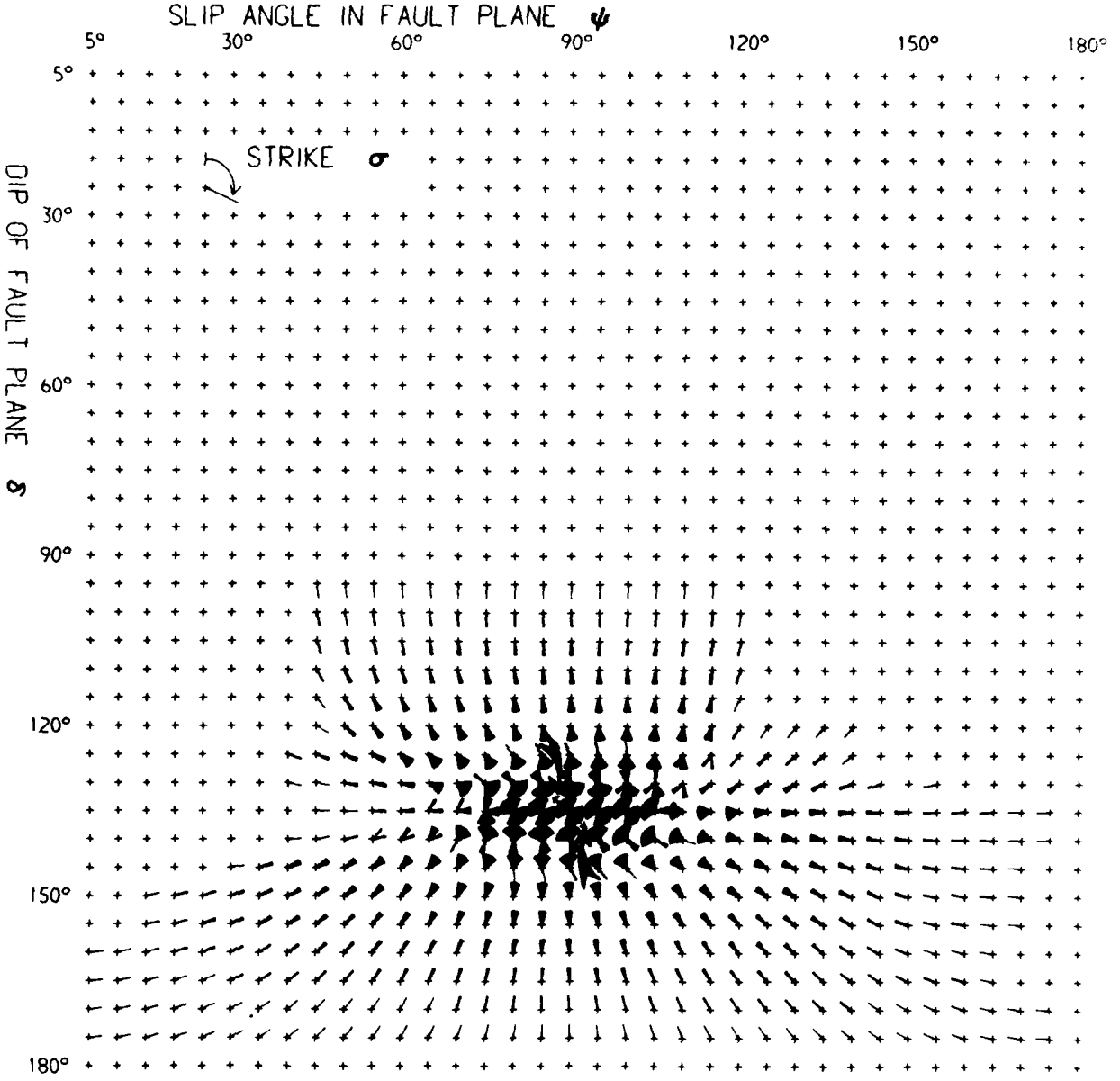

8 April 1976 03-30-49.3

(with allowance for velocity structure)

Number of compatible orientations = 2530

FIGURE 6(c)

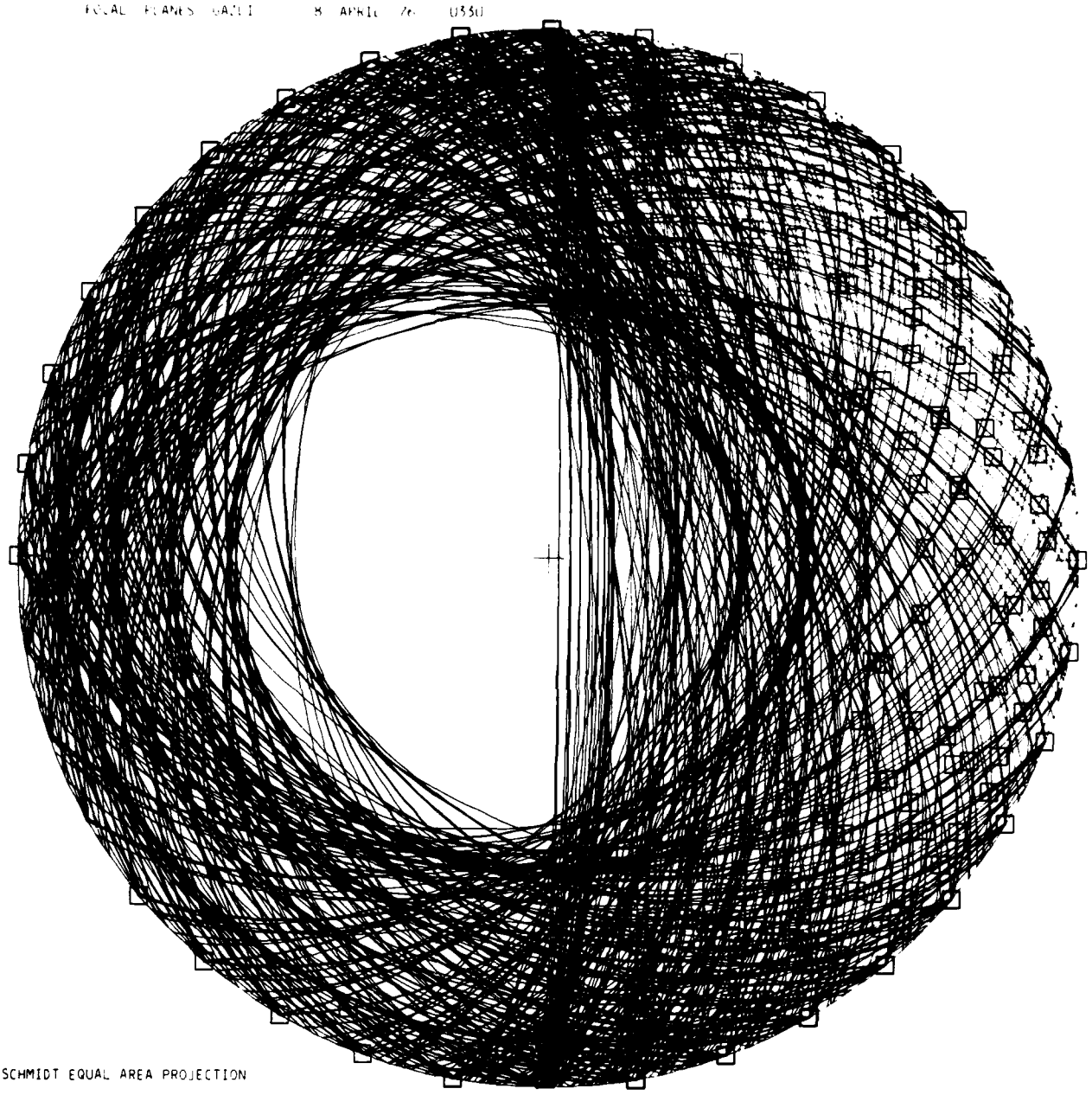

FIGURE 6(d)

(equivalent to figure 6(c))

EVENT NO. 7: 8 April 1976 06-16-50.0
DEPTH DEDUCED BY MODELLING: 9.49 km
MAGNITUDE m_b (NEIS): 4.7

SOURCE ORIENTATION USED IN MODEL:
Dip - 135°
Slip Angle - 75°
Strike - 135°

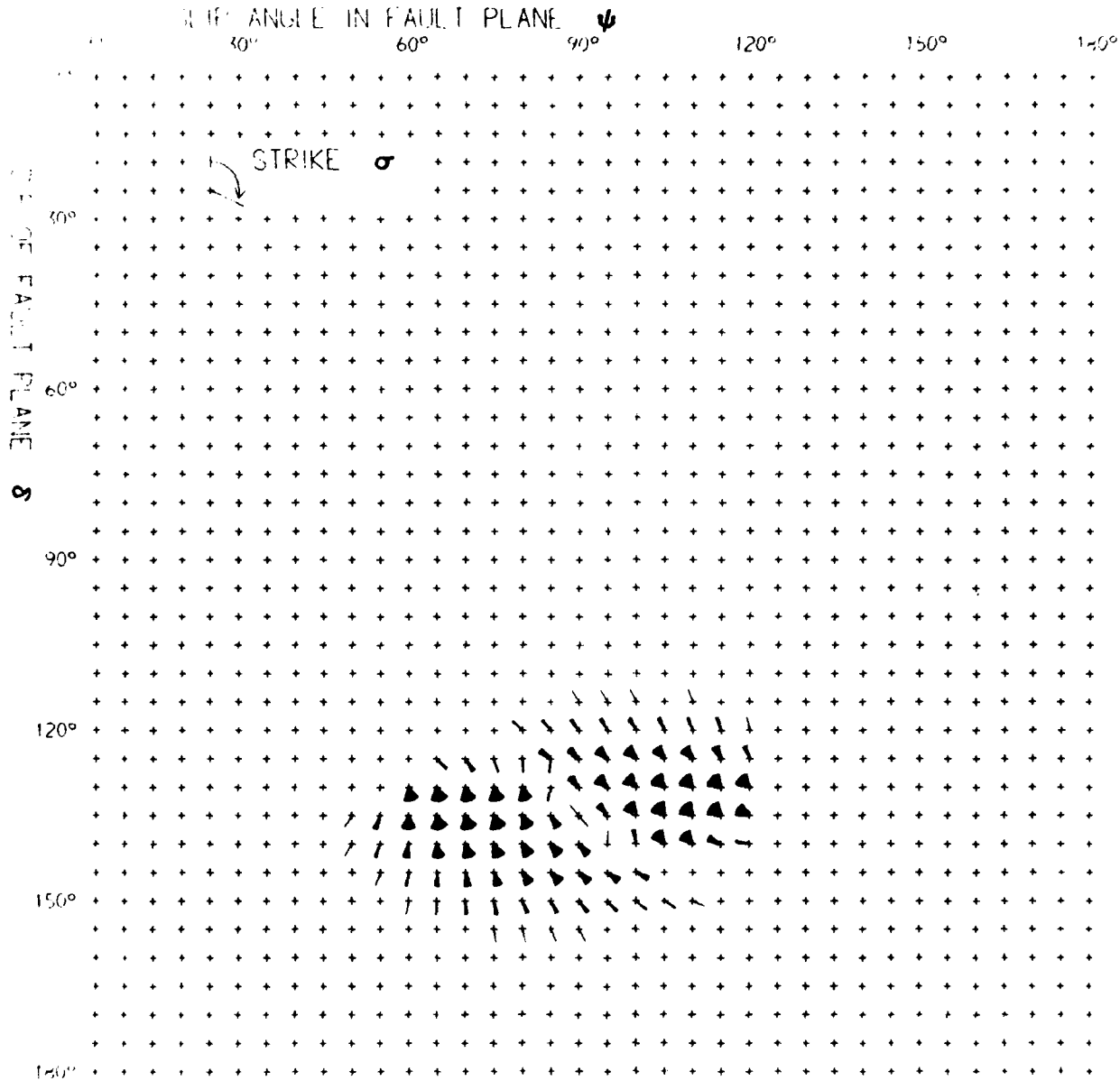

8 April 1976 06-16-50.0

(with no allowance for velocity structure)

Number of compatible orientations = 674

FIGURE 7(a)

EVENT NO. 7 (CATEGORY 2)

8 April 1976 06-16-50.0

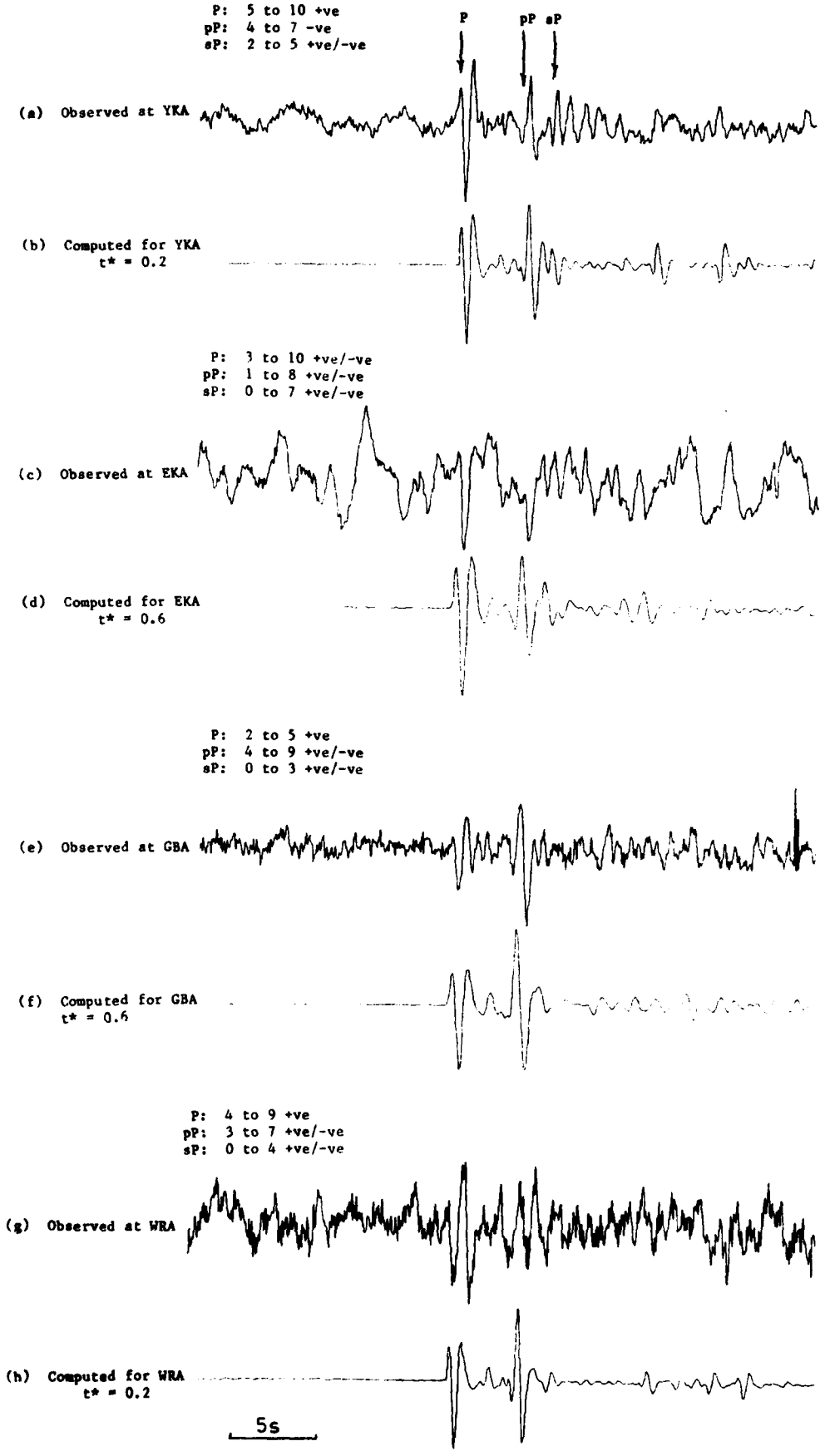

FIGURE 7(b)

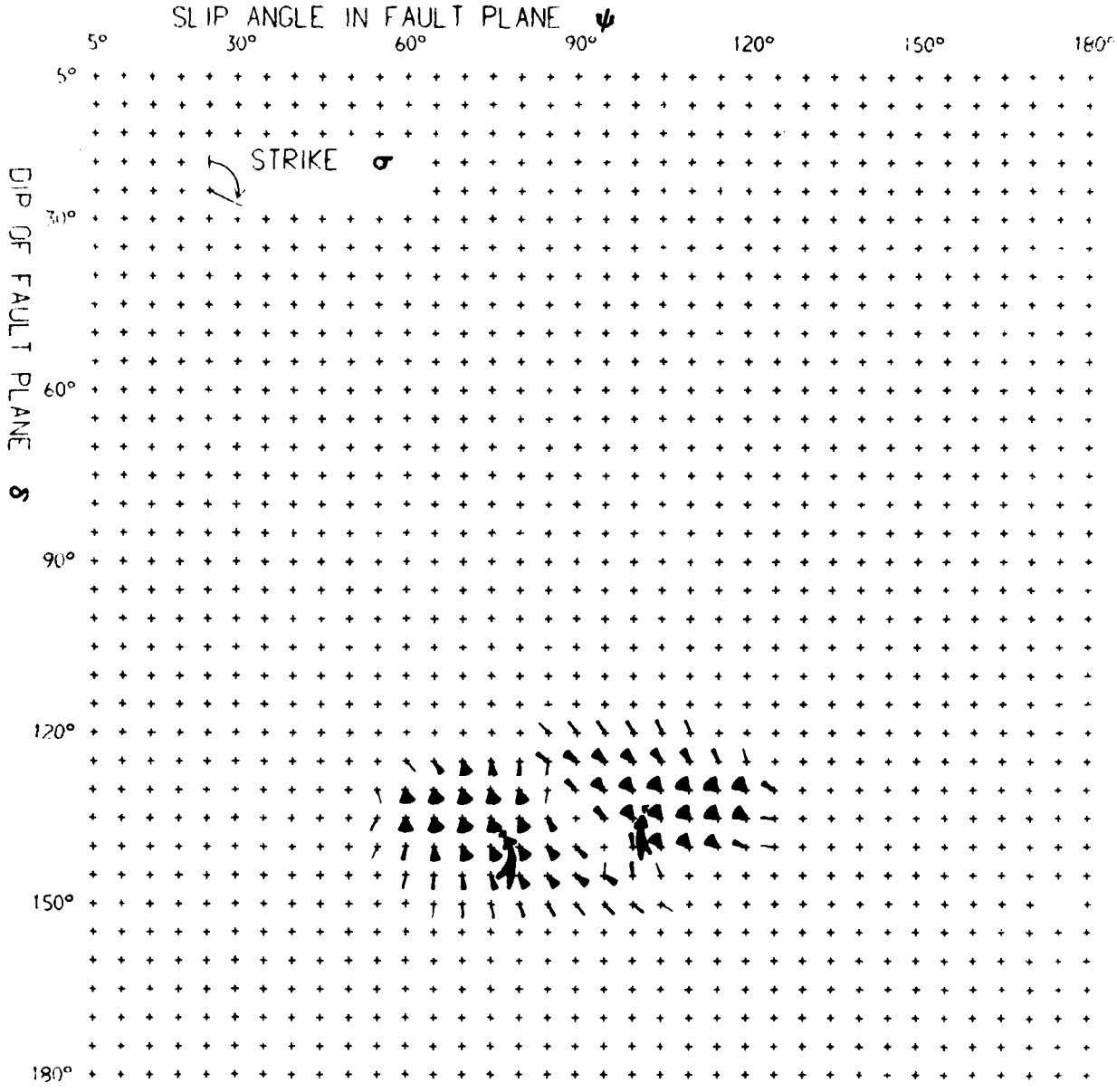

8 April 1976 06-16-50.0

(with allowance for velocity structure)

Number of compatible orientations = 625

FIGURE 7(c)

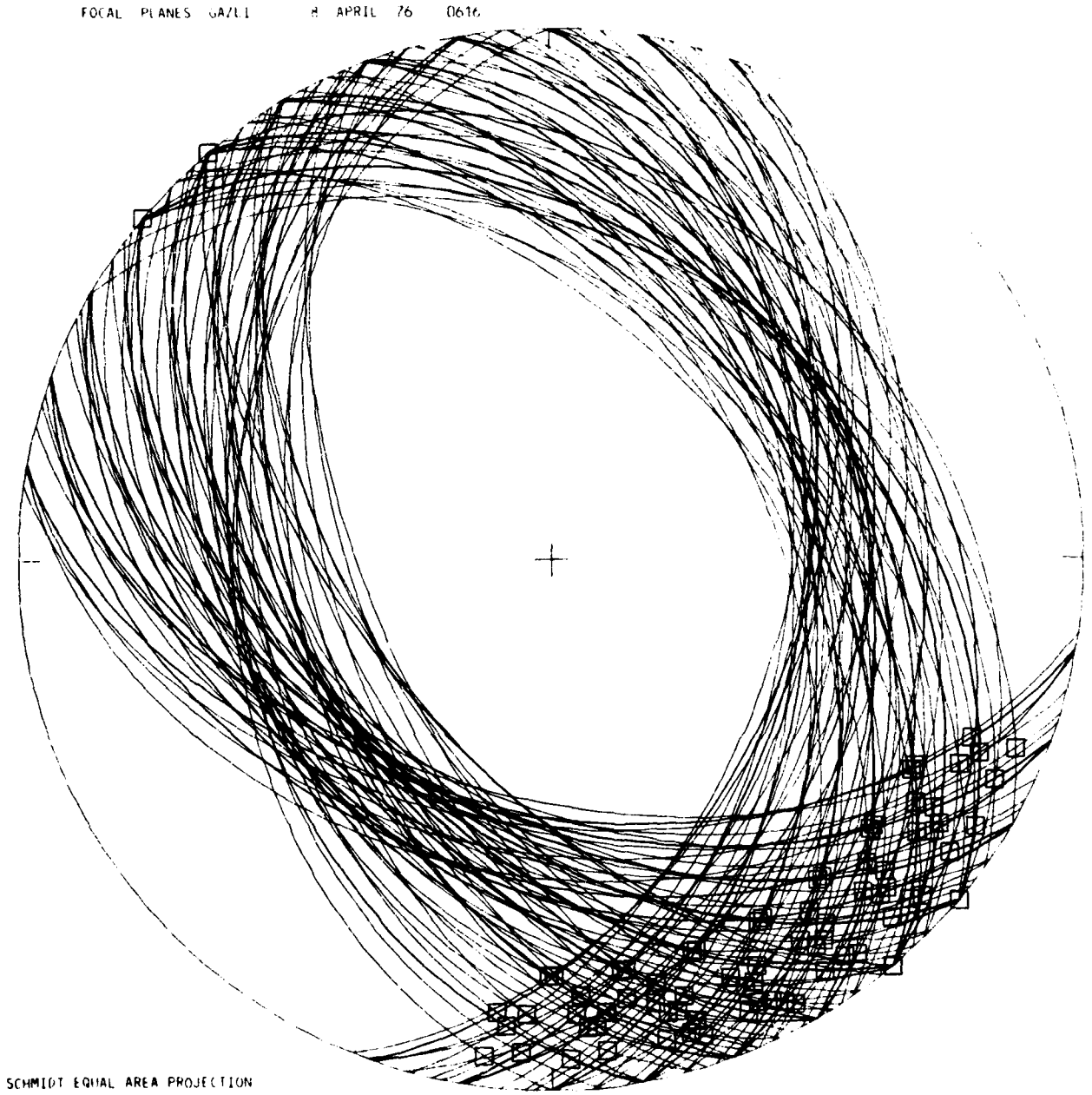

FIGURE 7(d)

(equivalent to figure 7(c))

EVENT NO. 8: 8 April 1976 09-10-07.7
DEPTH DEDUCED BY MODELLING: 8.57 km
MAGNITUDE m_b (NEIS): 4.2
SOURCE ORIENTATION USED IN MODEL:
Dip - 140°
Slip Angle - 50°
Strike - 340°

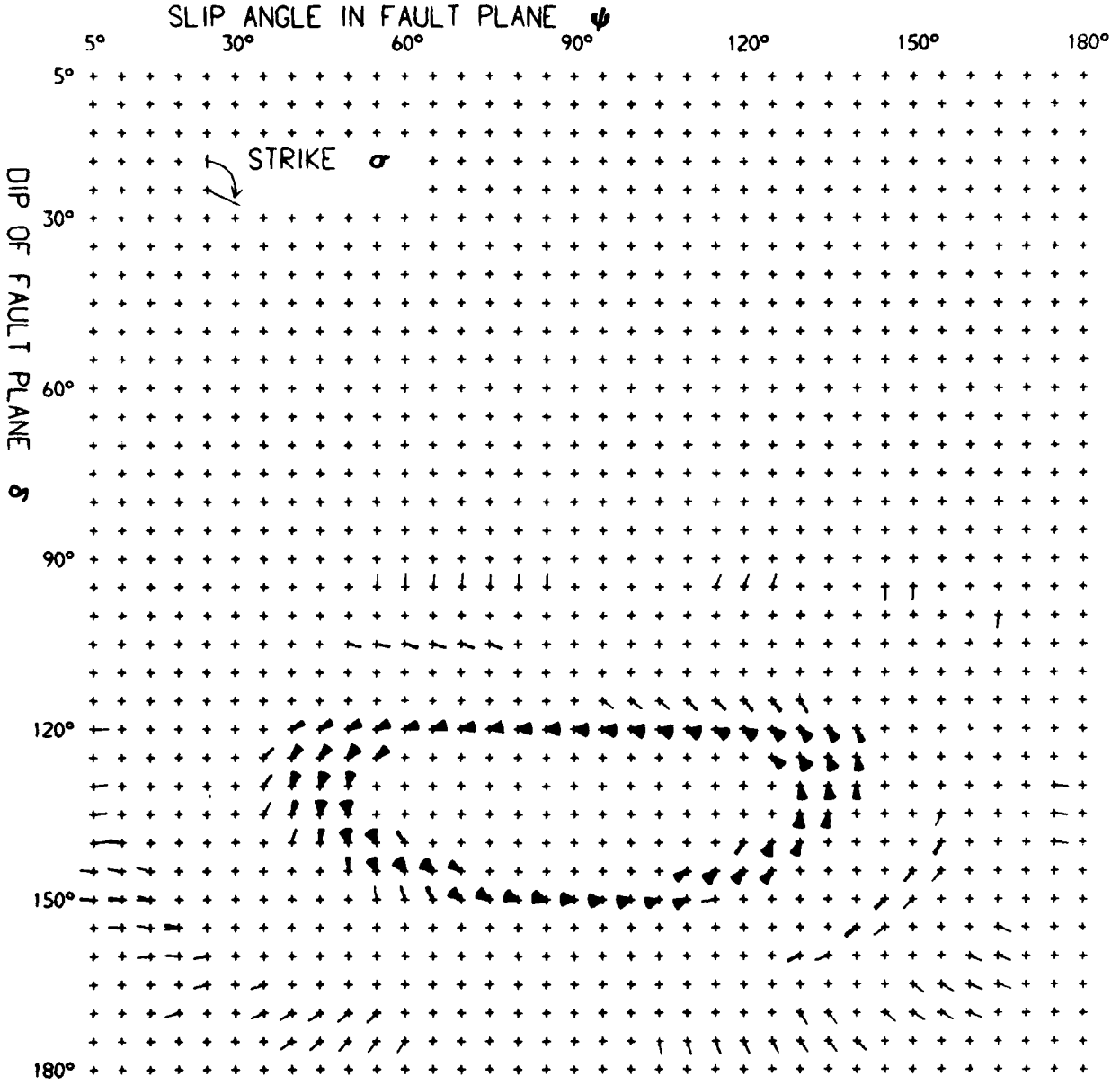

8 April 1976 09-10-07.7

(with no allowance for velocity structure)

Number of compatible orientations = 772

FIGURE 8(a)

EVENT NO. 8 (CATEGORY 2)

8 April 1976 09-10-07.7

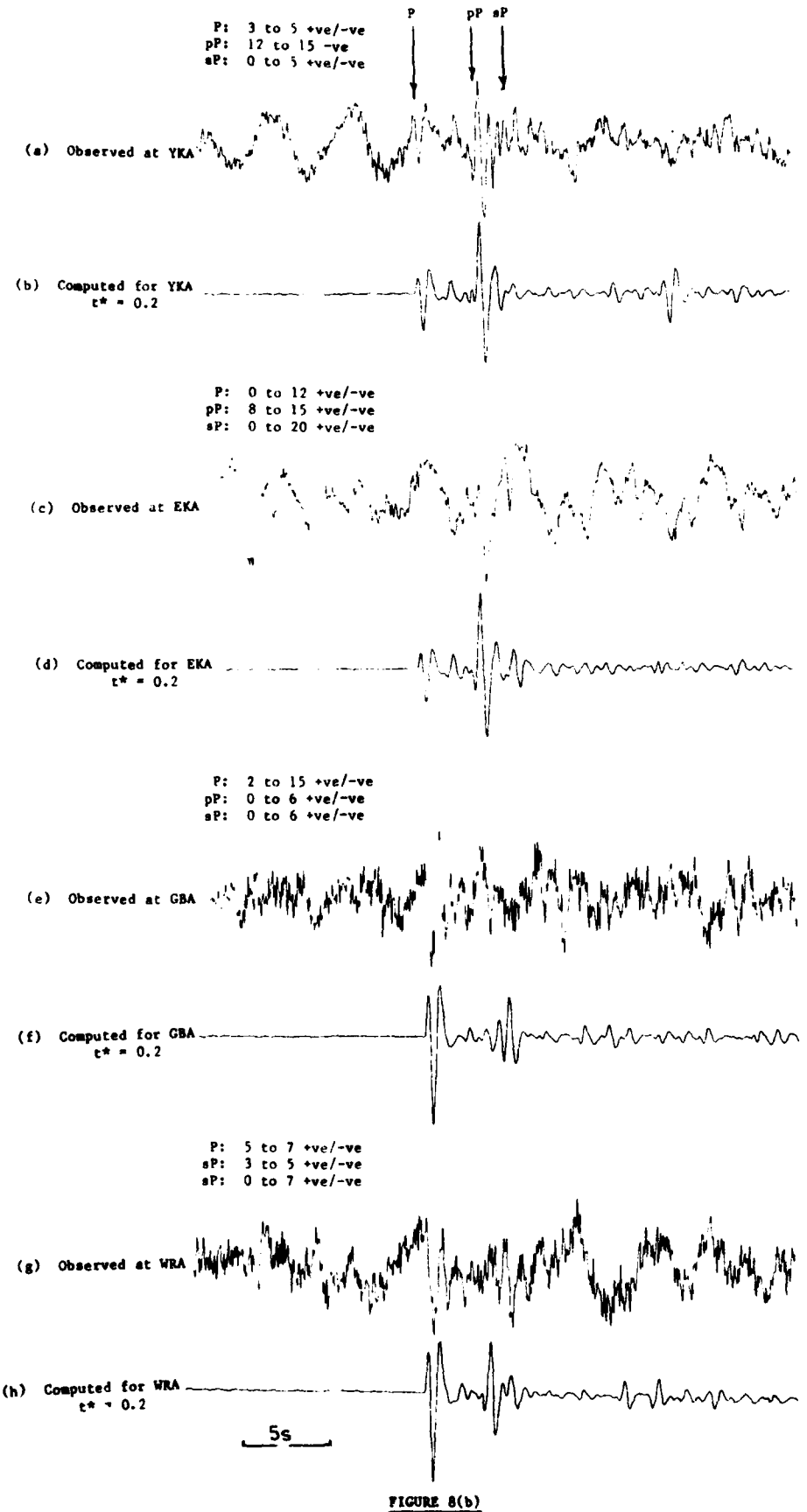

FIGURE 8(b)

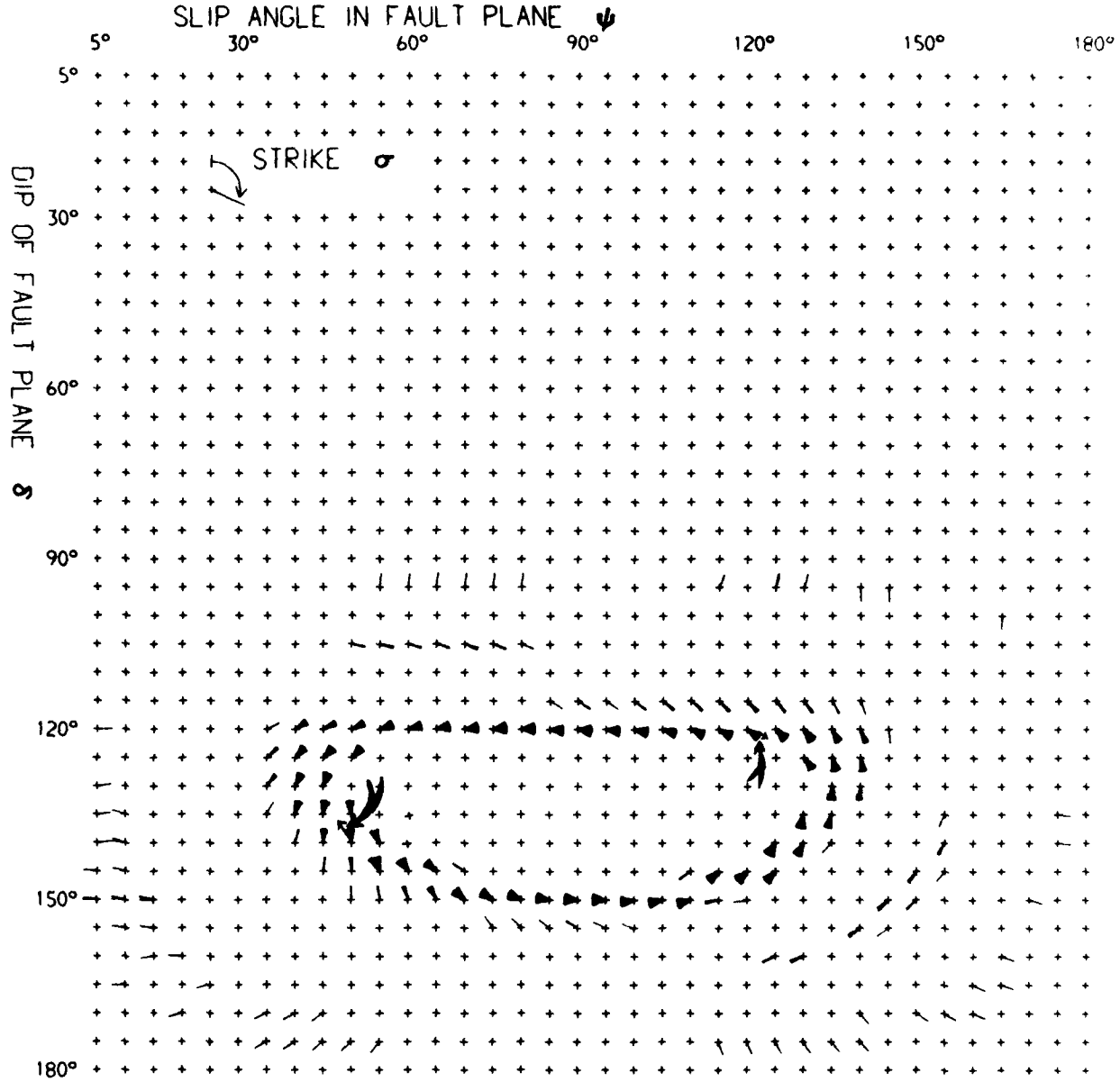

8 April 1976 09-10-07.7

(with allowance for velocity structure)

Number of compatible orientations = 690

FIGURE 8(c)

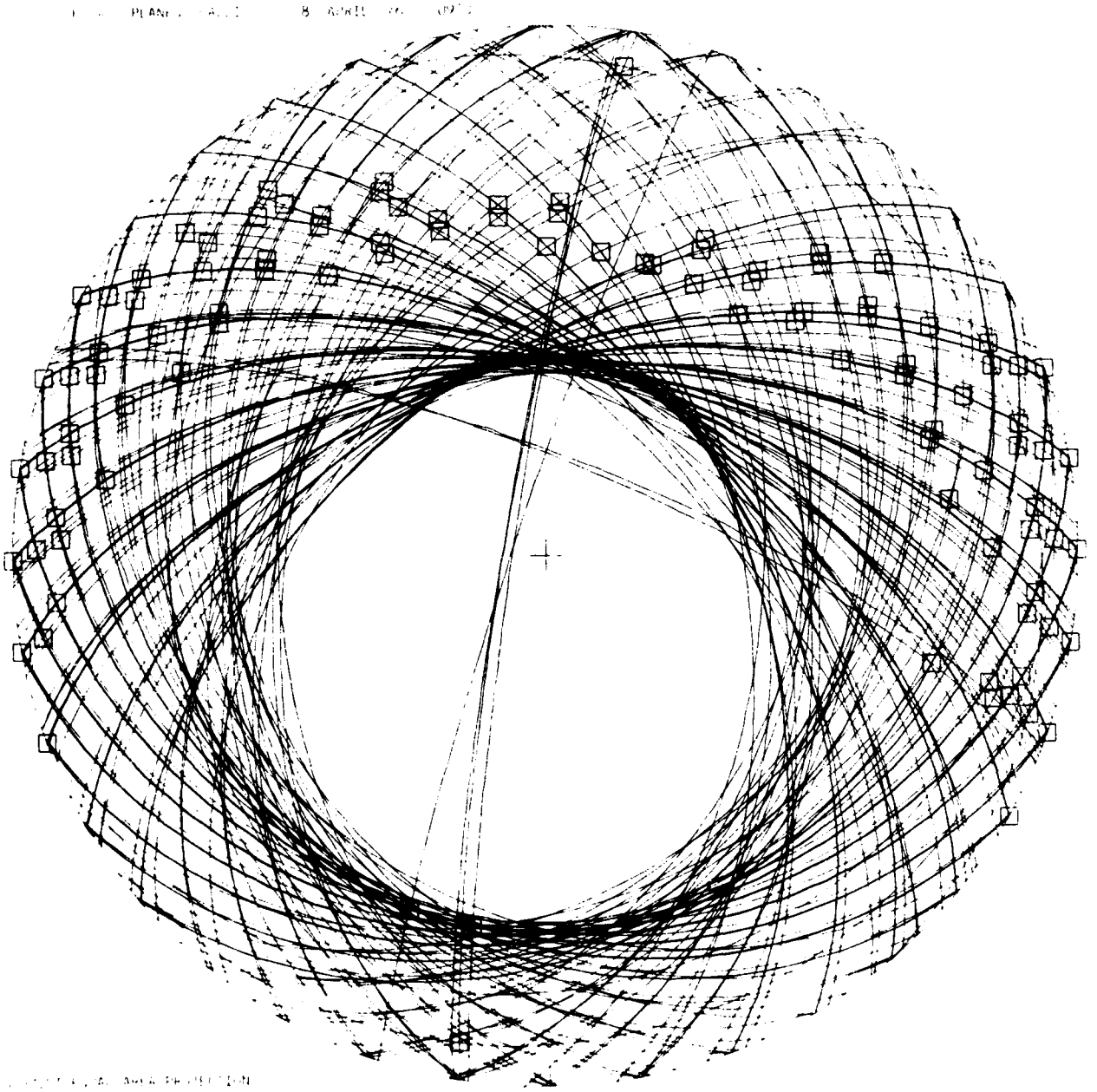

FIGURE 8(d)

(equivalent to figure 8(c))

EVENT NO. 9: 8 April 1976 12-03-41.1
DEPTH DEDUCED BY MODELLING: 7.96 km
MAGNITUDE m_b (NEIS): 5.1
SOURCE ORIENTATION USED IN MODEL: Dip - 140°
Slip Angle - 115°
Strike - 135°

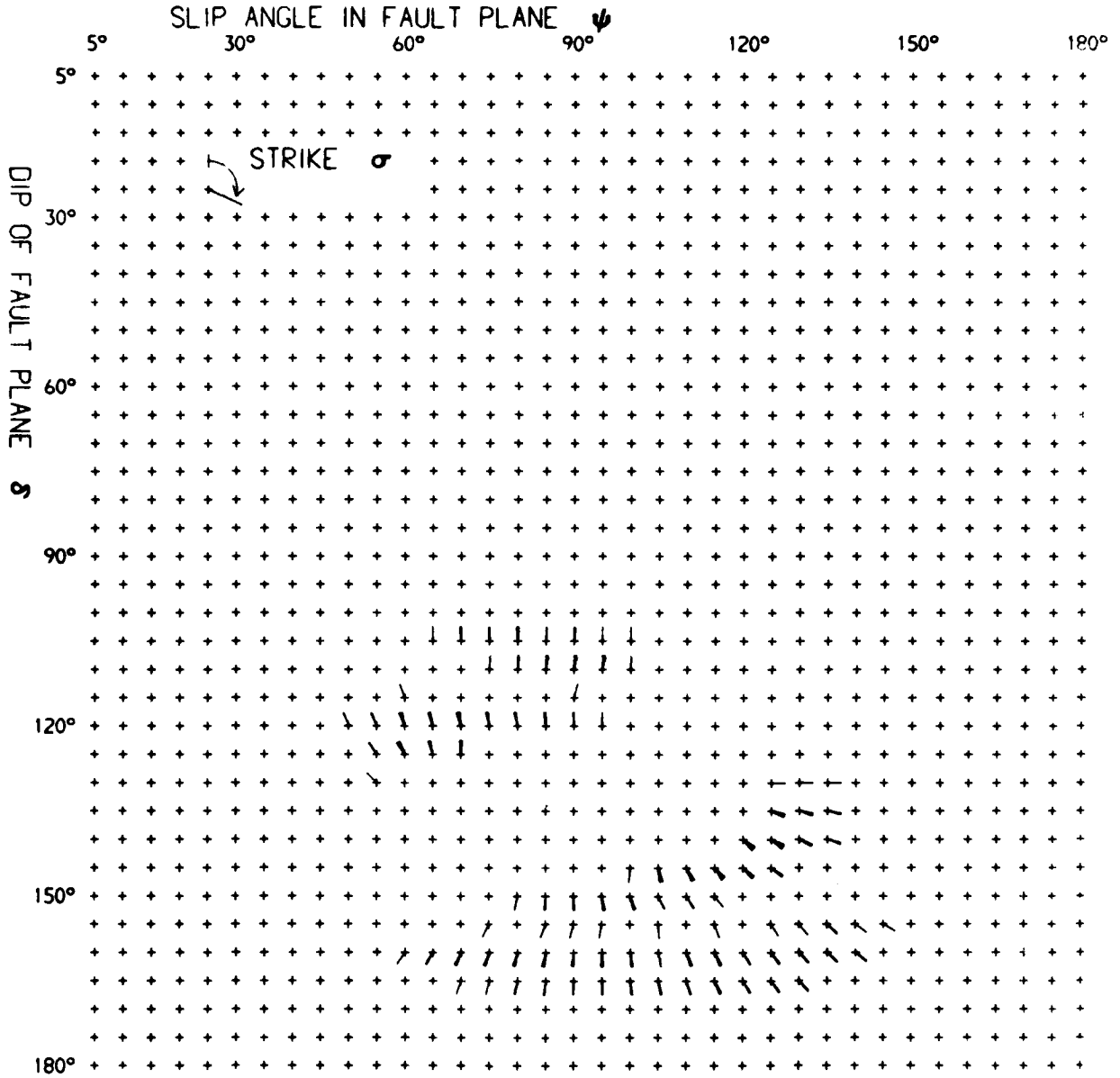

8 April 1976 12-03-41.1

(with no allowance for velocity structure)

Number of compatible orientations = 210

FIGURE 9(a)

EVENT NO. 9 (CATEGORY 2)

8 April 1976 12-03-41.1

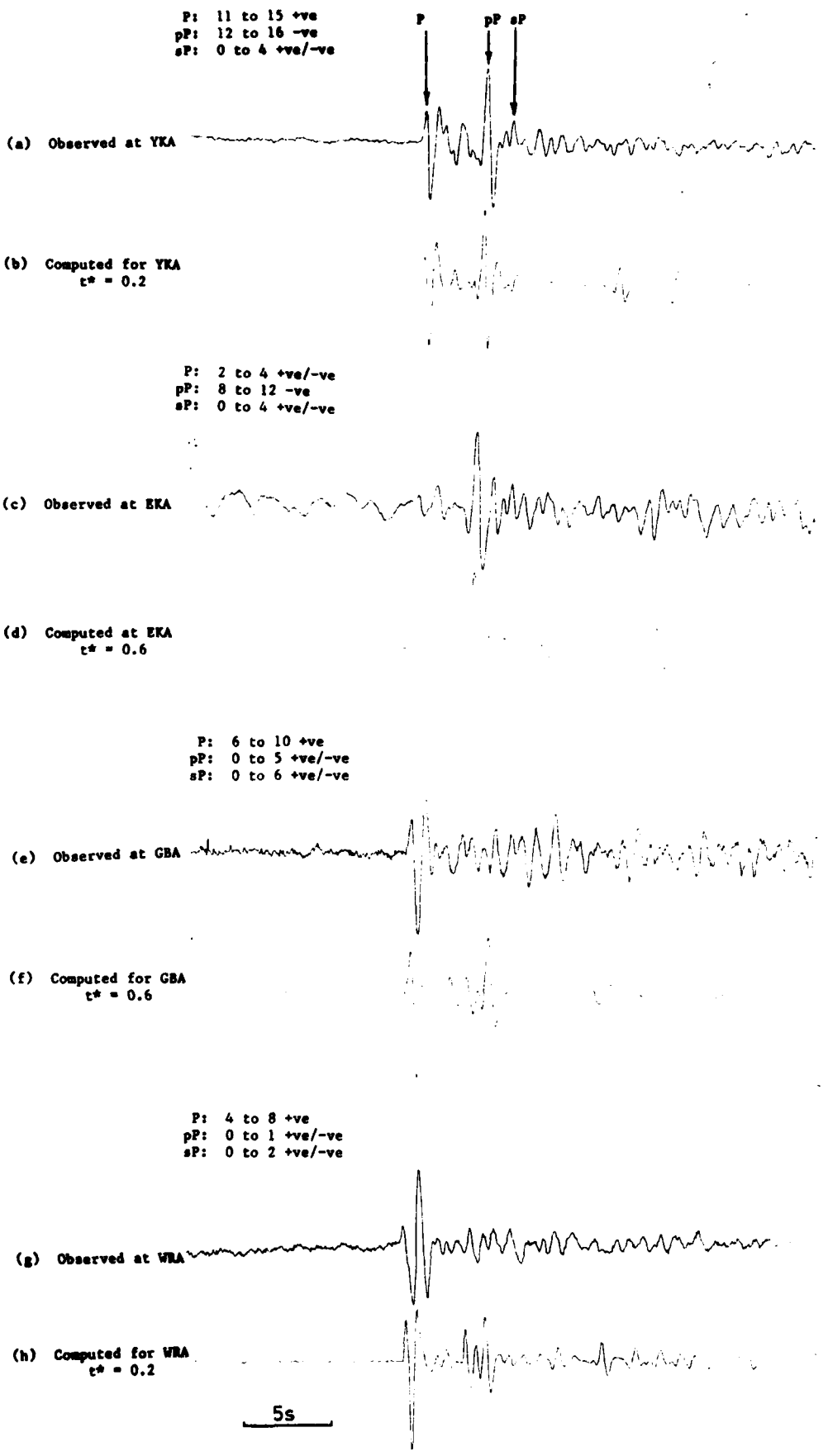

FIGURE 9(b)

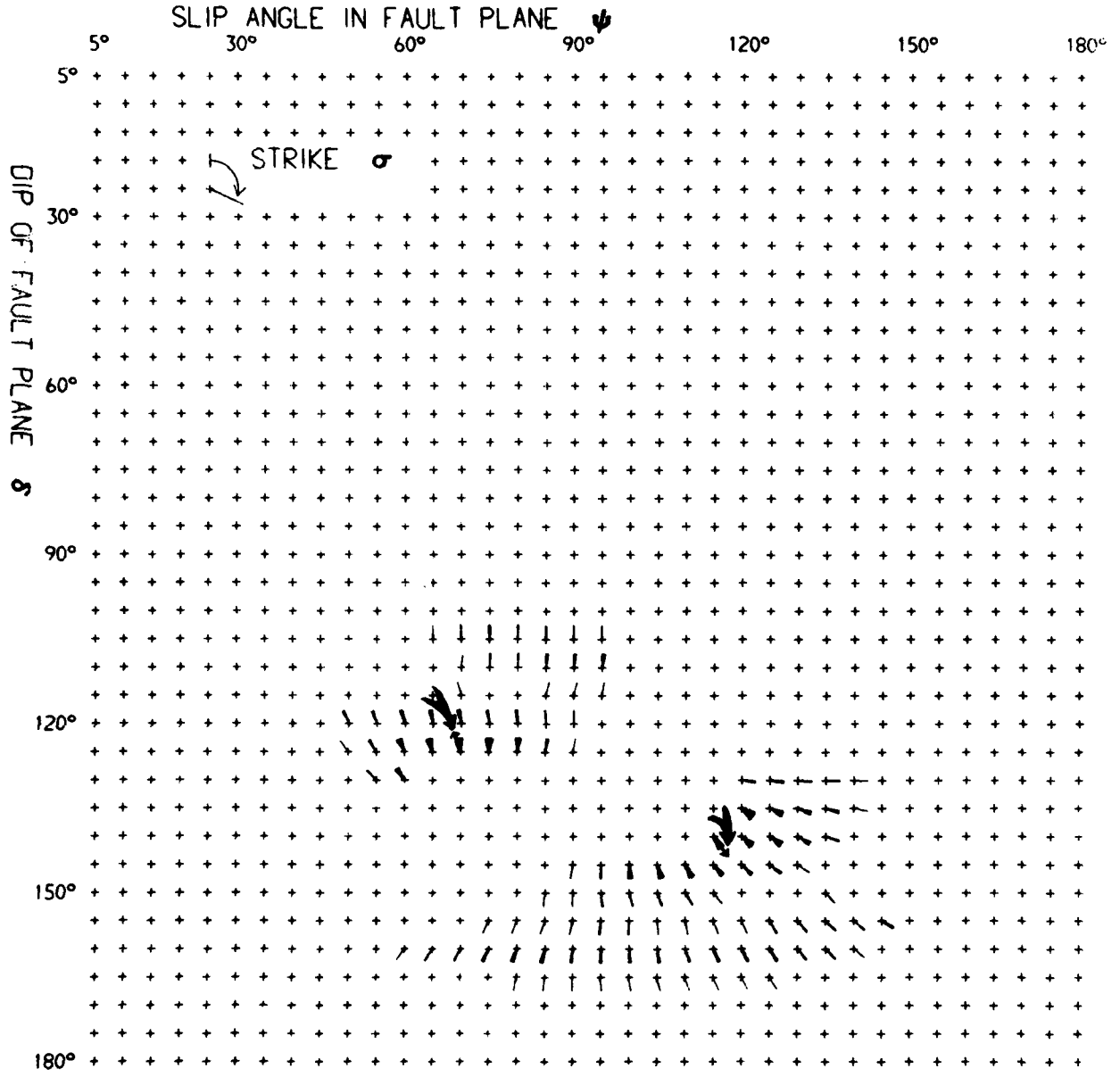

8 April 1976 12-03-41.1

(with allowance for velocity structure)

Number of compatible orientations = 288

FIGURE 9(c)

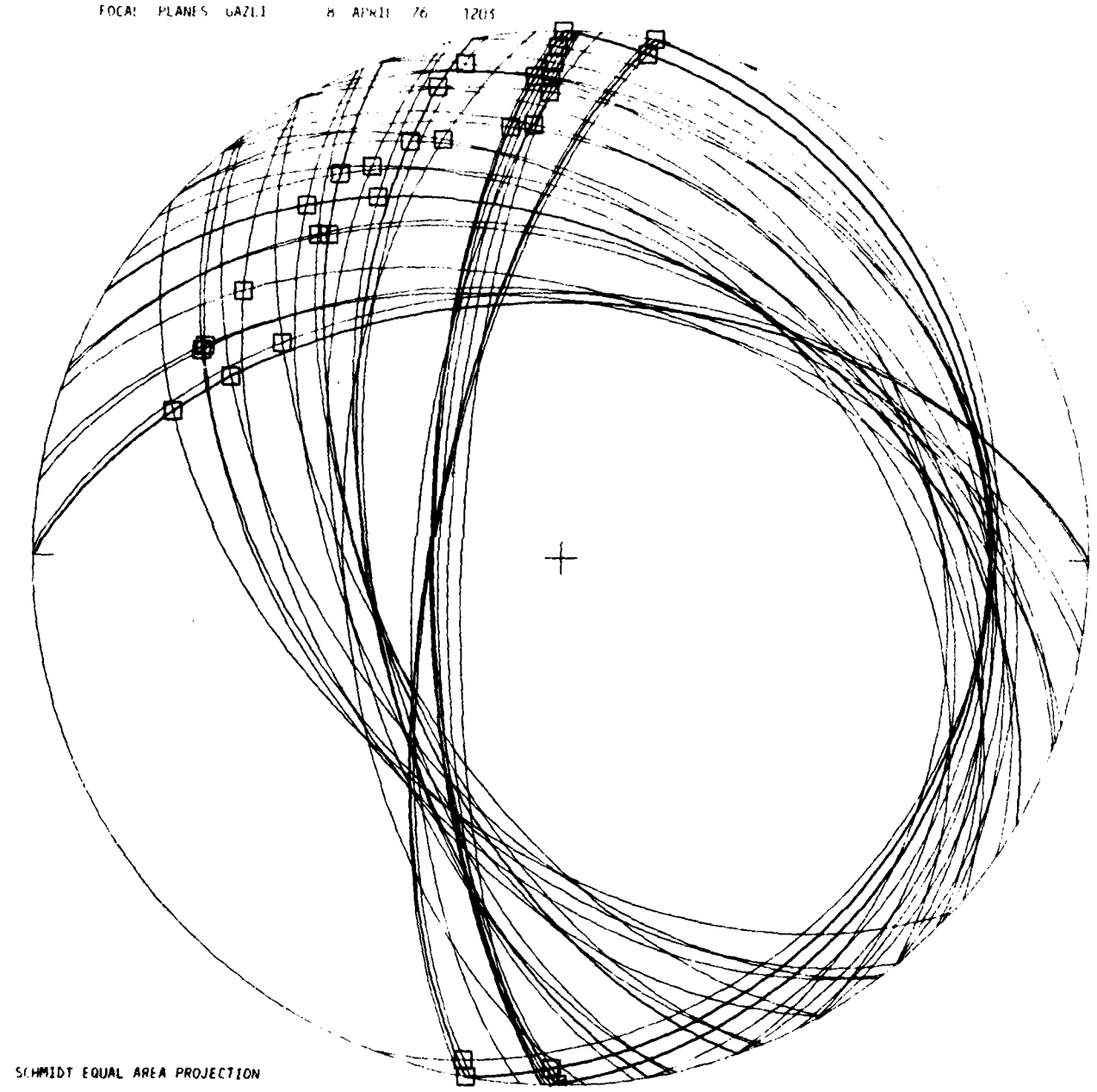

FIGURE 9(d)

(equivalent to figure 9(c))

EVENT NO. 19: 17 April 1976 12-11-14.2
DEPTH DEDUCED BY MODELLING: 9.9 km
MAGNITUDE m_b (NEIS) 4.4
SOURCE ORIENTATION USED IN MODEL: Dip - 135°
Slip Angle - 90°
Strike - 135°

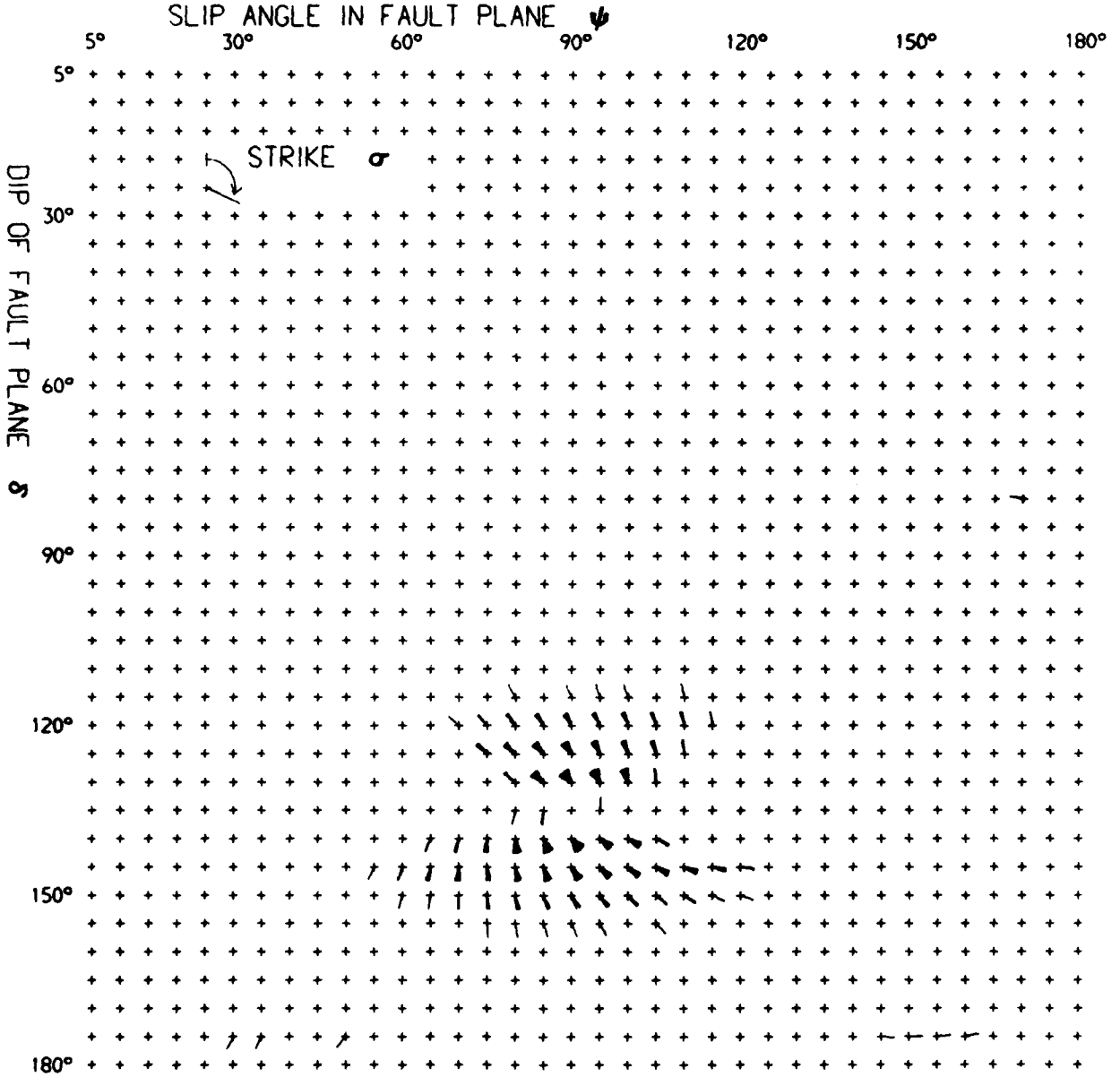

17 April 1976 12-11-14.2

(with no allowance for velocity structure)

Number of compatible orientations = 296

FIGURE 10(a)

EVENT NO. 19 (CATEGORY 2)

17 April 1976 12-11-14.2

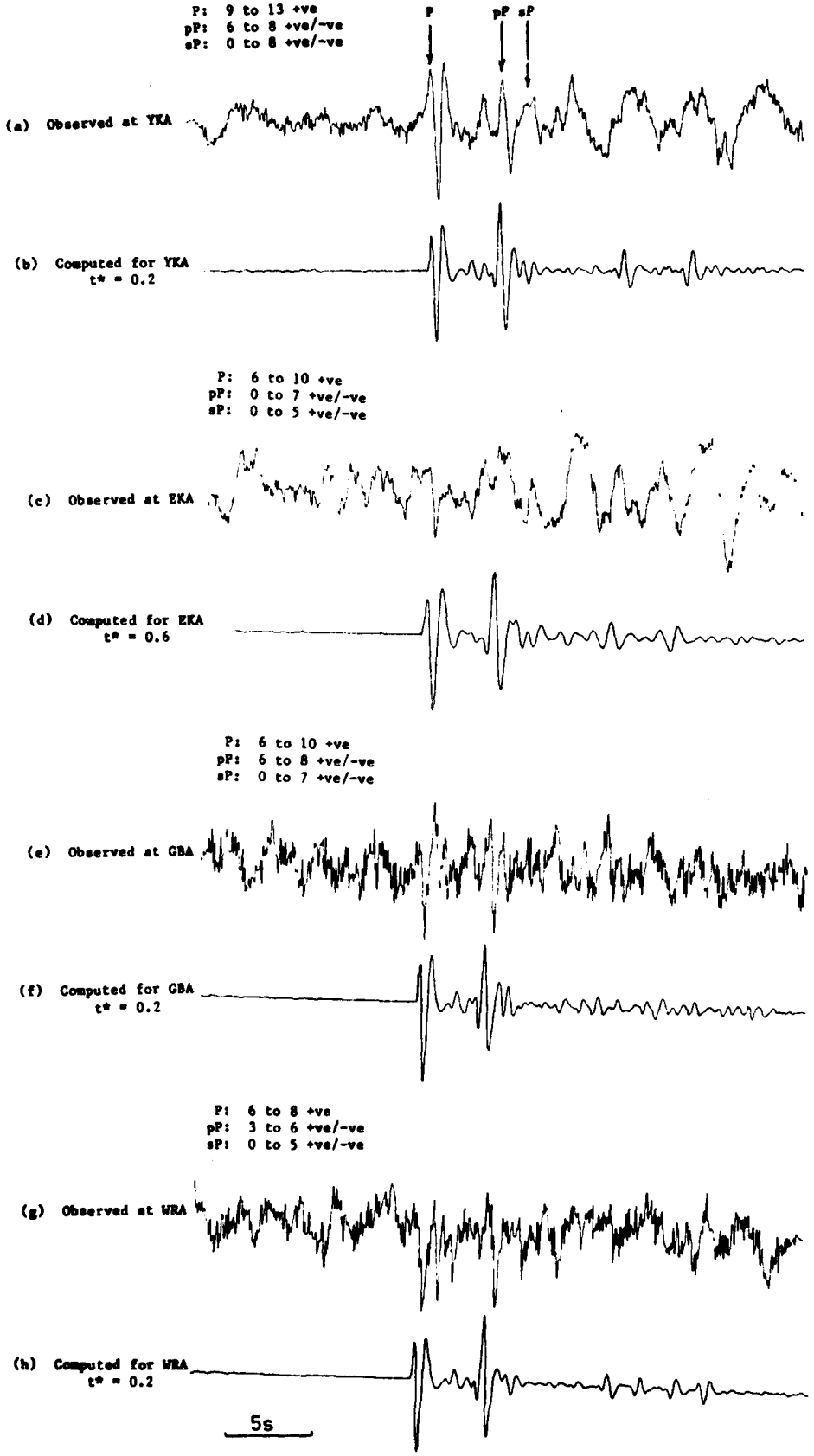

FIGURE 10(b)

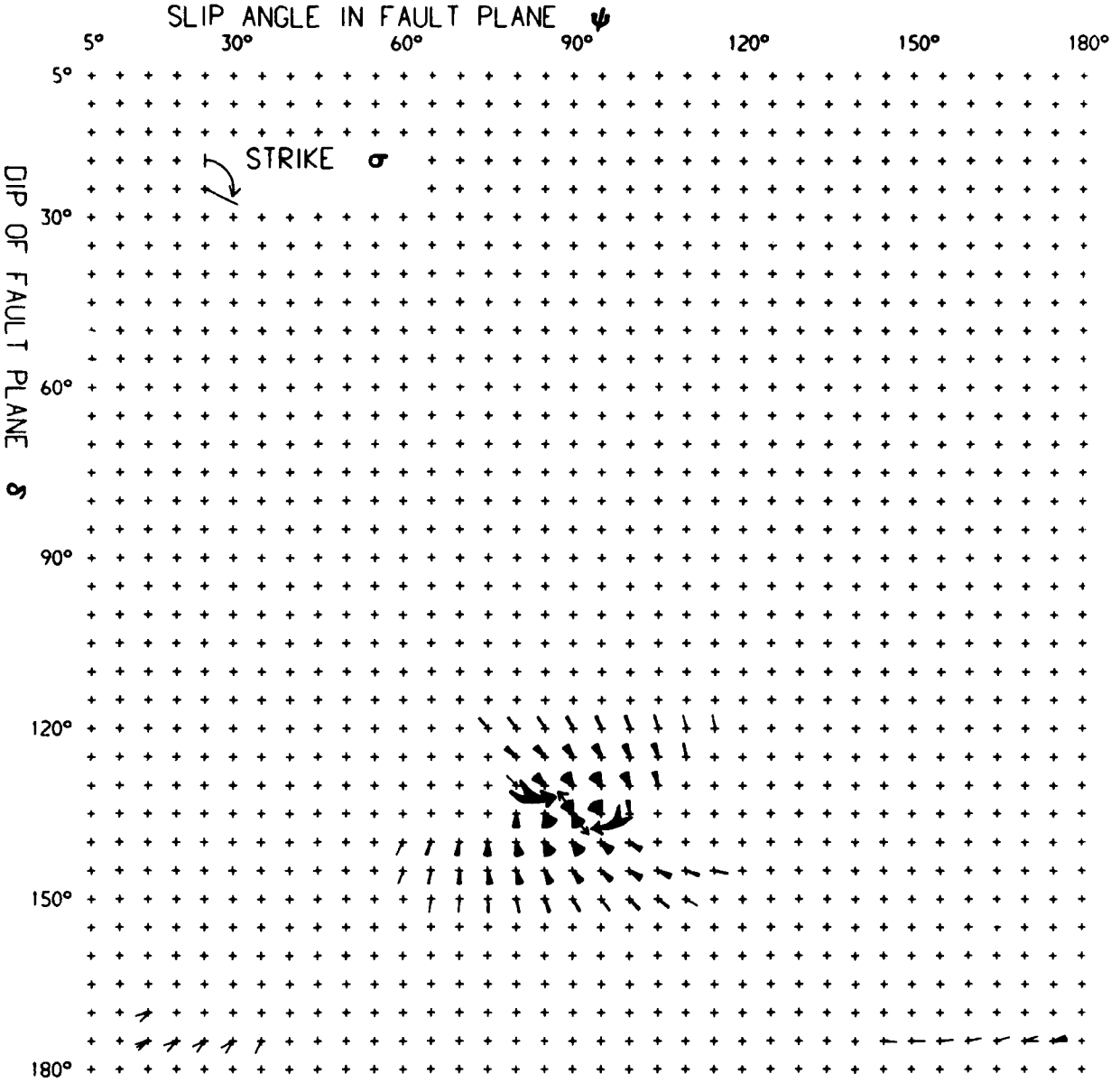

17 April 1976 12-11-14.2

(with allowance for velocity structure)

Number of compatible orientations = 337

FIGURE 10(c)

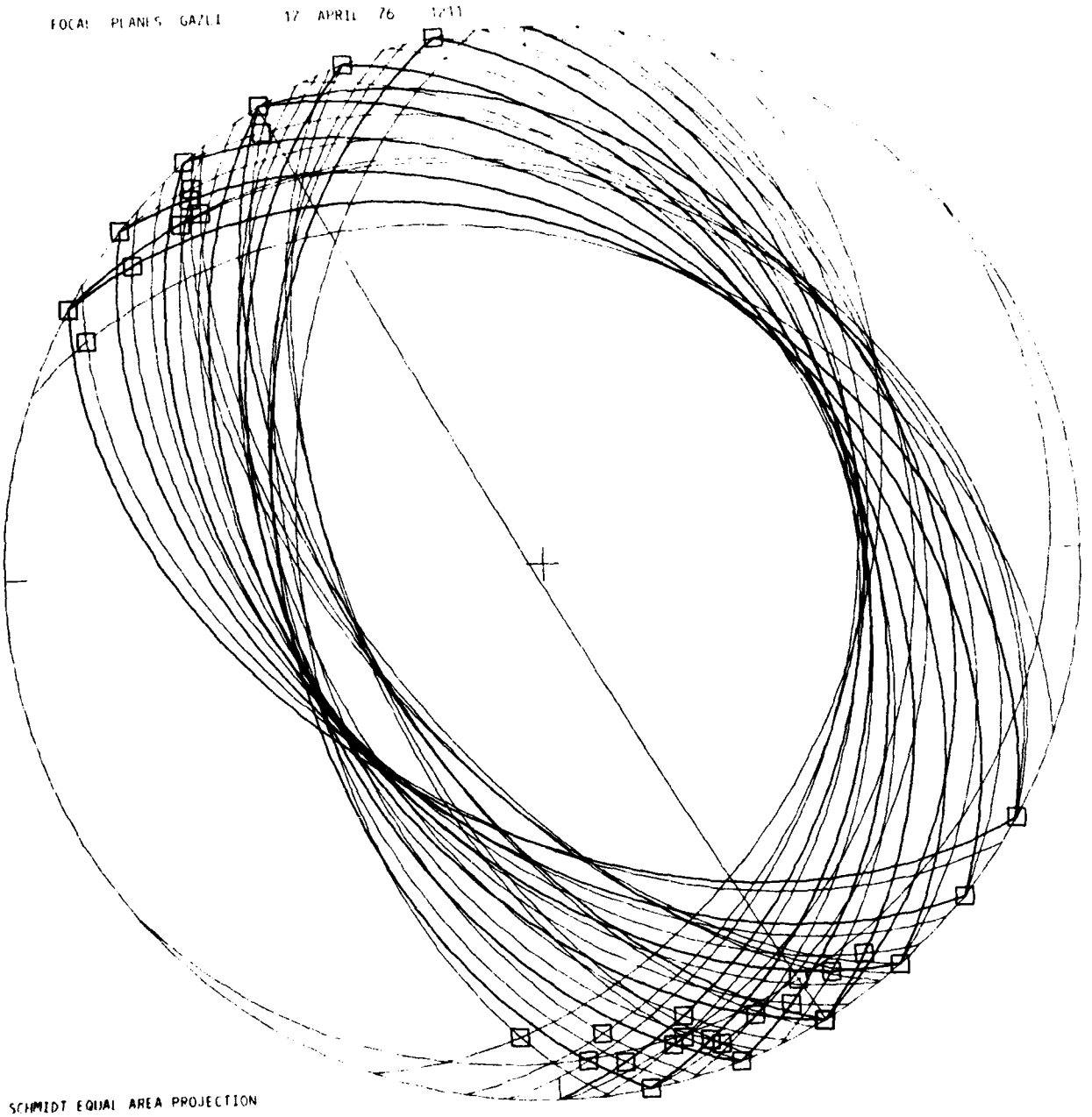

FIGURE 10(d)

(equivalent to figure 10(c))

EVENT NO. 22: 18 April 1976 22-37-39.7
DEPTH DEDUCED BY MODELLING: 6.1 km
MAGNITUDE m_b (NEIS): 4.7

SOURCE ORIENTATION USED IN MODEL:
Dip - 140°
Slip Angle - 60°
Strike - 20°

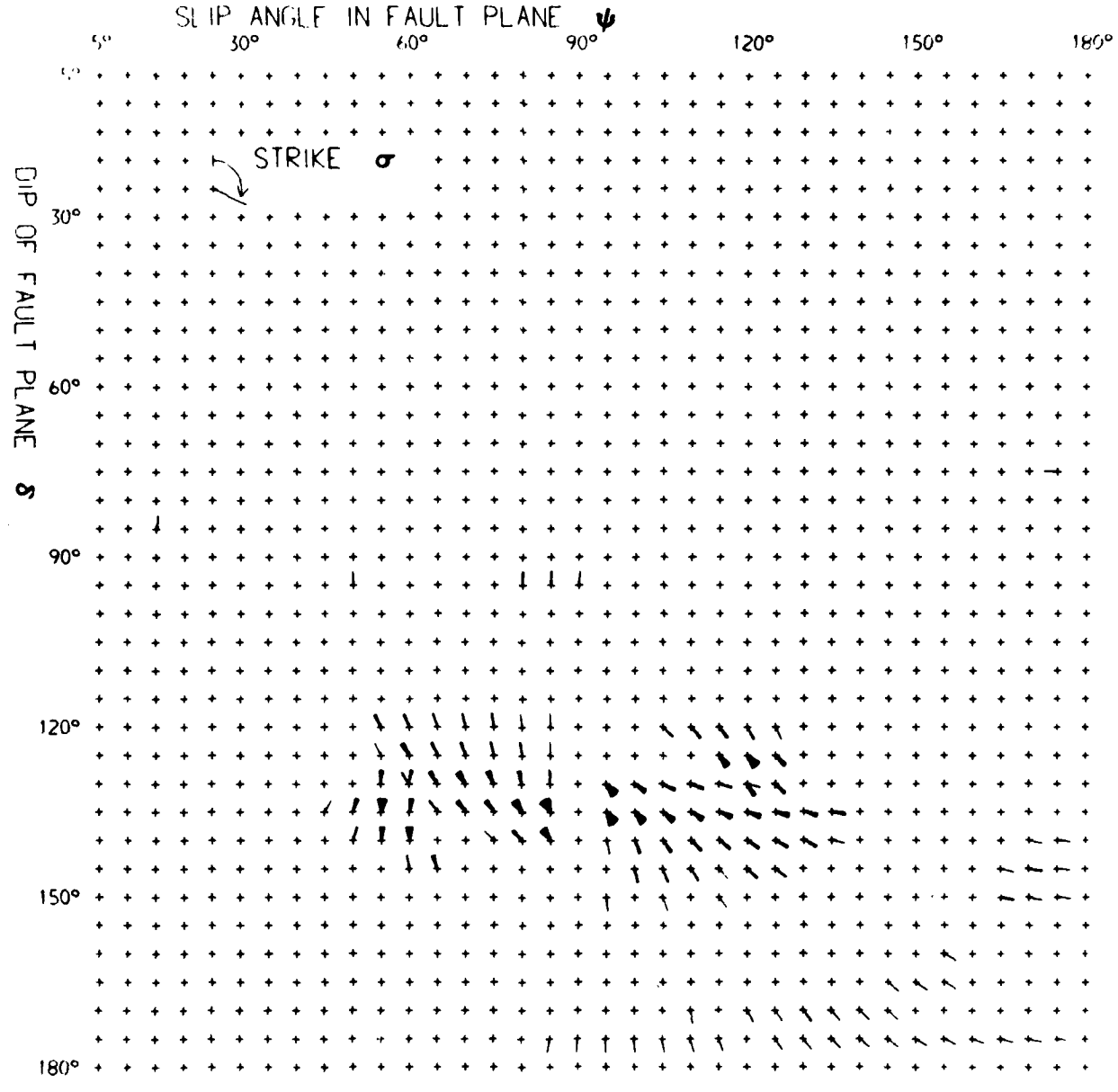

18 April 1976 22-37-39.7

(with no allowance for velocity structure)

Number of compatible orientations = 341

FIGURE 11(a)

EVENT NO. 22 (CATEGORY 2)

18 April 1976 22-37-39.7

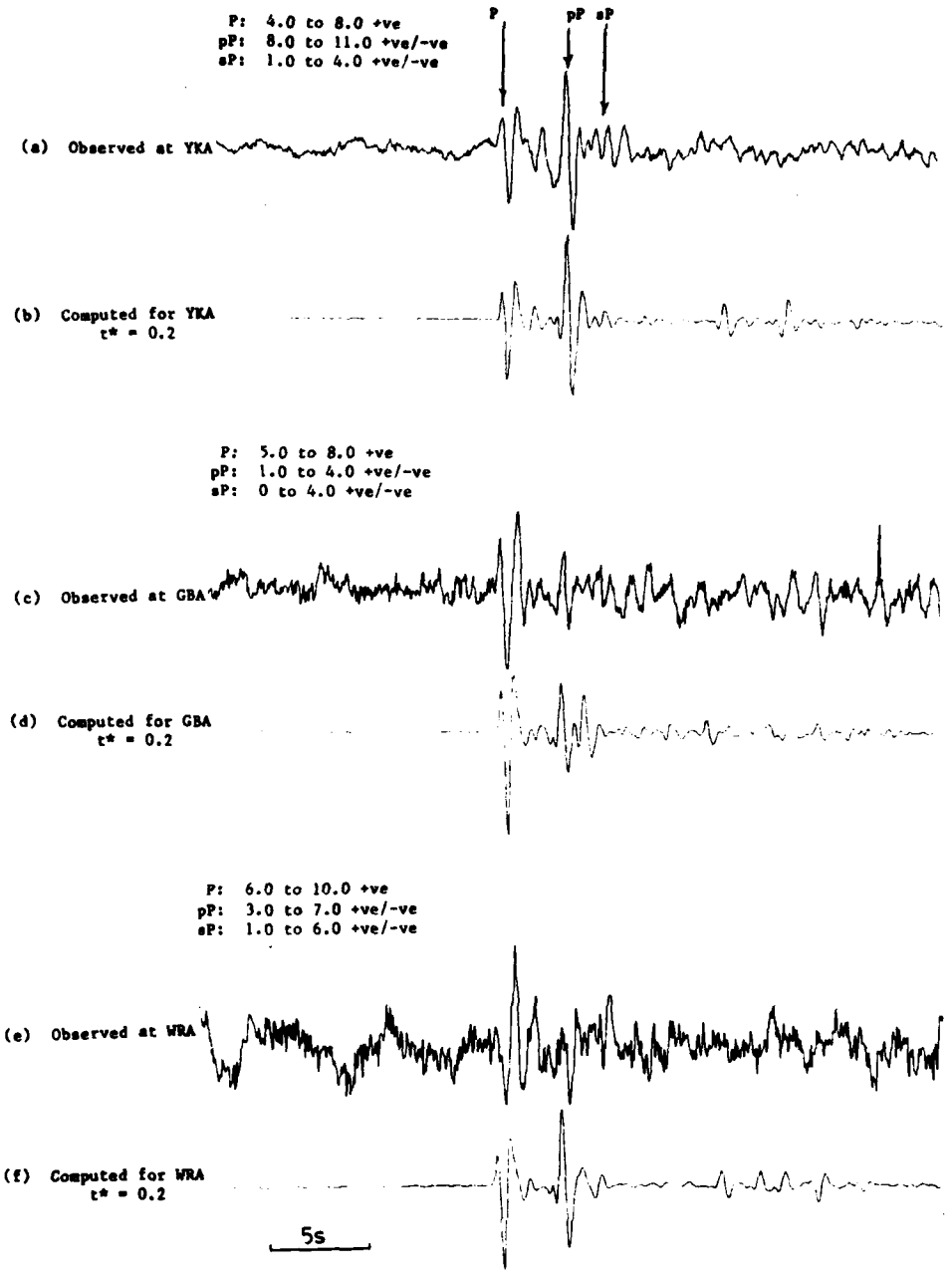

FIGURE 11(b)

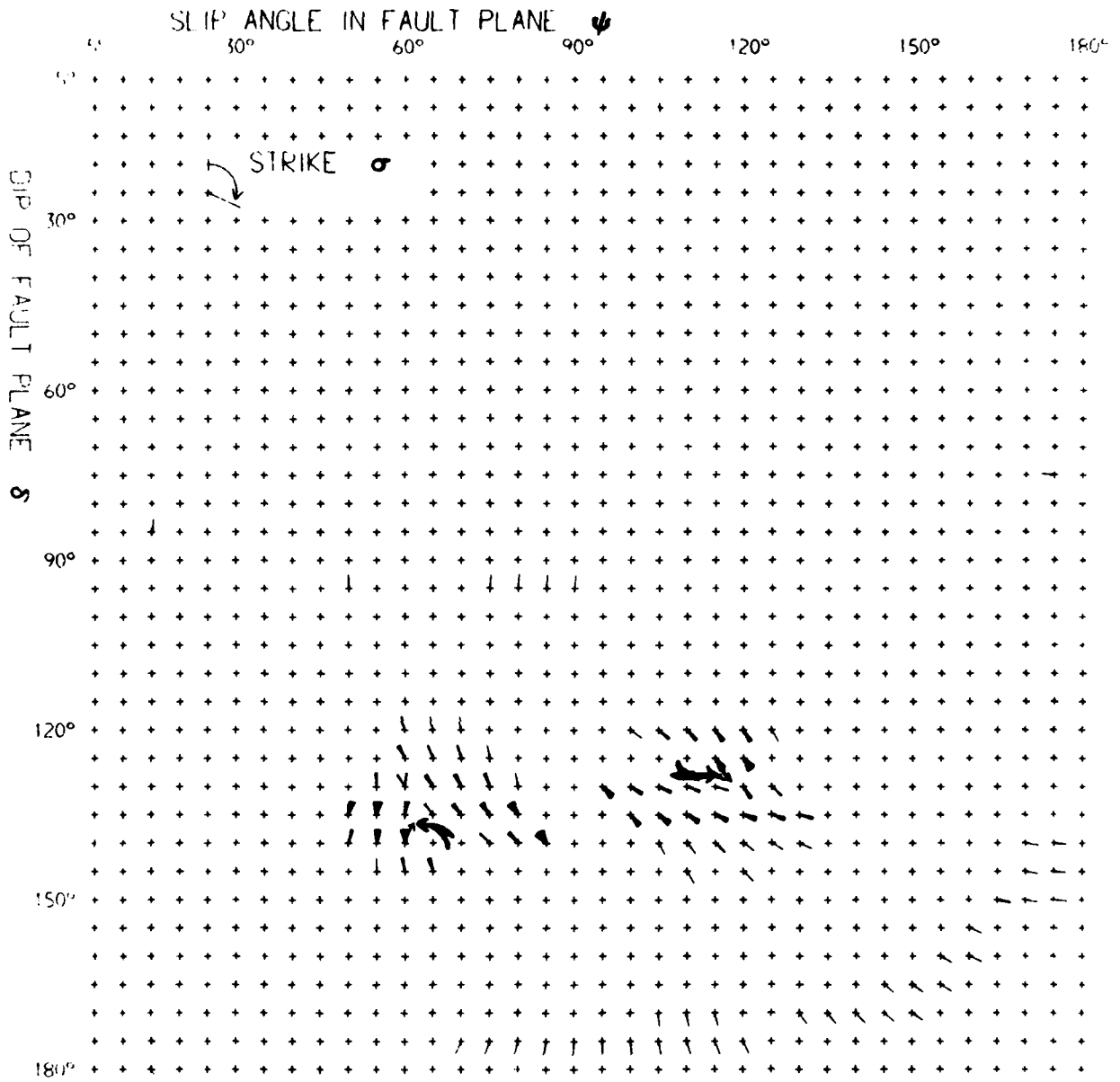

18 April 1976 22-37-39.7

(with allowance for velocity structure)

Number of compatible orientations = 255

FIGURE 11(c)

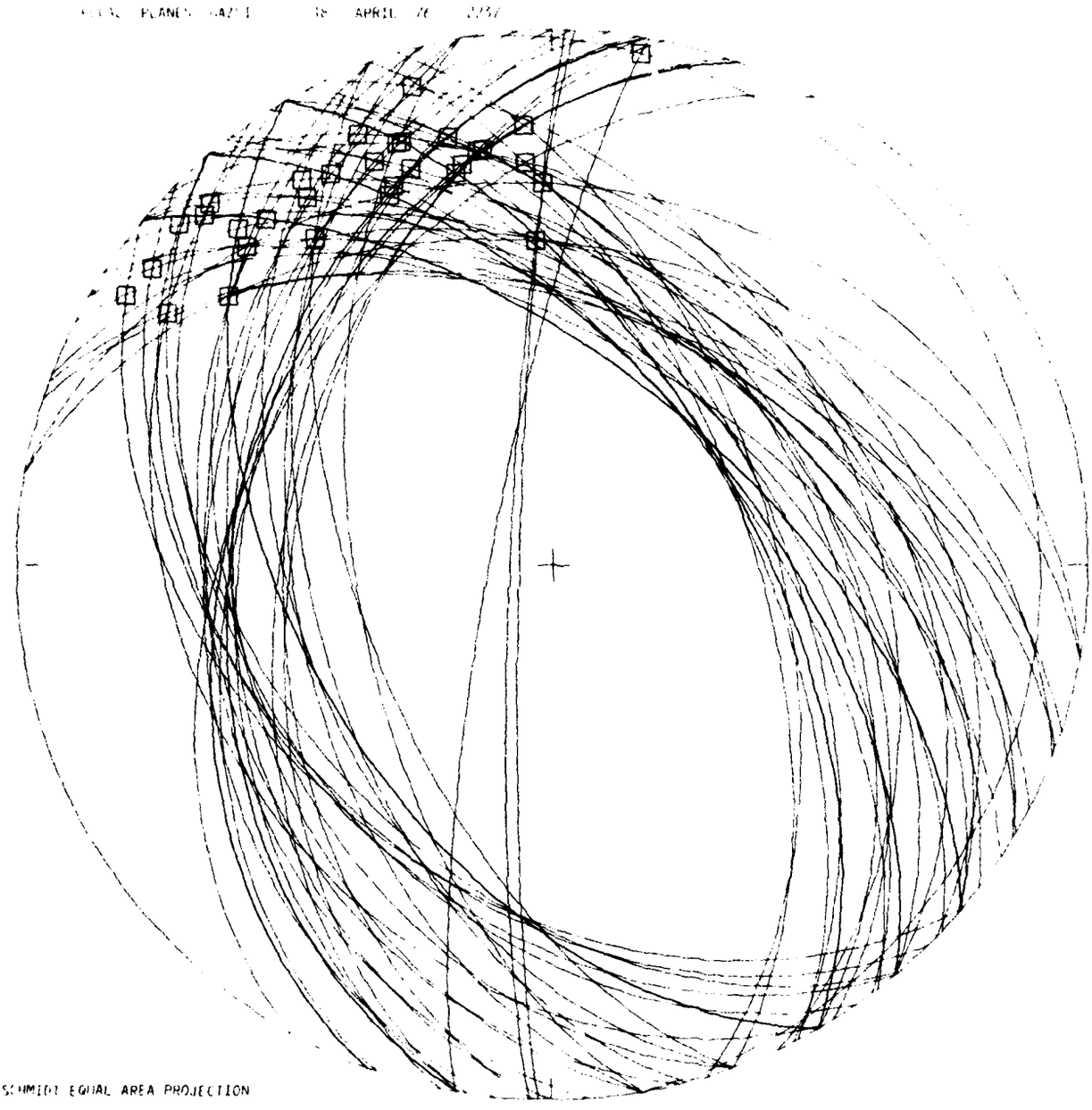

FIGURE 11(d)

(equivalent to figure 11(c))

EVENT NO. 23: 21 April 1976 14-41-34.6
DEPTH DEDUCED BY MODELLING: 8.57 km
MAGNITUDE m_b (NEIS): 5.0
SOURCE ORIENTATION USED IN MODEL: Dip - 135°
Slip Angle - 90°
Strike - 135°

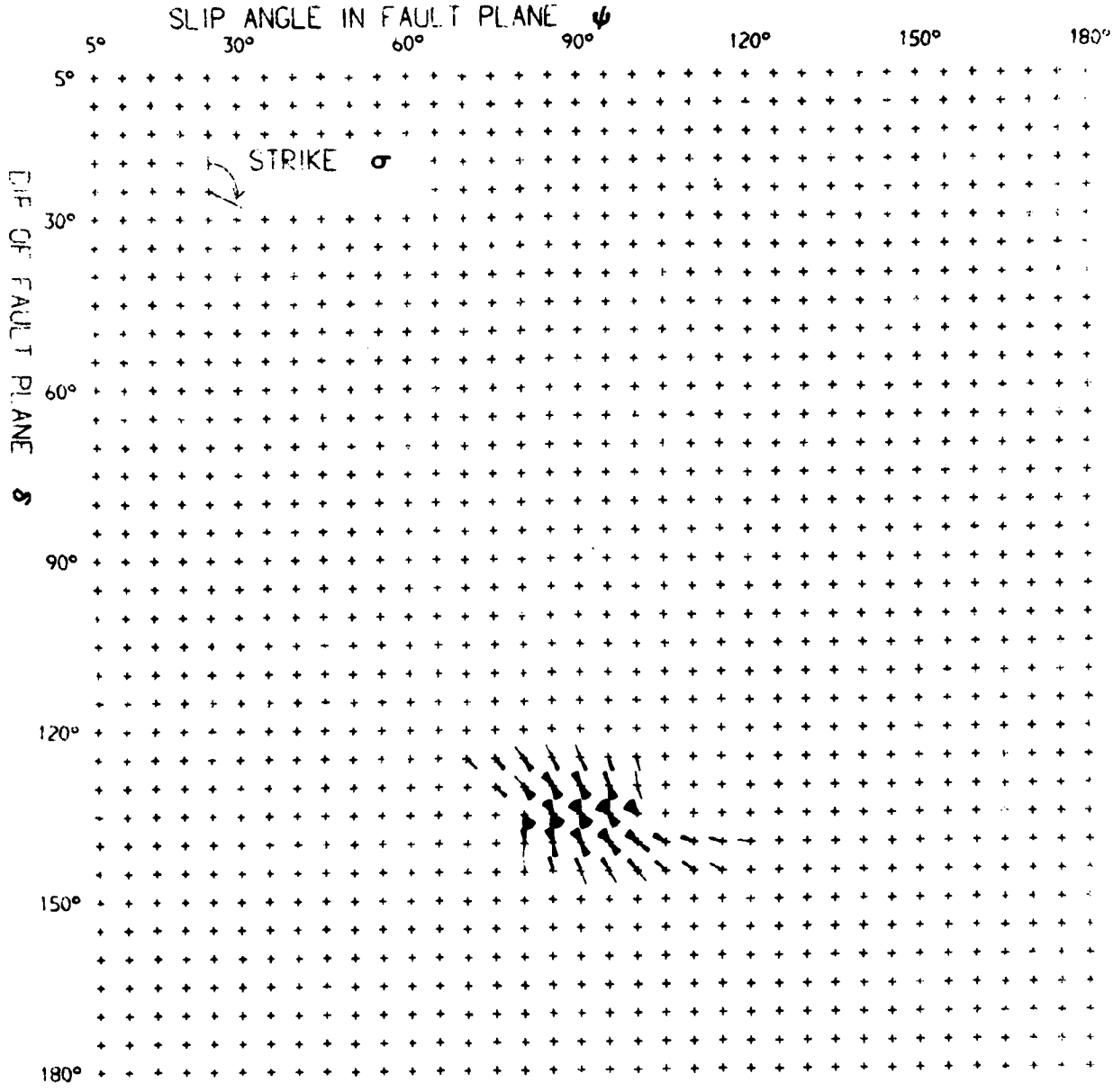

21 April 1976 14-41-34.6

(with no allowance for velocity structure)

Number of compatible orientations = 282

FIGURE 12(a)

EVENT NO. 23 (CATEGORY 2)

21 April 1976 14-41-34.6

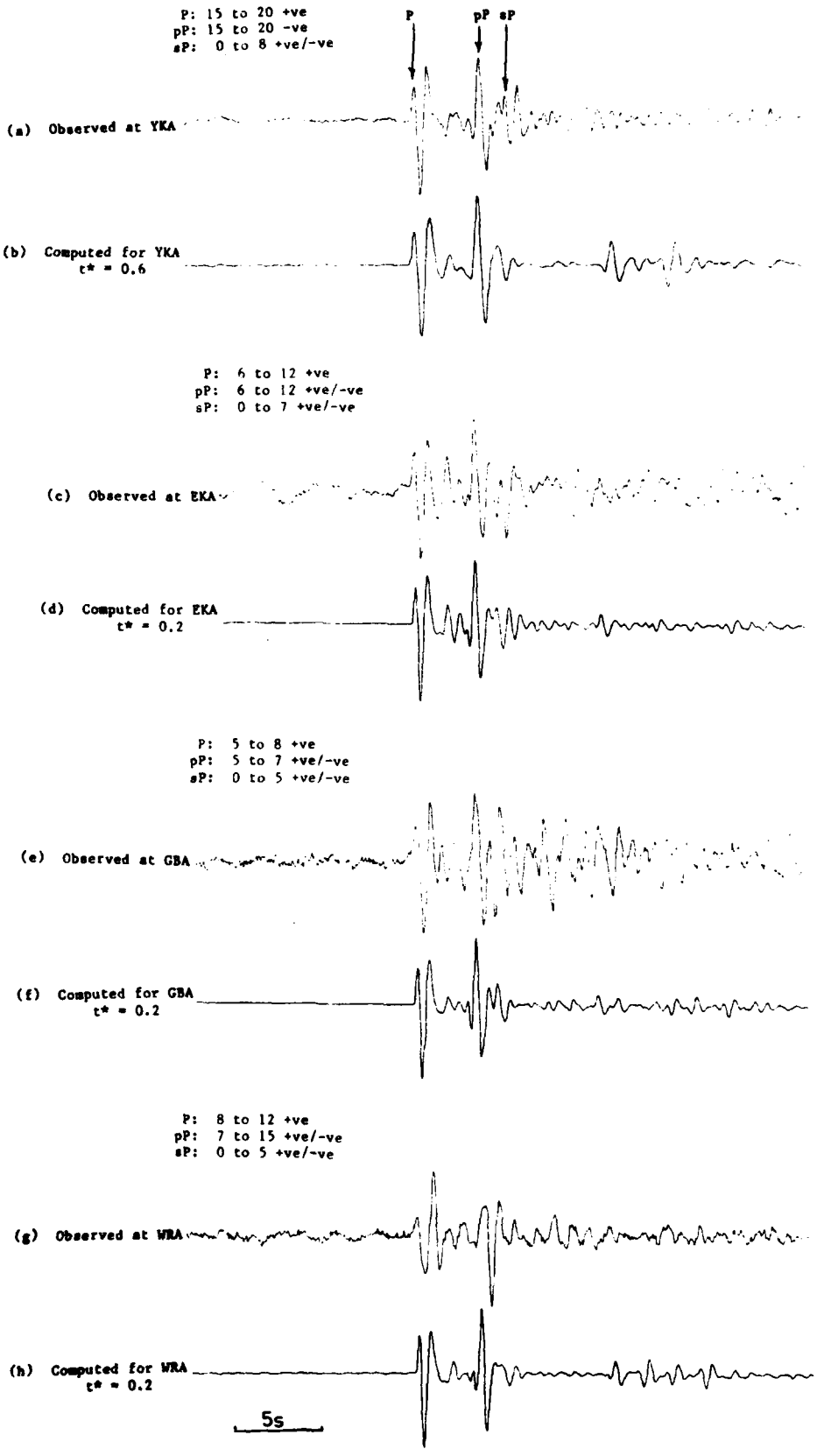

FIGURE 12(b)

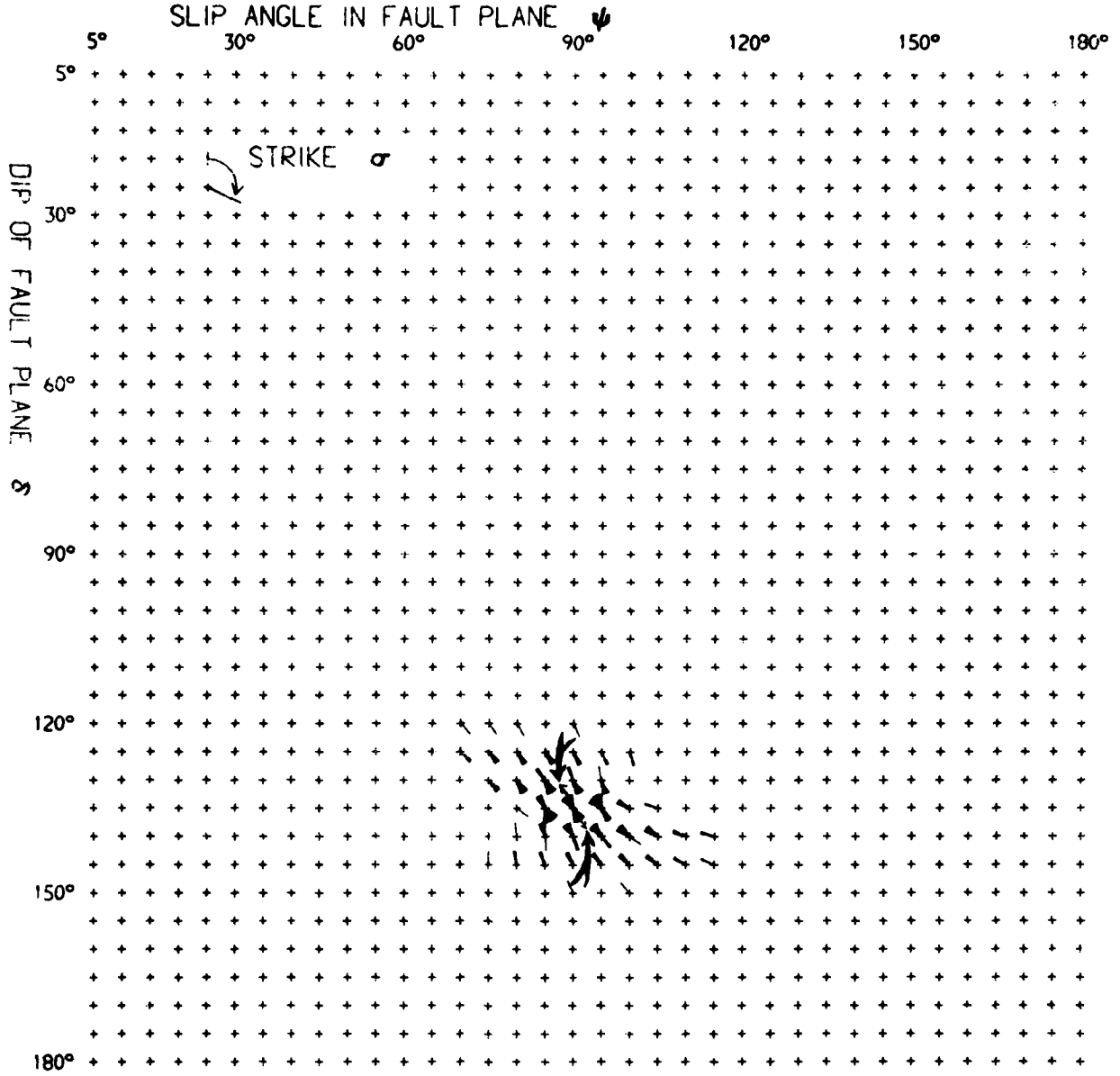

21 April 1976 14-41-34.6

(with allowance for velocity structure)

Number of compatible orientations = 229

FIGURE 12(c)

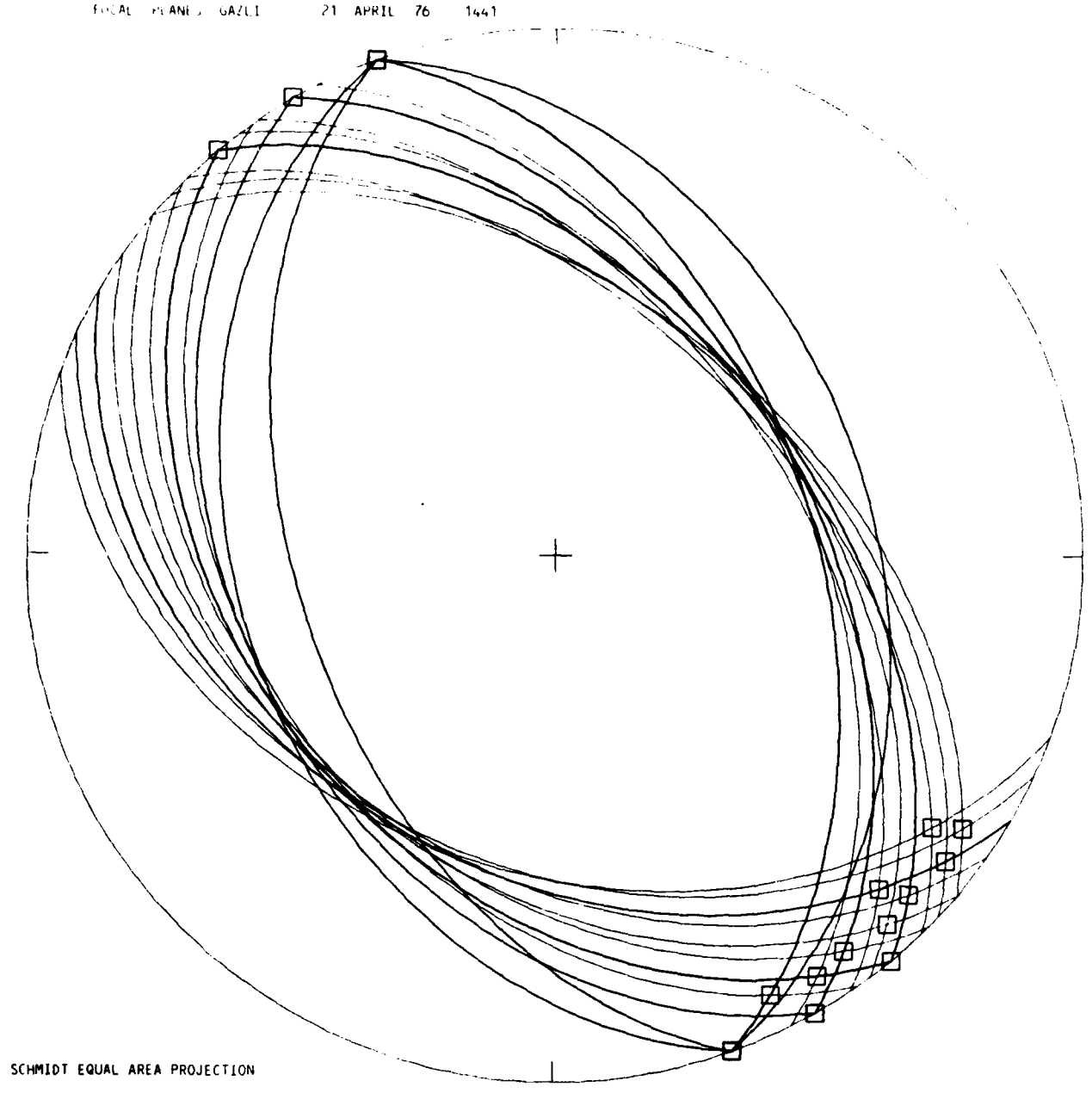

FIGURE 12(d)

(equivalent to figure 12(c))

EVENT NO. 26: 23 April 1976 01-56-48.3
DEPTH DEDUCED BY MODELLING: 9.49 km
MAGNITUDE m_b (NEIS): 4.7

SOURCE ORIENTATION USED IN MODEL:
Dip - 140°
Slip Angle - 90°
Strike - 100°

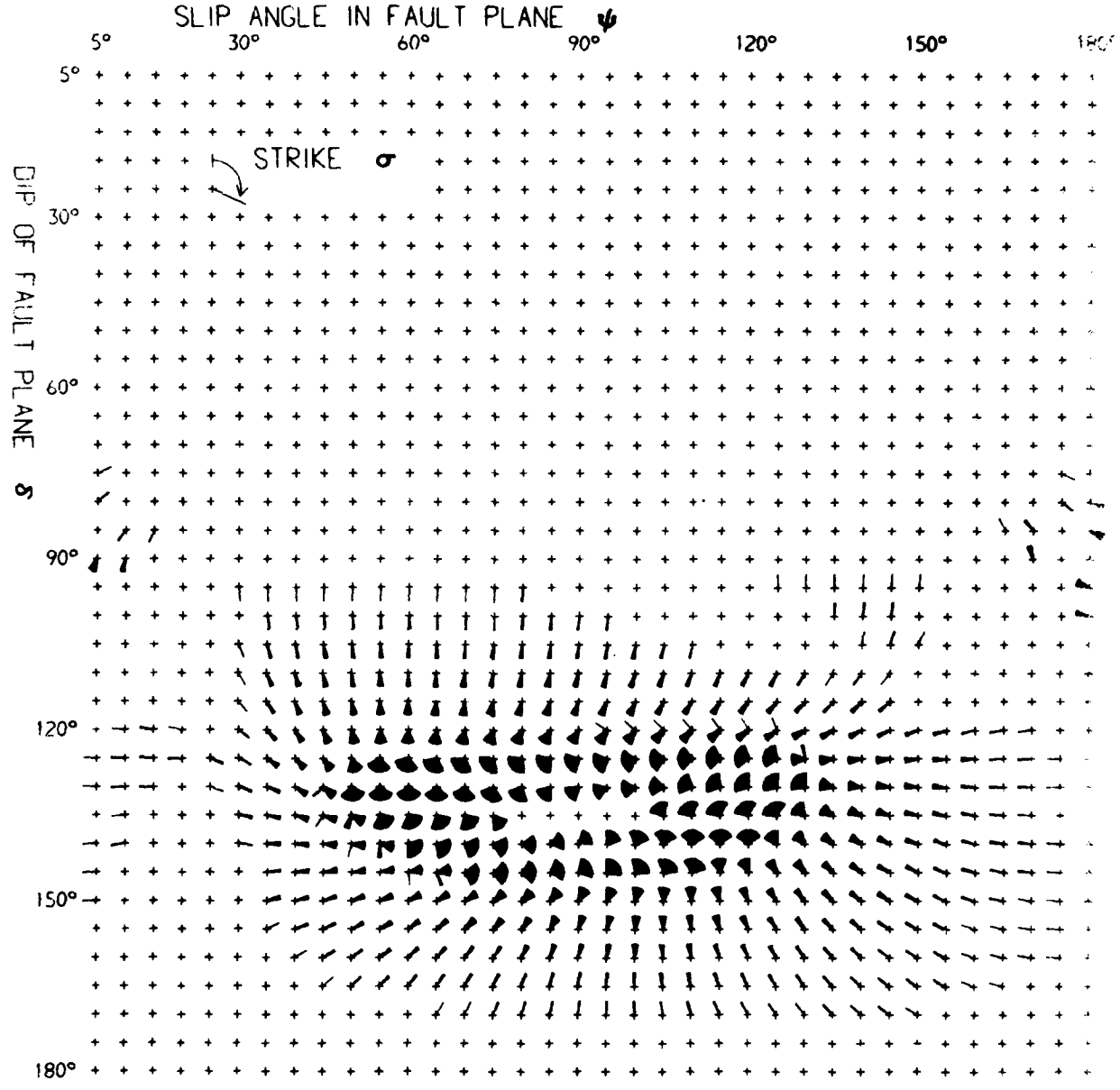

23 April 1976 01-56-48.3

(with no allowance for velocity structure)

Number of compatible orientations = 3059

FIGURE 13(a)

EVENT NO. 26 (CATEGORY 2)

23 April 1976 01-56-48.3

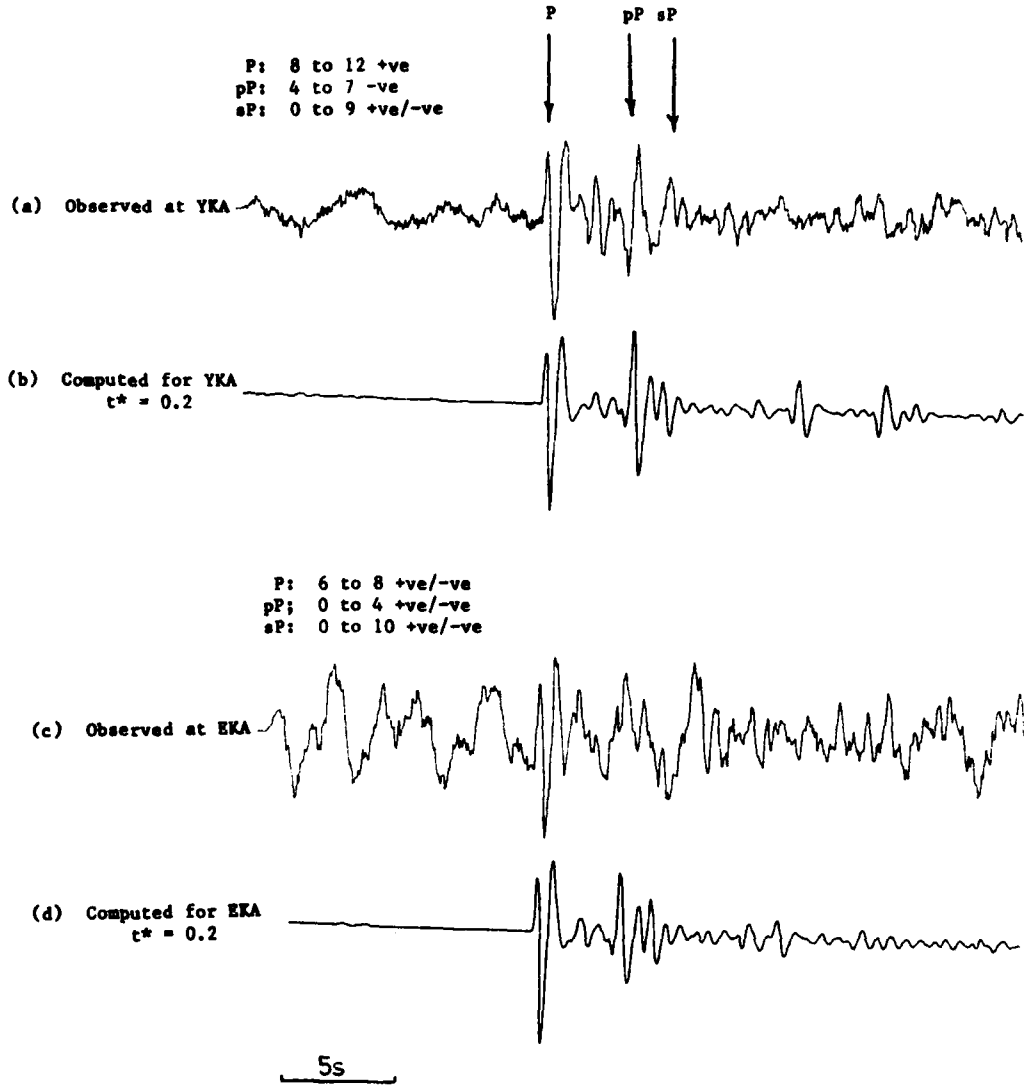

FIGURE 13(b)

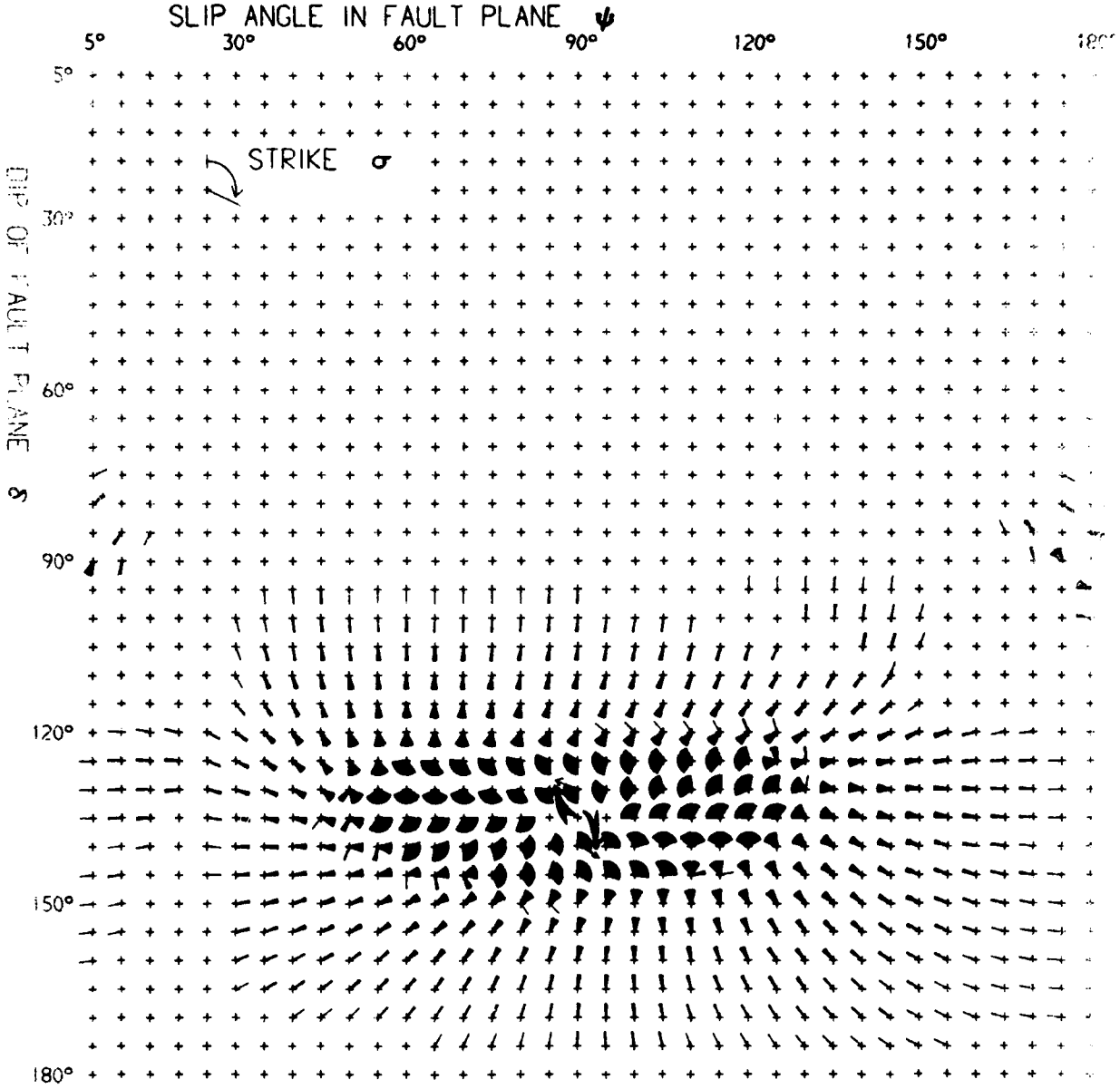

23 April 1976 01-56-48.3

(with allowance for velocity structure)

Number of compatible orientations = 4461

FIGURE 13(c)

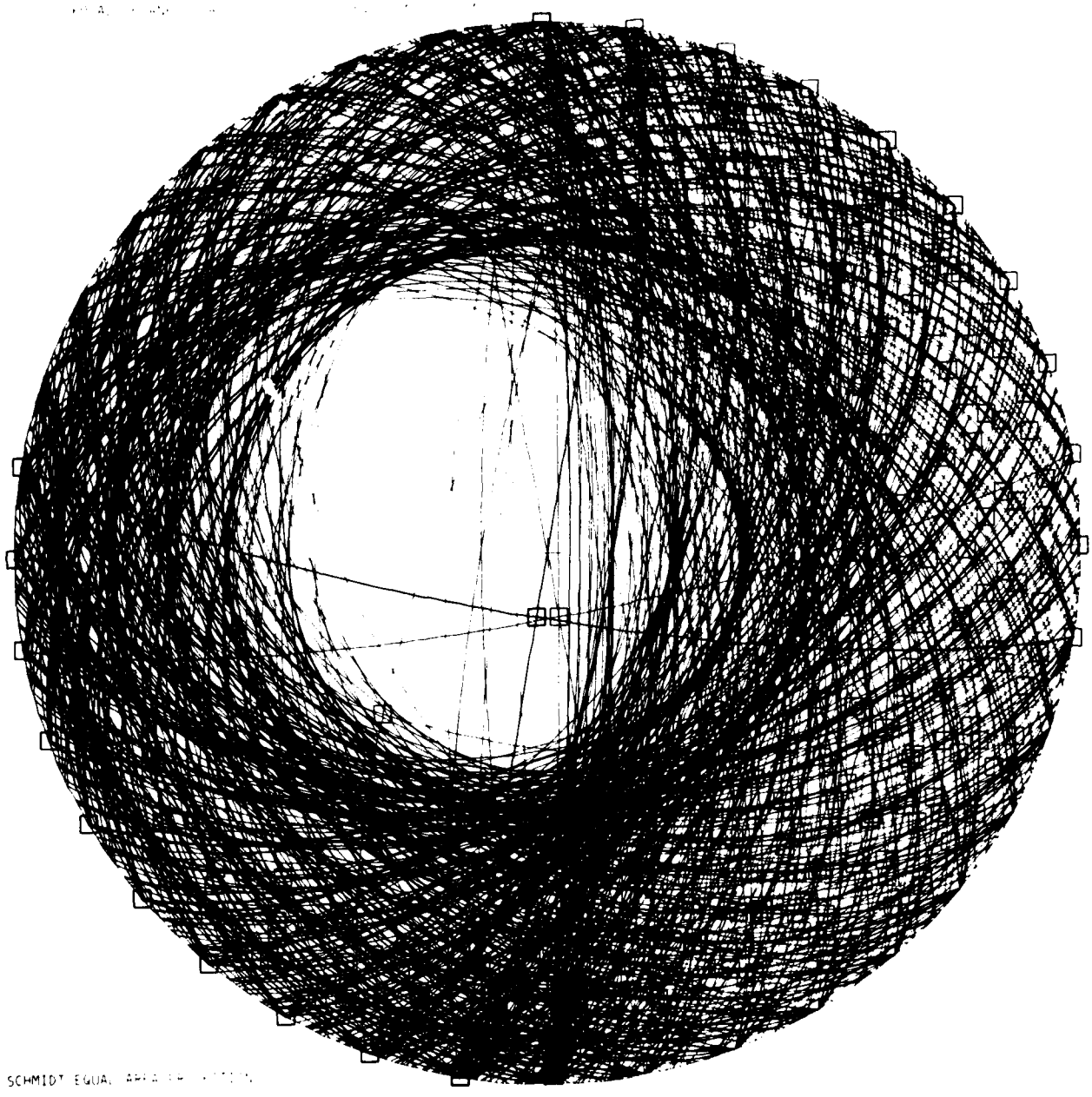

FIGURE 13(d)

(equivalent to figure 13(c))

EVENT NO. 28: 24 April 1976 13-57-01.0
DEPTH DEDUCED BY MODELLING: 9.18 km
MAGNITUDE m_b (NEIS) 4.7

SOURCE ORIENTATION USED IN MODEL:
Dip - 130°
Slip Angle - 55°
Strike - 260°

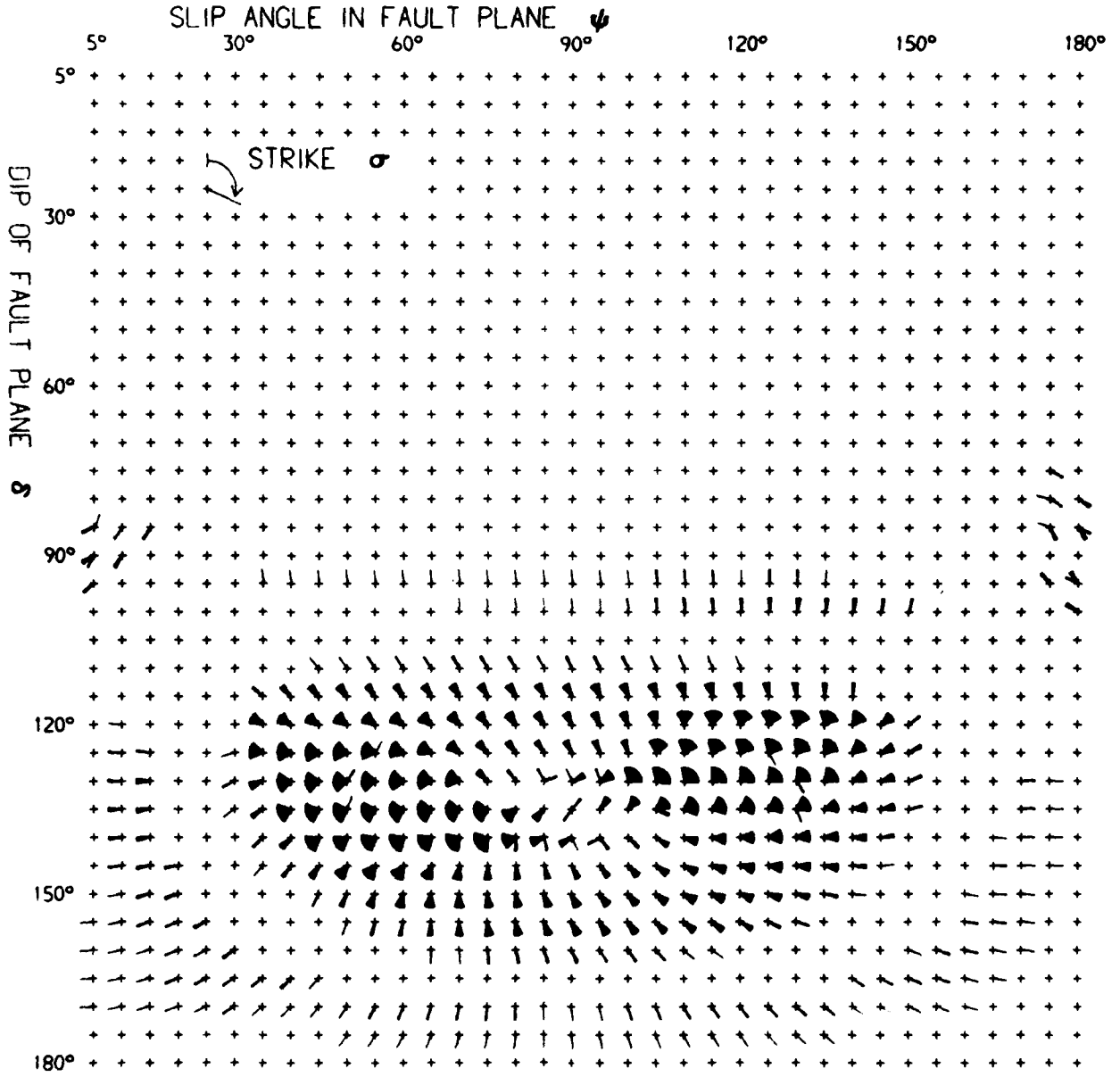

24 April 1976 13-57-01.0
(with no allowance for velocity structure)
Number of compatible orientations = 2526

FIGURE 14(a)

EVENT NO. 28 (CATEGORY 2)

24 April 1976 13-57-01.0

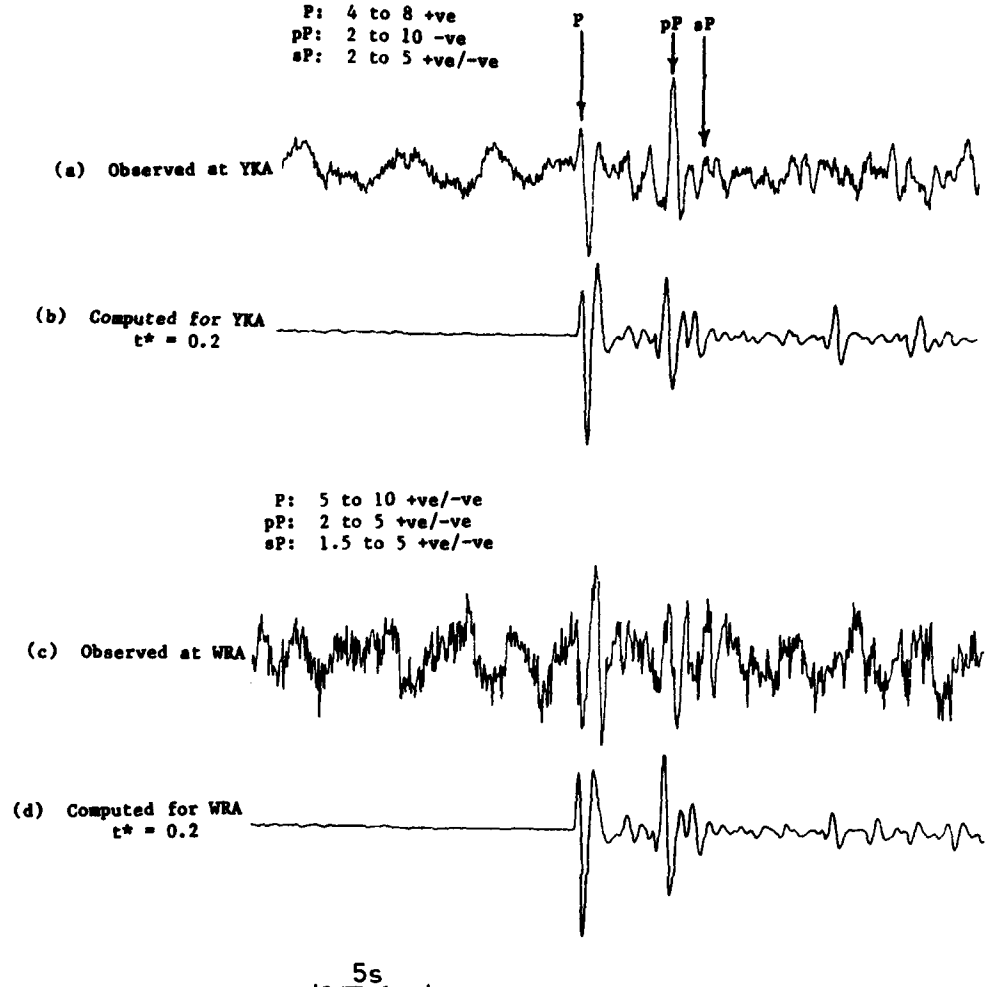

FIGURE 14(b)

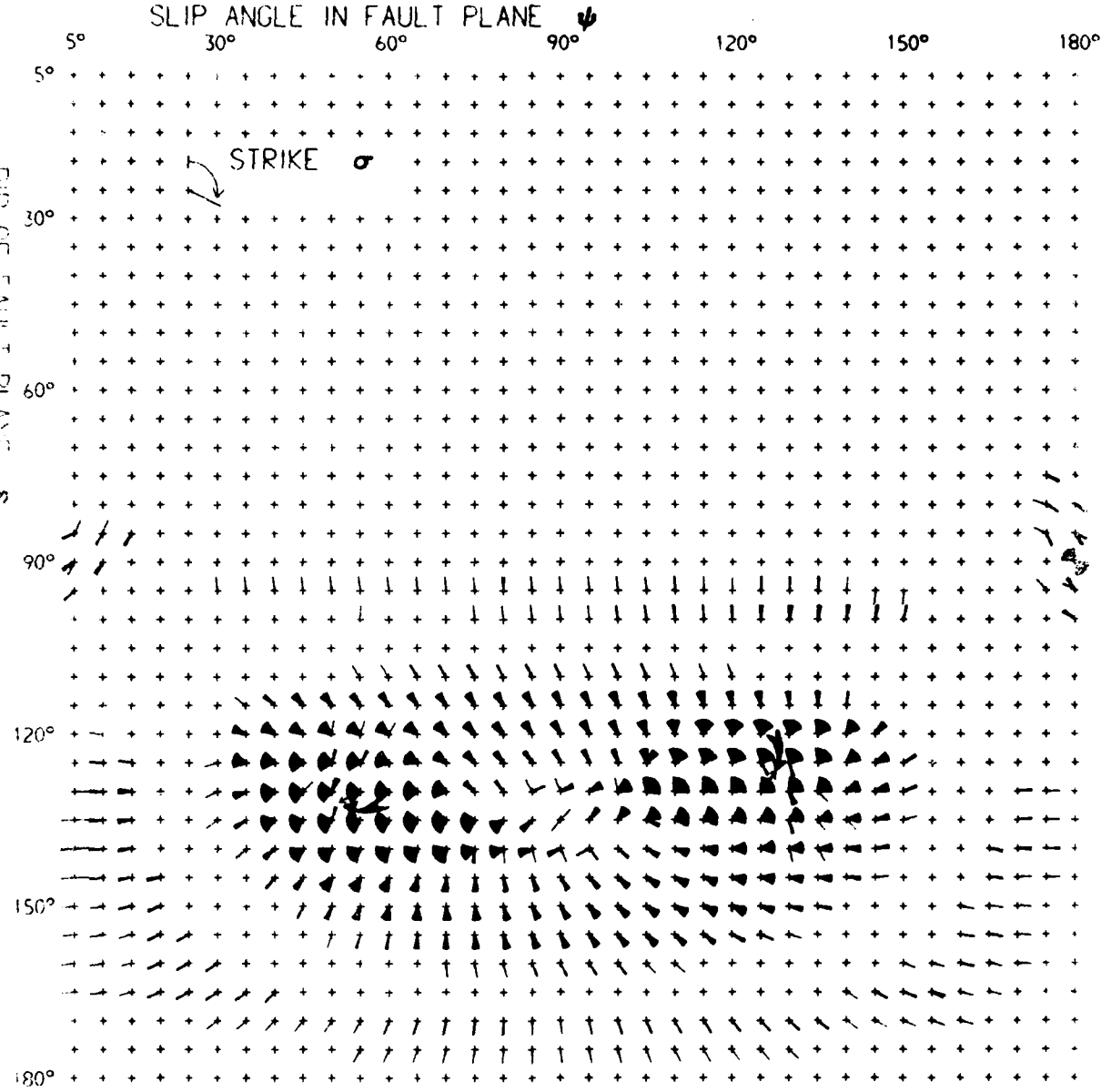

24 April 1976 13-57-01.0

(with allowance for velocity structure)

Number of compatible orientations = 4461

FIGURE 14(c)

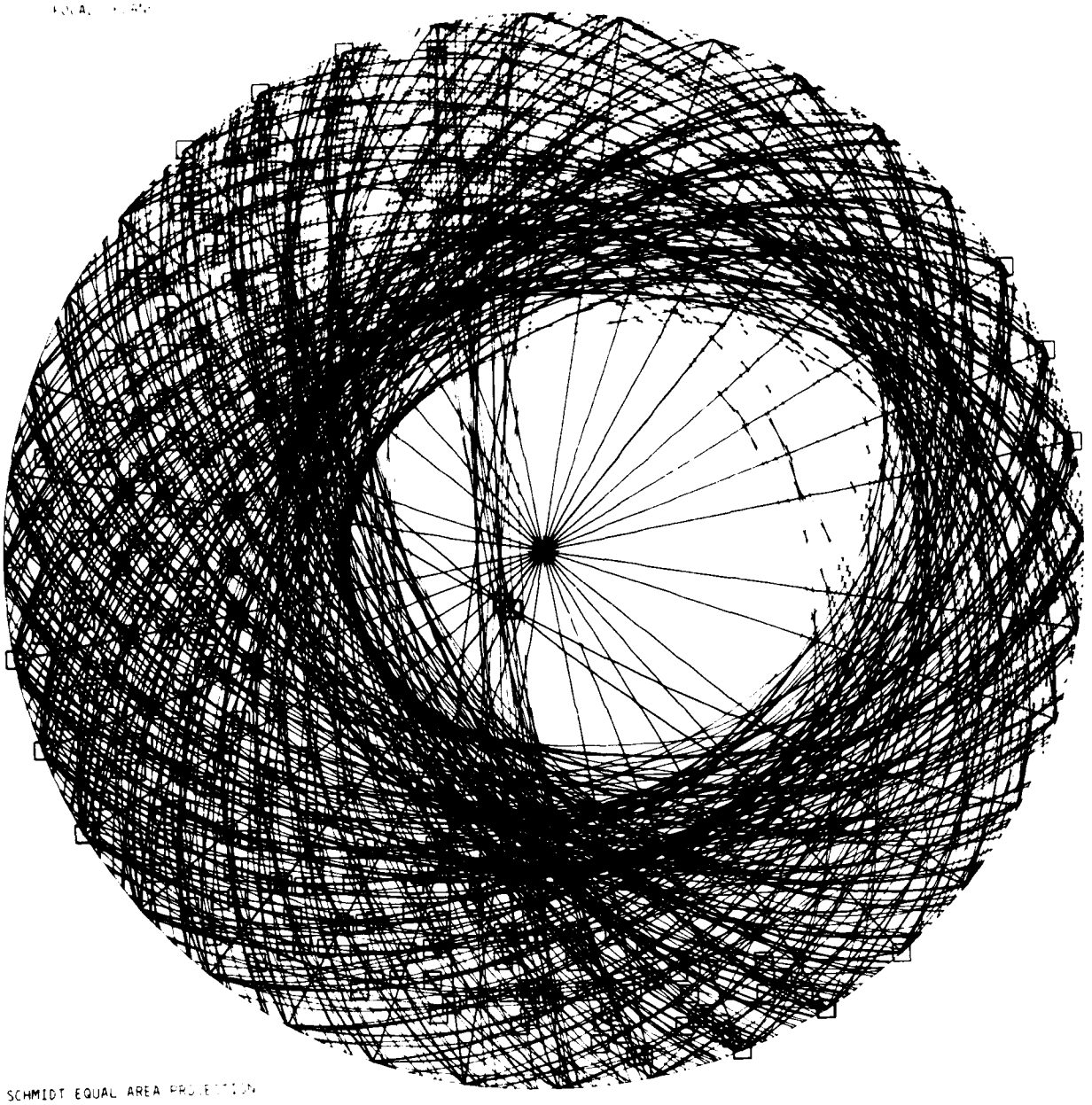

FIGURE 14(d)

(equivalent to figure 14(c))

EVENT NO. 30: 7 May 1976 00-10-49.4
DEPTH DEDUCED BY MODELLING: 5.22 km
MAGNITUDE m_b (NEIS): 4.8

SOURCE ORIENTATION USED IN MODEL:
Dip - 135°
Slip Angle - 90°
Strike - 135°

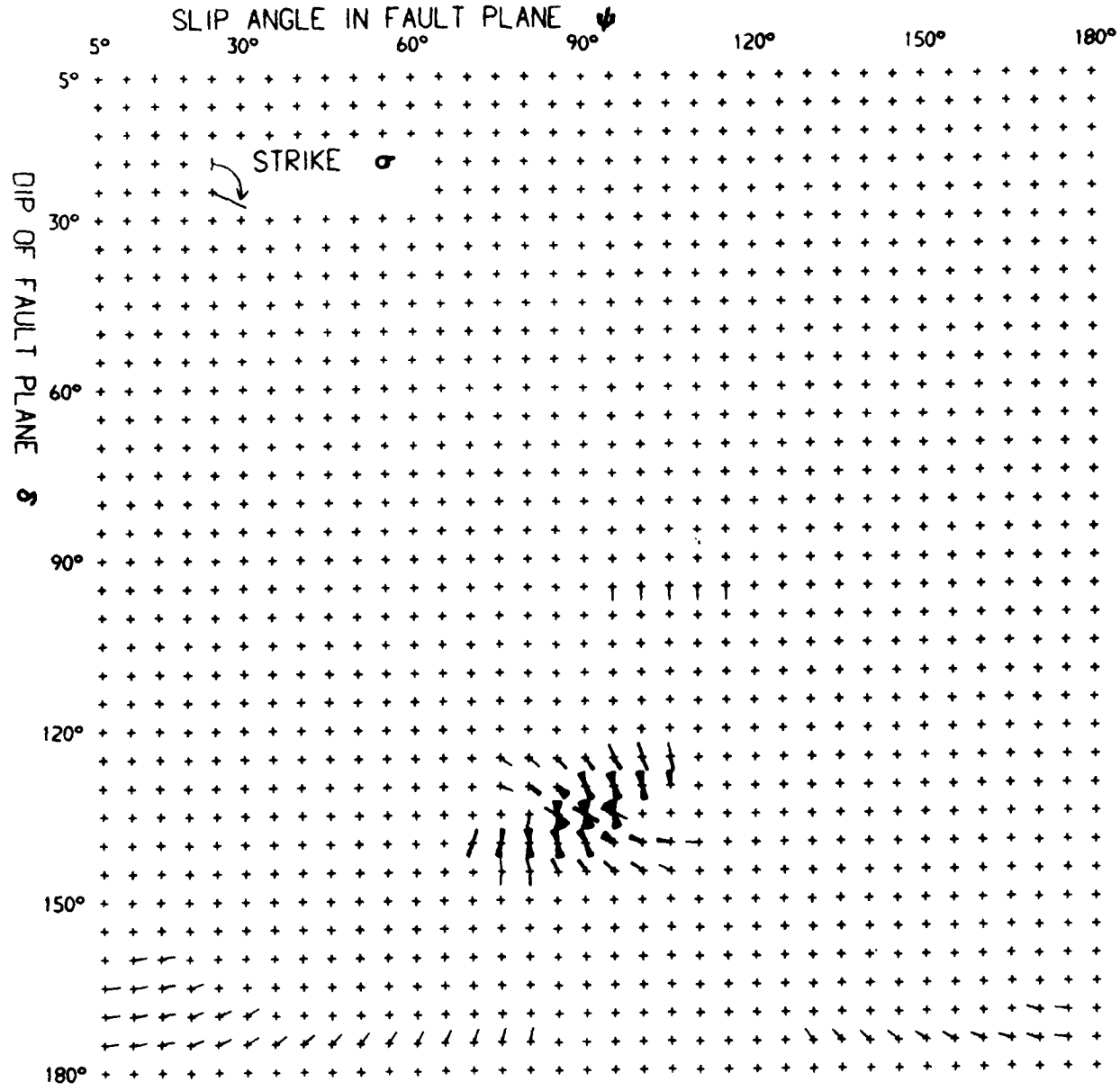

7 May 1976 00-10-49.4

(with no allowance for velocity structure)

Number of compatible orientations = 288

FIGURE 15(a)

EVENT NO. 30 (CATEGORY 2)

7 May 1976 00-10-49.4

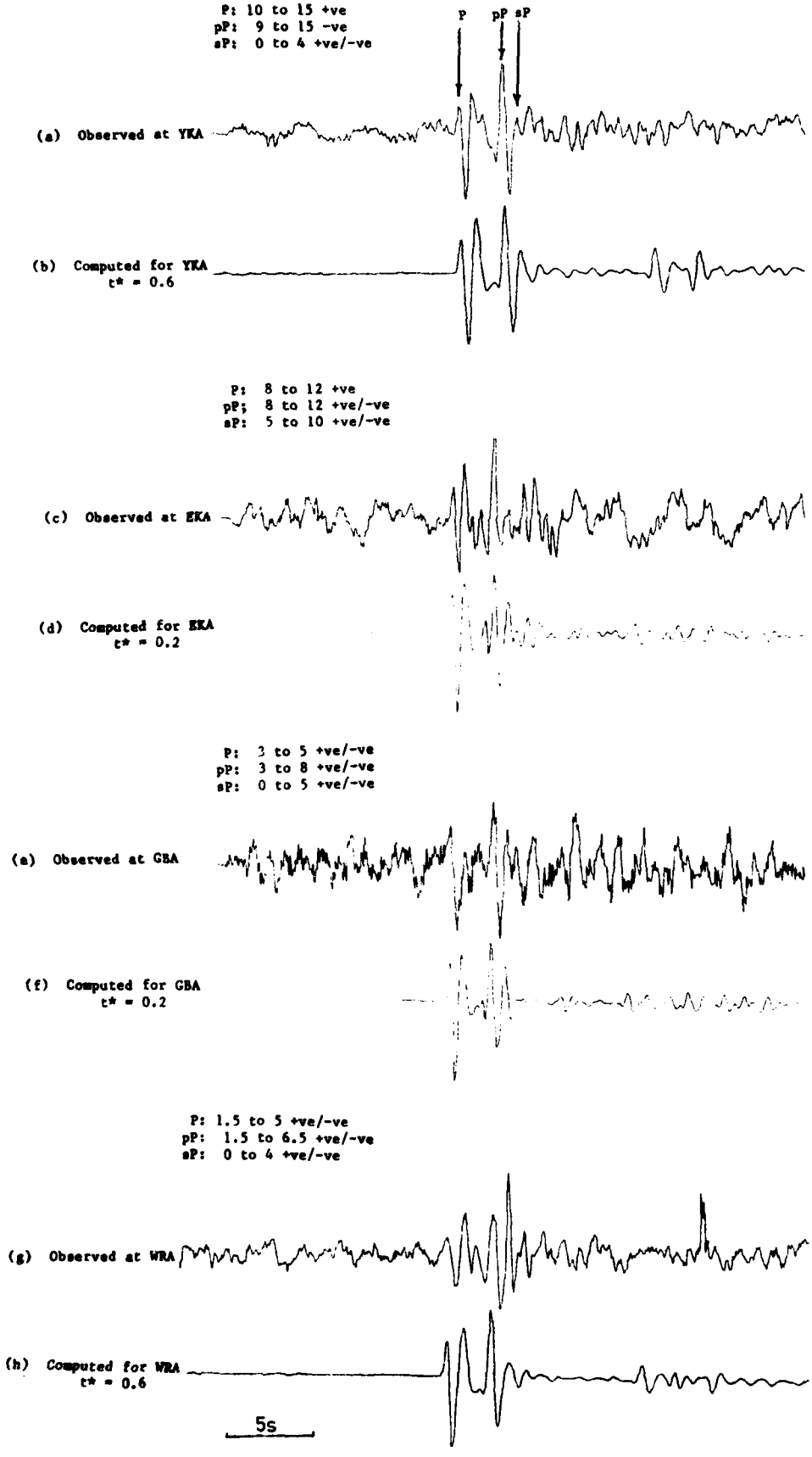

FIGURE 15(b)

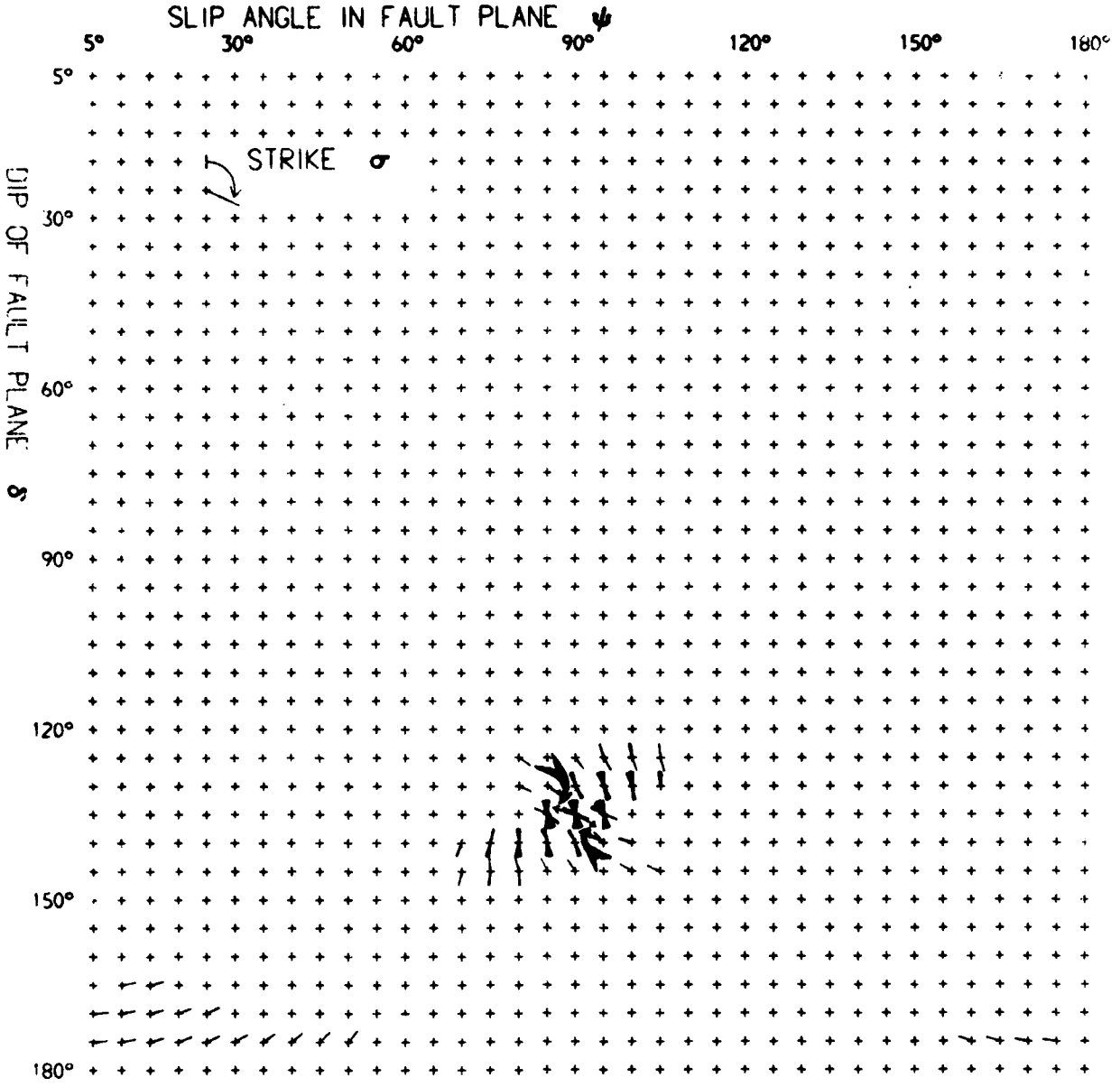

7 May 1976 00-10-49.4

(with allowance for velocity structure)

Number of compatible orientations = 184

FIGURE 15(c)

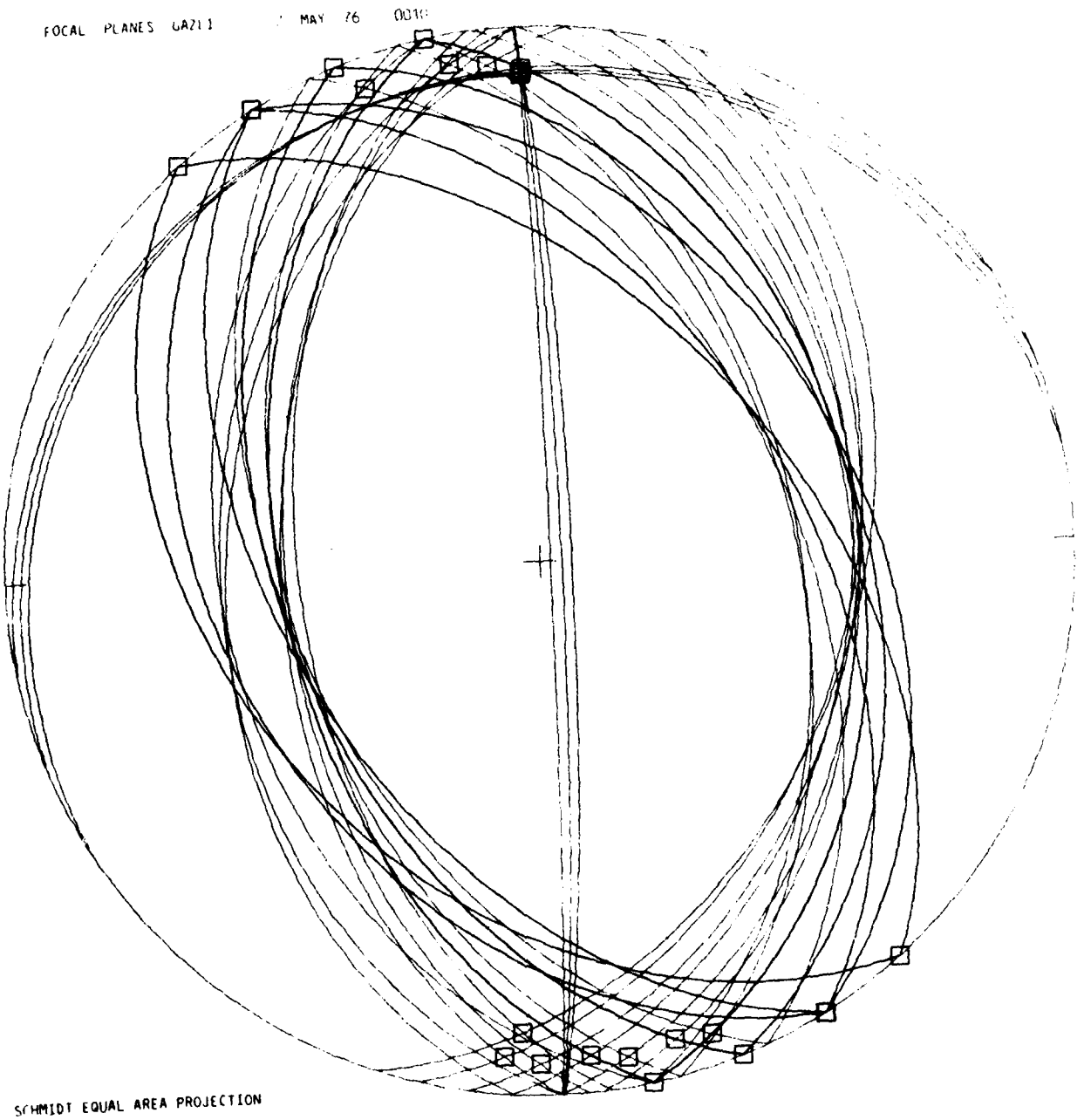

FIGURE 15(d)

(equivalent to figure 15(c))

EVENT NO. 31: 9 May 1976 07-51-16.7
DEPTH DEDUCED BY MODELLING: 10.1 km
MAGNITUDE m_b (NEIS) 5.1
SOURCE ORIENTATION USED IN MODEL: Dip - 125°
Slip Angle - 90°
Strike - 330°

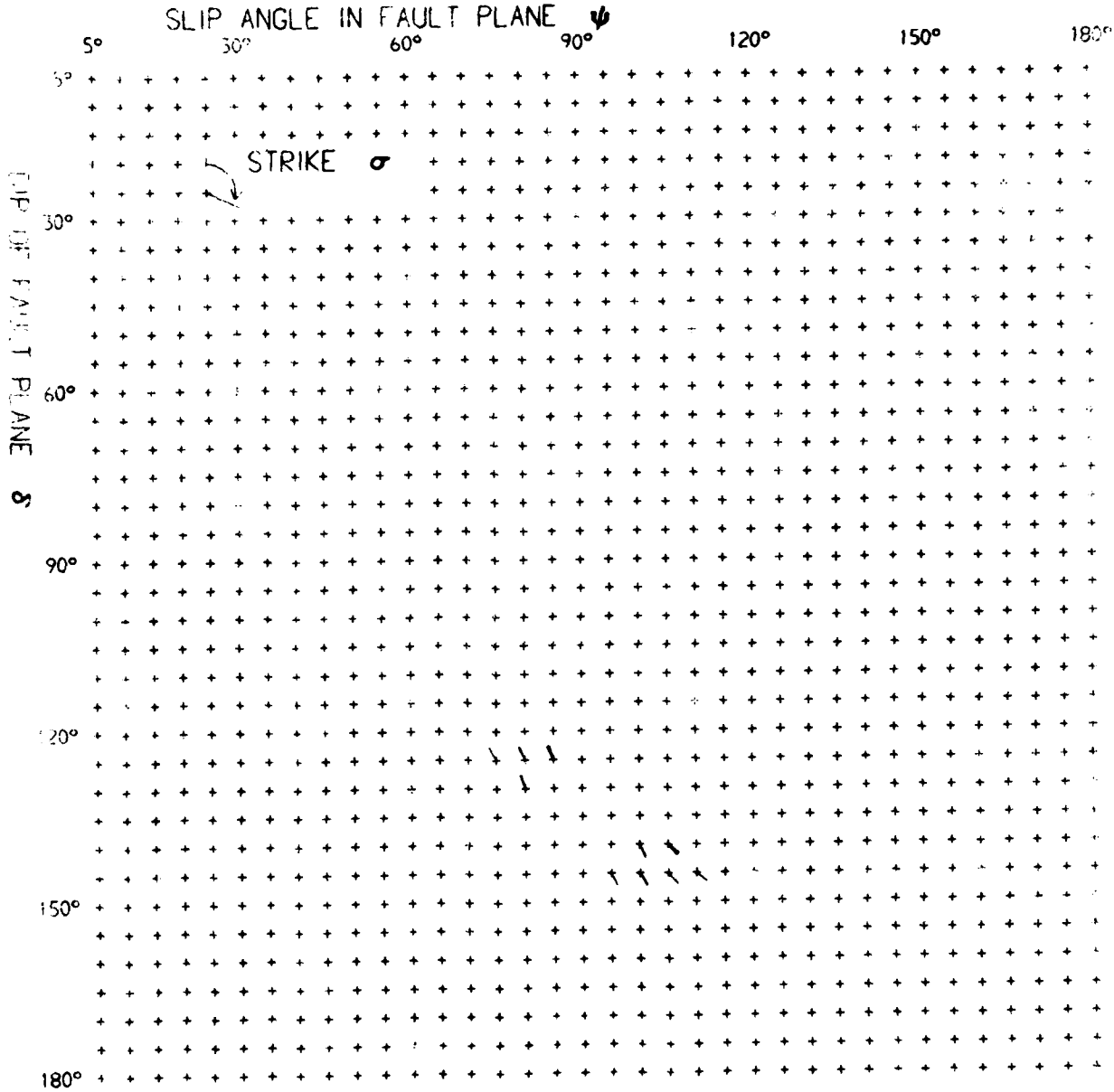

9 May 1976 07-51-16.7

(with no allowance for velocity structure)

Number of compatible orientations = 20

FIGURE 16(a)

EVENT NO. 31 (CATEGORY 2)

9 May 1976 07-51-16.7

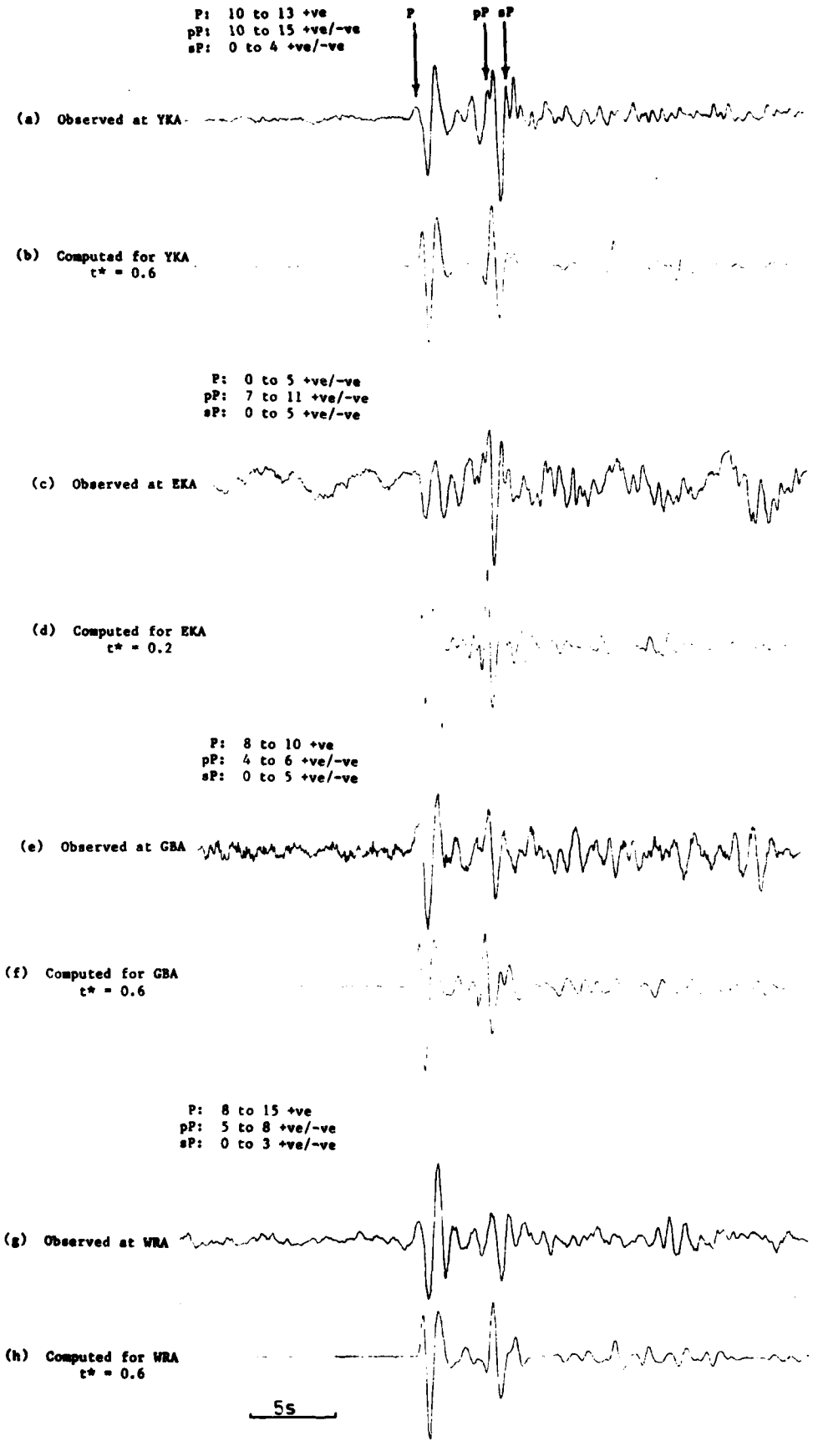

FIGURE 16(b)

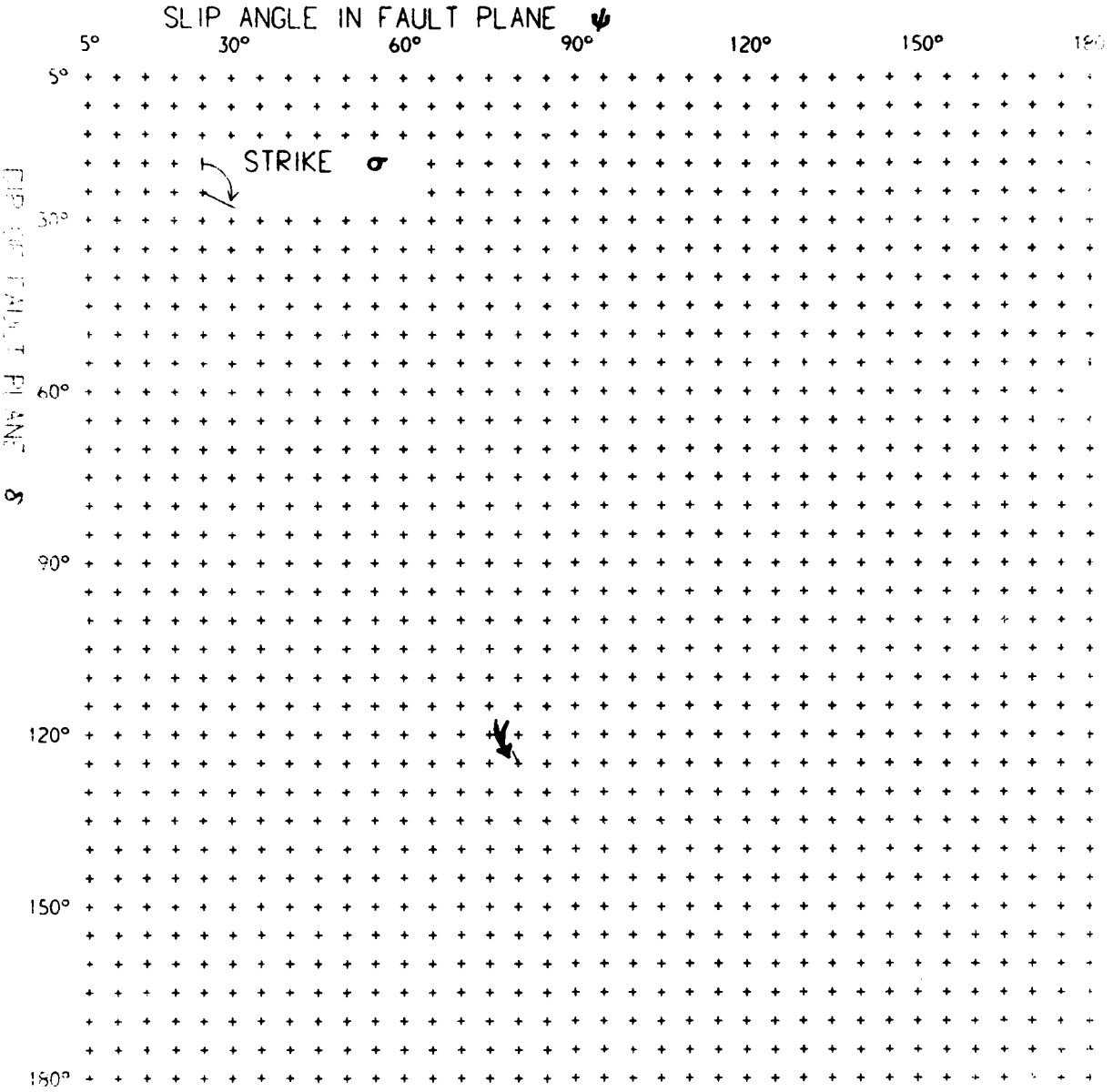

9 May 1976 07-51-16.7

(with allowance for velocity structure)

Number of compatible orientations = 1

FIGURE 16(c)

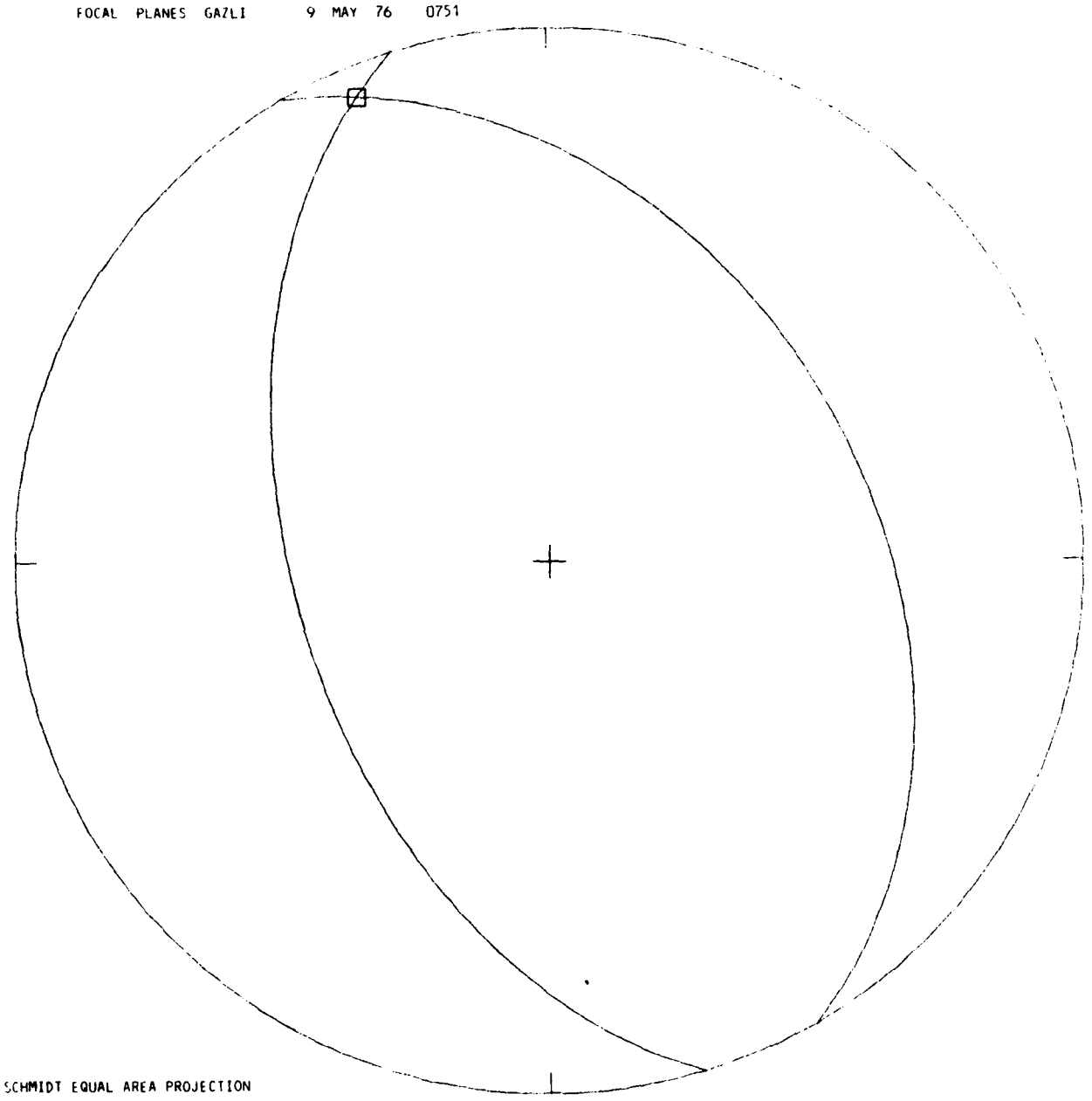

FIGURE 16(d)

(equivalent to figure 16(c))

EVENT NO. 34:	**17 May 1976**	**04-53-51.7**
DEPTH DEDUCED BY MODELLING:	**6.1 km**	
MAGNITUDE m_b (NEIS):	**4.7**	
SOURCE ORIENTATION USED IN MODEL:	**Dip - 130°**	
	Slip Angle - 90°	
	Strike - 125°	

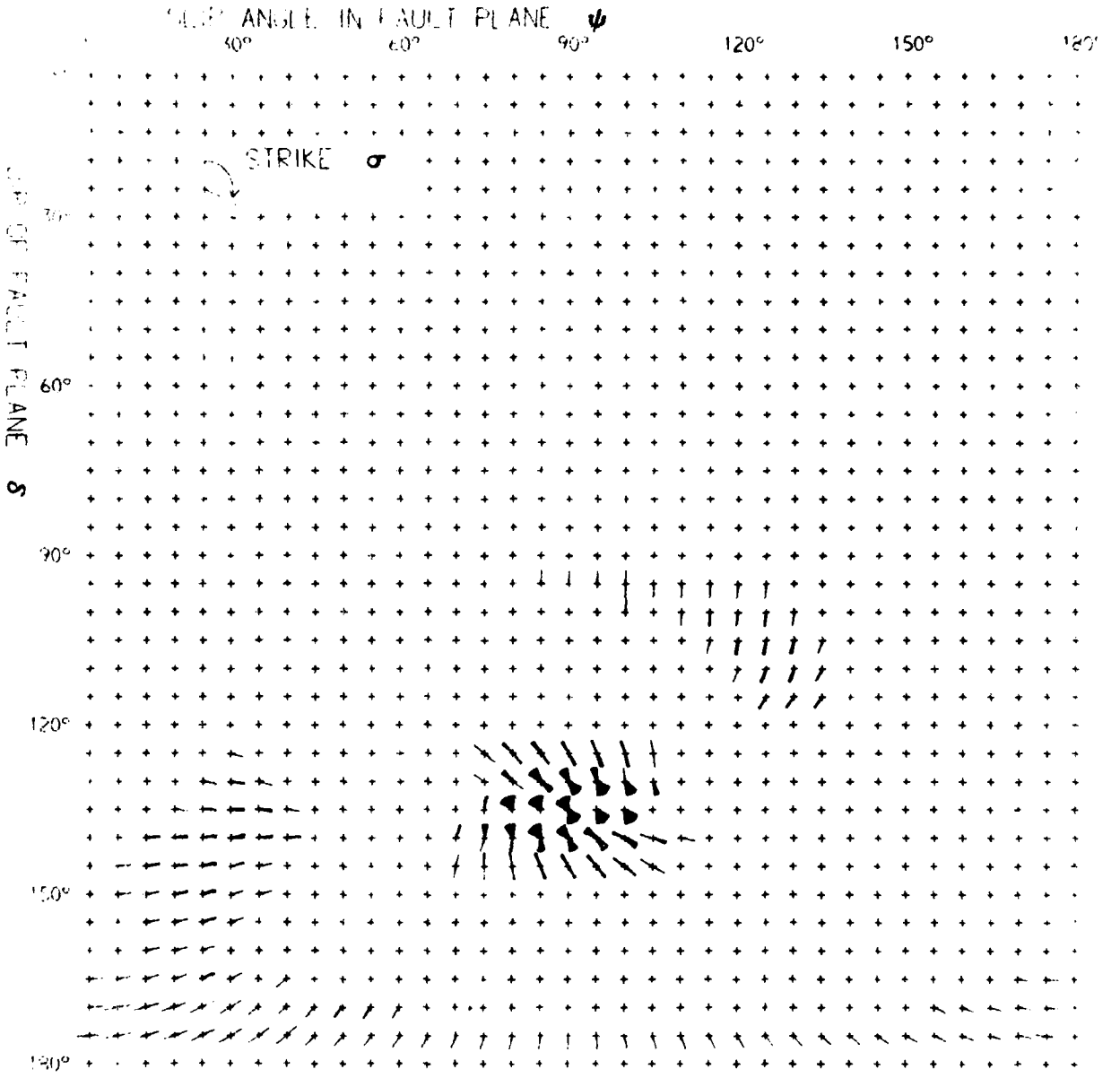

17 May 1976 04-53-51.7

(with no allowance for velocity structure)

Number of compatible orientations = 514

FIGURE 17(a)

EVENT NO. 34 (CATEGORY 2)

17 May 1976 04-53-51.7

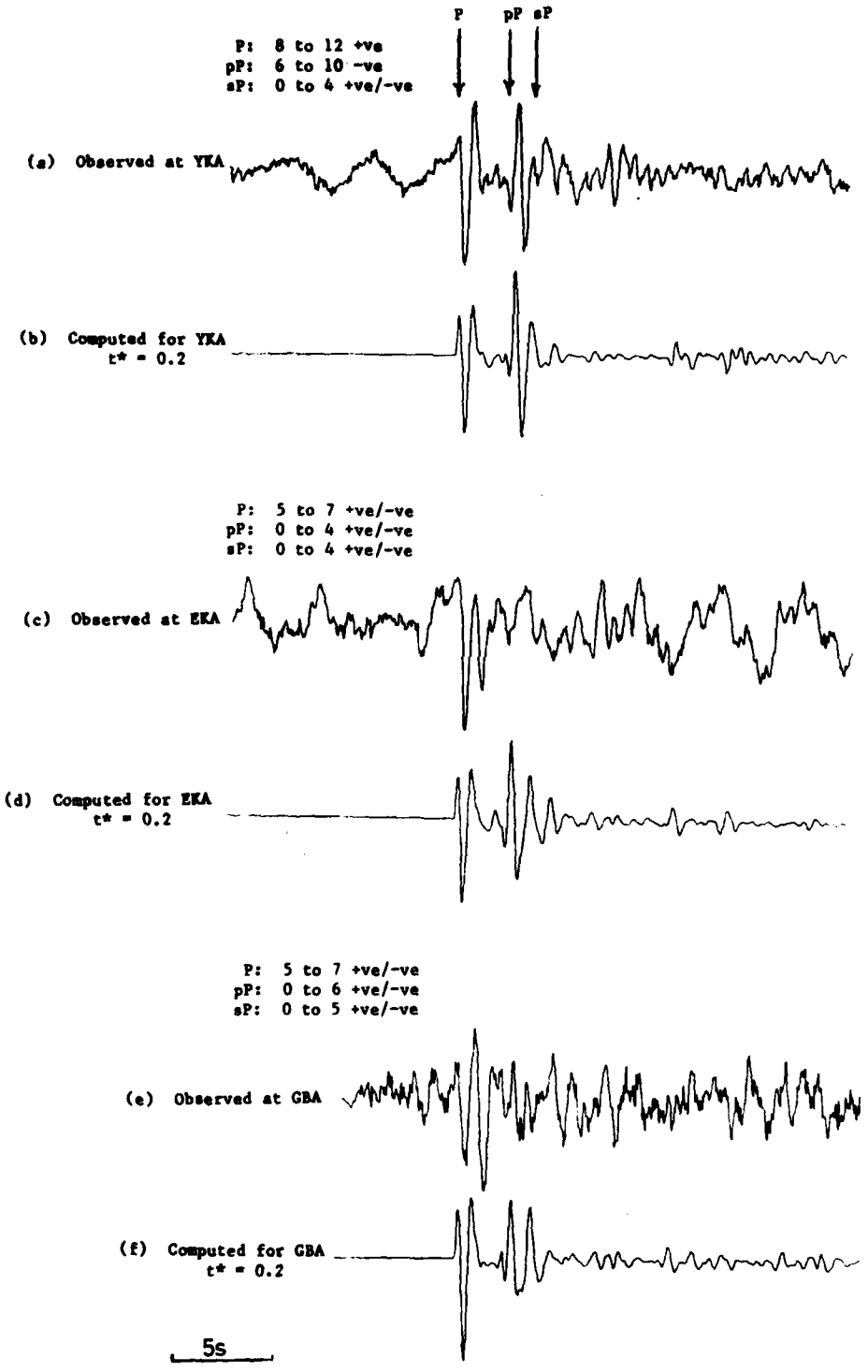

FIGURE 17(b)

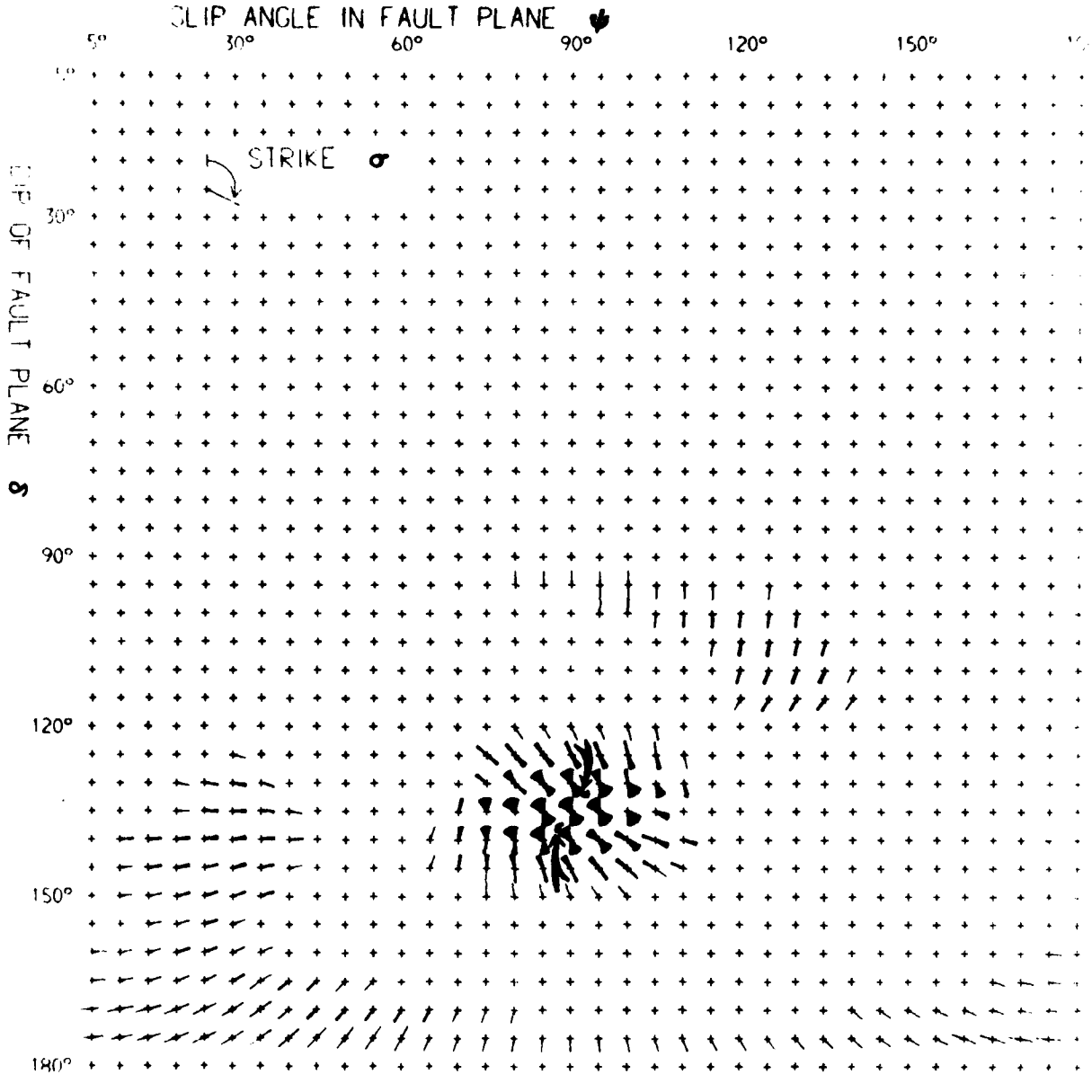

17 May 1976 04-53-51.7

(with allowance for velocity structure)

Number of compatible orientations = 737

FIGURE 17(c)

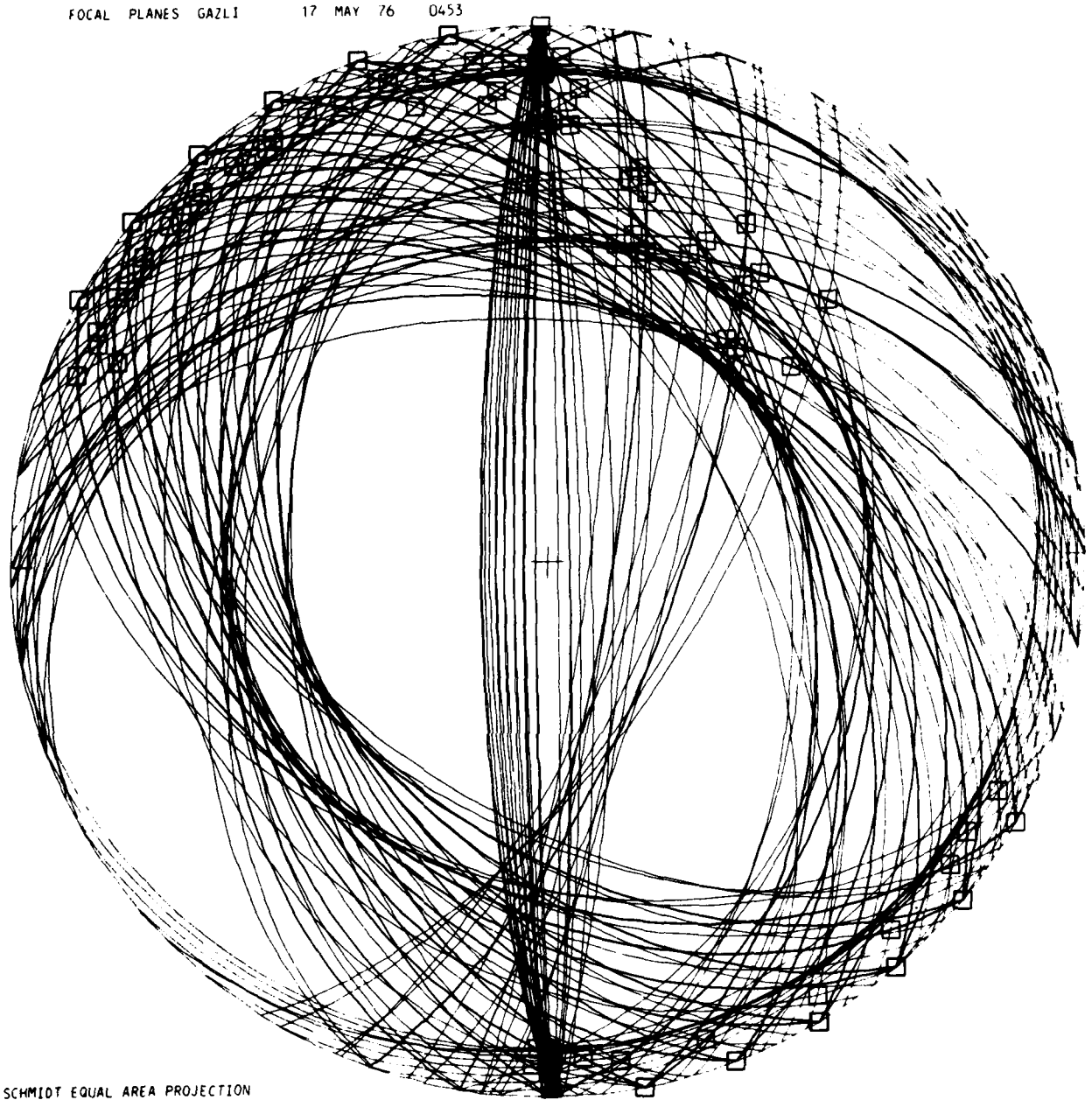

FIGURE 17(d)

(equivalent to figure 17(c))

EVENT NO. 41: 19 May 1976 15-54-45.6
DEPTH DEDUCED BY MODELLING: 13.15 km
MAGNITUDE m_b (NEIS): 5.0
SOURCE ORIENTATION USED IN MODEL: Dip - 135°
Slip Angle - 90°
Strike - 135°

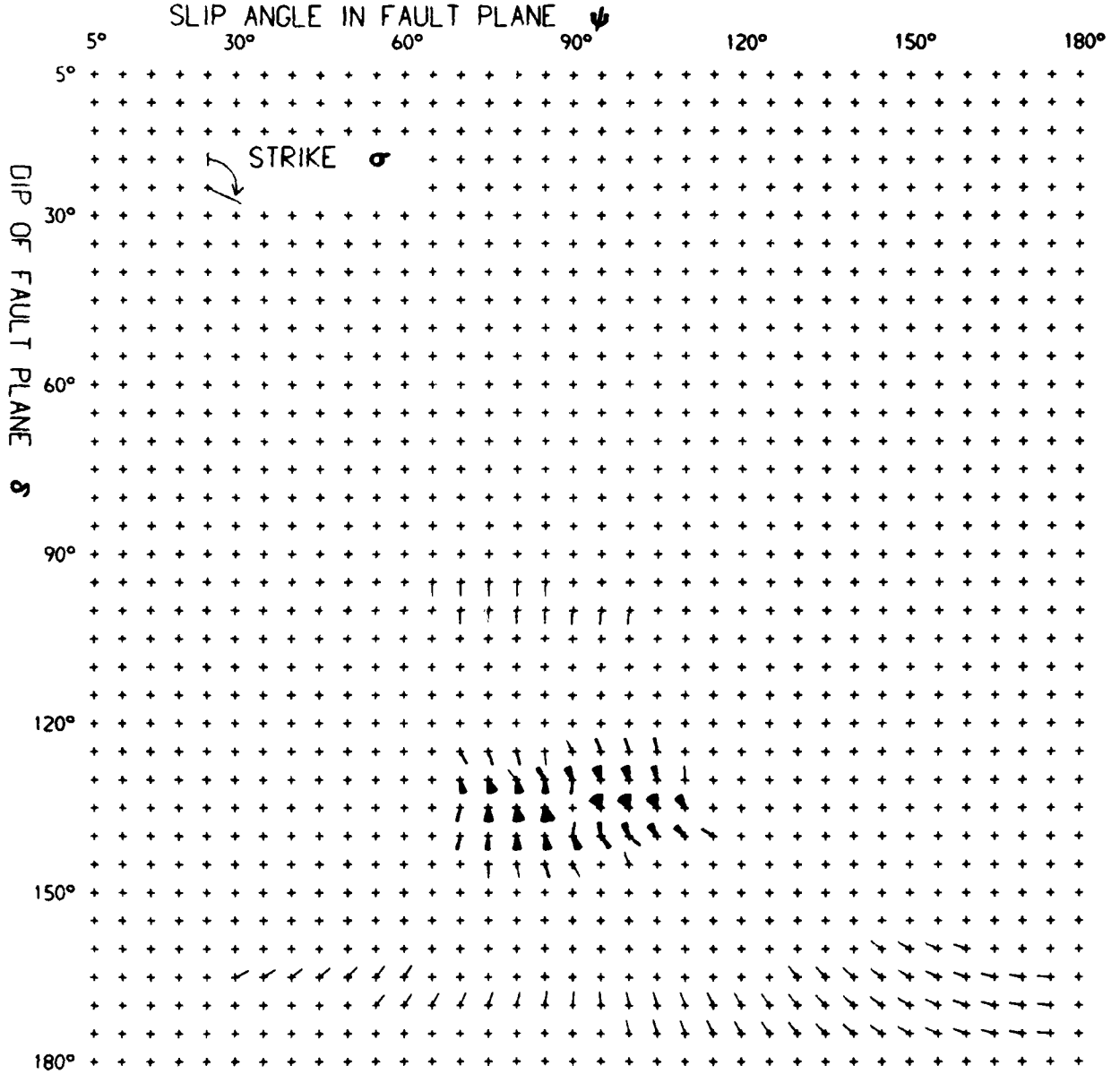

19 May 1976 15-54-45.6
(with no allowance for velocity structure)
Number of compatible orientations = 304

FIGURE 18(a)

EVENT NO. 41 (CATEGORY 2)

19 May 1976 15-54-45.6

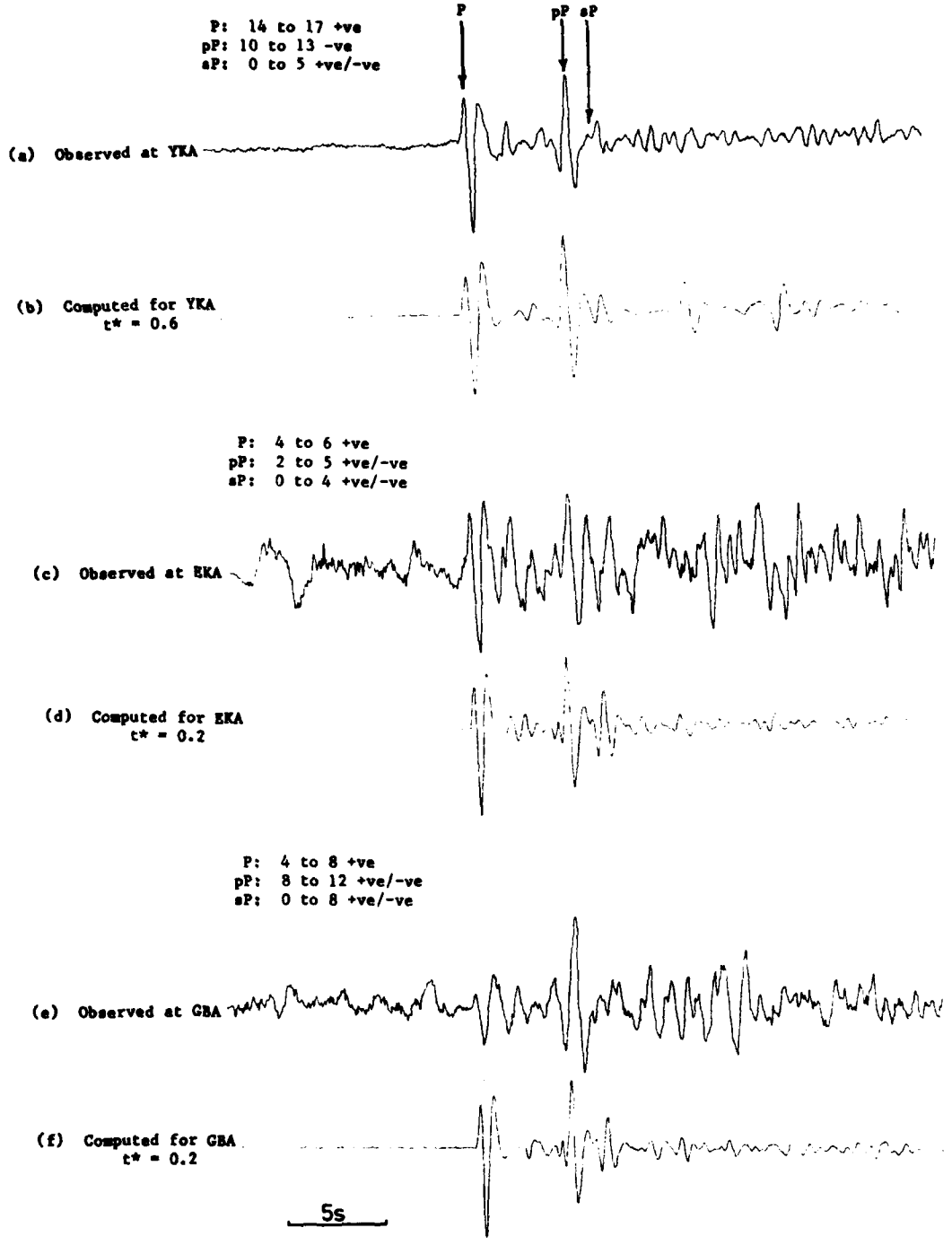

FIGURE 18(b)

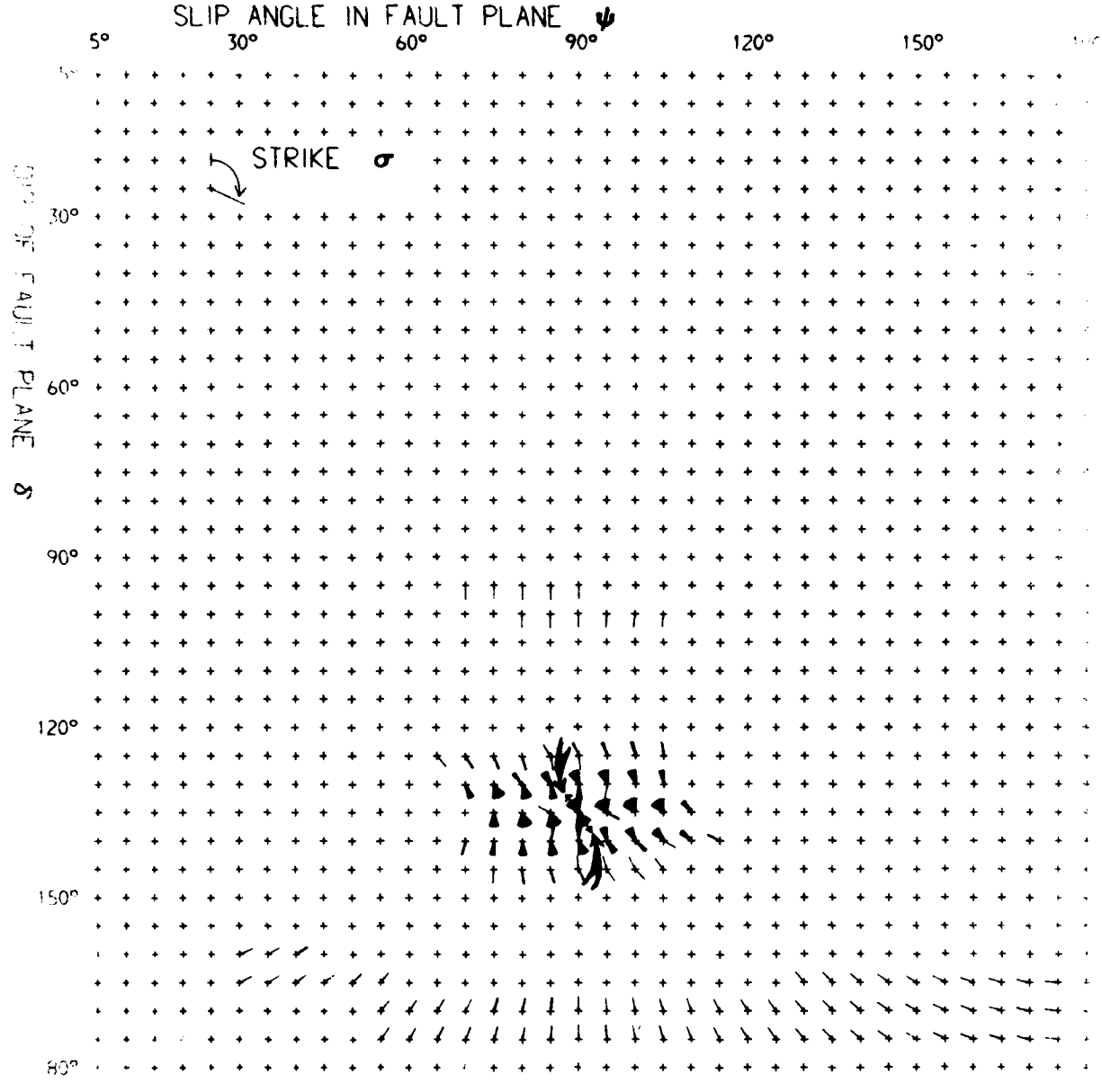

19 May 1976 15-54-45.6

(with allowance for velocity structure)

Number of compatible orientations = 403

FIGURE 18(c)

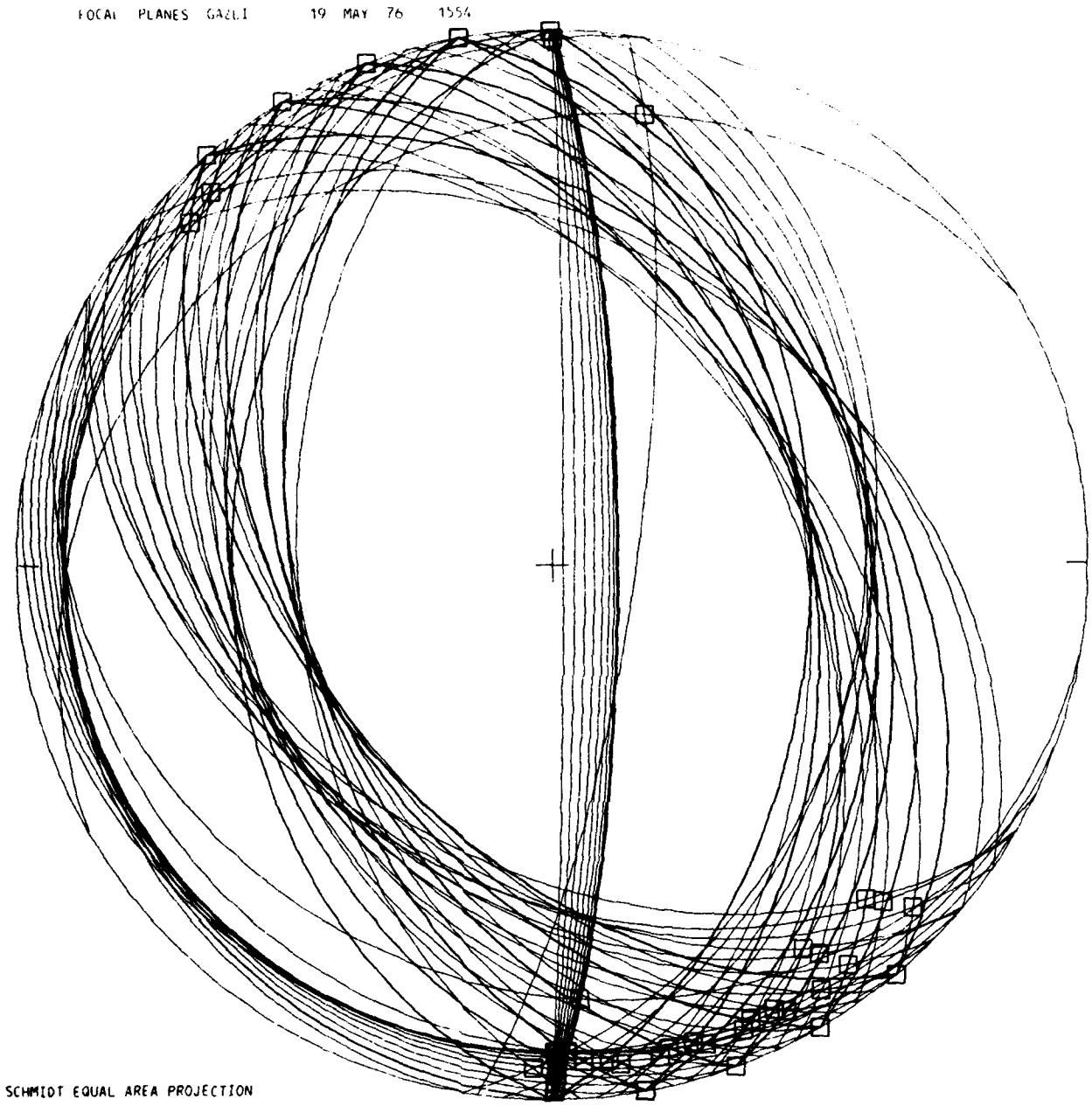

FIGURE 18(d)

(equivalent to figure 18(c))

EVENT NO. 48: 28 May 1976 14-05-37.3
DEPTH DEDUCED BY MODELLING: 7.96 km
MAGNITUDE m_b (NEIS): 4.9
SOURCE ORIENTATION USED IN MODEL: Dip - 135°
Slip Angle - 110°
Strike - 330°

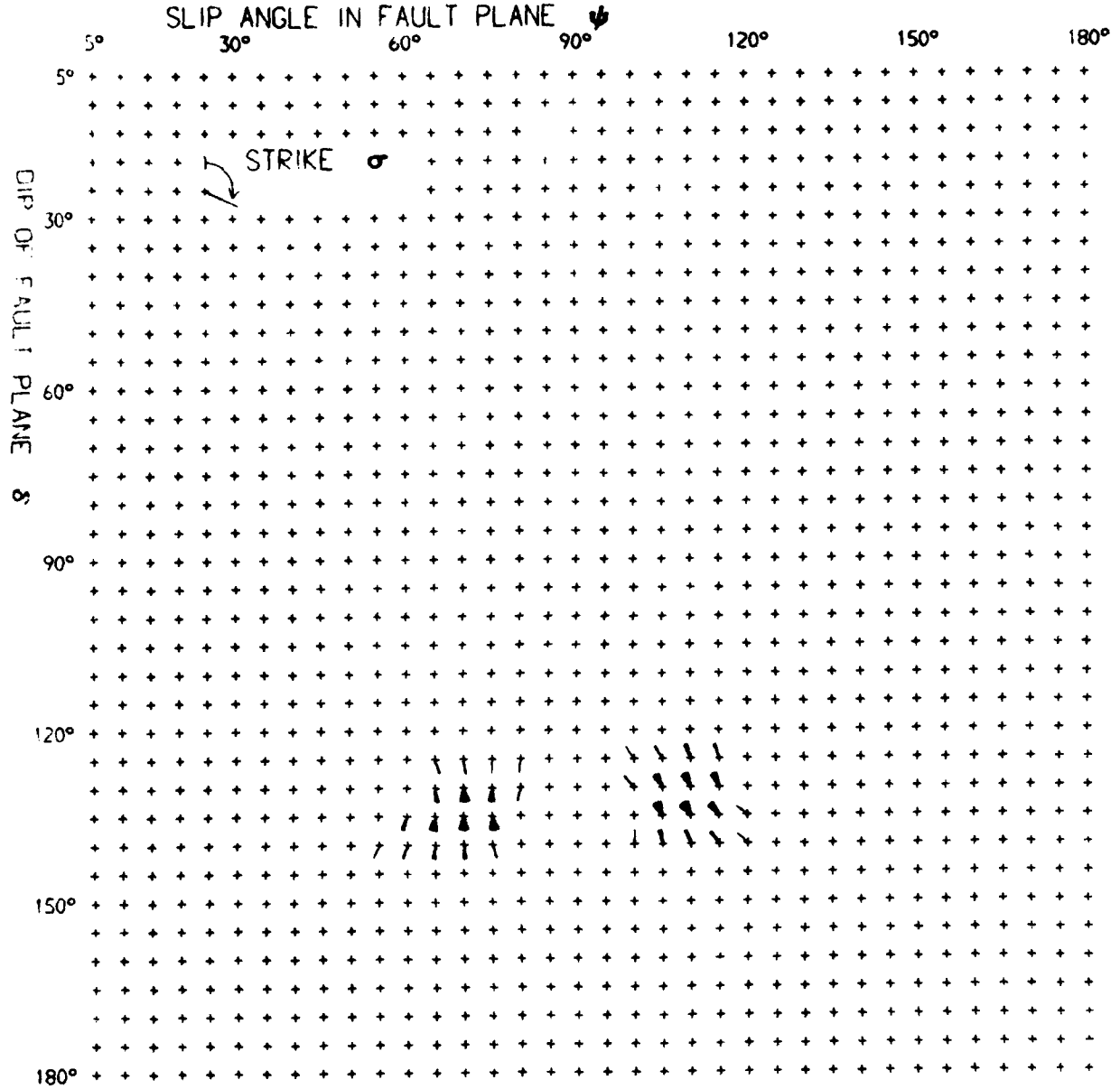

28 May 1976 14-05-37.3
(with no allowance for velocity structure)
Number of compatible orientations = 143

FIGURE 19(a)

EVENT NO. 48 (CATEGORY 2)

28 May 1976 14-05-37.3

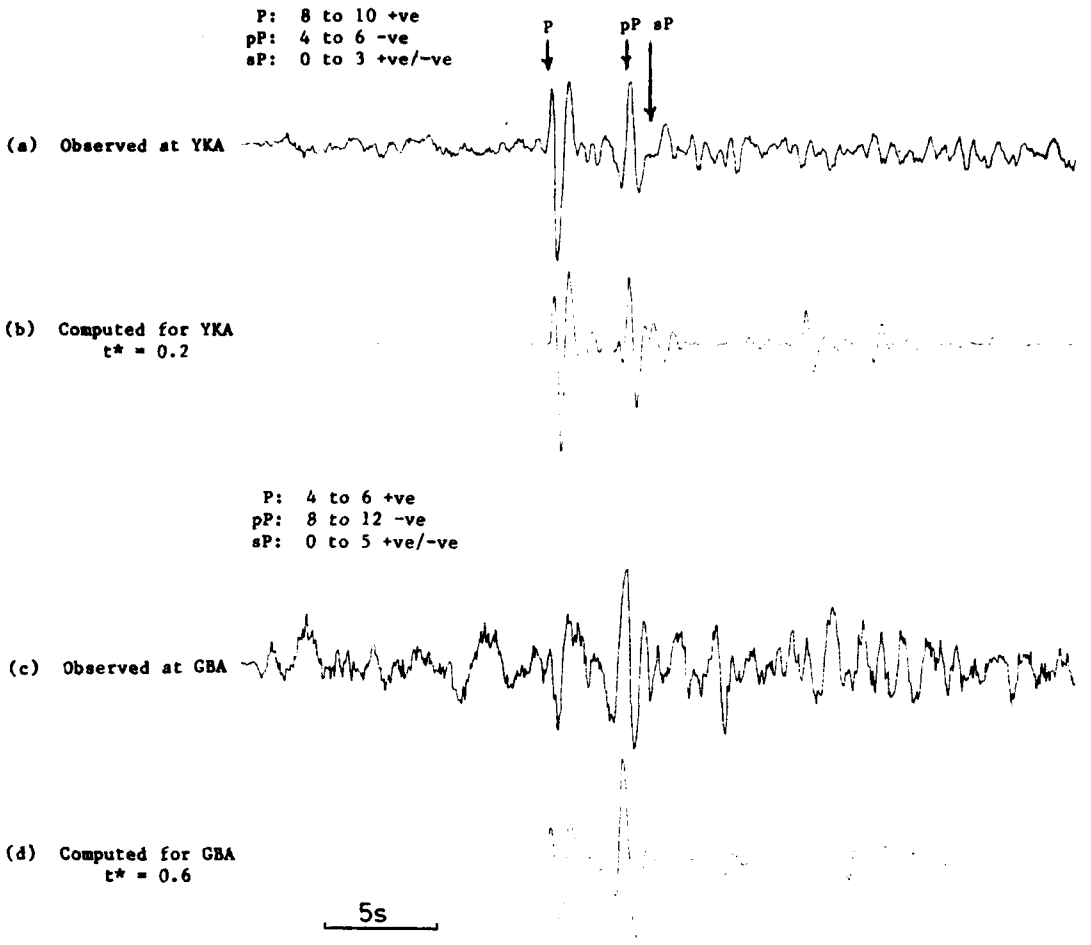

FIGURE 19(b)

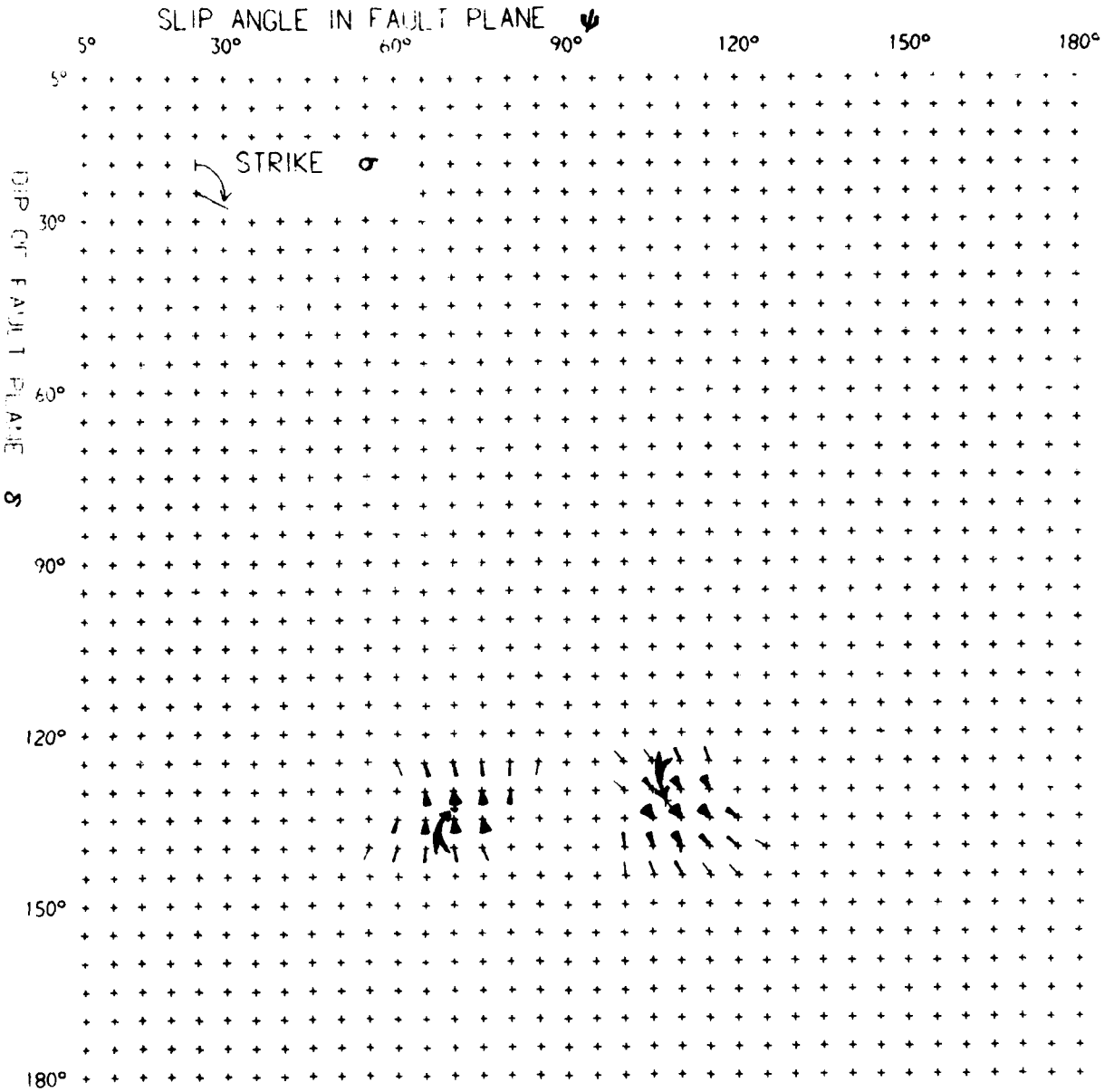

28 May 1976 14-05-37.3

(with allowance for velocity structure)

Number of compatible orientations = 192

FIGURE 19(c)

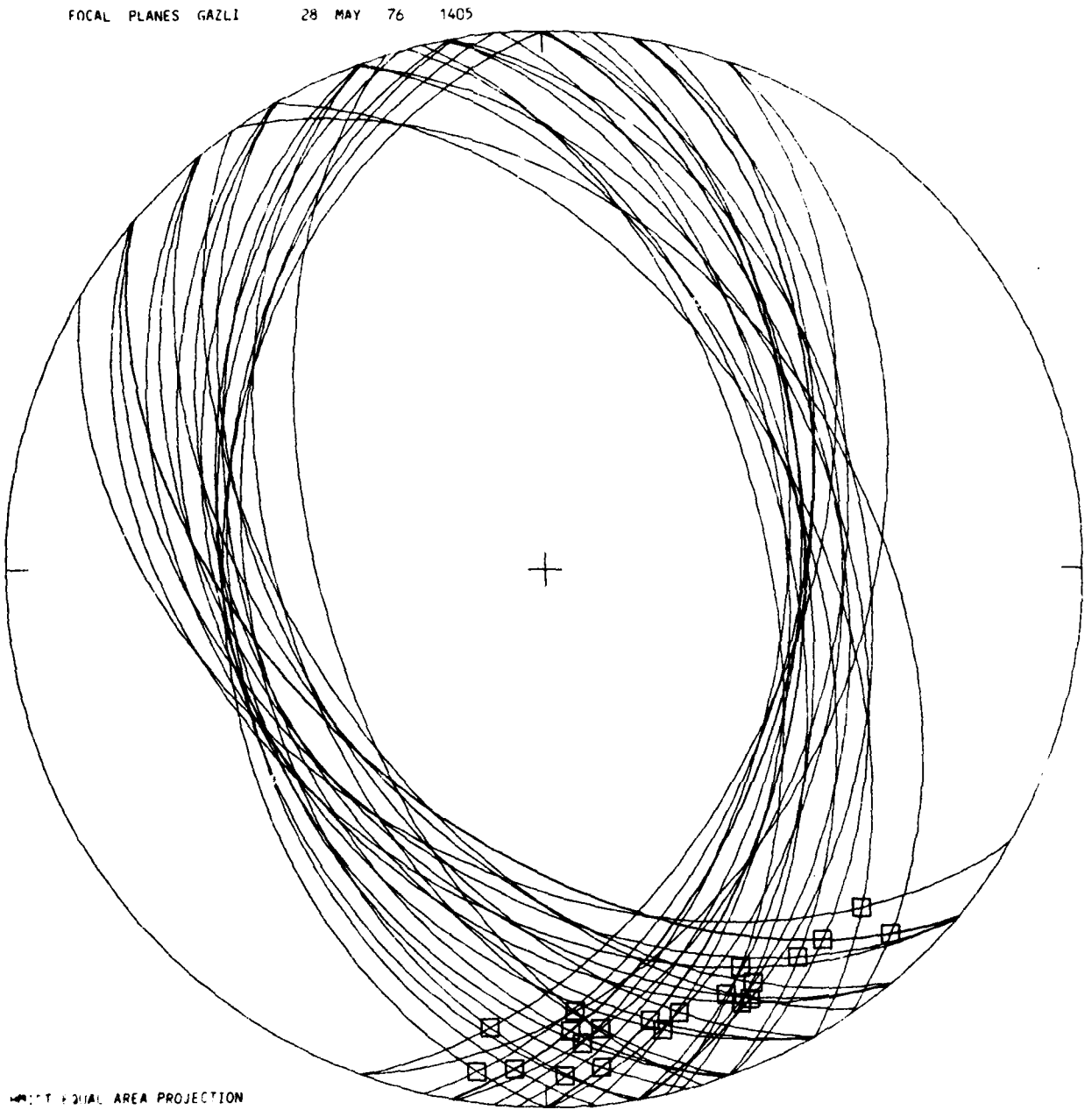

FIGURE 19(d)

(equivalent to figure 19(c))

EVENT NO. 52: 20 June 1976 23-33-48.8
DEPTH DEDUCED BY MODELLING: 10.1 km
MAGNITUDE m_b (NEIS): 5.3
SOURCE ORIENTATION USED IN MODEL: Dip - 145°
Slip Angle - 100°
Strike - 200°

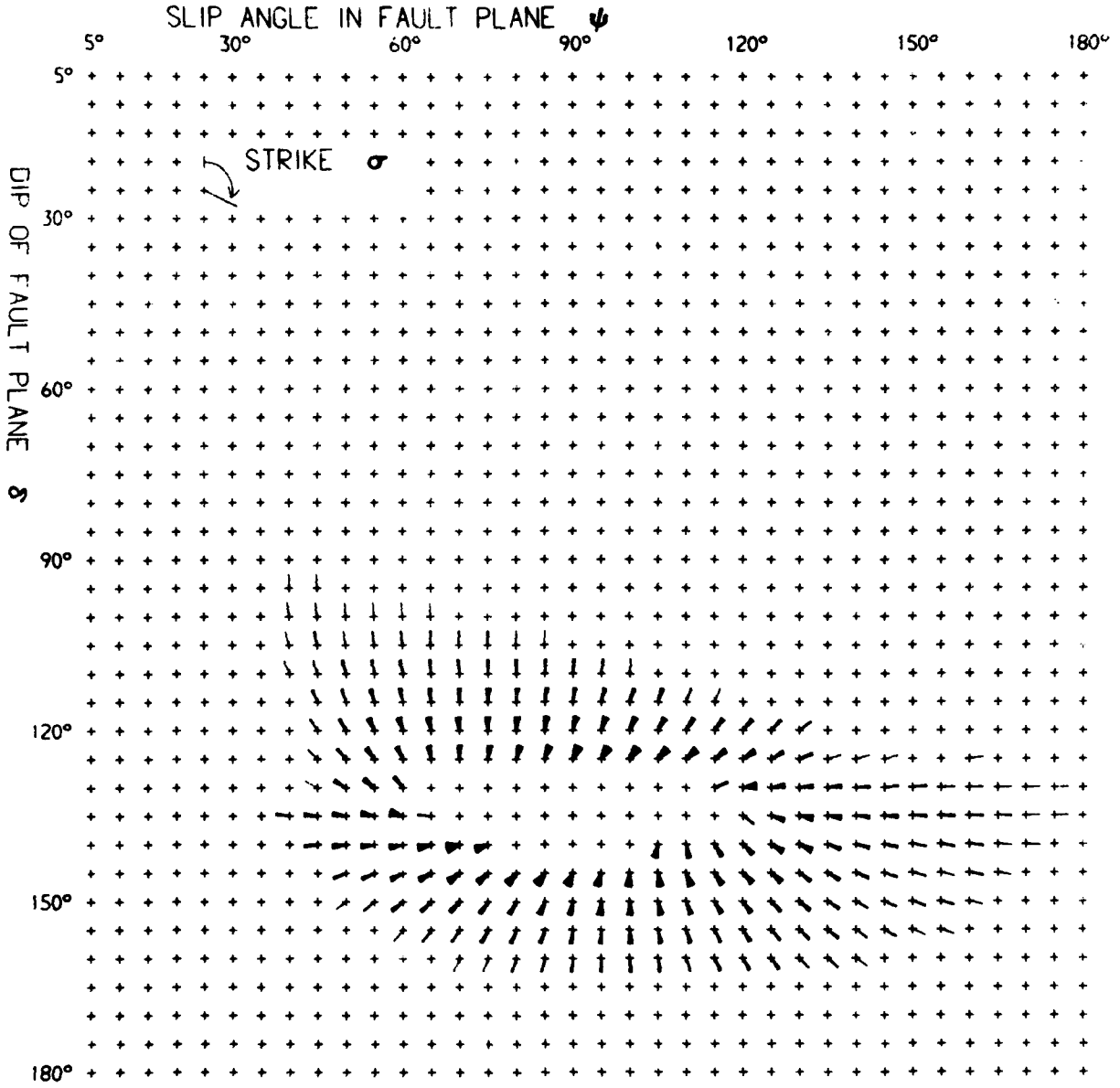

20 June 1976 23-33-48.8

(with no allowance for velocity structure)

Number of compatible orientations = 836

FIGURE 20(a)

EVENT NO. 52 (CATEGORY 2)

20 June 1976 23-33-48.8

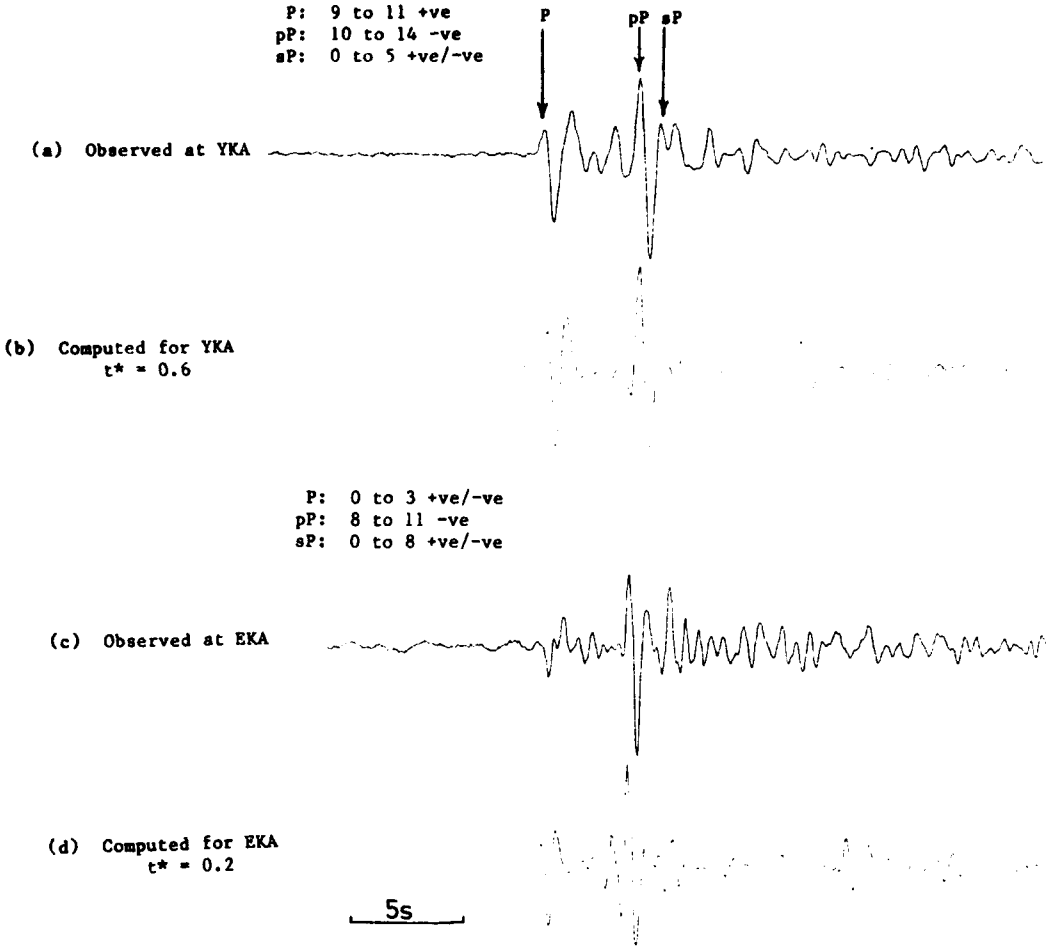

FIGURE 20(b)

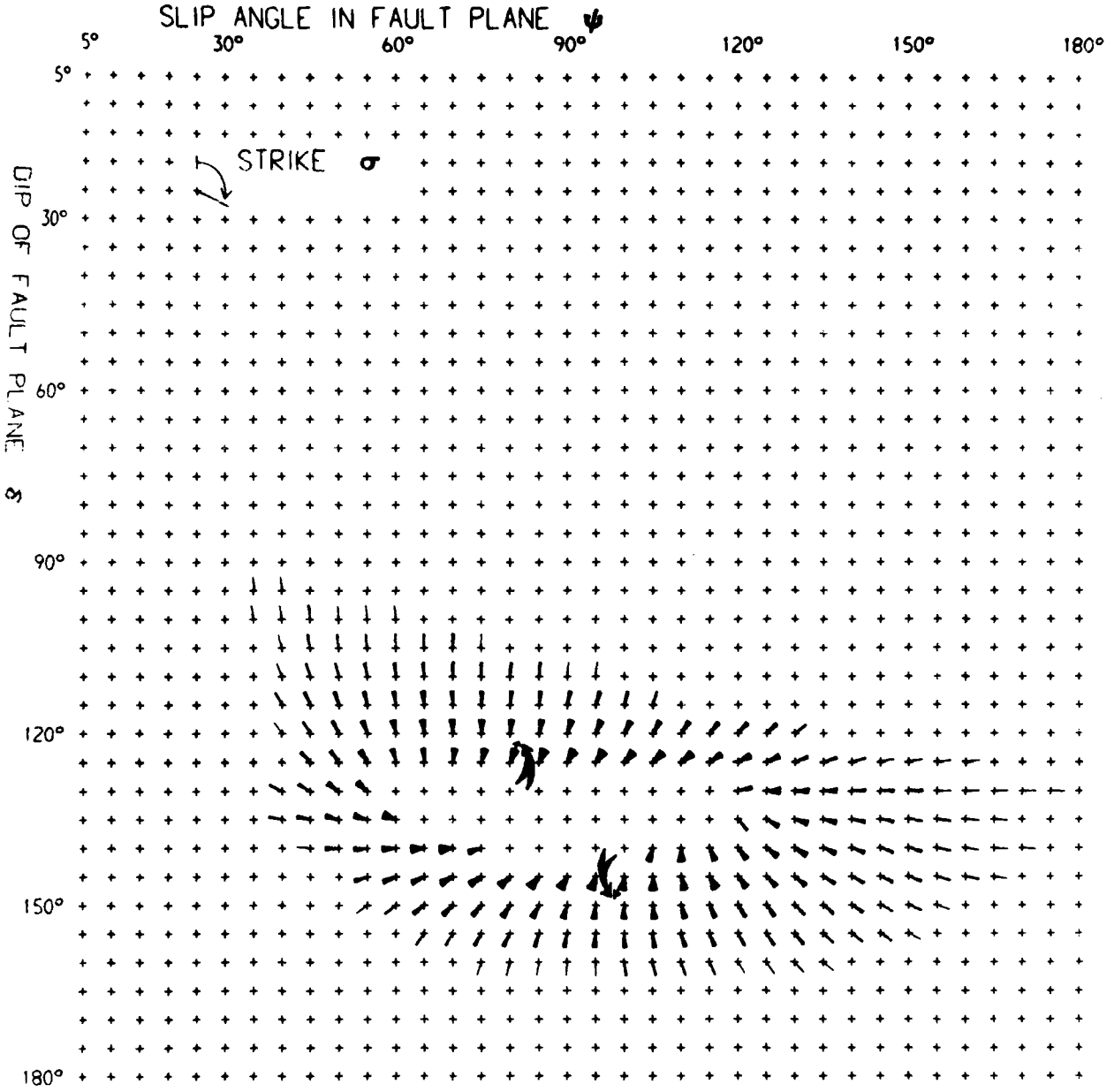

20 June 1976 23-33-48.8

(with allowance for velocity structure)

Number of compatible orientations = 809

FIGURE 20(c)

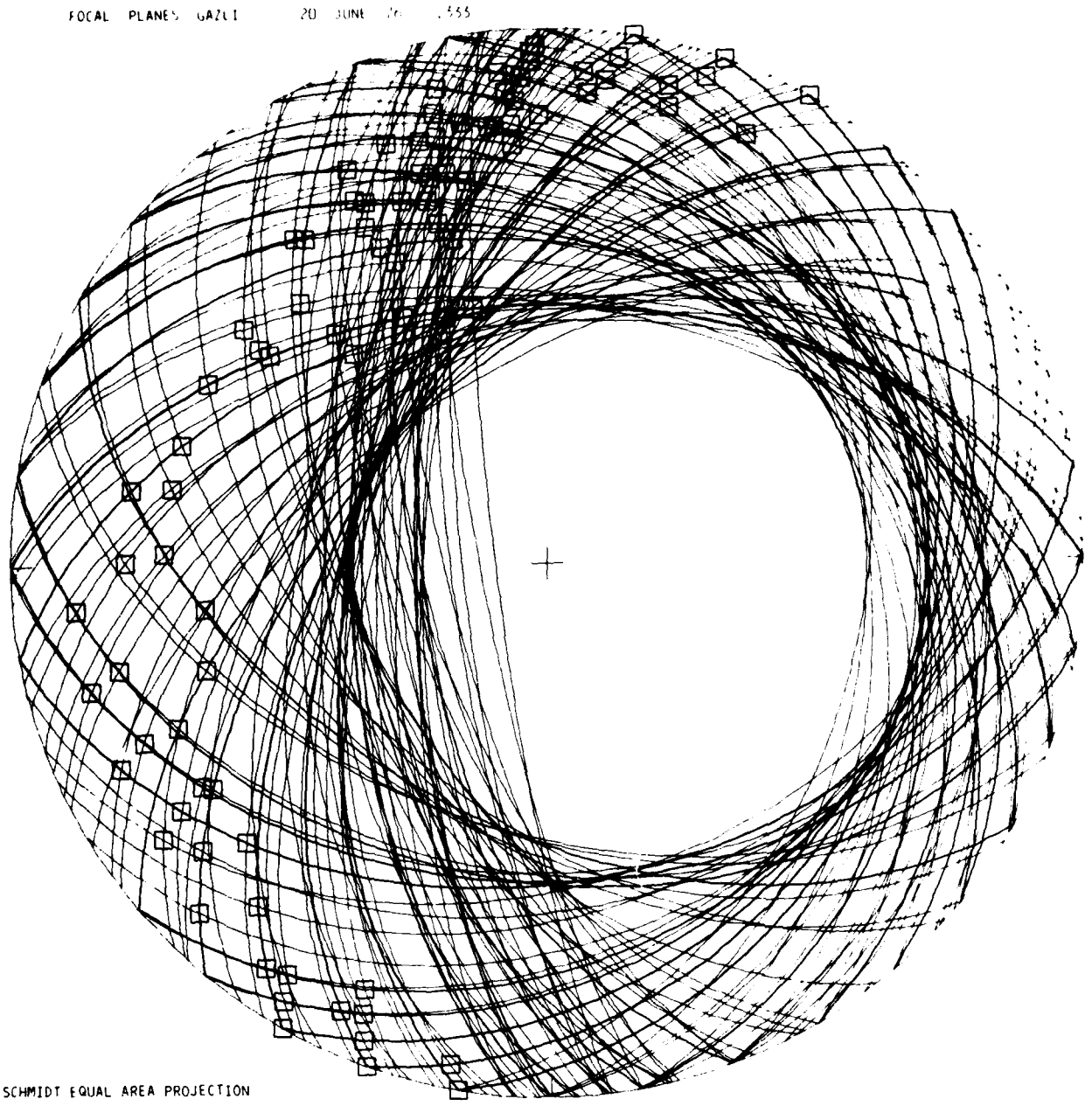

FIGURE 20(d)

(equivalent to figure 20(c))

EVENT NO. 53:	**23 June 1976**	**09-49-32.8**
DEPTH DEDUCED BY MODELLING:	**4.6 km**	
MAGNITUDE m_b (NEIS):	**4.8**	
SOURCE ORIENTATION USED IN MODEL:	**Dip - 130°**	
	Slip Angle - 90°	
	Strike - 130°	

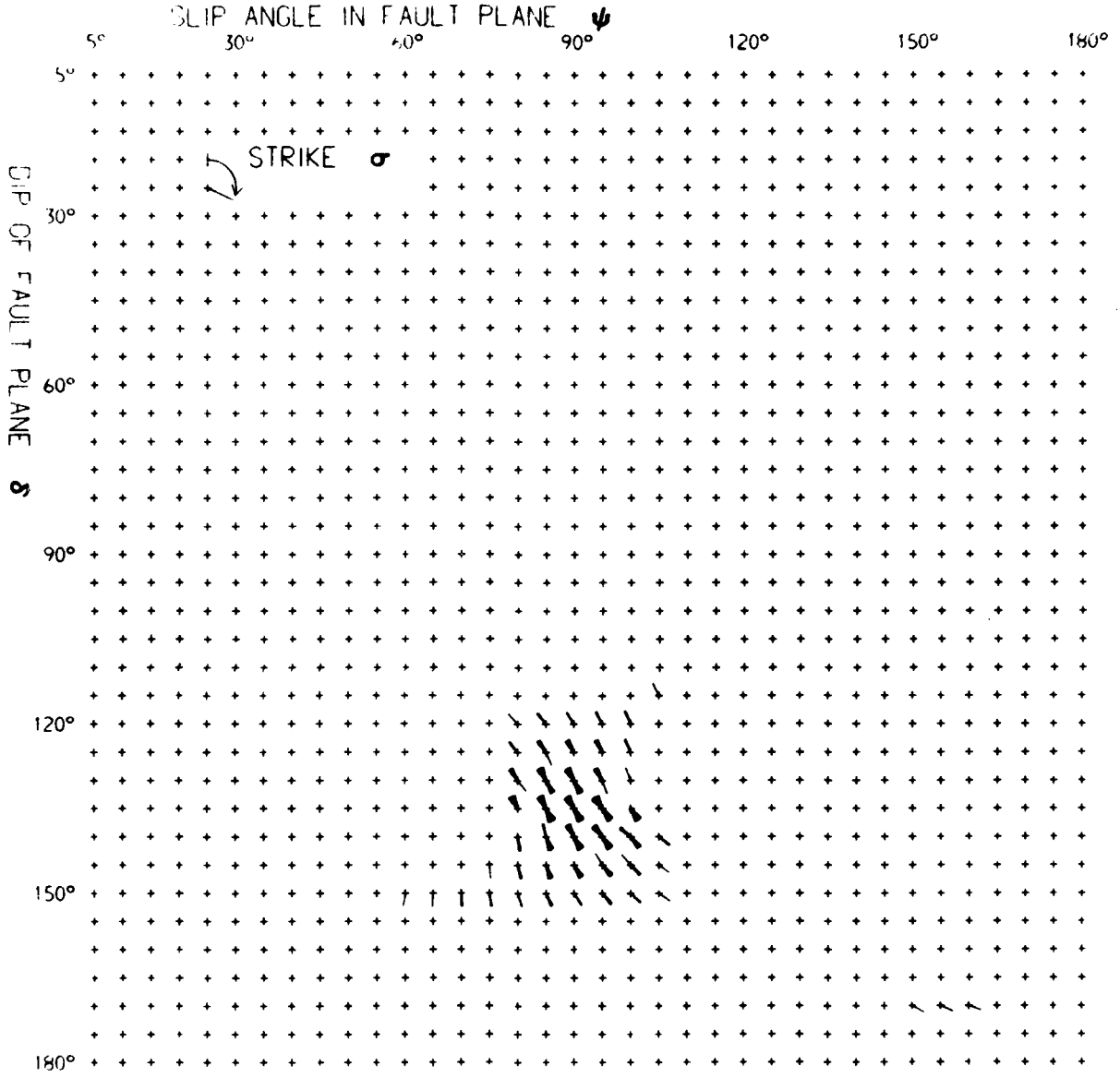

23 June 1976 09-49-32.8

(with no allowance for velocity structure)

Number of compatible orientations = 218

FIGURE 21(a)

EVENT NO. 53 (CATEGORY 2)

23 June 1976 09-49-32.8

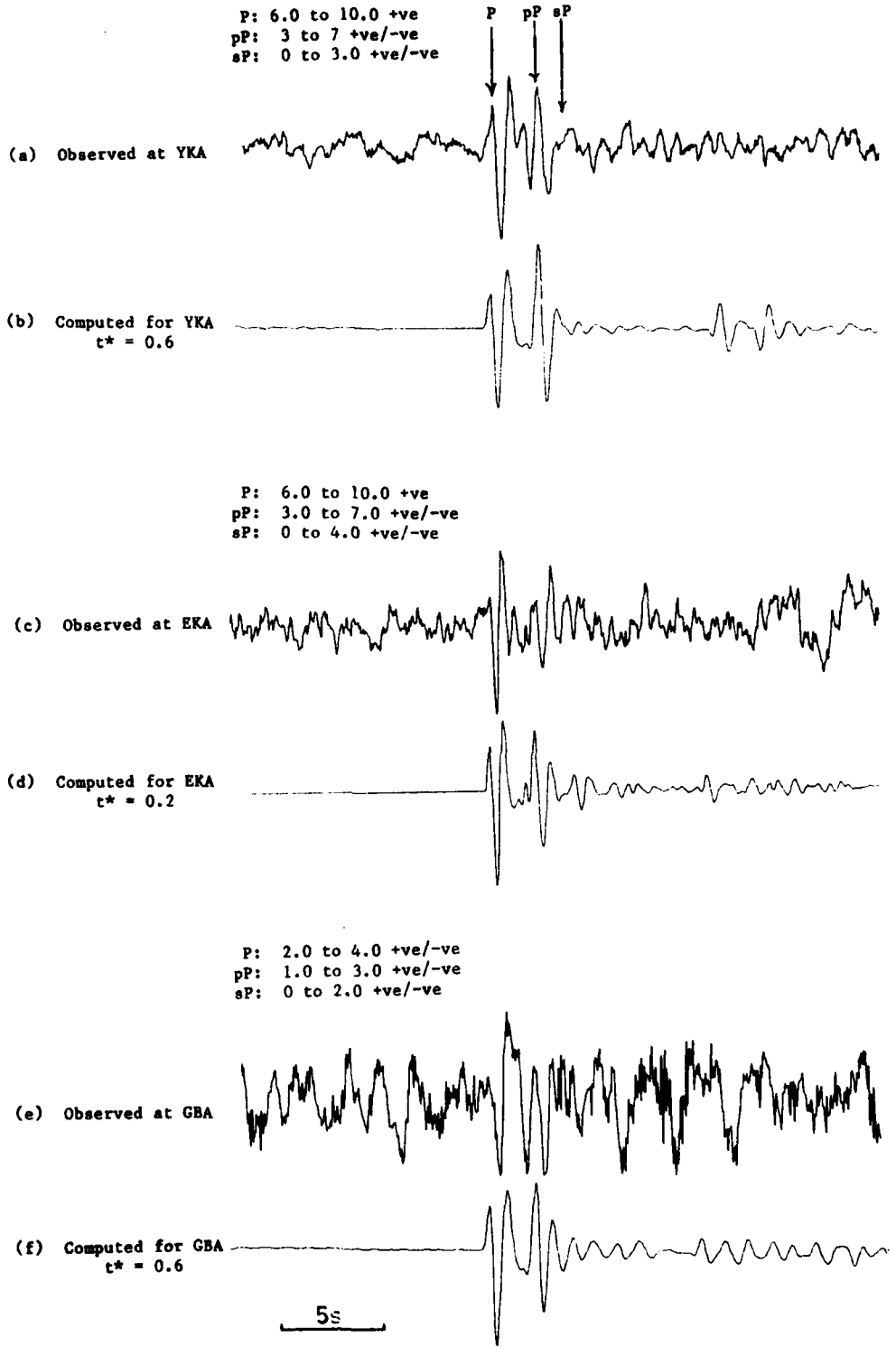

FIGURE 21(b)

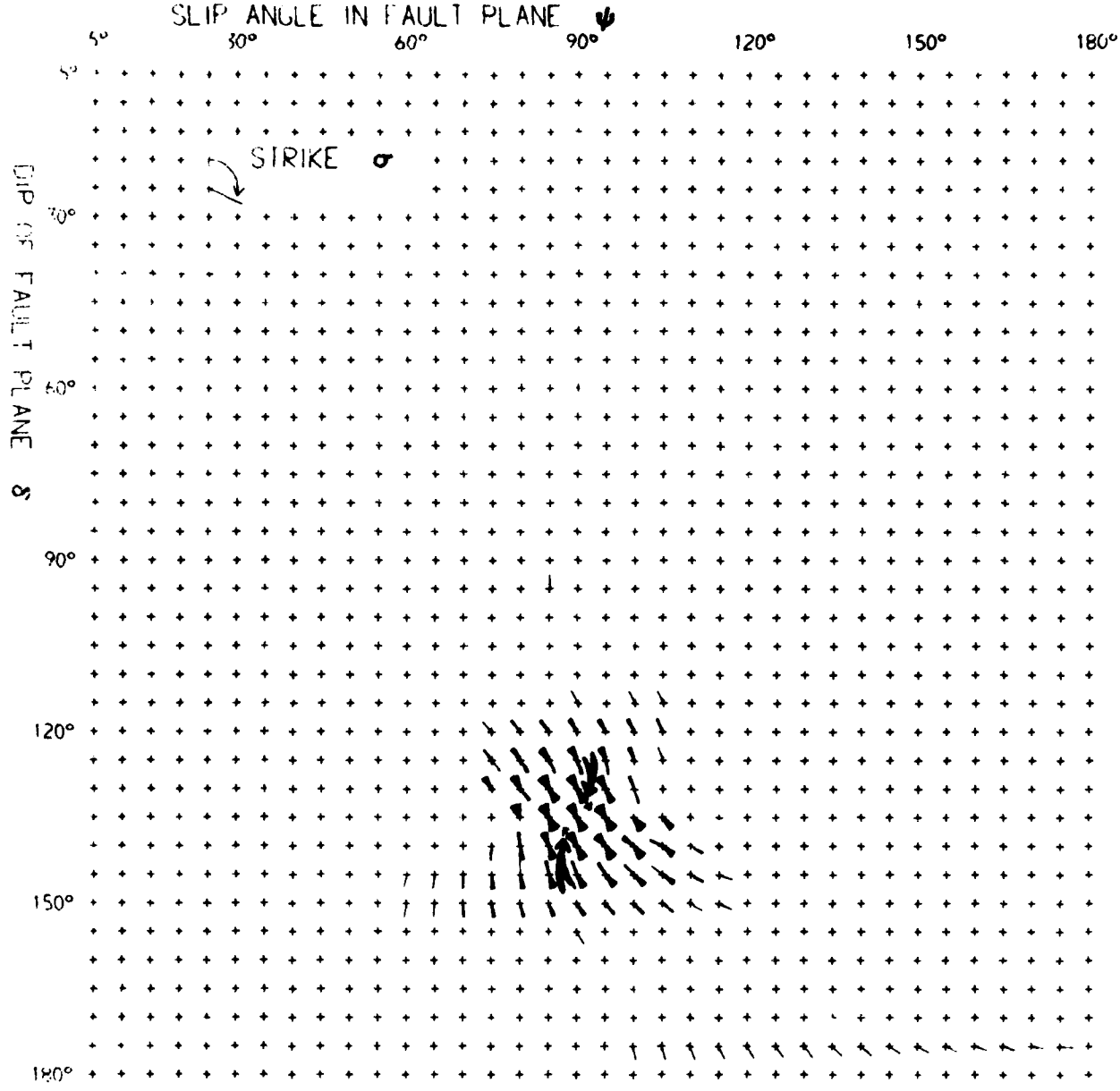

23 June 1976 09-49-32.8

(with allowance for velocity structure)

Number of compatible orientations = 414

FIGURE 21(c)

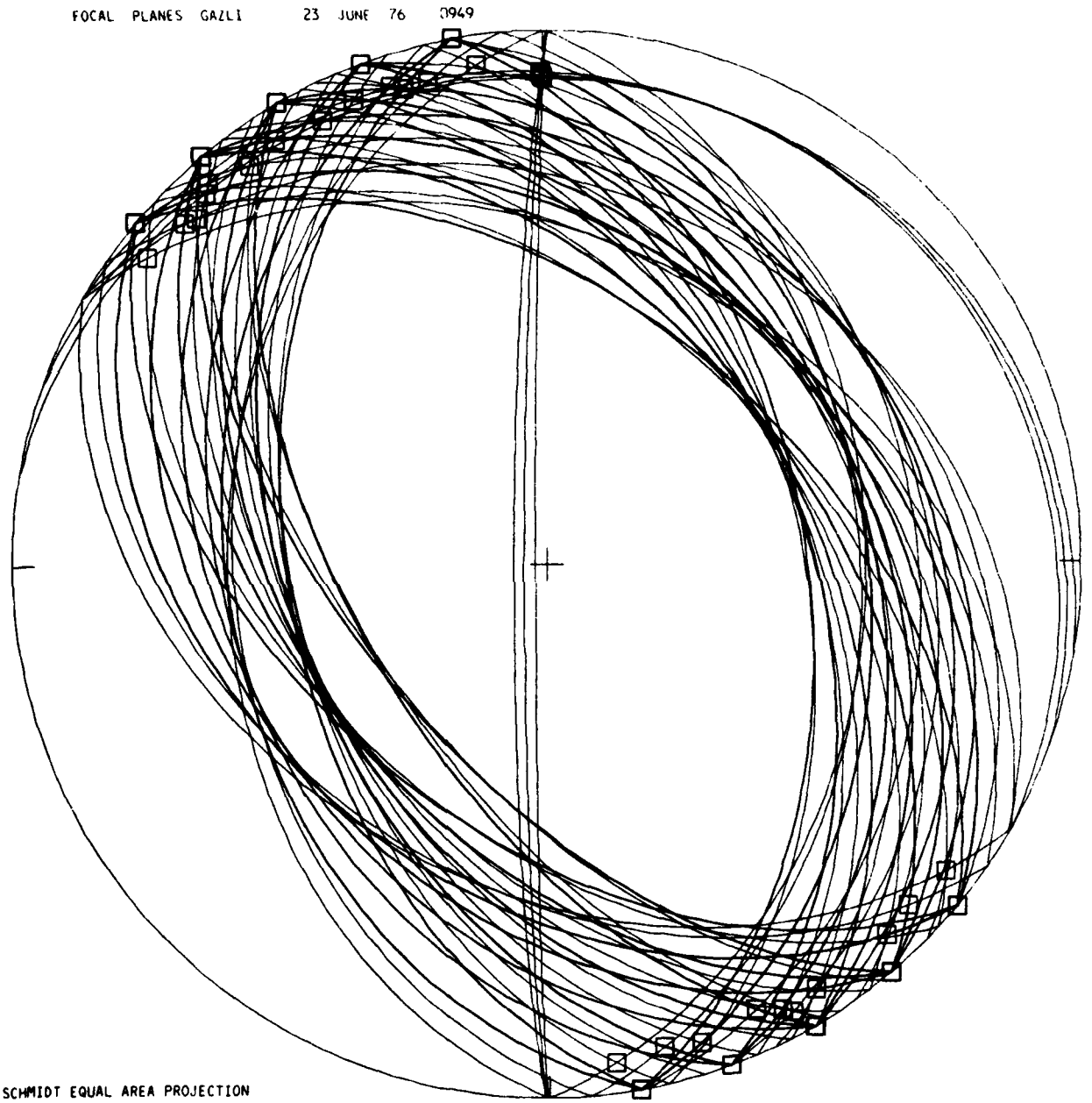

FIGURE 21(d)

(equivalent to figure 21(c))

EVENT NO. 54: 8 July 1976 23-35-38.0
DEPTH DEDUCED BY MODELLING: 7.96 km
MAGNITUDE m_b (NEIS): 4.7

SOURCE ORIENTATION USED IN MODEL:
Dip - 135°
Slip Angle - 100°
Strike - 320°

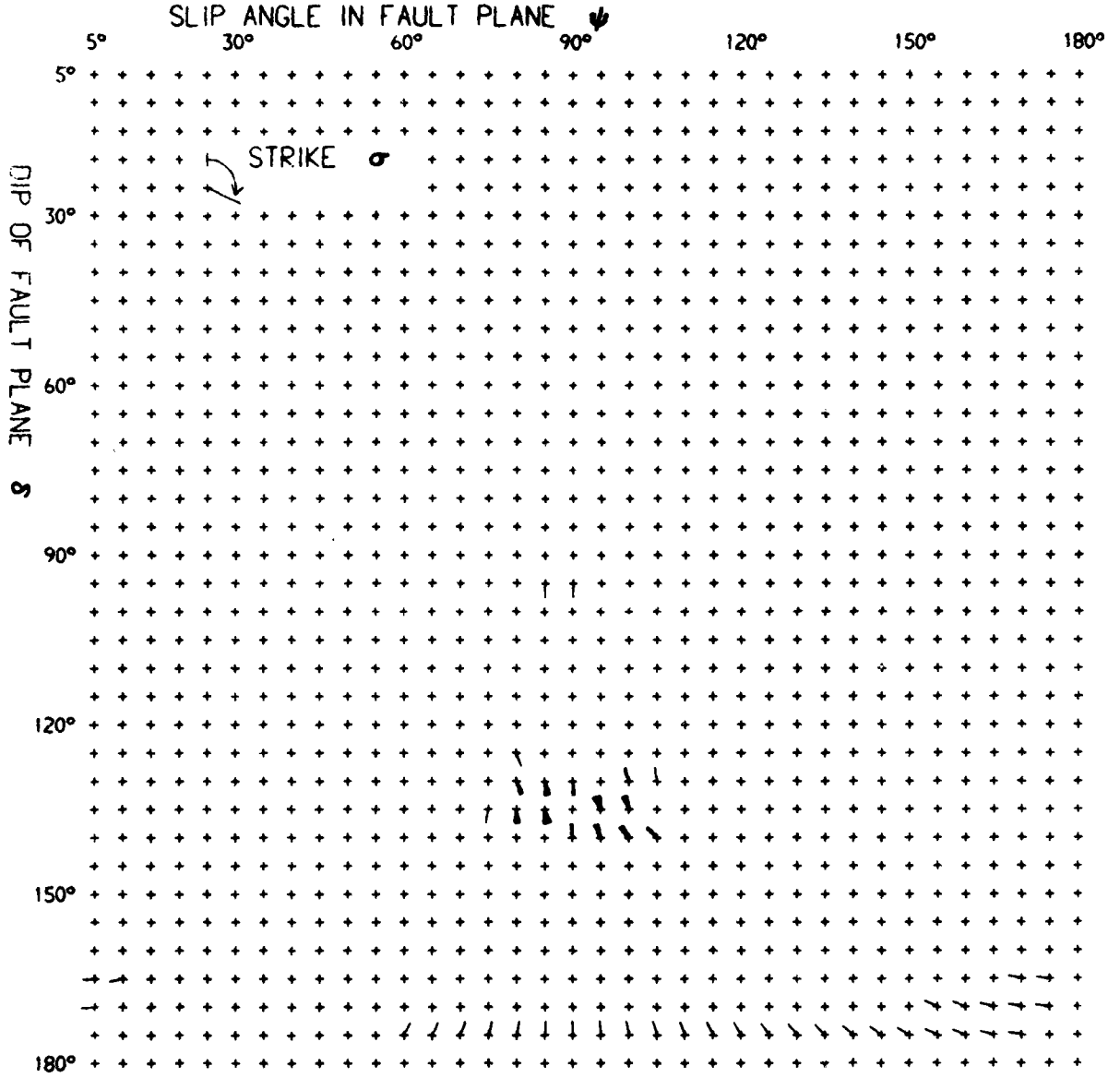

8 July 1976 23-35-38.0

(with no allowance for velocity structure)

Number of compatible orientations = 97

FIGURE 22(a)

EVENT NO. 54 (CATEGORY 2)

8 July 1976 23-35-38.0

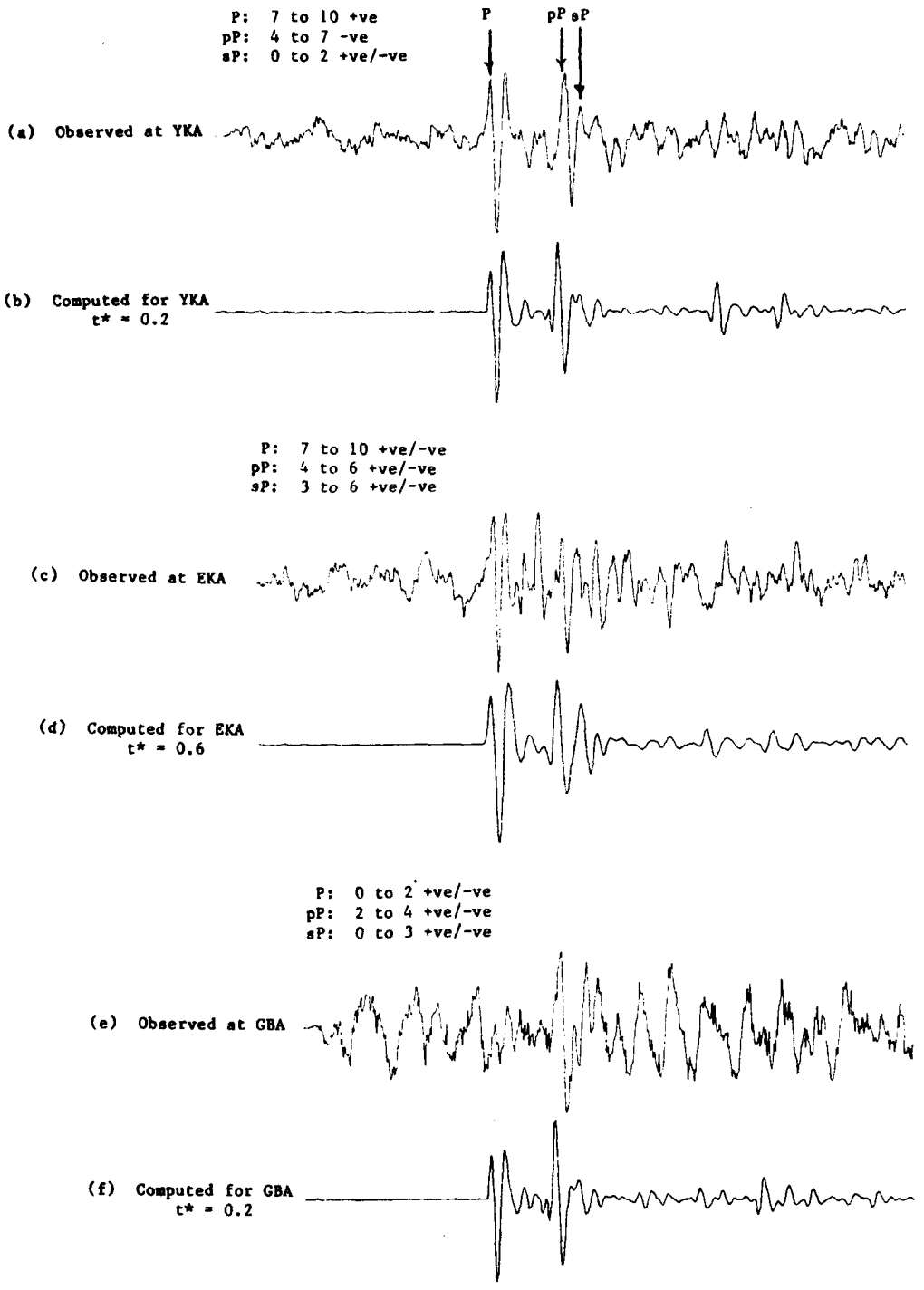

FIGURE 22(b)

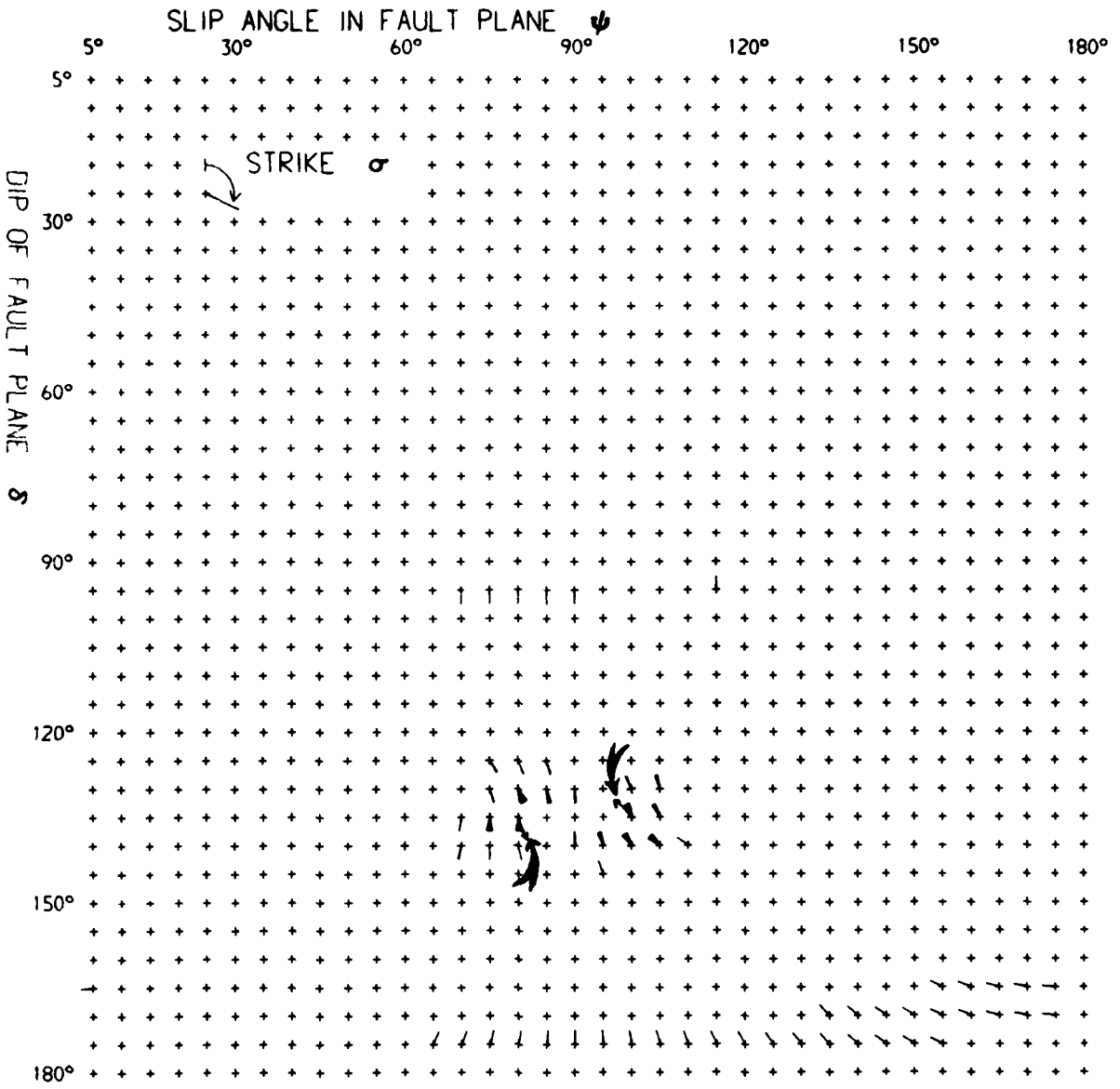

8 July 1976 23-35-38.0

(with allowance for velocity structure)

Number of compatible orientations = 116

FIGURE 22(c)

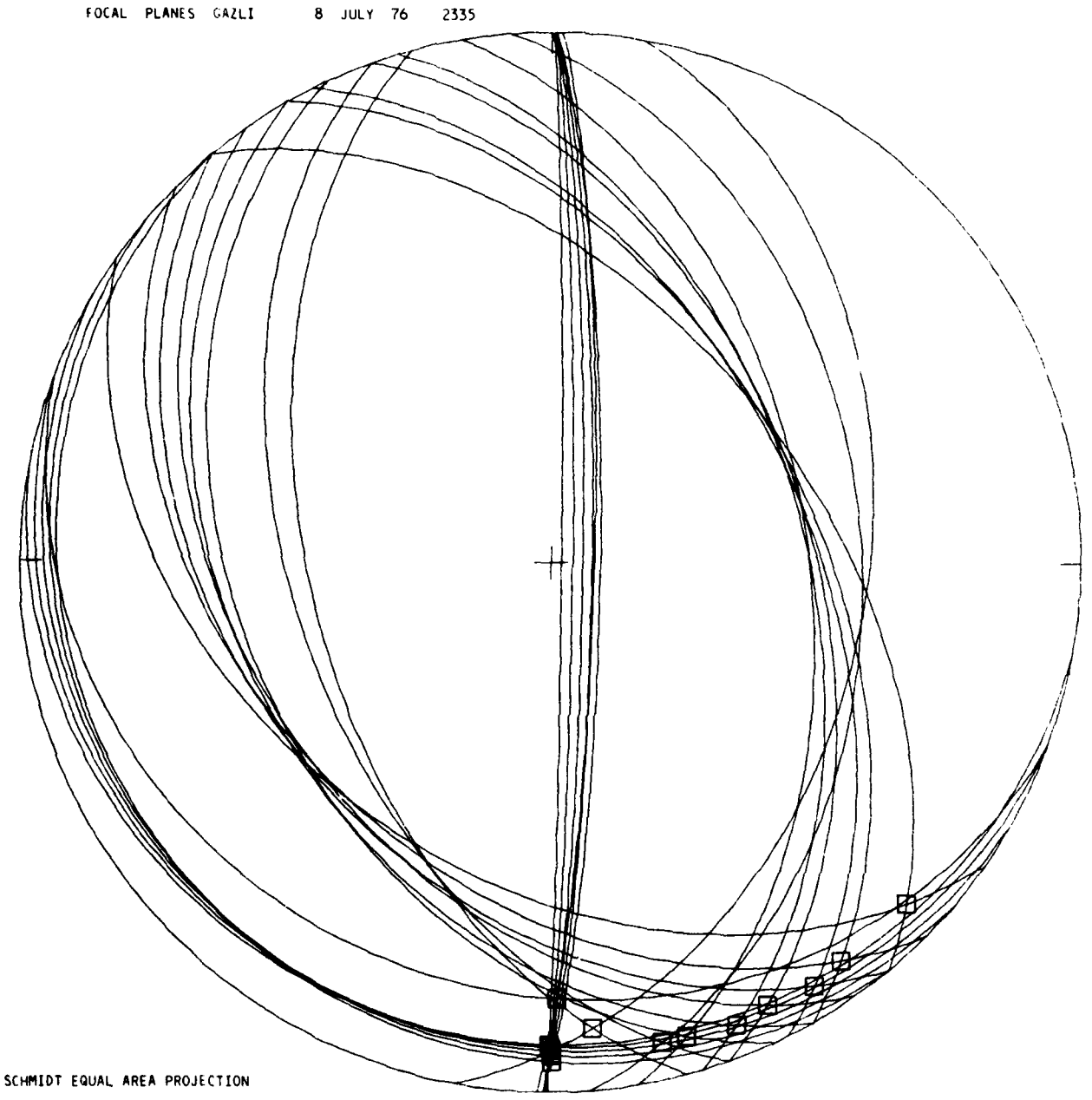

FIGURE 22(d)

(equivalent to figure 22(c))

EVENT NO. 58: 22 September 1976 21-49-42.6
DEPTH DEDUCED BY MODELLING: 12.84 km
MAGNITUDE m_b (NEIS): 4.7

SOURCE ORIENTATION USED IN MODEL:
Dip - 130°
Slip Angle - 90°
Strike - 130°

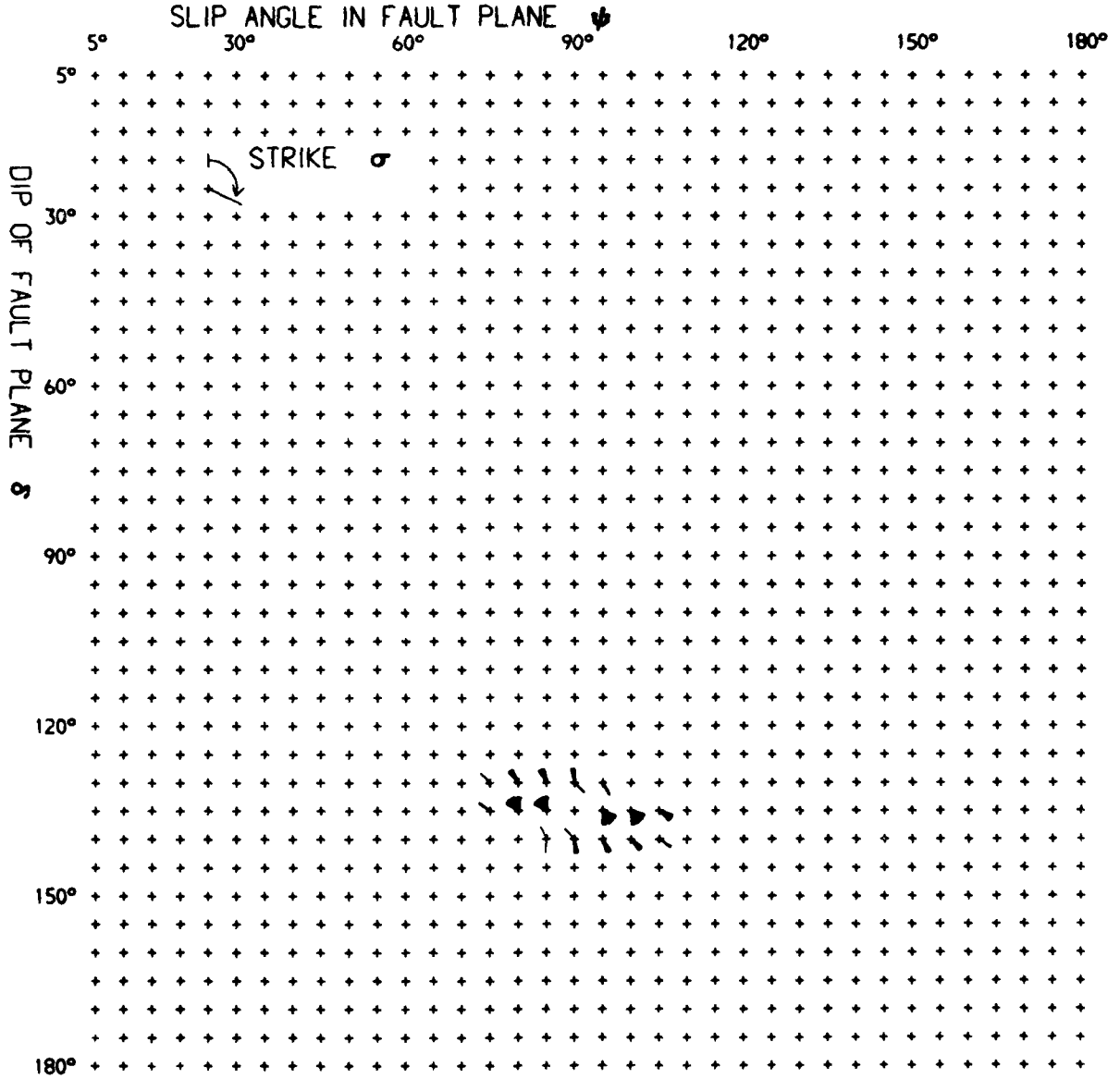

22 September 1976 21-49-42.6
(with no allowance for velocity structure)
Number of compatible orientations = 106

FIGURE 23(a)

AD-A089 512 ATOMIC WEAPONS RESEARCH ESTABLISHMENT ALDERMASTON (EN--ETC F/G 8/11
THE 1976 EARTHQUAKE SEQUENCE IN UZBEKISTAN - FOCAL MECHANISMS D--ETC(U)
JUL 80 R G PEARCE, H BAINBRIDGE, P F KEY
UNCLASSIFIED AWRE-027/80 DRIC-BR-74998 NL

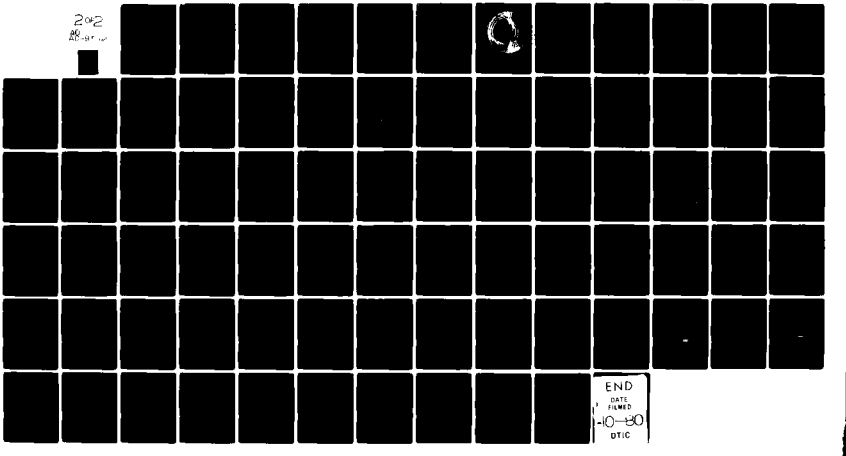

END
DATE FILMED
10-80
DTIC

EVENT NO. 58 (CATEGORY 2)

22 September 1976 21-49-42.6

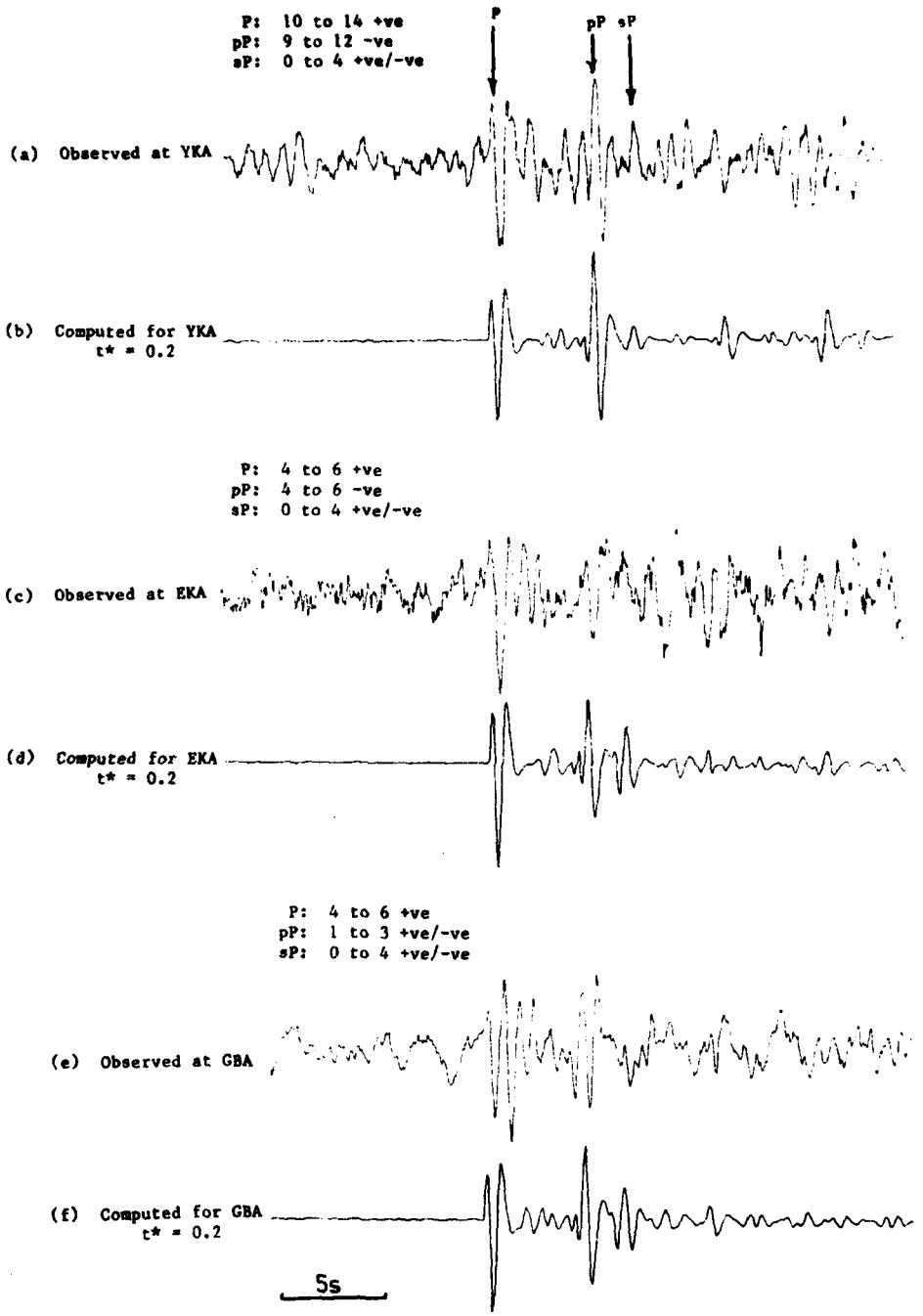

FIGURE 23(b)

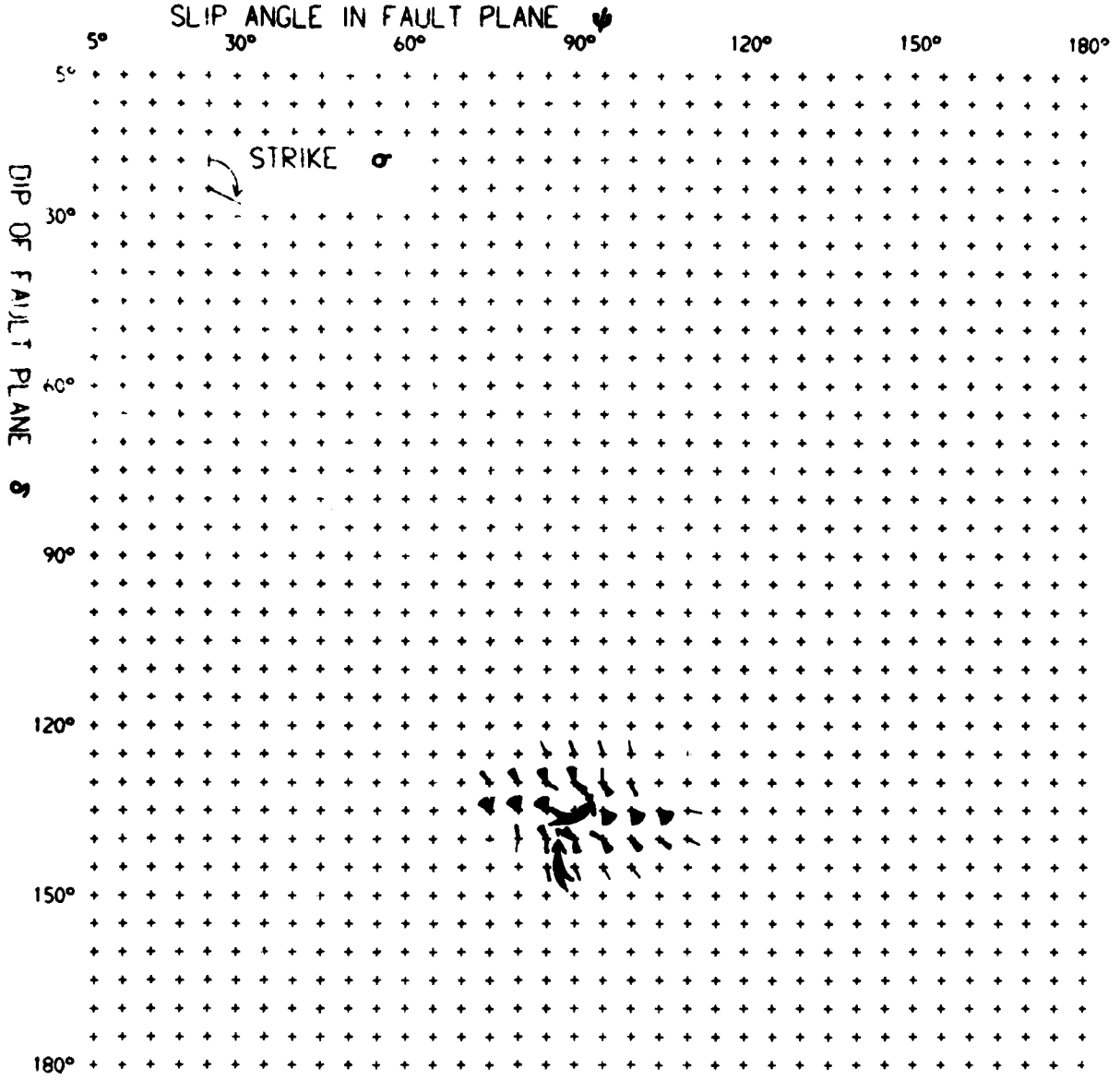

22 September 1976 21-49-42.6

(with allowance for velocity structure)

Number of compatible orientations = 200

FIGURE 23(c)

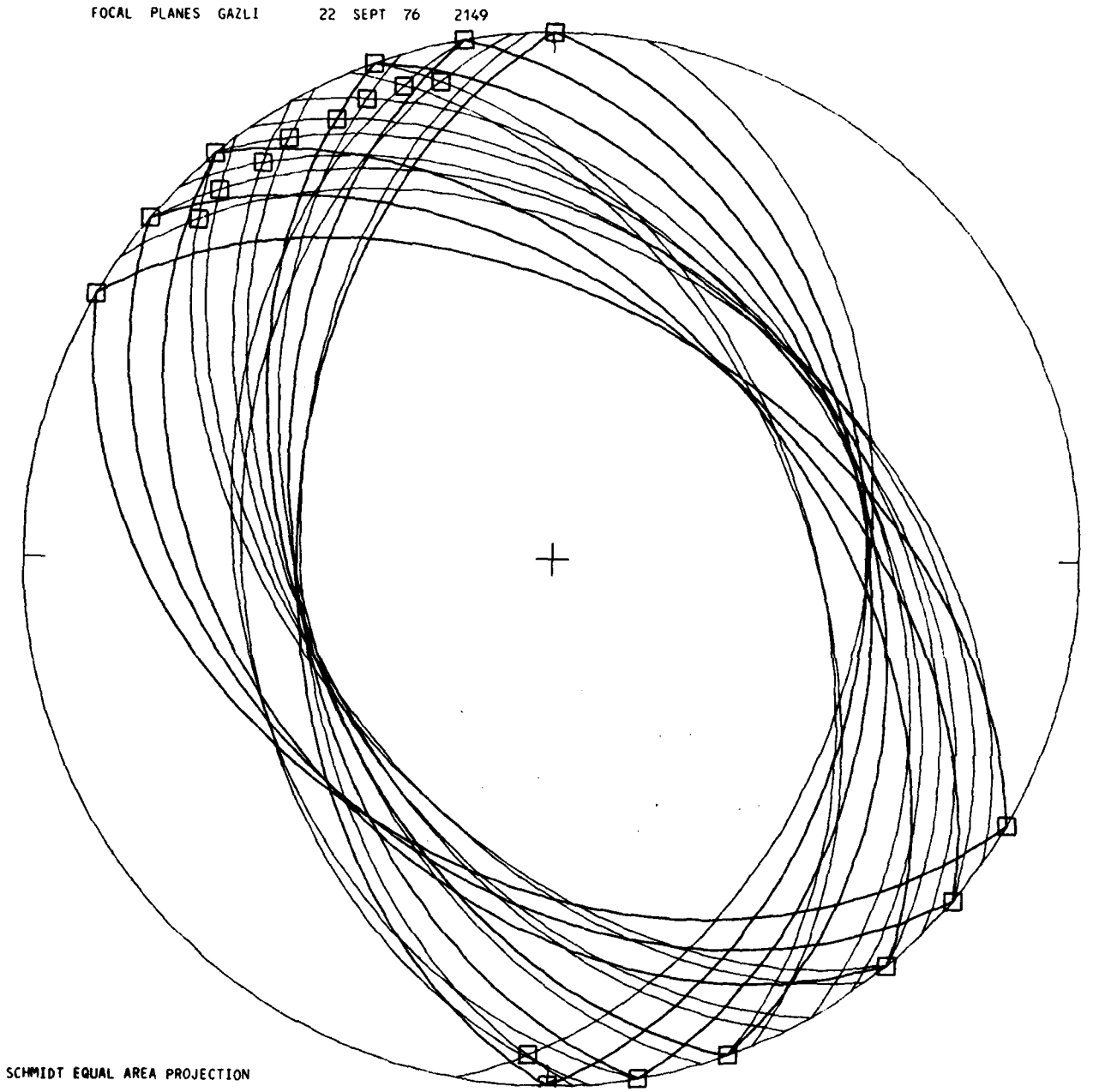

FIGURE 23(d)

(equivalent to figure 23(d))

EVENT NO. 34:	**17 May 1976**	**04-53-51.7**
DEPTH DEDUCED BY MODELLING:	**6.1 km**	
MAGNITUDE m_b (NEIS):	**4.7**	
SOURCE ORIENTATION USED IN MODEL:	**Dip - 95°**	
	Slip Angle - 180°	
	Strike - 275°	

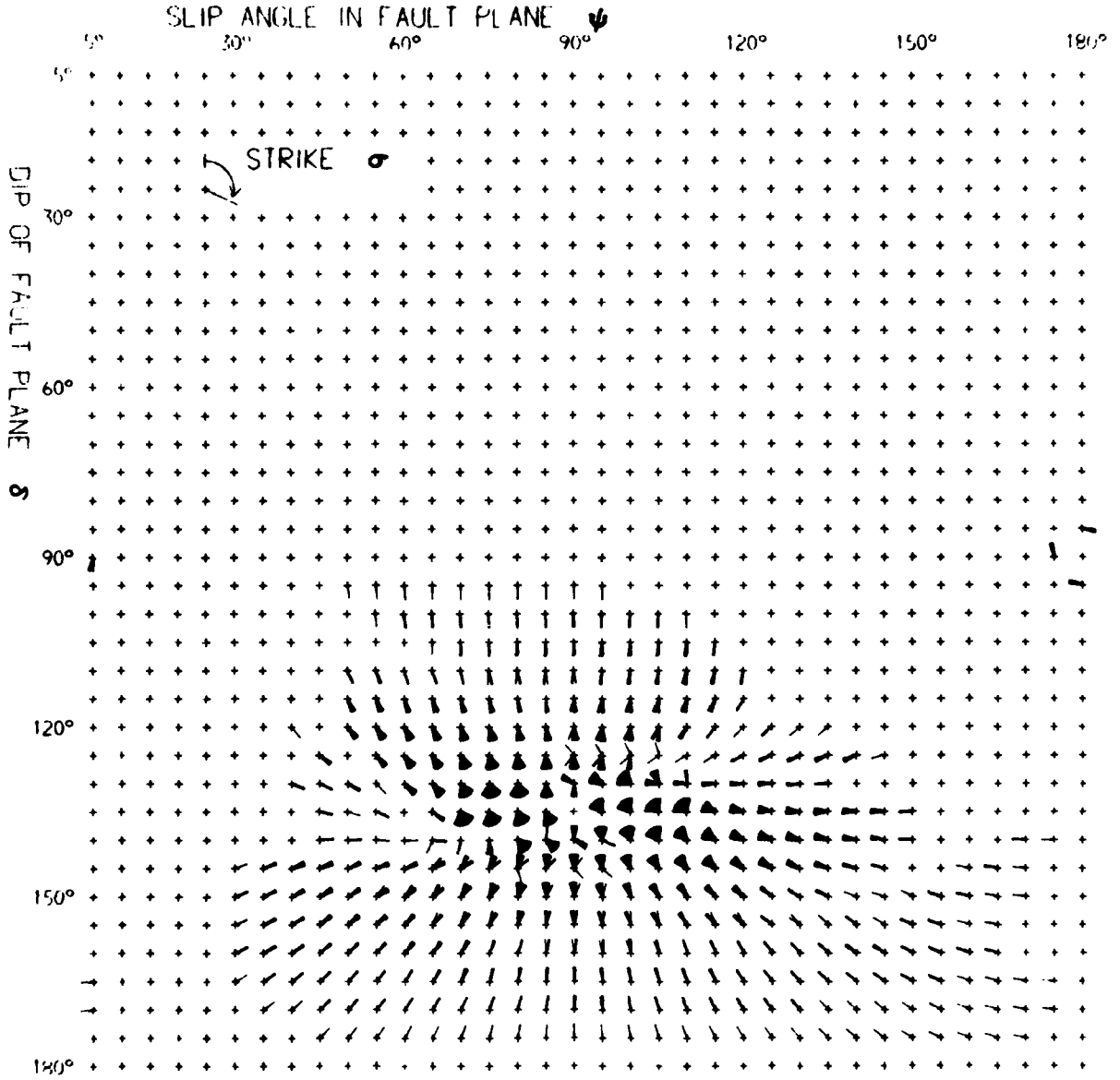

17 May 1976 04-53-51.7

(with no allowance for velocity structure)

Number of compatible orientations = 1612

FIGURE 24(a)

EVENT NO. 34 (CATEGORY 2)

17 May 1976 04-53-51.7

(strike-slip orientation)

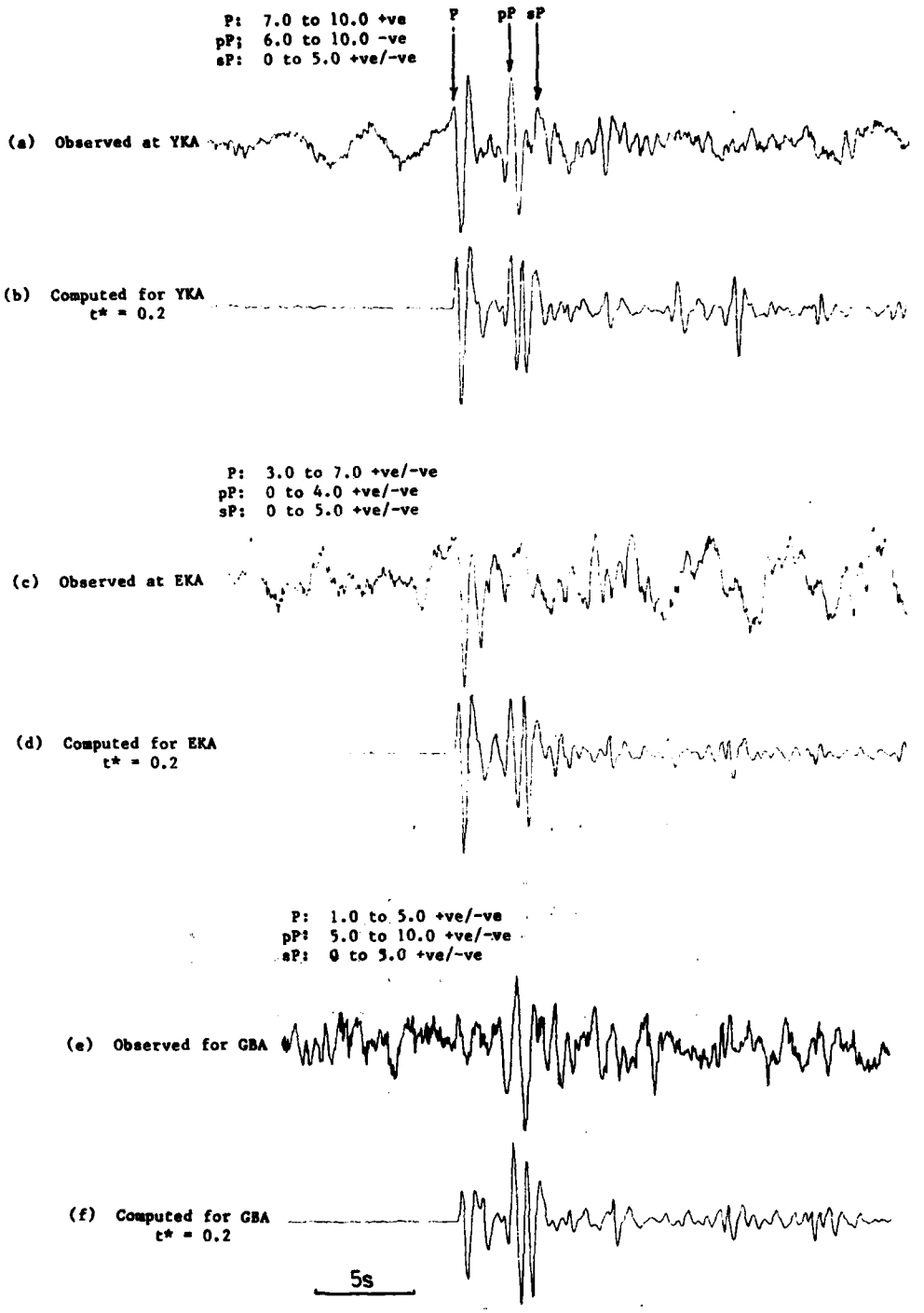

FIGURE 24(b)

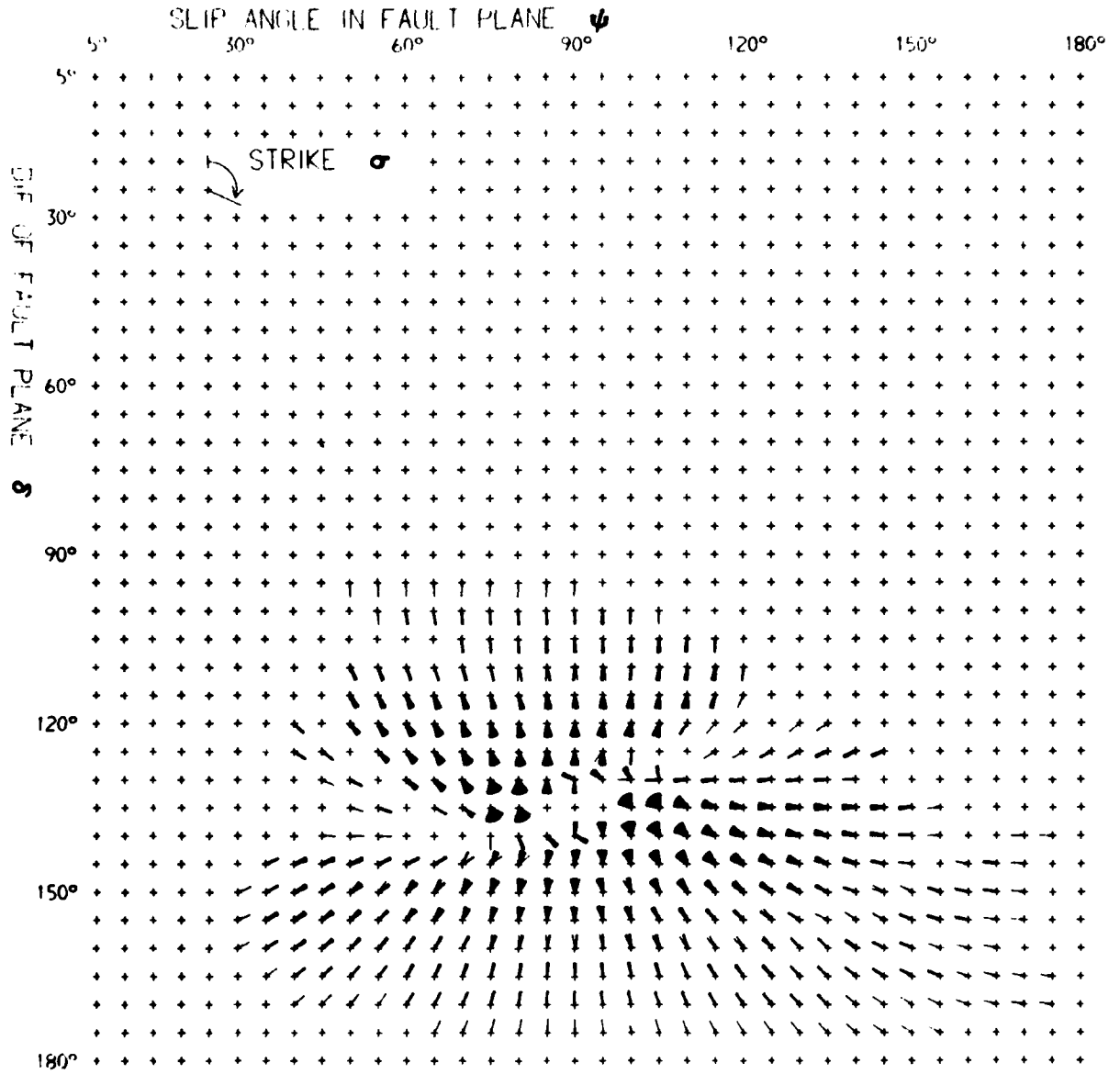

17 May 1976 04-53-51.7

(with allowance for velocity structure)

Number of compatible orientations = 1323

FIGURE 24(c)

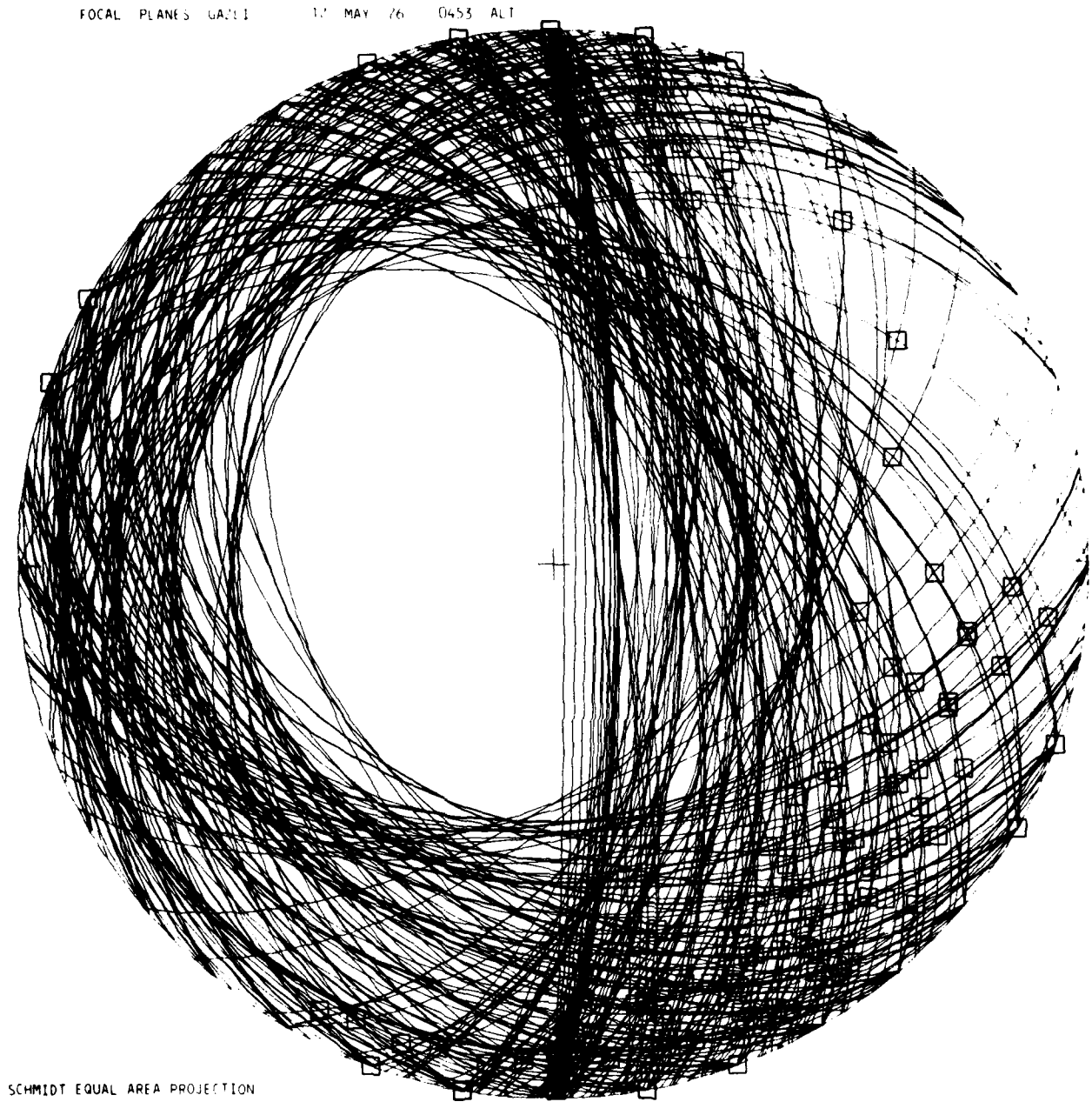

FIGURE 24(d)

(equivalent to figure 24(c))

EVENT NO. 1 - CATEGORY 1

8 April 1976 02-40-27.0

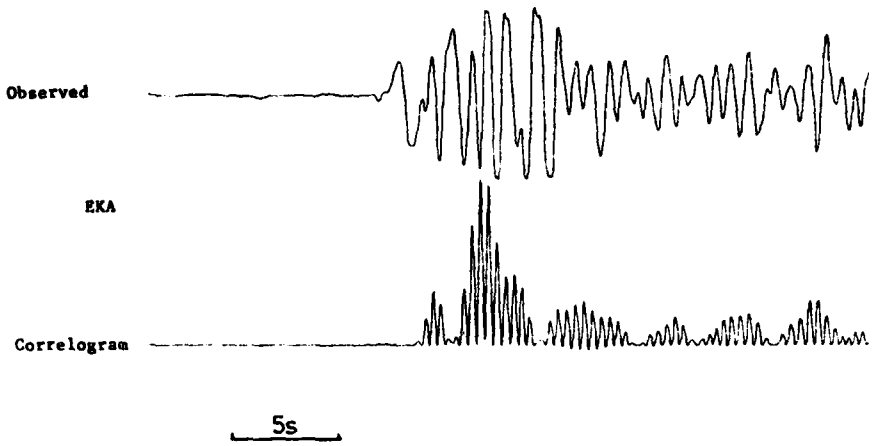

FIGURE 25

(Seismograms were recorded at the other arrays but were overloaded. This also applies to all four array seismograms for Event 2.)

EVENT NO. 5 - CATEGORY 5

8 April 1976 04-46-08.9

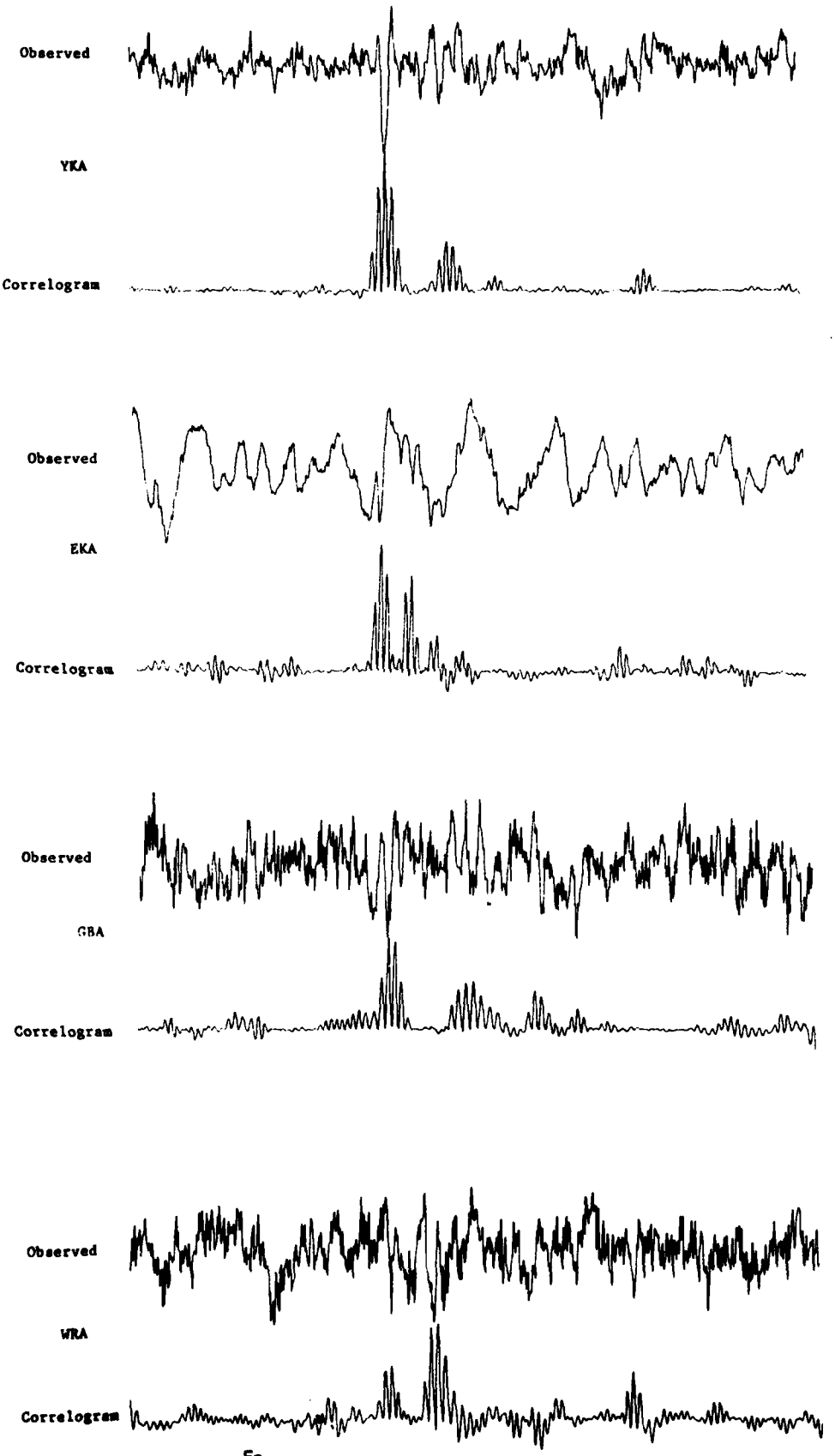

FIGURE 26

EVENT NO. 6 - CATEGORY 5

8 April 1976 04-58-53.9

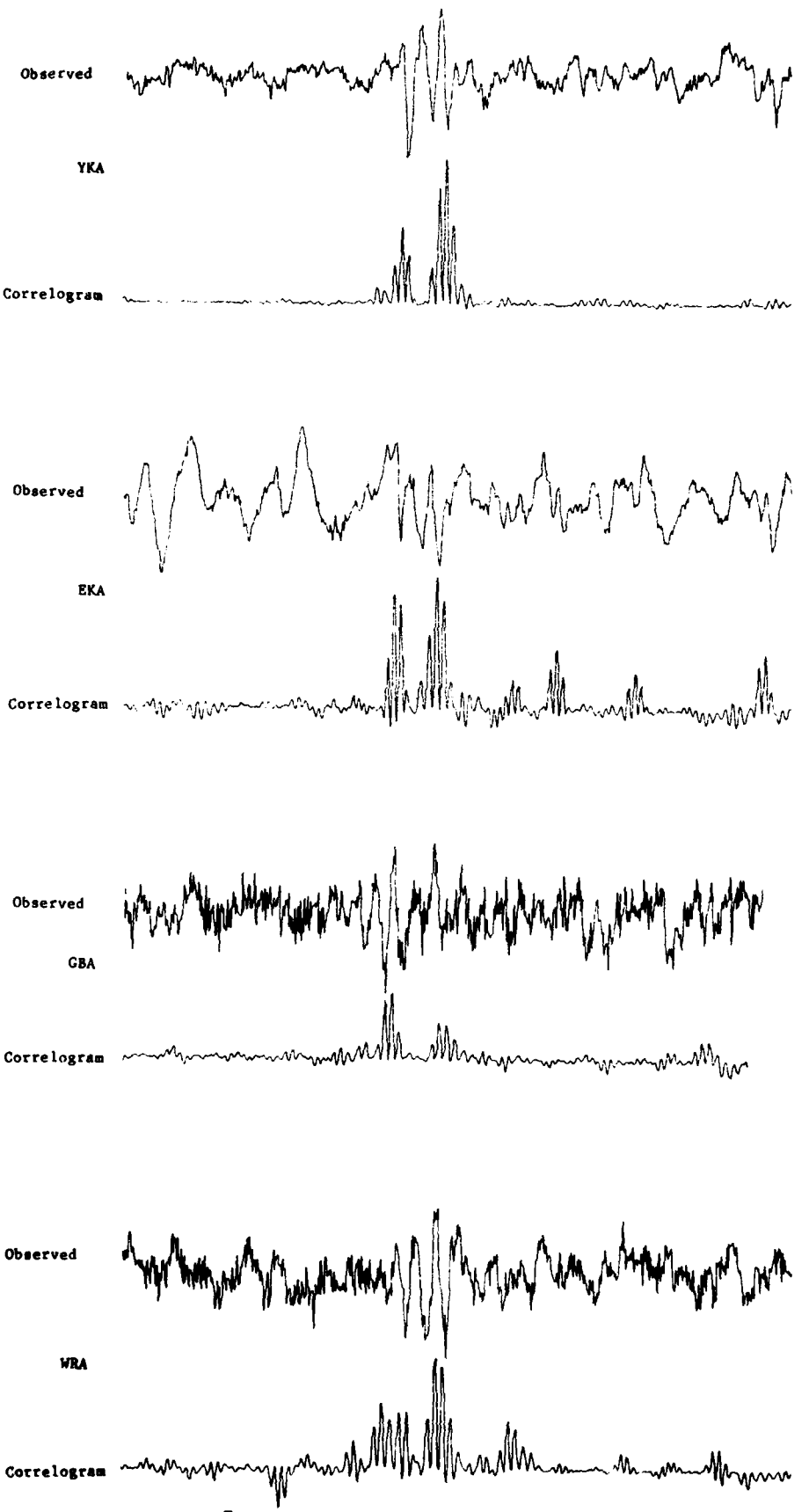

FIGURE 27

EVENT NO. 10 - CATEGORY 5

8 April 1976 22-54-17.8

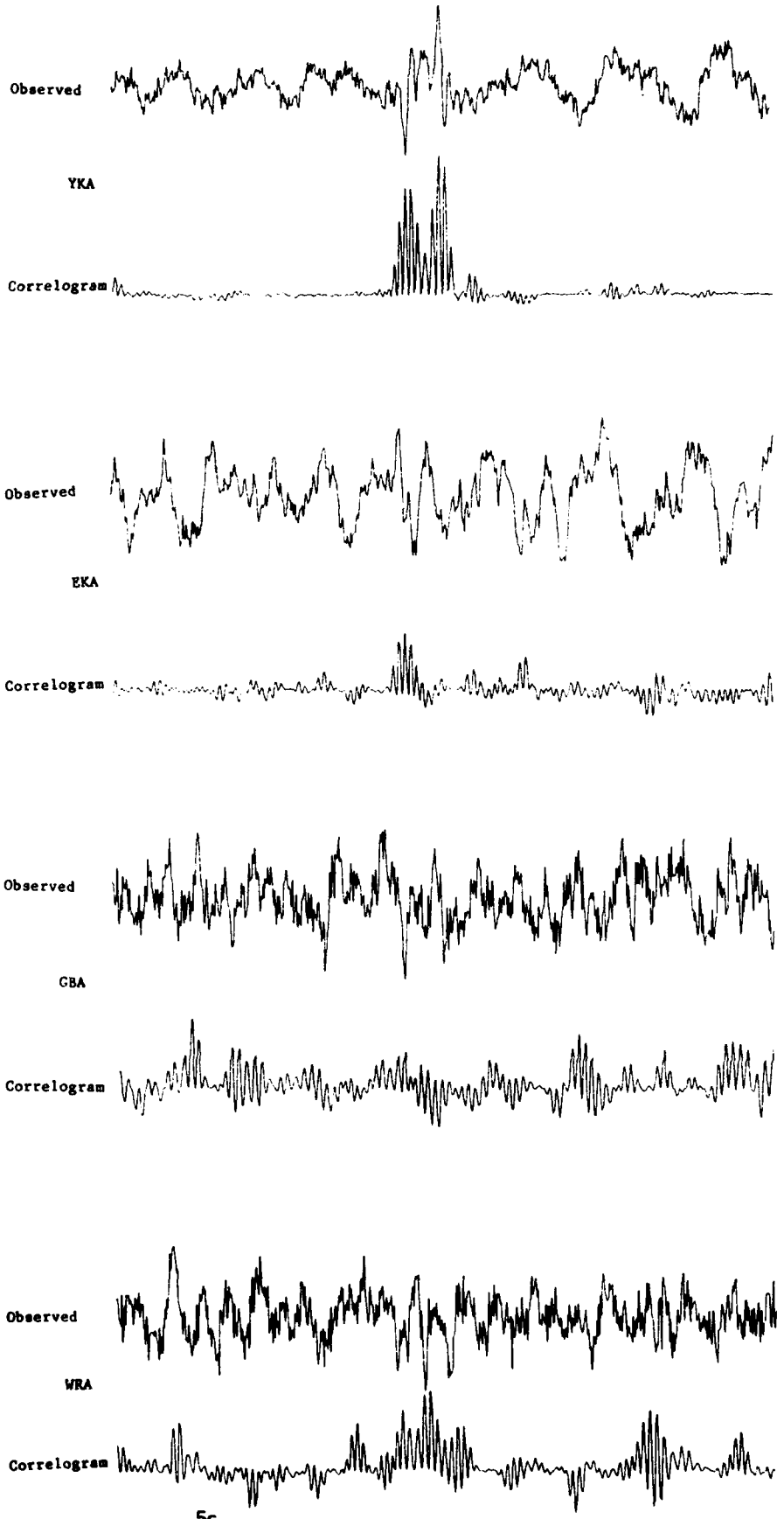

FIGURE 28

EVENT NO. 11 - CATEGORY 5

9 April 1976 02-46-23.9

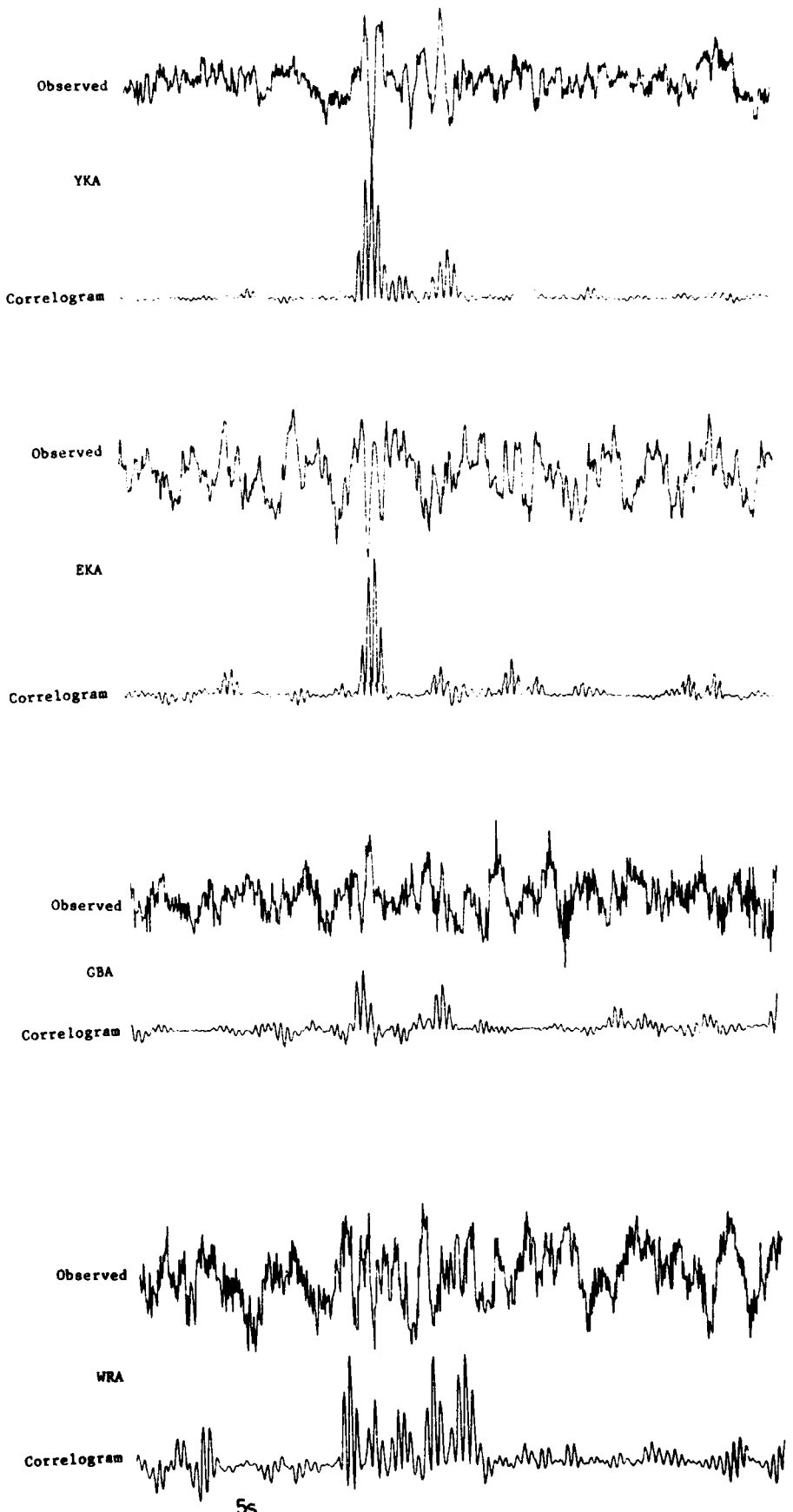

FIGURE 29

EVENT NO. 12 - CATEGORY 5

12 April 1976 06-35-23.5

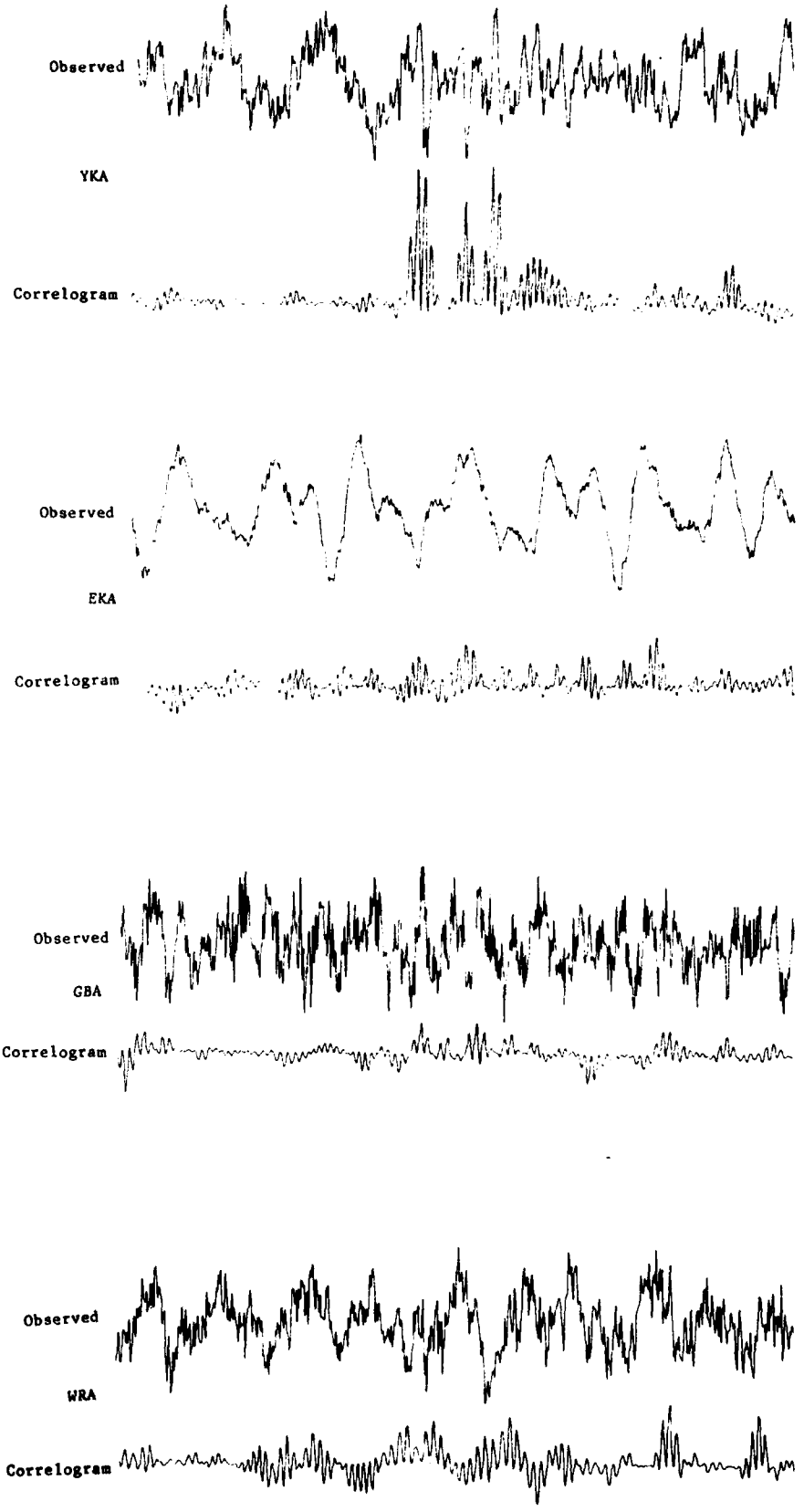

FIGURE 30

EVENT NO. 13 - CATEGORY 5

12 April 1976 16-12-58.9

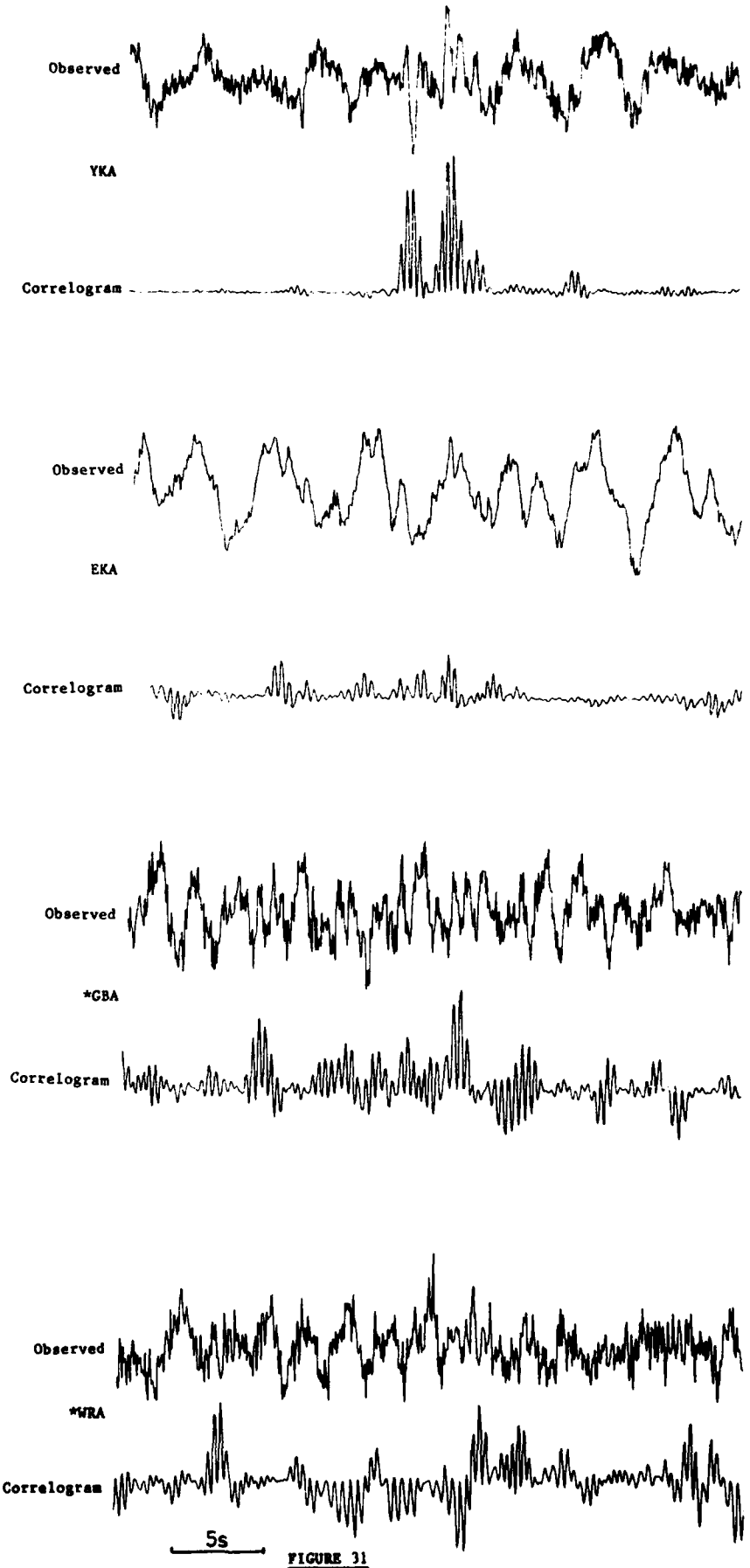

FIGURE 31

EVENT NO. 14 - CATEGORY 5

14 April 1976 07-51-06.5

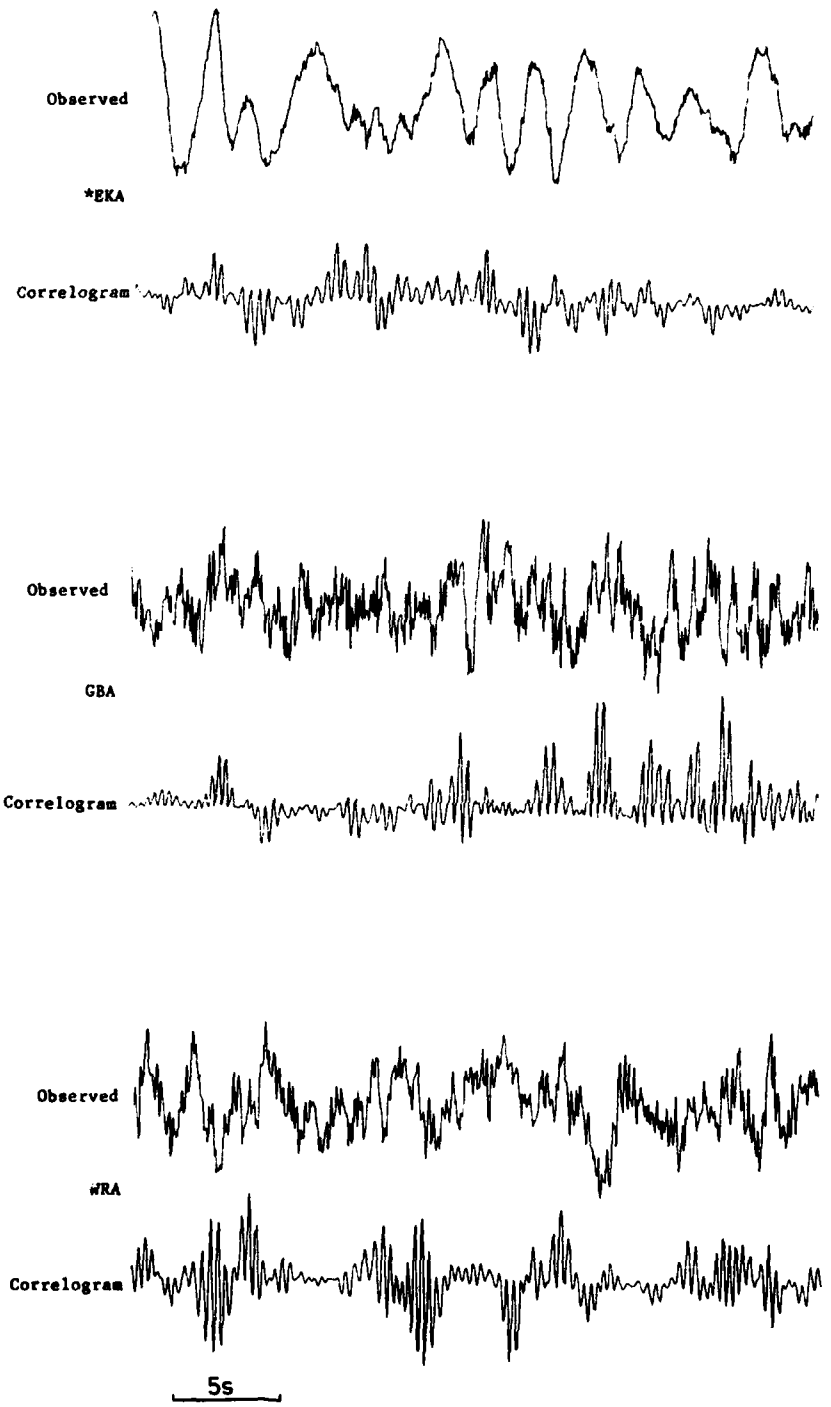

FIGURE 32

EVENT NO. 15 - CATEGORY 5

14 April 1976 19-26-55.8

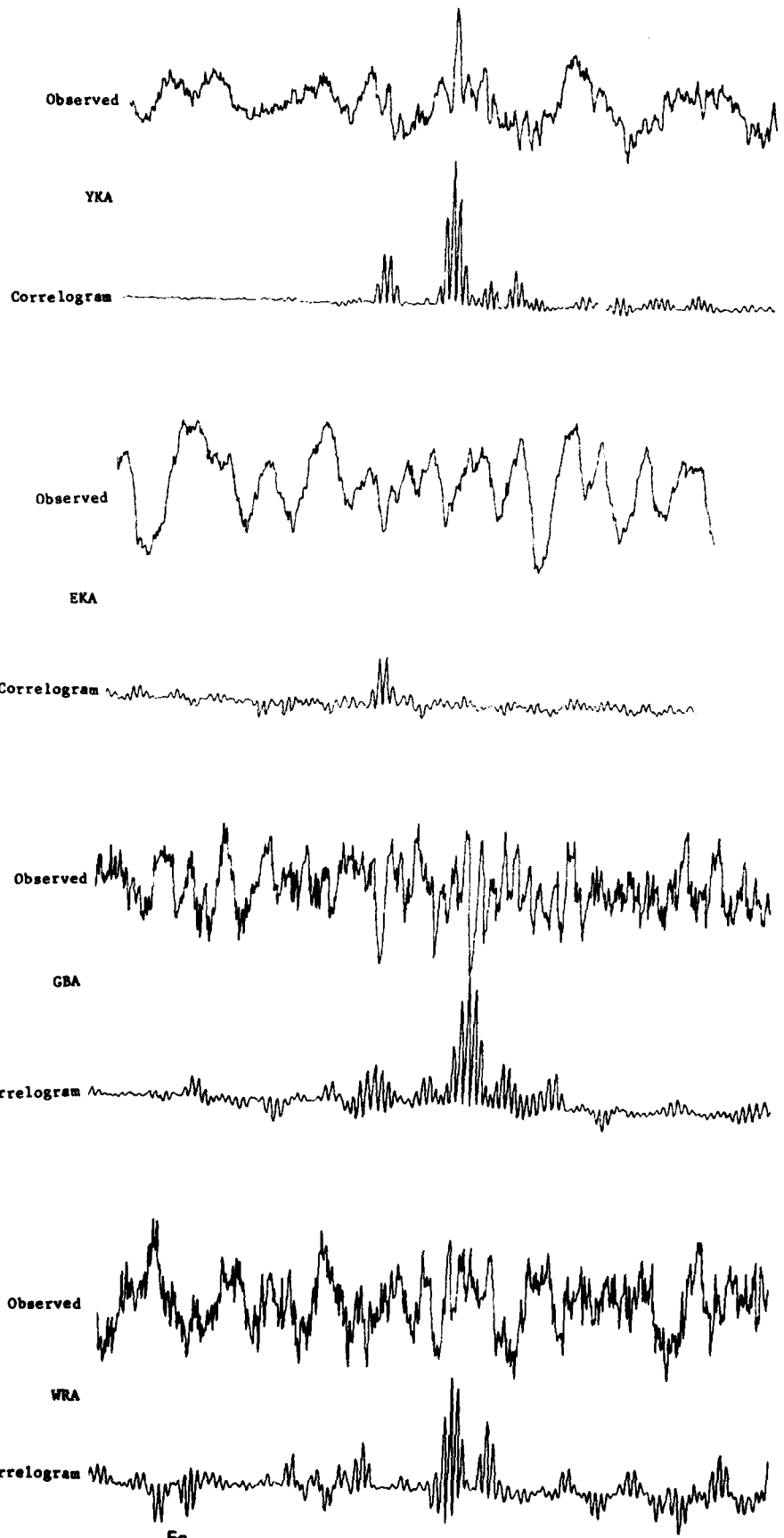

FIGURE 33

EVENT NO. 16 - CATEGORY 5

15 April 1976 06-15-21.1

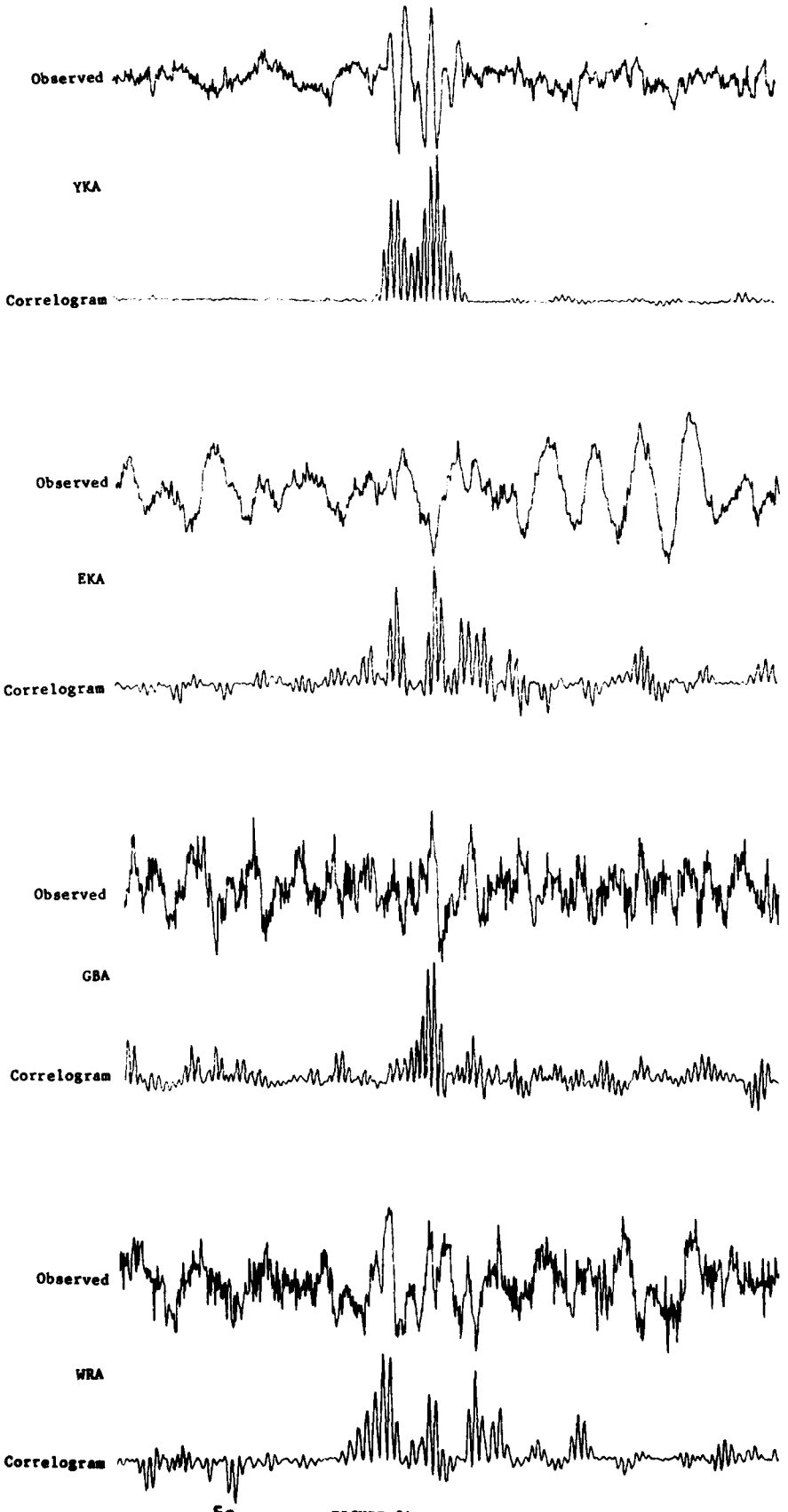

FIGURE 34

EVENT NO. 17 - CATEGORY 5

15 April 1976 16-35-15.7

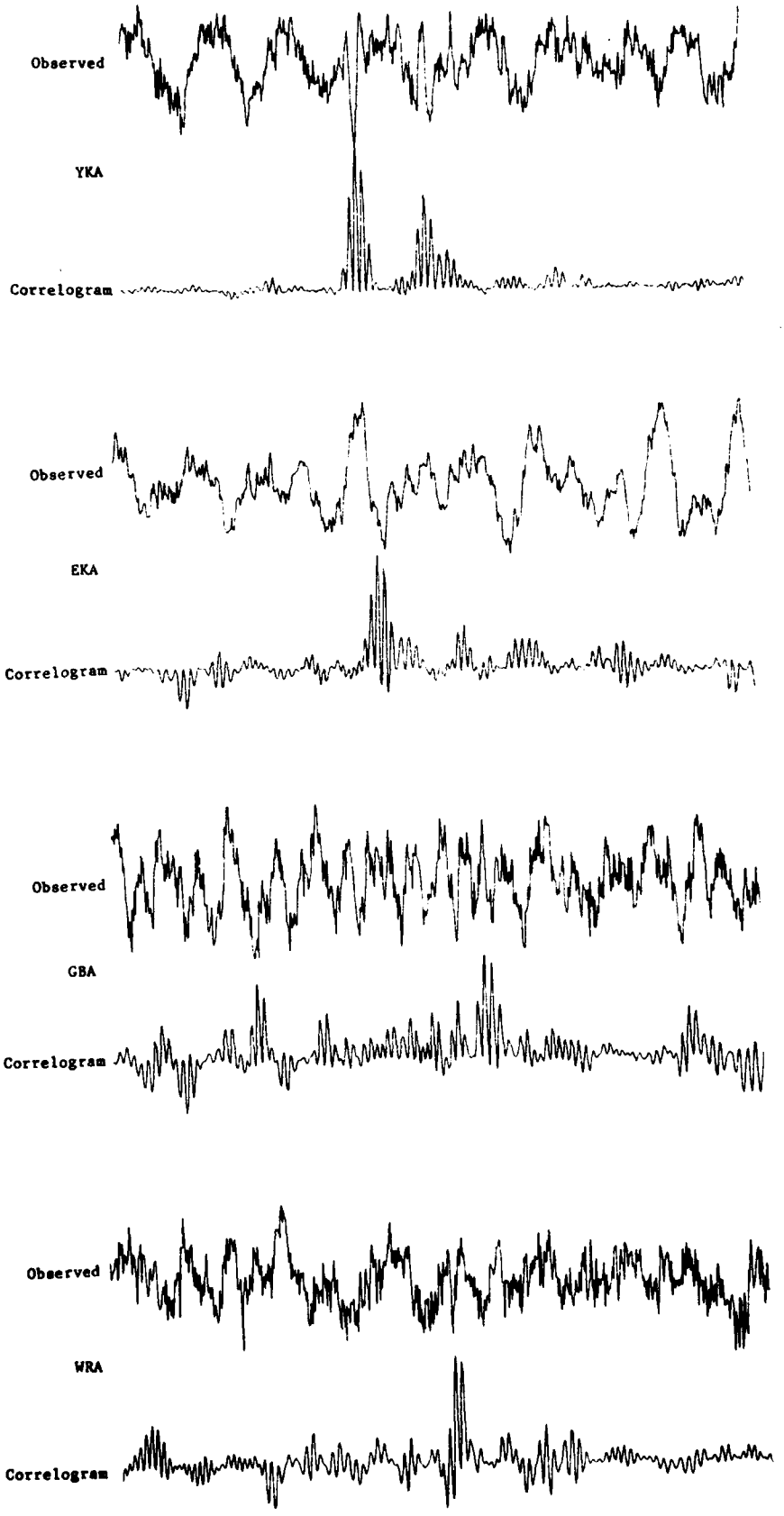

FIGURE 35

EVENT NO. 18 - CATEGORY 5

16 April 1976 02-36-45.8

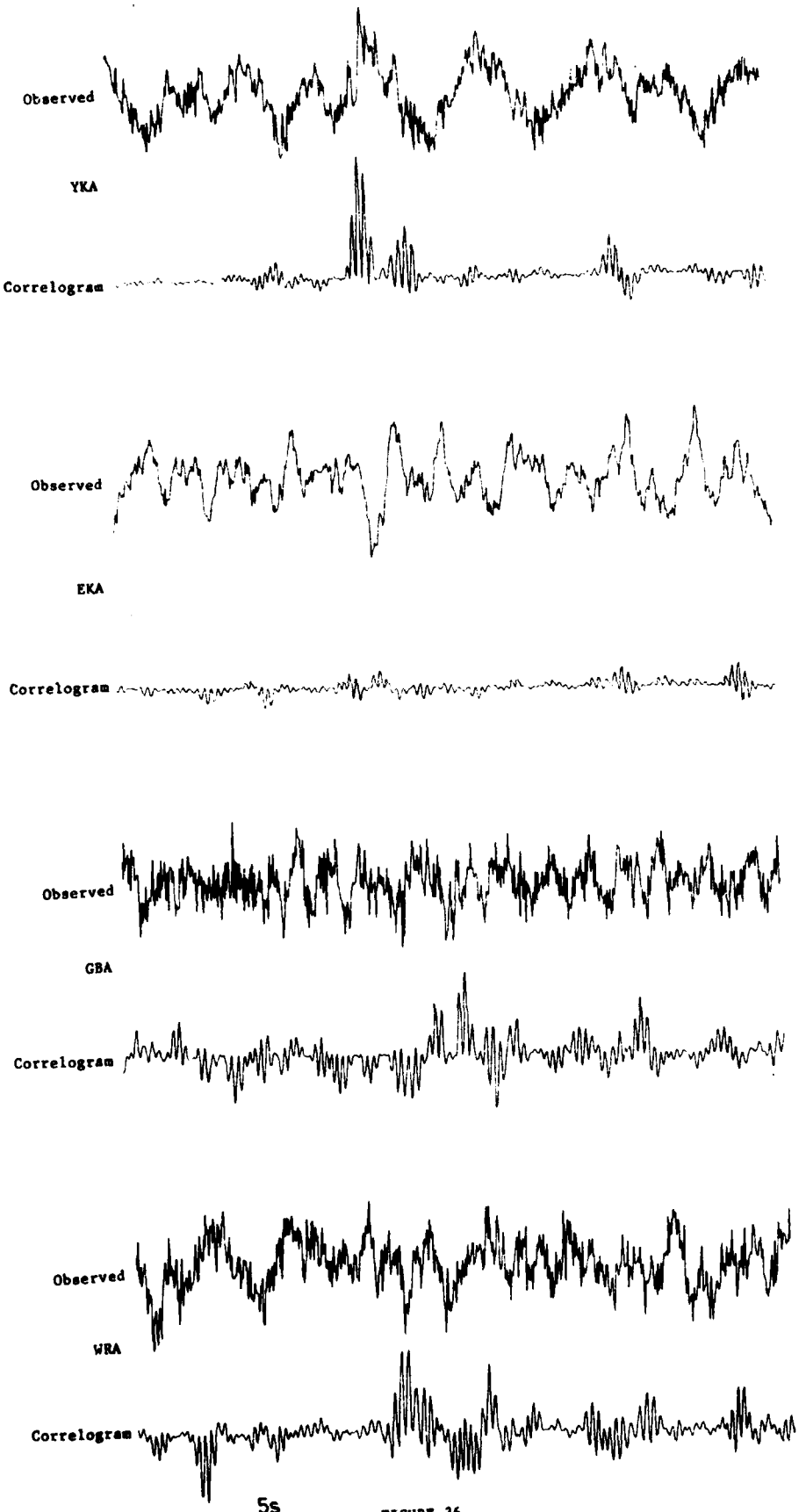

FIGURE 36

EVENT NO. 20 - CATEGORY 5

17 April 1976 13-47-55.1

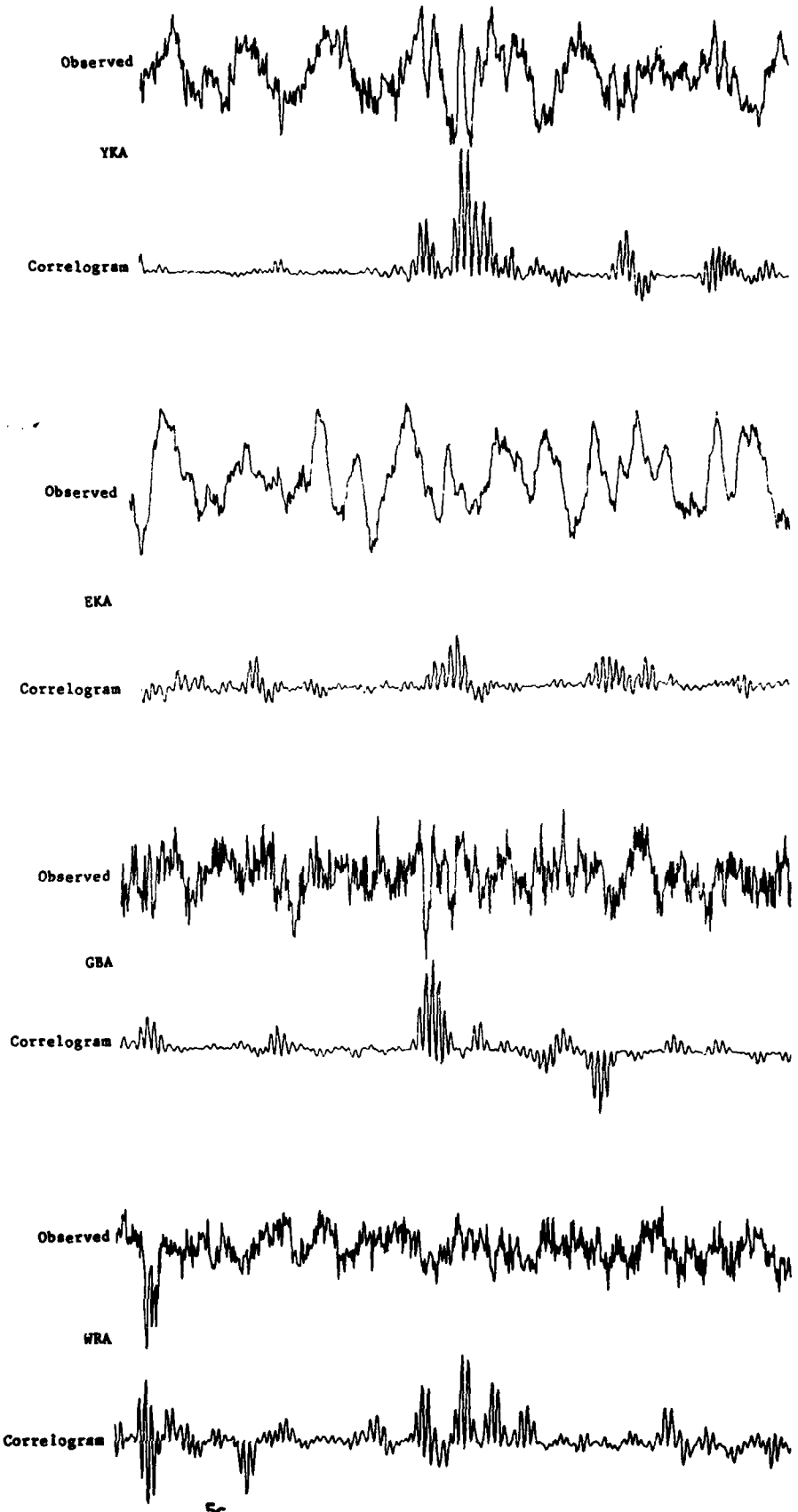

FIGURE 37

EVENT NO. 21 - CATEGORY 5

17 April 1976 20-21-47.2

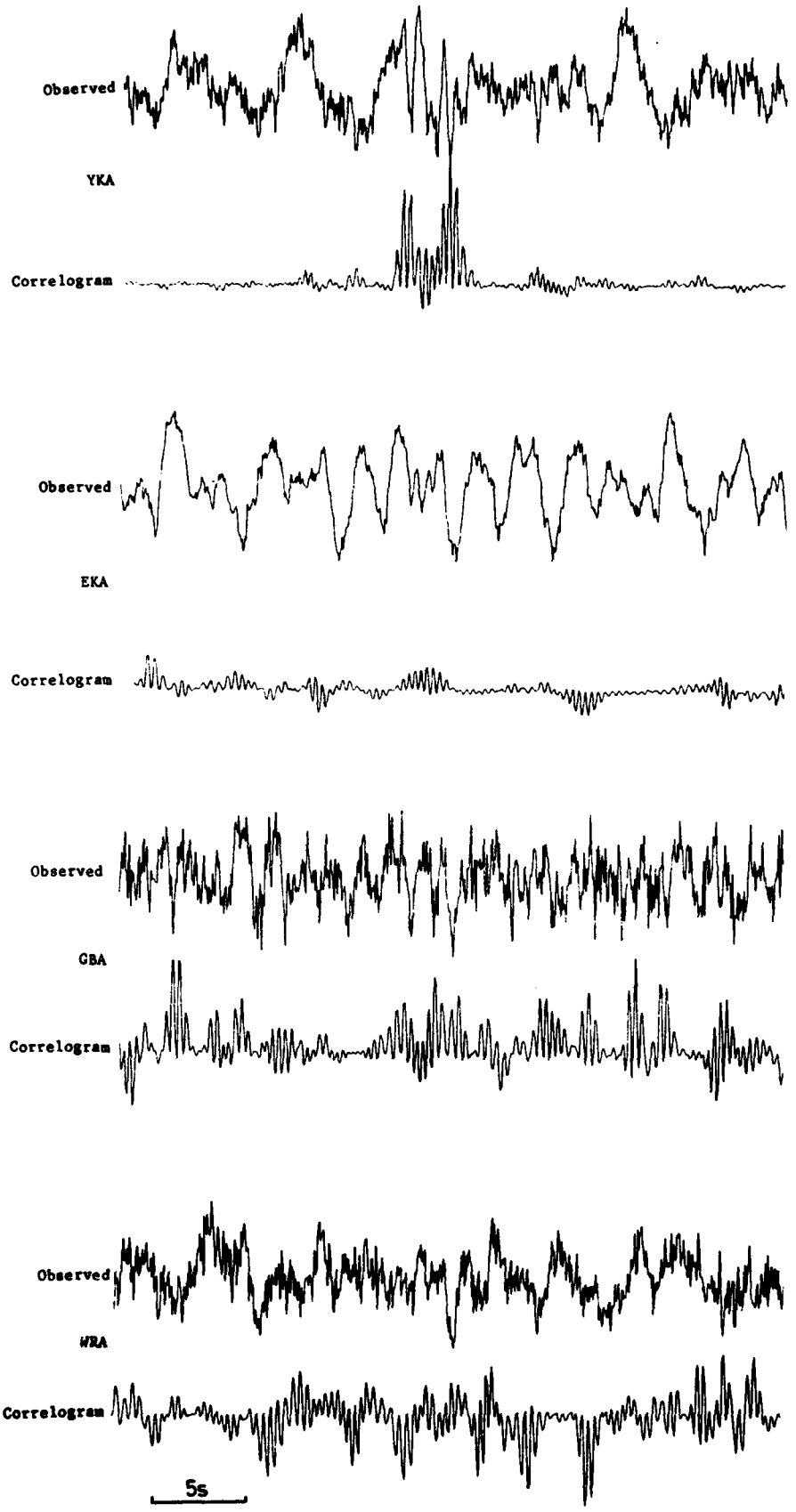

FIGURE 38

EVENT NO. 24 - CATEGORY 5

21 April 1976 22-33-29.8

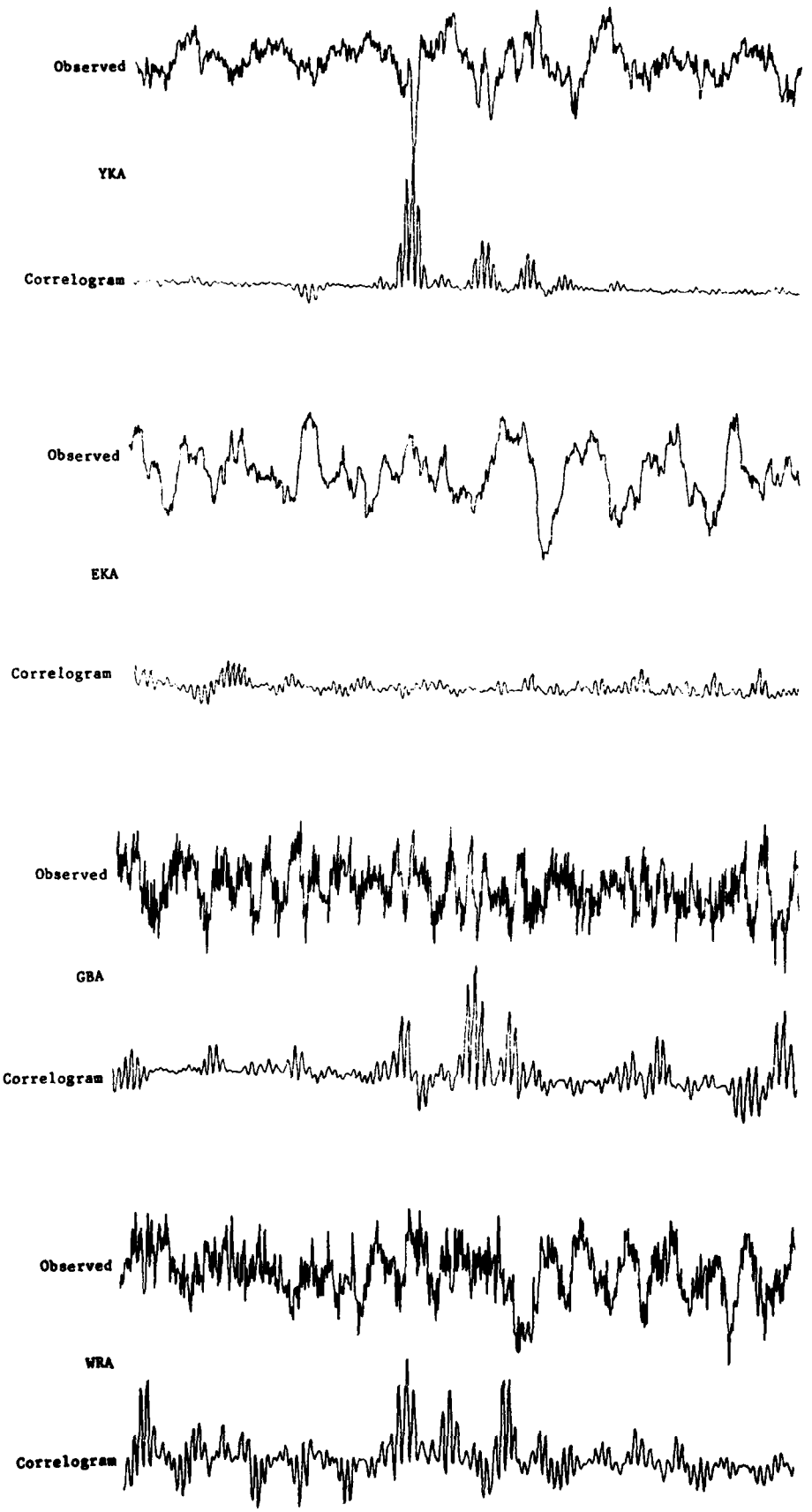

FIGURE 39

EVENT NO. 25 - CATEGORY 5

21 April 1976 23-18-33.9

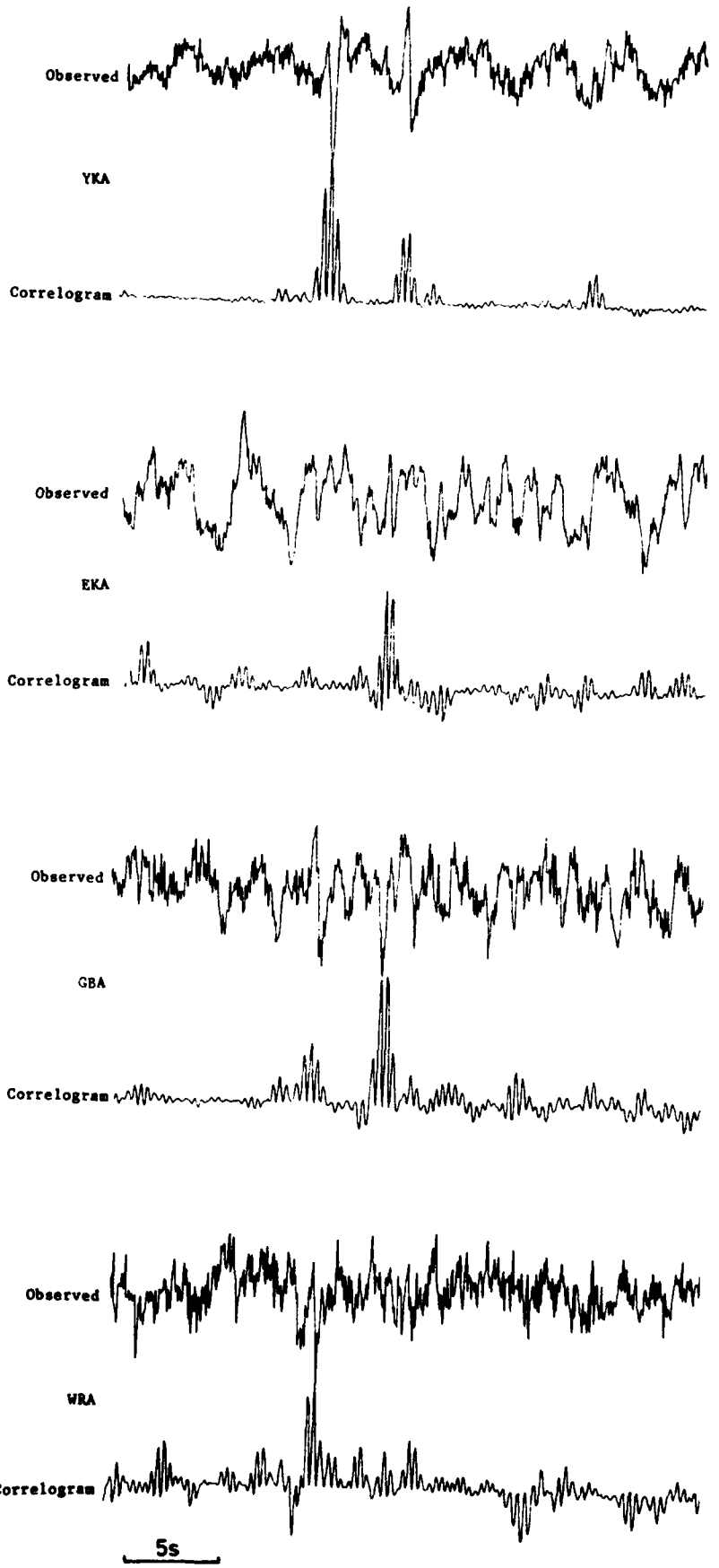

FIGURE 40

EVENT NO. 27 - CATEGORY 2 (See also Figure 80)

23 April 1976 20-55-31.7

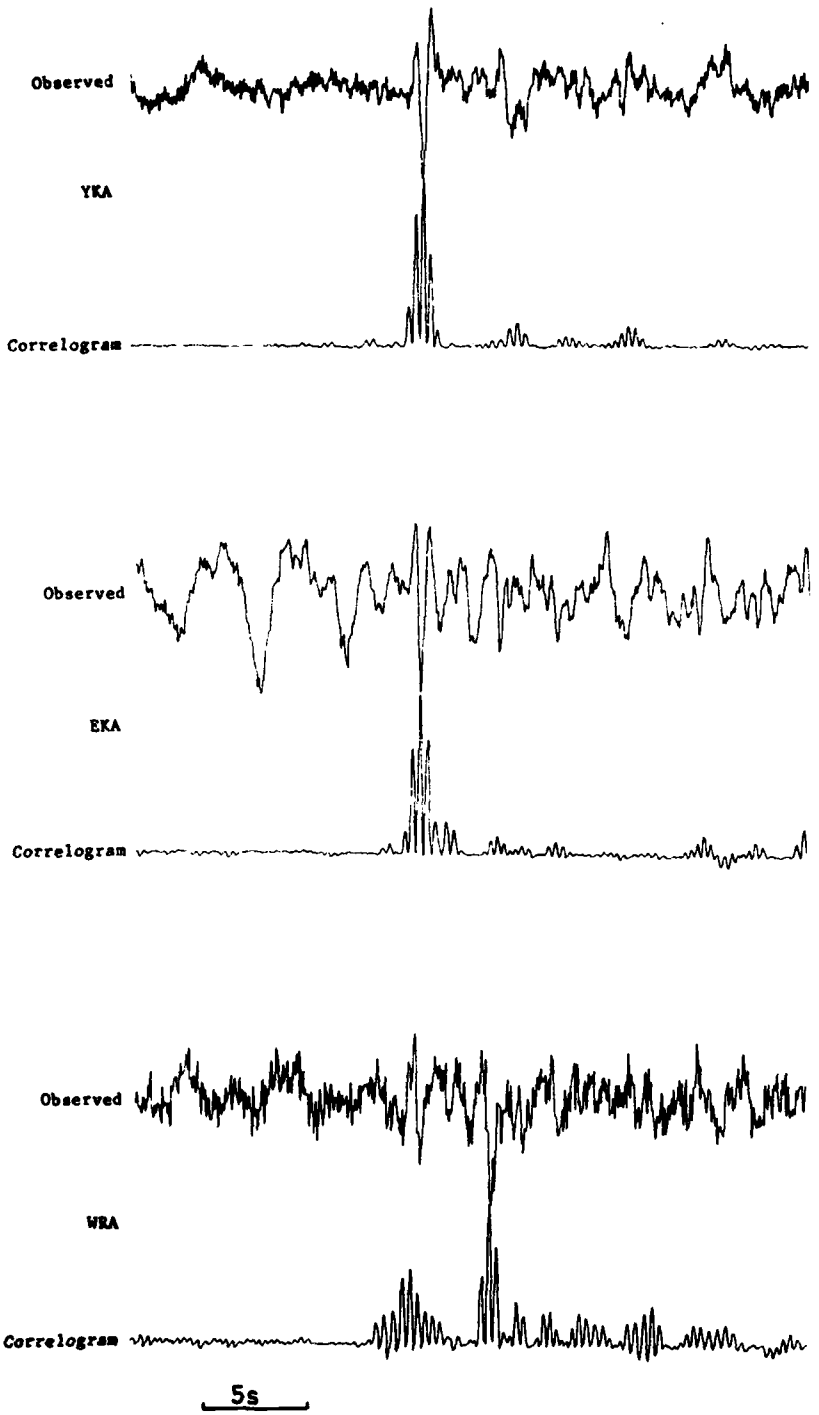

FIGURE 41

EVENT NO. 29 - CATEGORY 5

2 May 1976 15-41-36.7

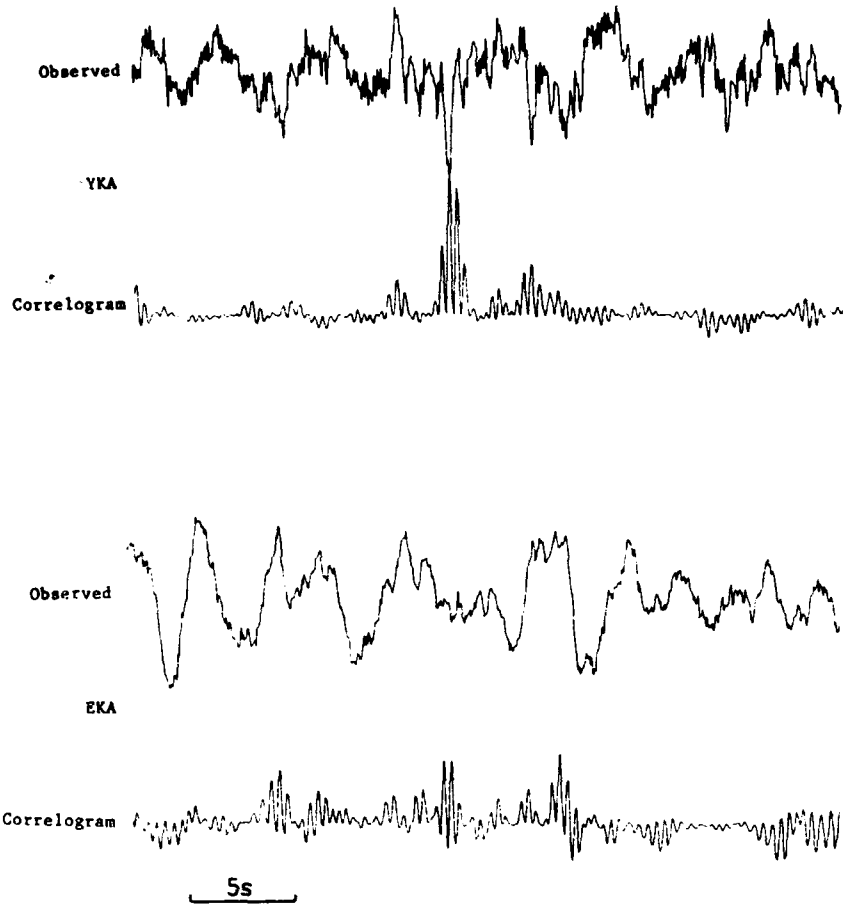

FIGURE 42

EVENT NO. 32 - CATEGORY 1

17 May 1976 02-58-40.6

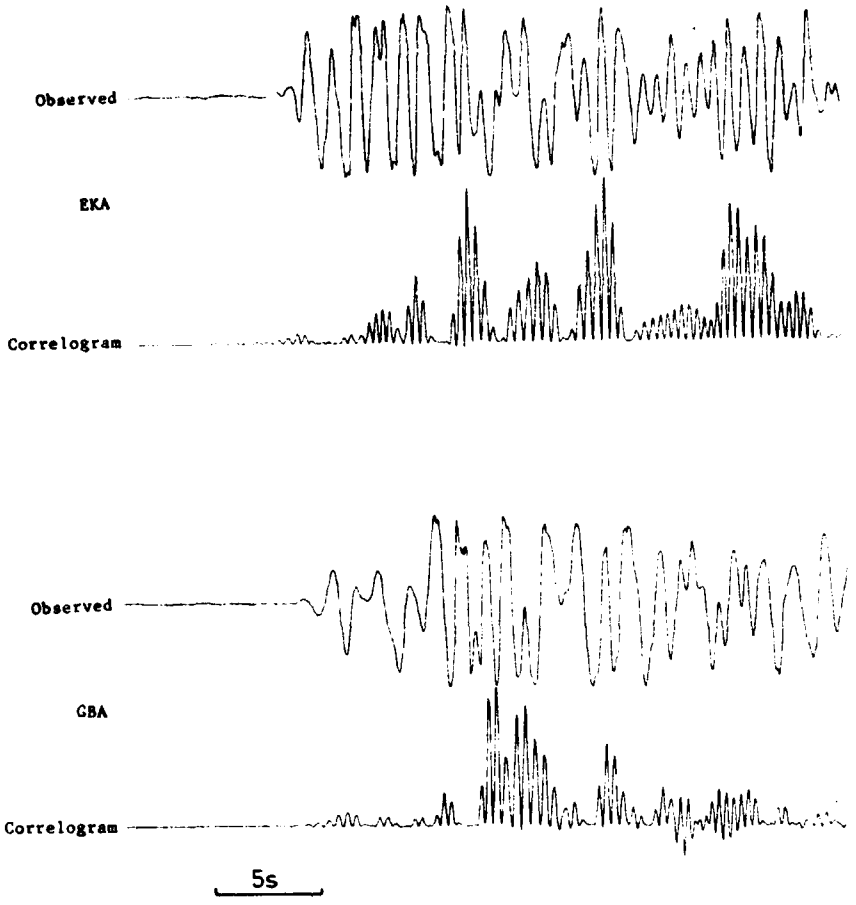

FIGURE 43

(YKA was available but overloaded)

EVENT NO. 33 - CATEGORY 4

17 May 1976 04-14-15.6

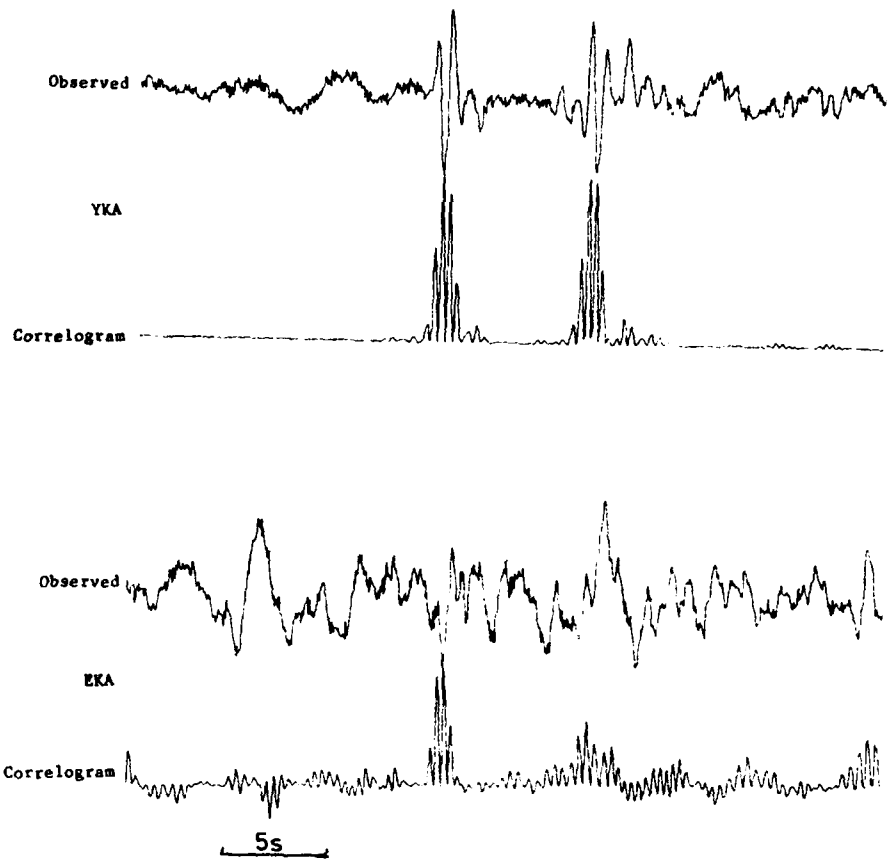

FIGURE 44

EVENT NO. 35 - CATEGORY 5

17 May 1976 11-01-26.3

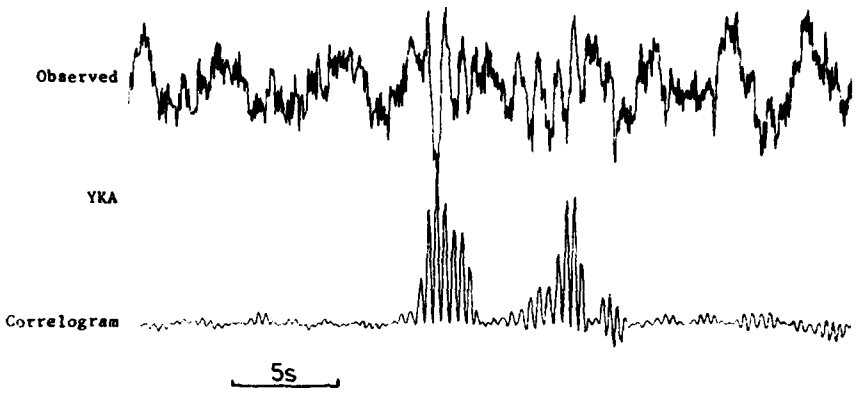

FIGURE 45

EVENT NO. 36 - CATEGORY 3

17 May 1976 17-46-17.2

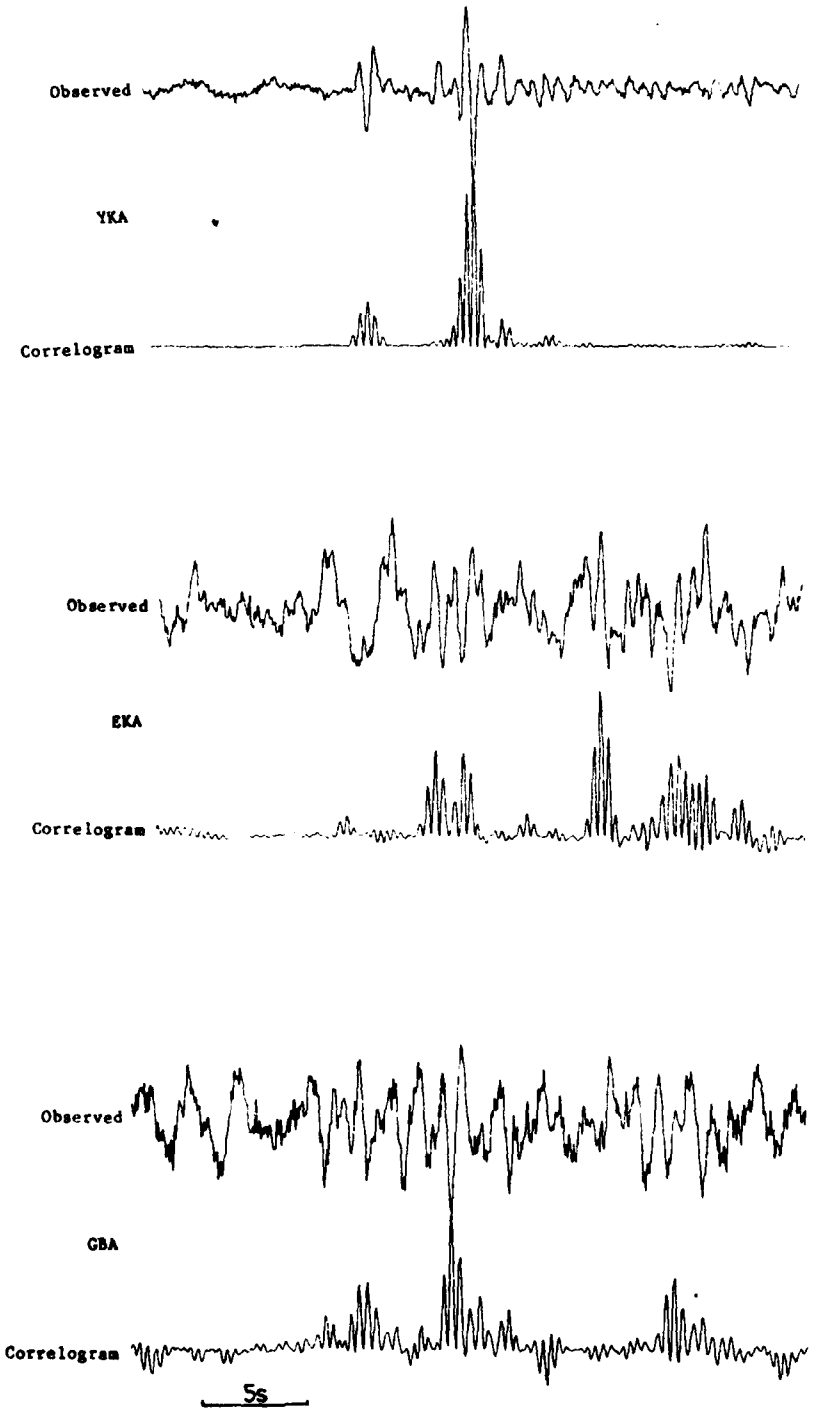

FIGURE 46

EVENT NO. 37 -CATEGORY 3

18 May 1976 04-16-25.9

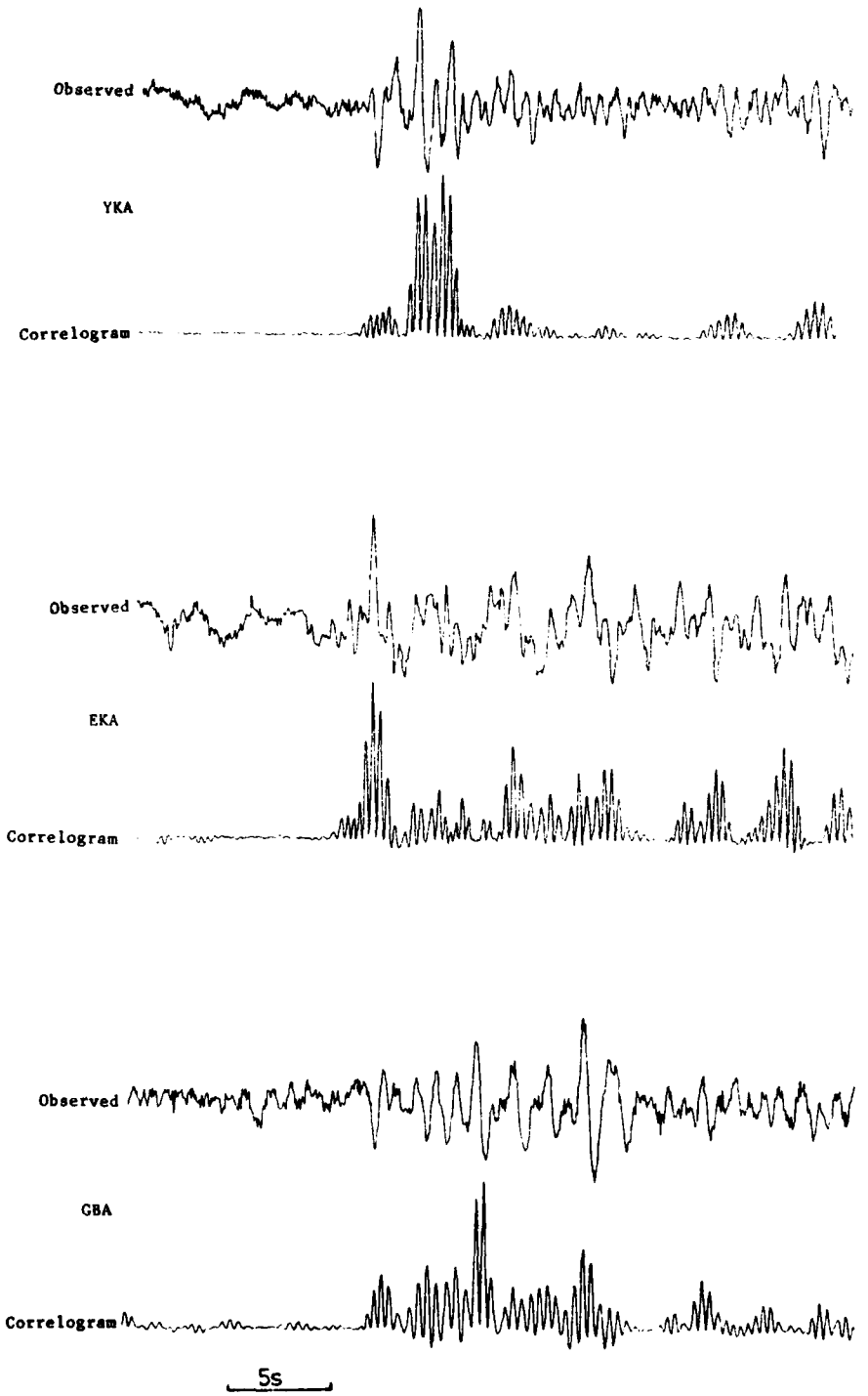

FIGURE 47

EVENT NO. 38 - CATEGORY 3

18 May 1976 08-57-29.4

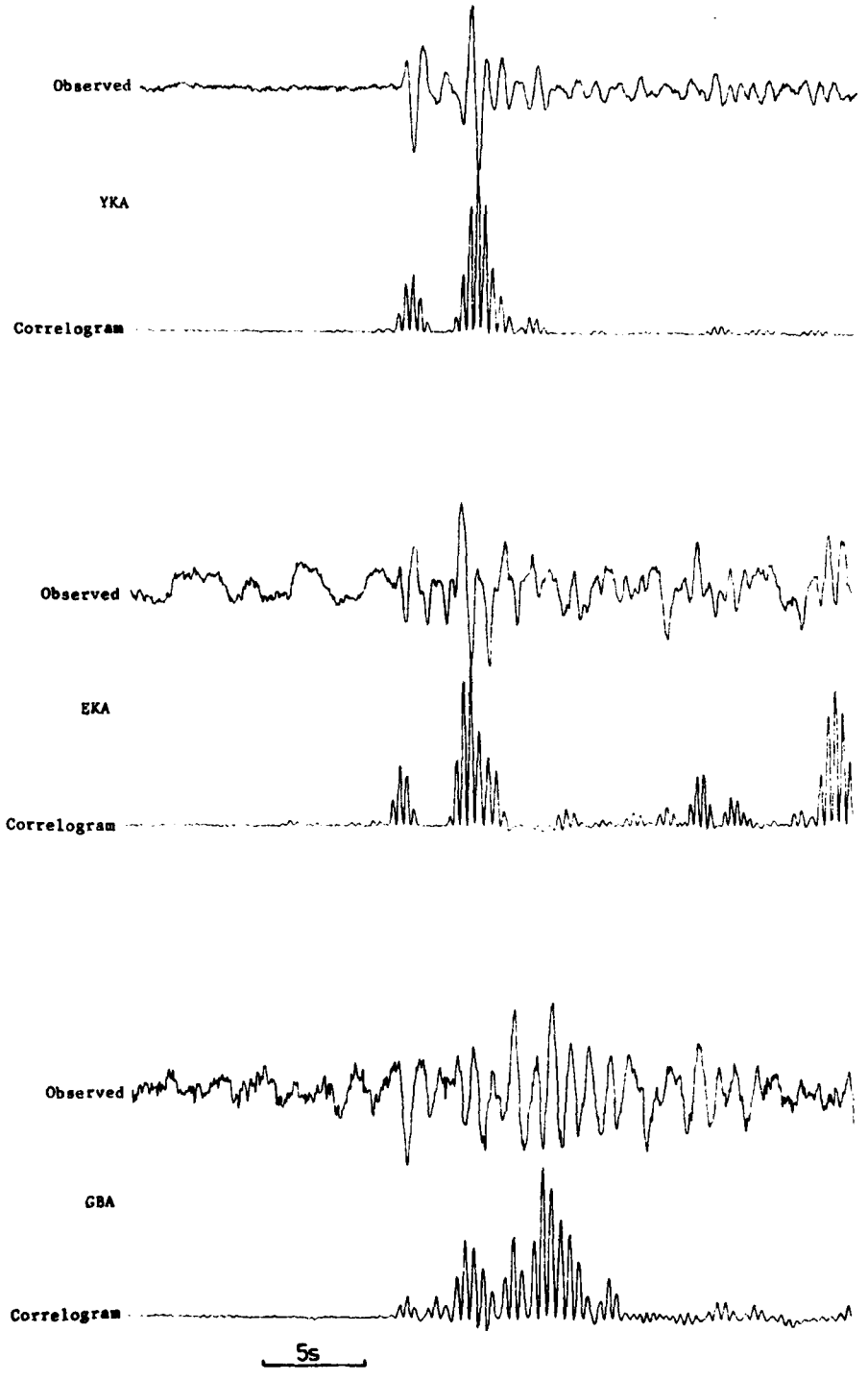

FIGURE 48

EVENT NO. 39 - CATEGORY 3

18 May 1976 13-54-23.9

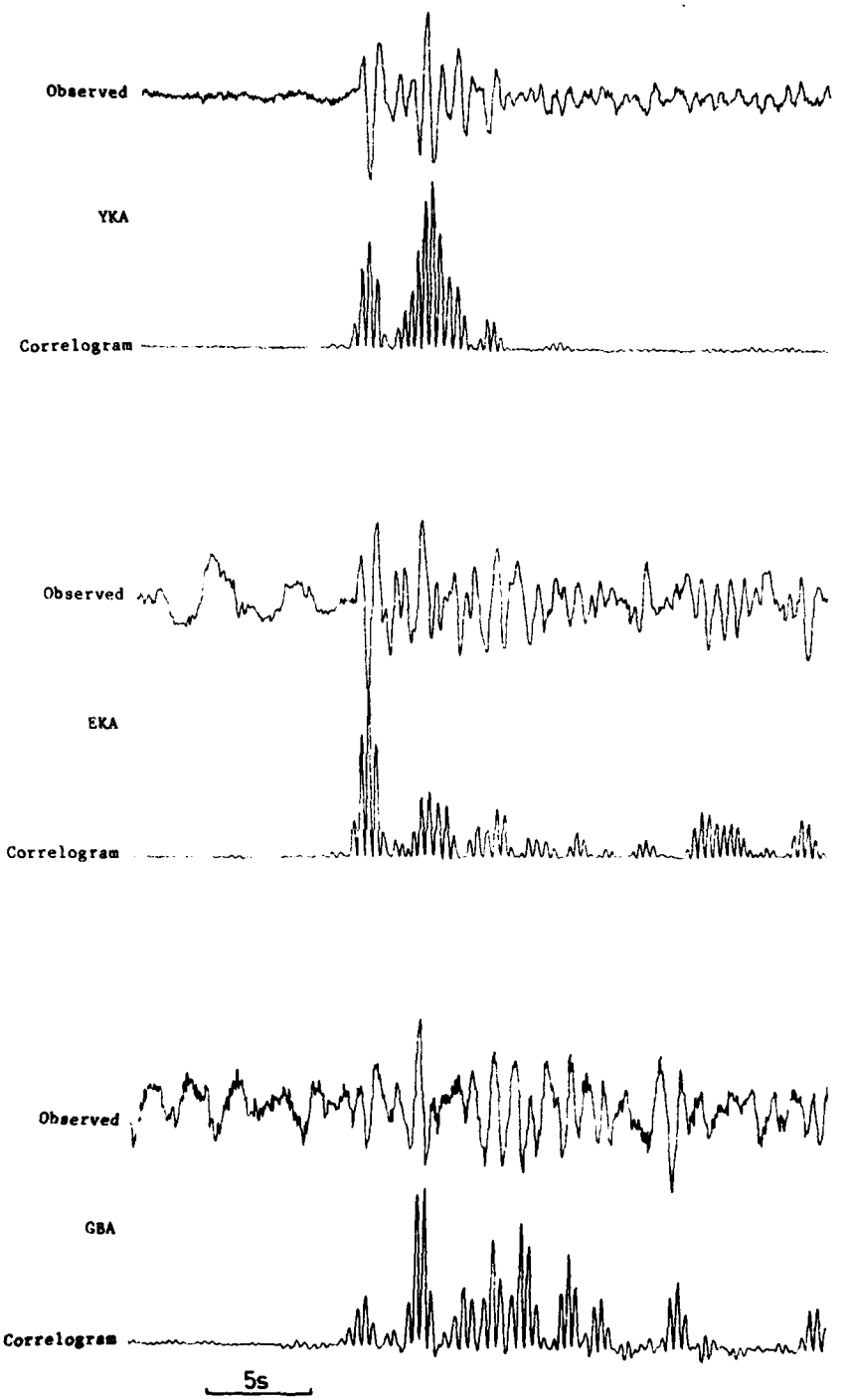

FIGURE 49

EVENT NO. 40 - CATEGORY 5

19 May 1976 01-11-20.8

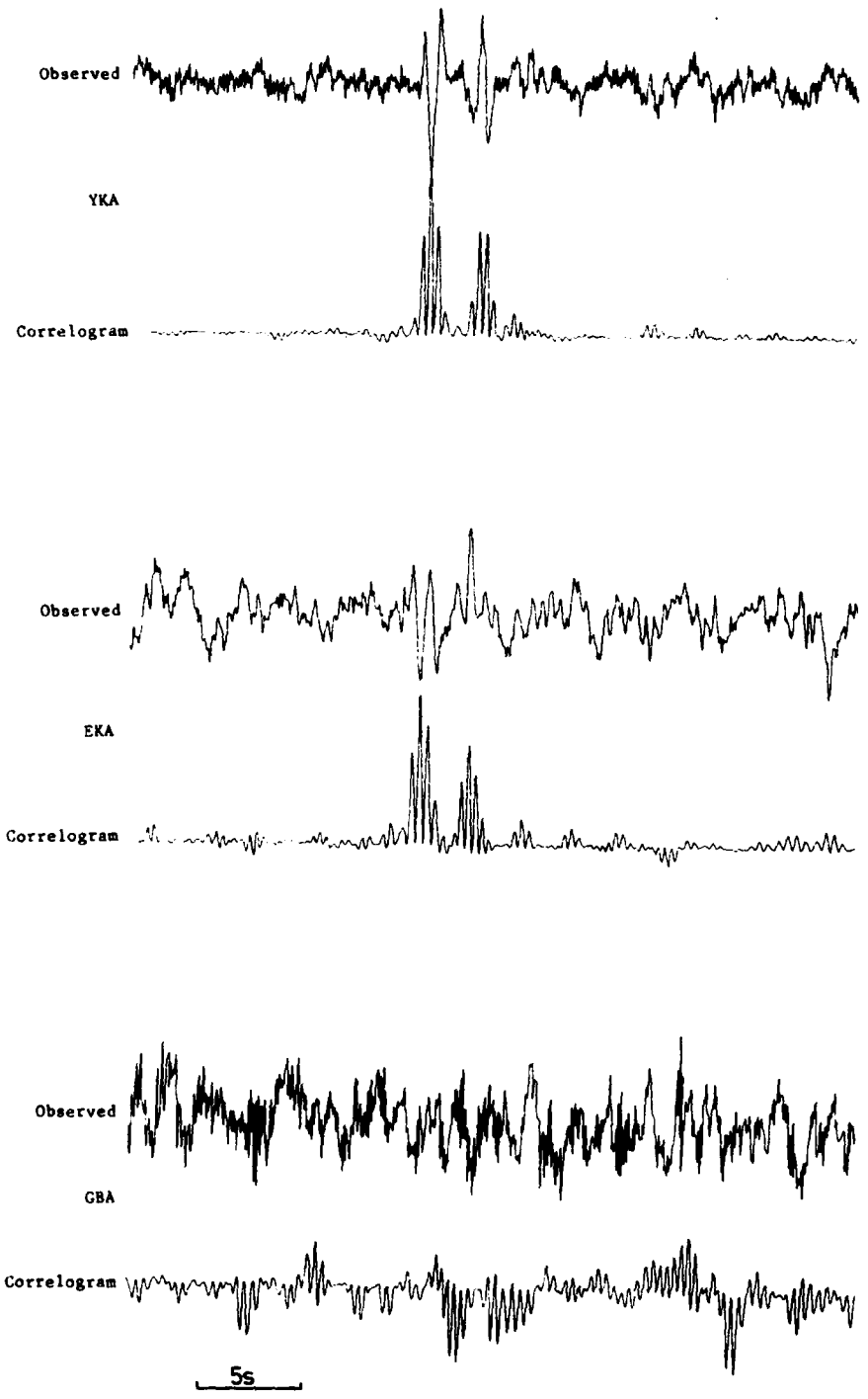

FIGURE 50

EVENT NO. 42 - CATEGORY 5

19 May 1976 16-21-44.9

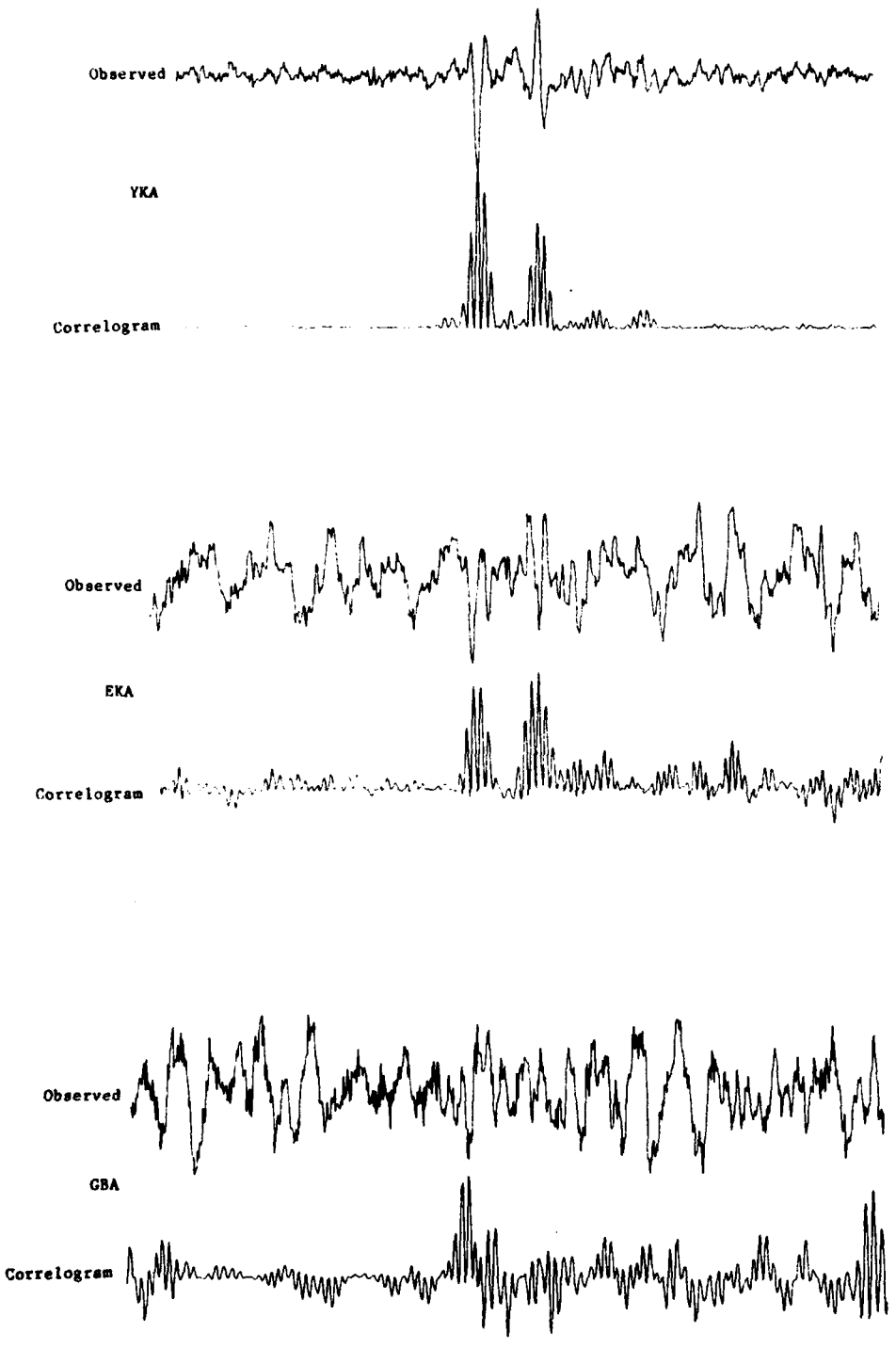

FIGURE 51

EVENT NO. 43 - CATEGORY 5

21 May 1976 16-05-28.5

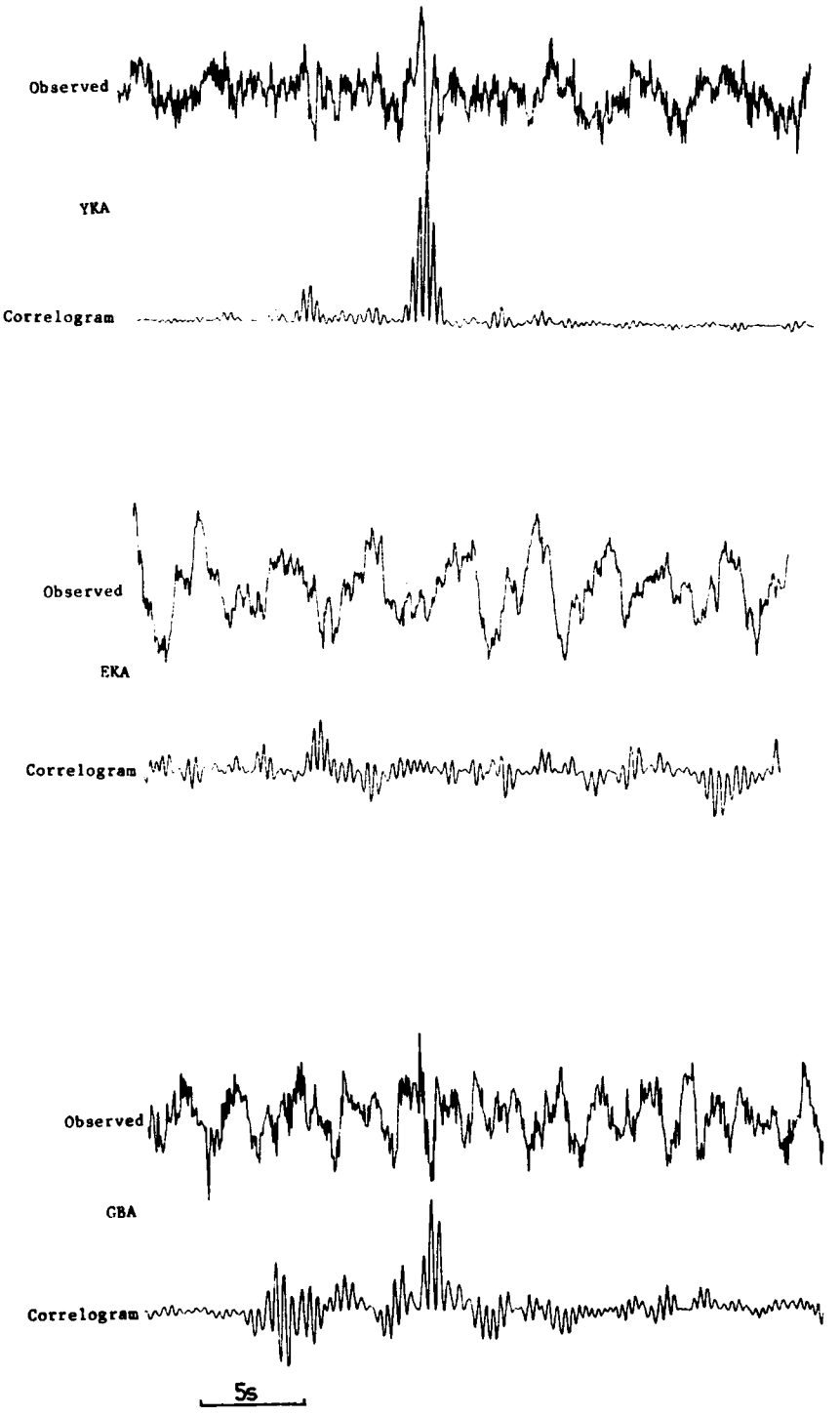

FIGURE 52

EVENT NO. 44 - CATEGORY 5

21 May 1976 18-28-57.3

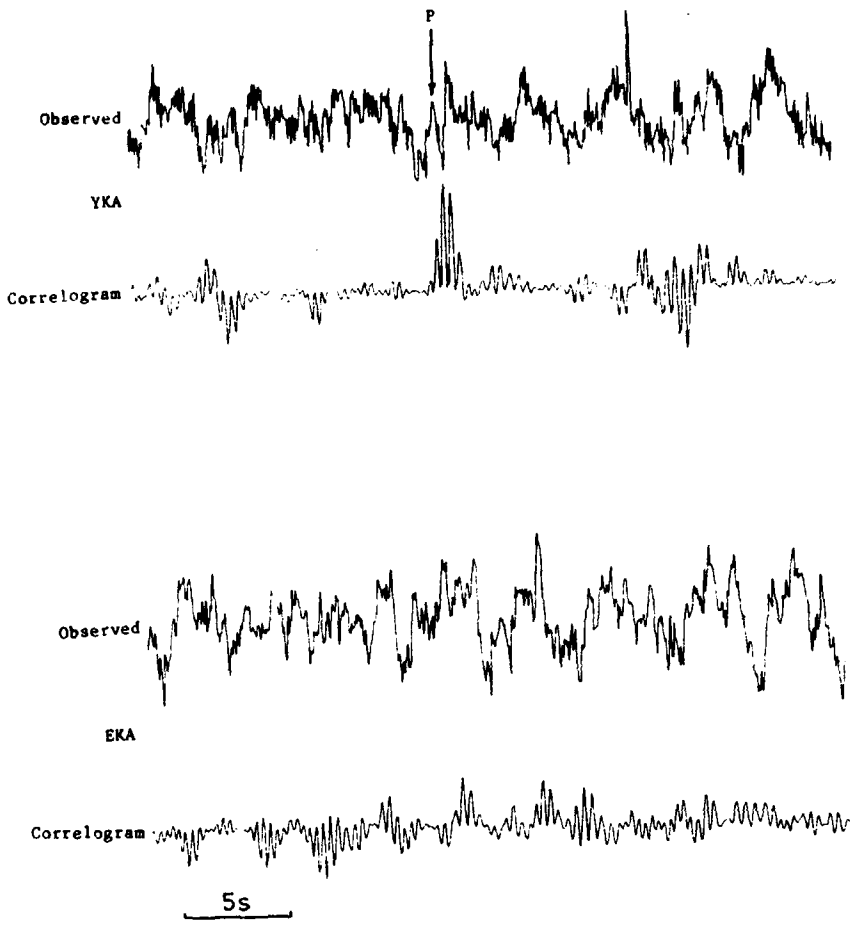

FIGURE 53

EVENT NO. 45 - CATEGORY 5

23 May 1976 09-49-21.3

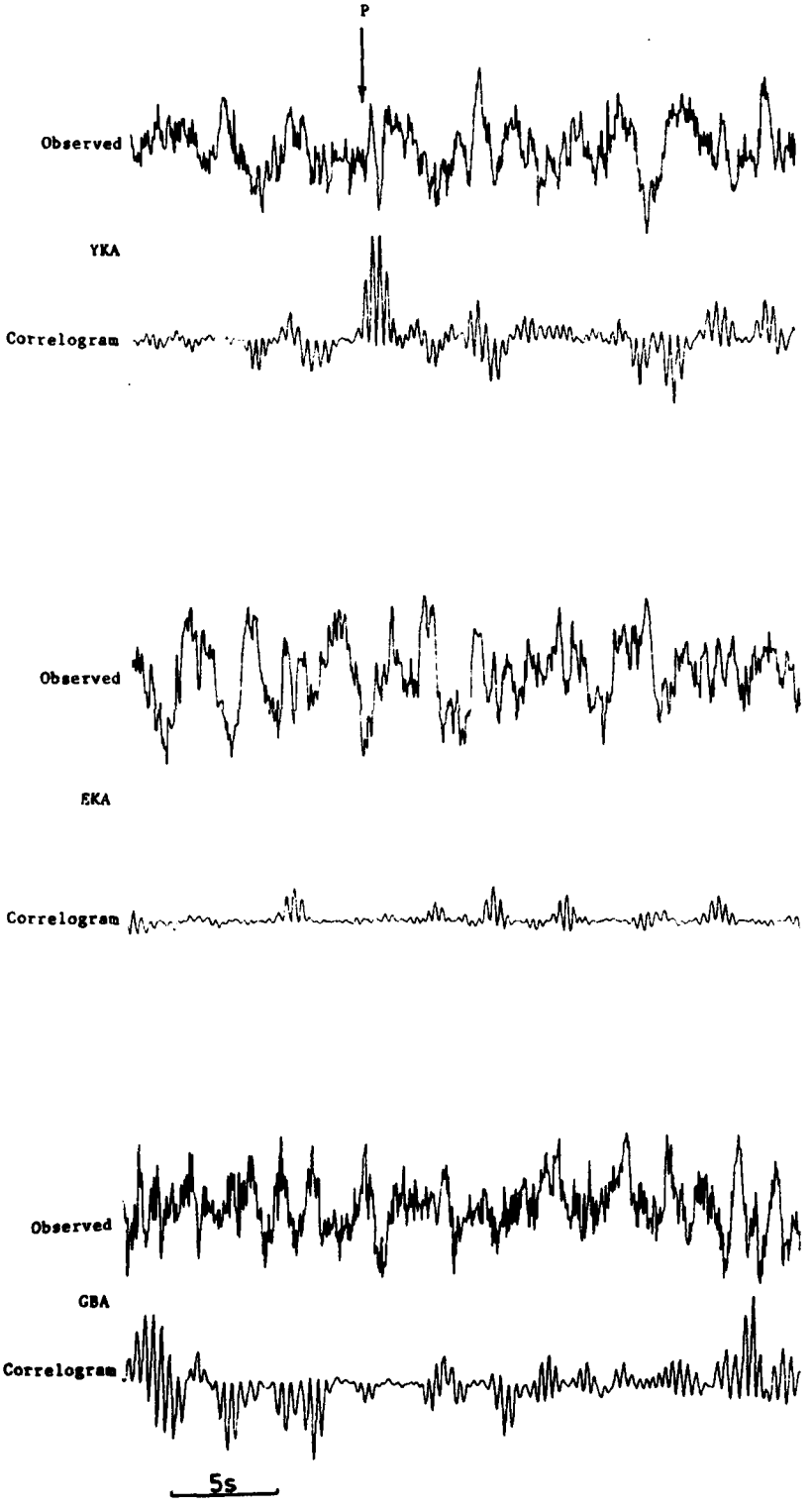

FIGURE 54

EVENT NO. 46 - CATEGORY 5

24 May 1976 06-10-54.4

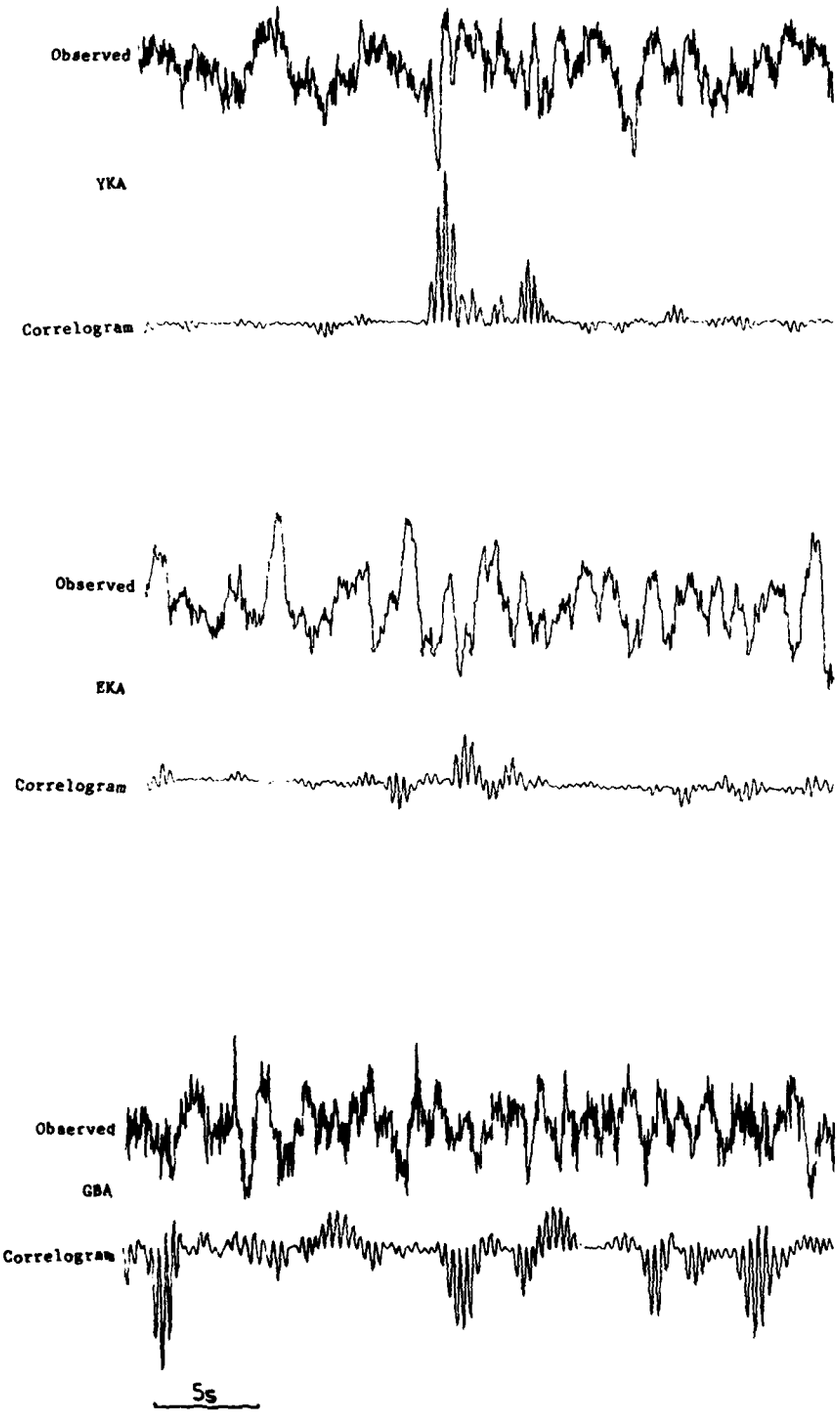

FIGURE 55

EVENT NO. 47 - CATEGORY 5

24 May 1976 14-56-12.8

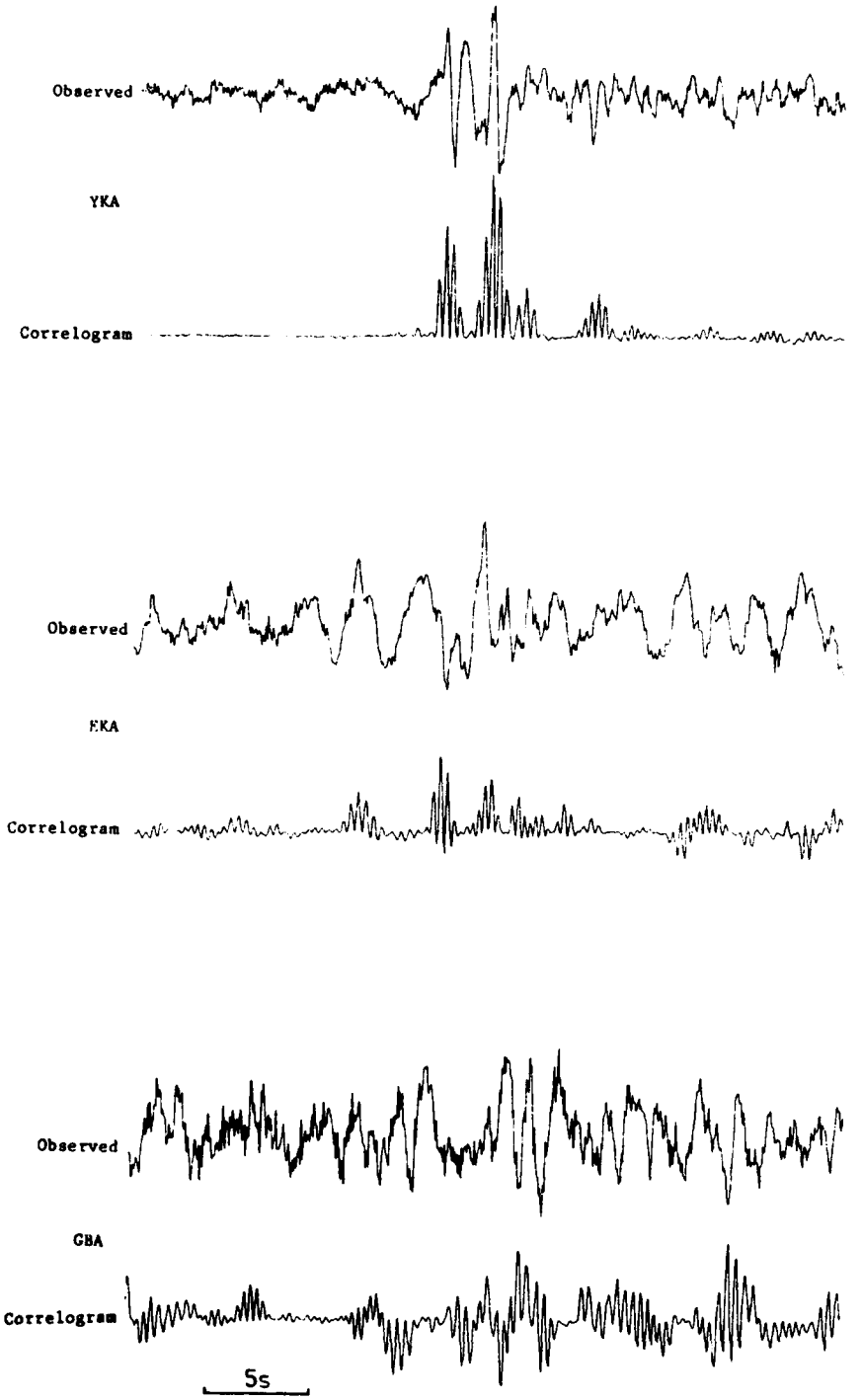

FIGURE 56

EVENT NO. 49 - CATEGORY A

(See also Figure 81)

1 June 1976 07-31-59.2

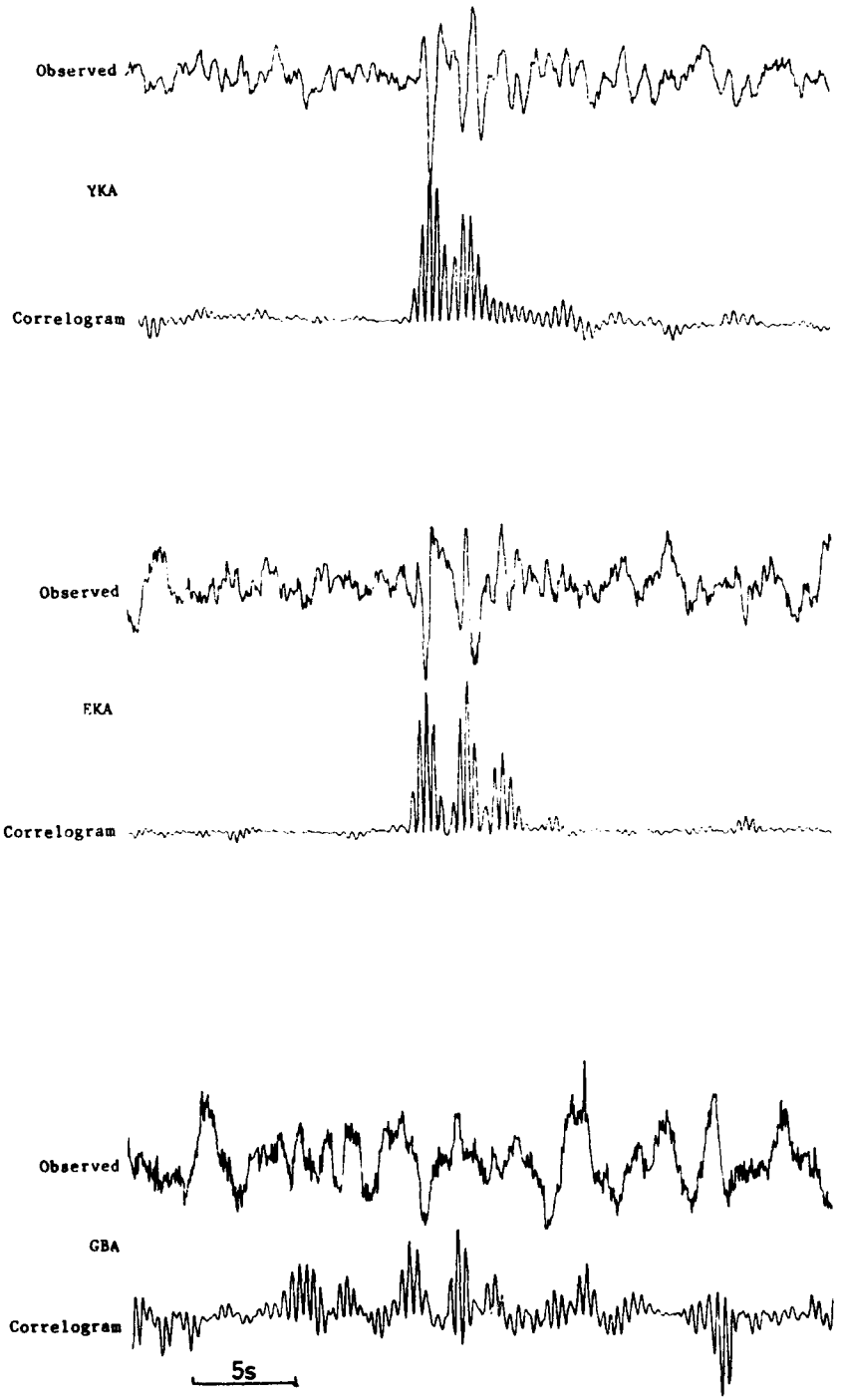

FIGURE 57

EVENT NO. 50 - CATEGORY 5

6 June 1976 04-19-09.7

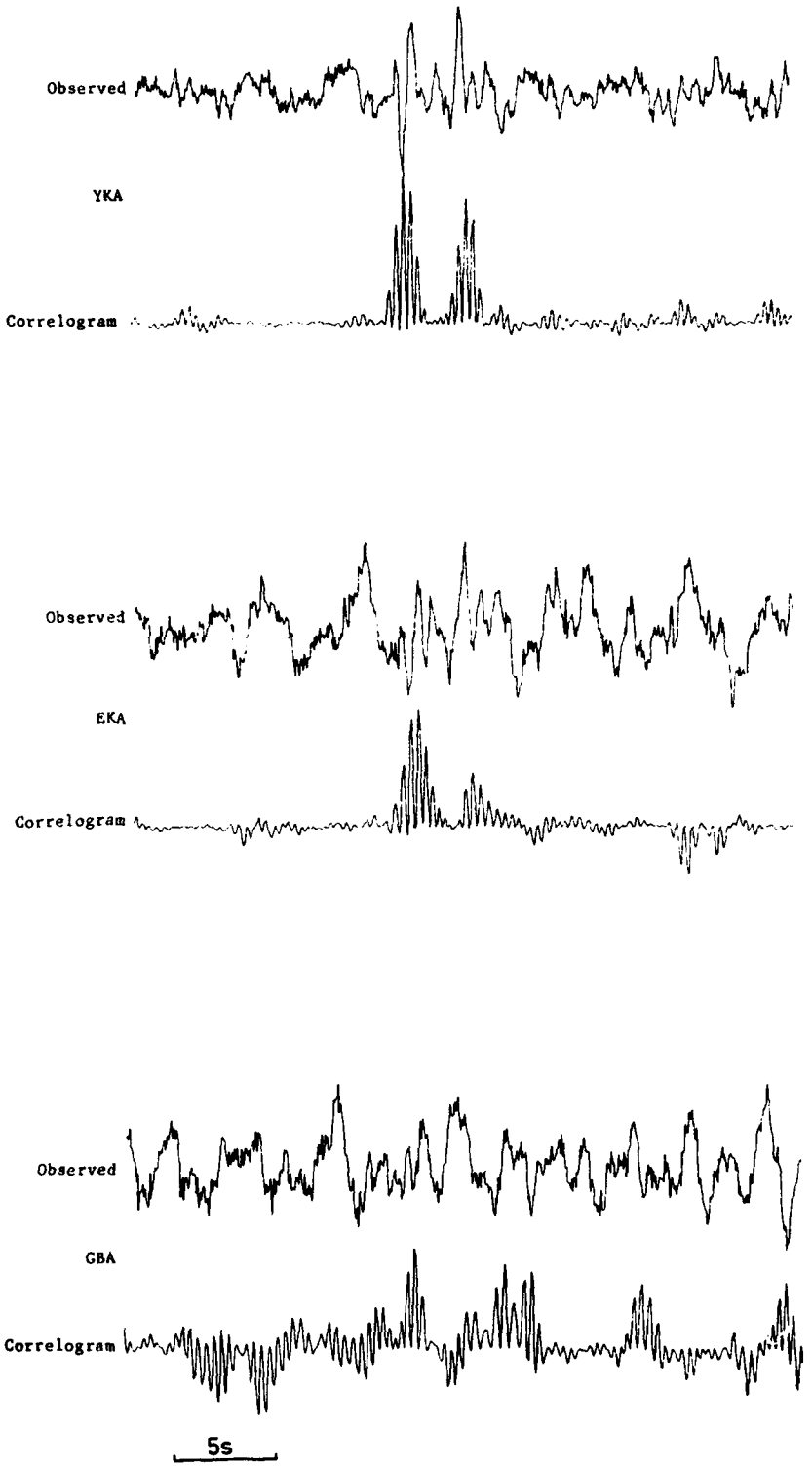

FIGURE 58

EVENT NO. 51 - CATEGORY 5

11 June 1976 13-42-37.1

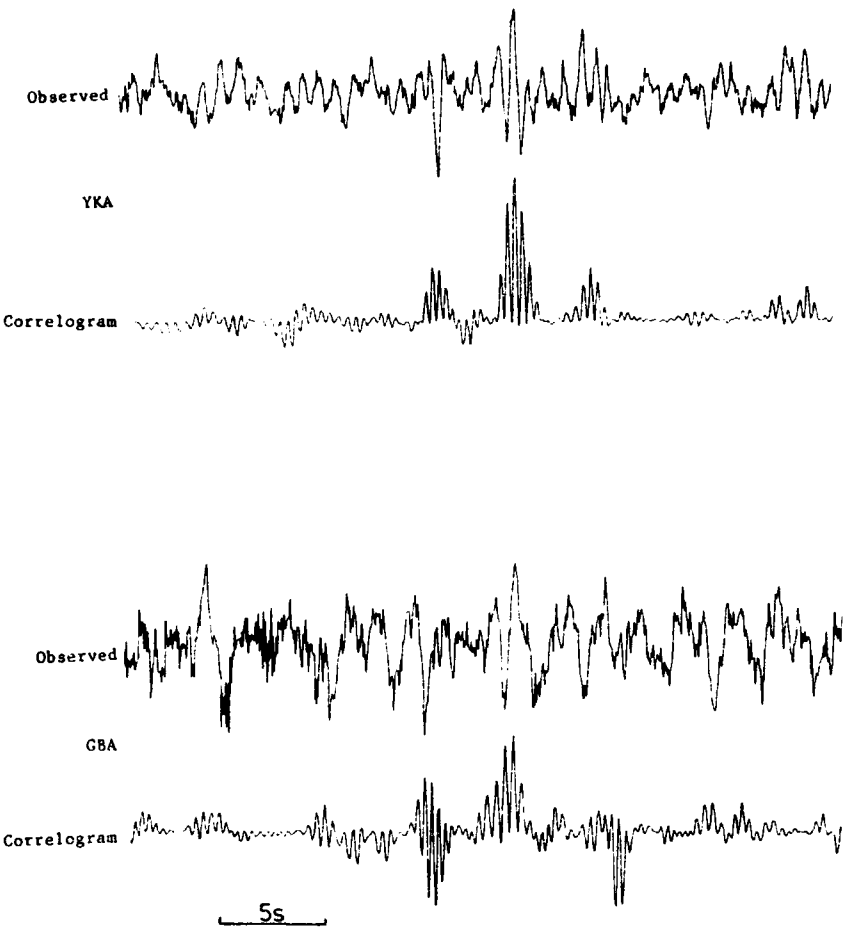

FIGURE 59

EVENT NO. 55 - CATEGORY 5

4 August 1976 02-23-44.1

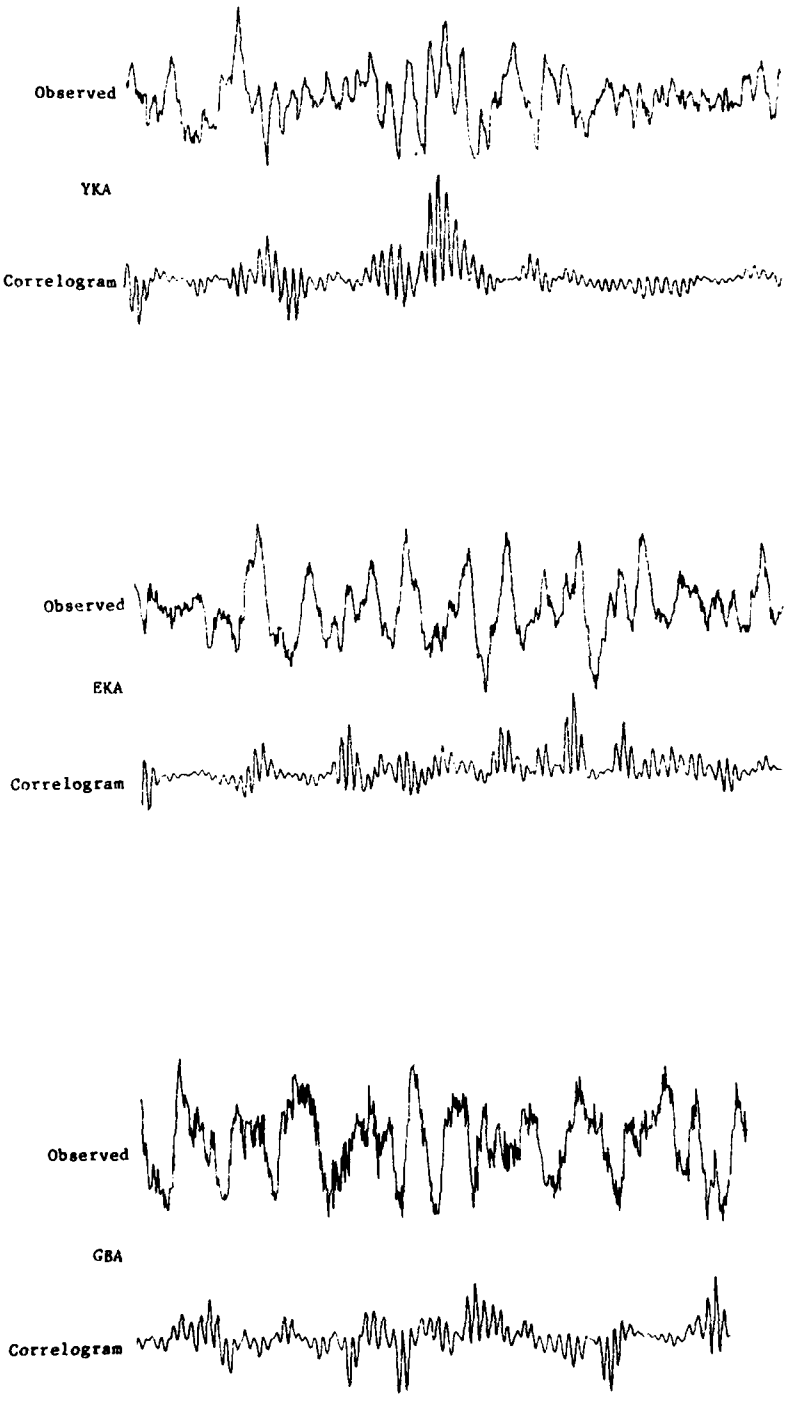

FIGURE 60

EVENT NO. 56 - CATEGORY 5

18 August 1976 23-17-55.0

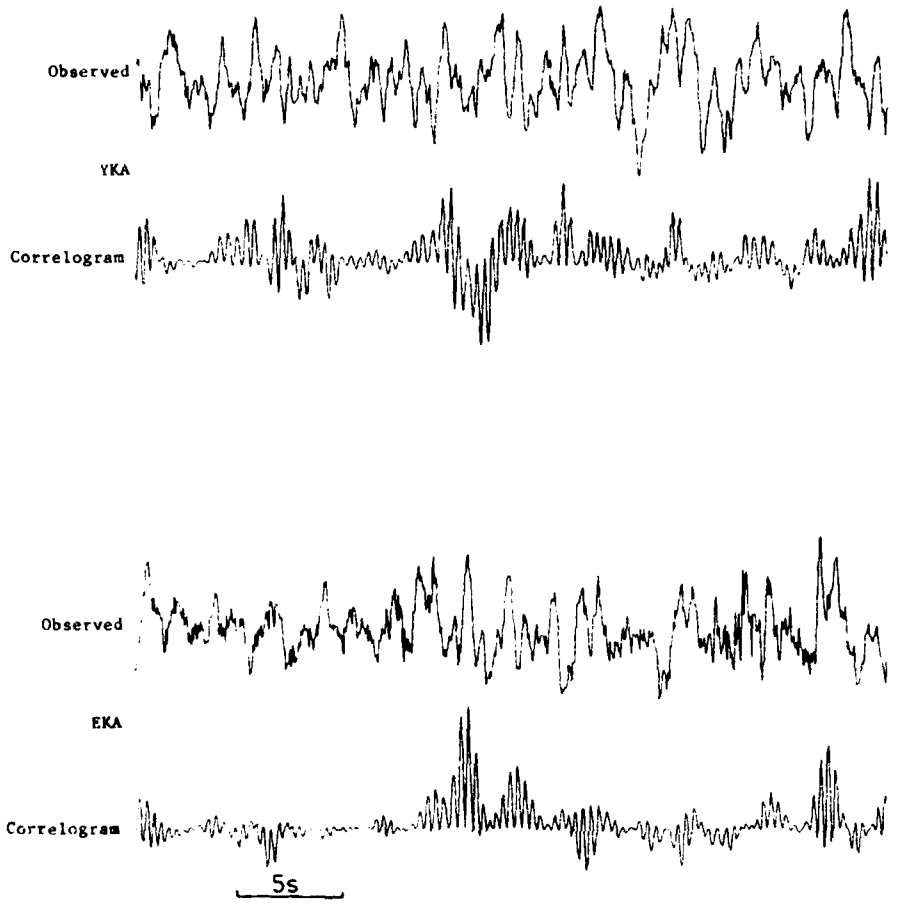

FIGURE 61

EVENT NO. 57 - CATEGORY 5

21 August 1976 12-15-32.3

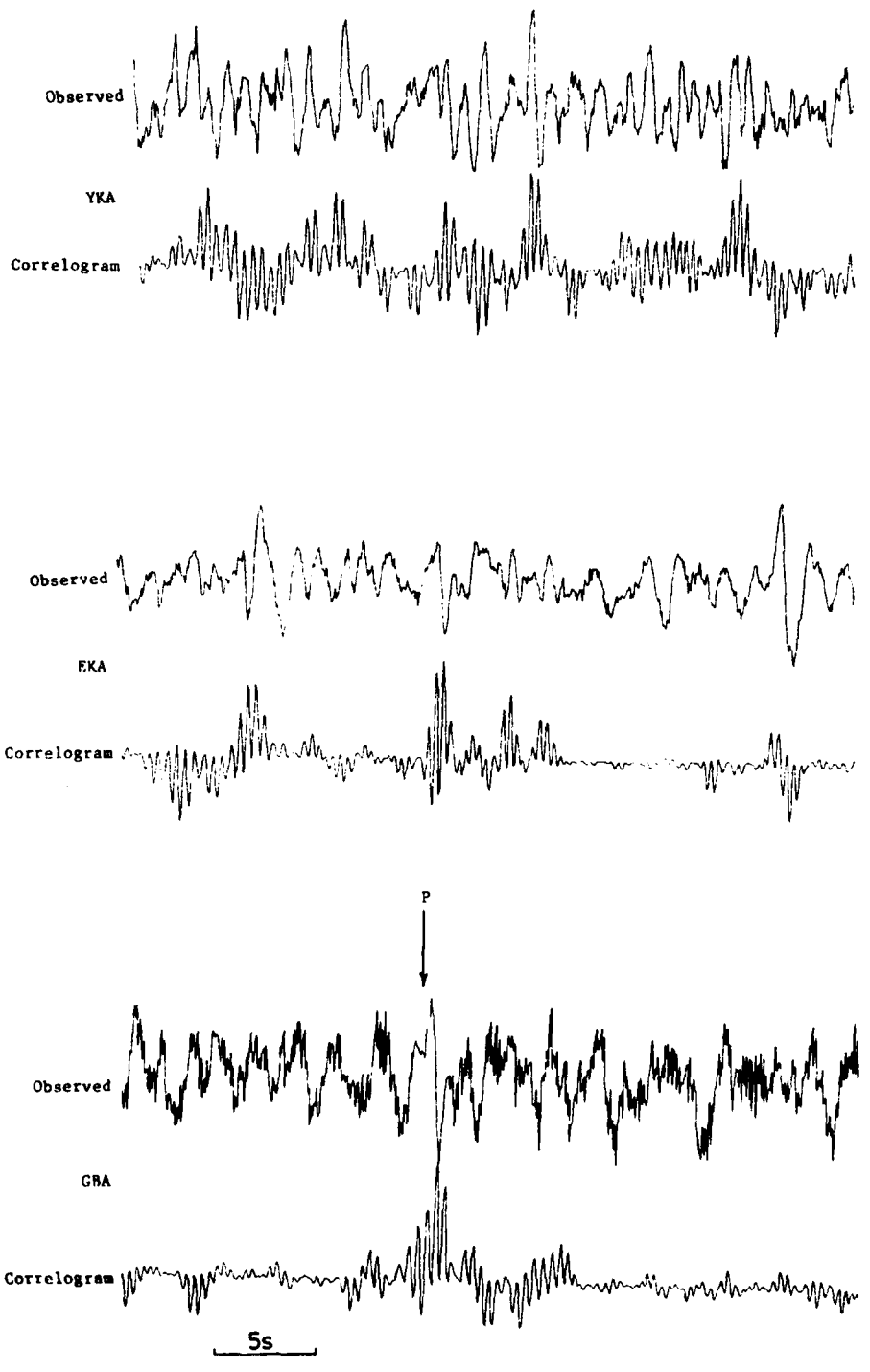

FIGURE 62

EVENT NO. 59 - CATEGORY 5

9 October 1976 16-04-19.1

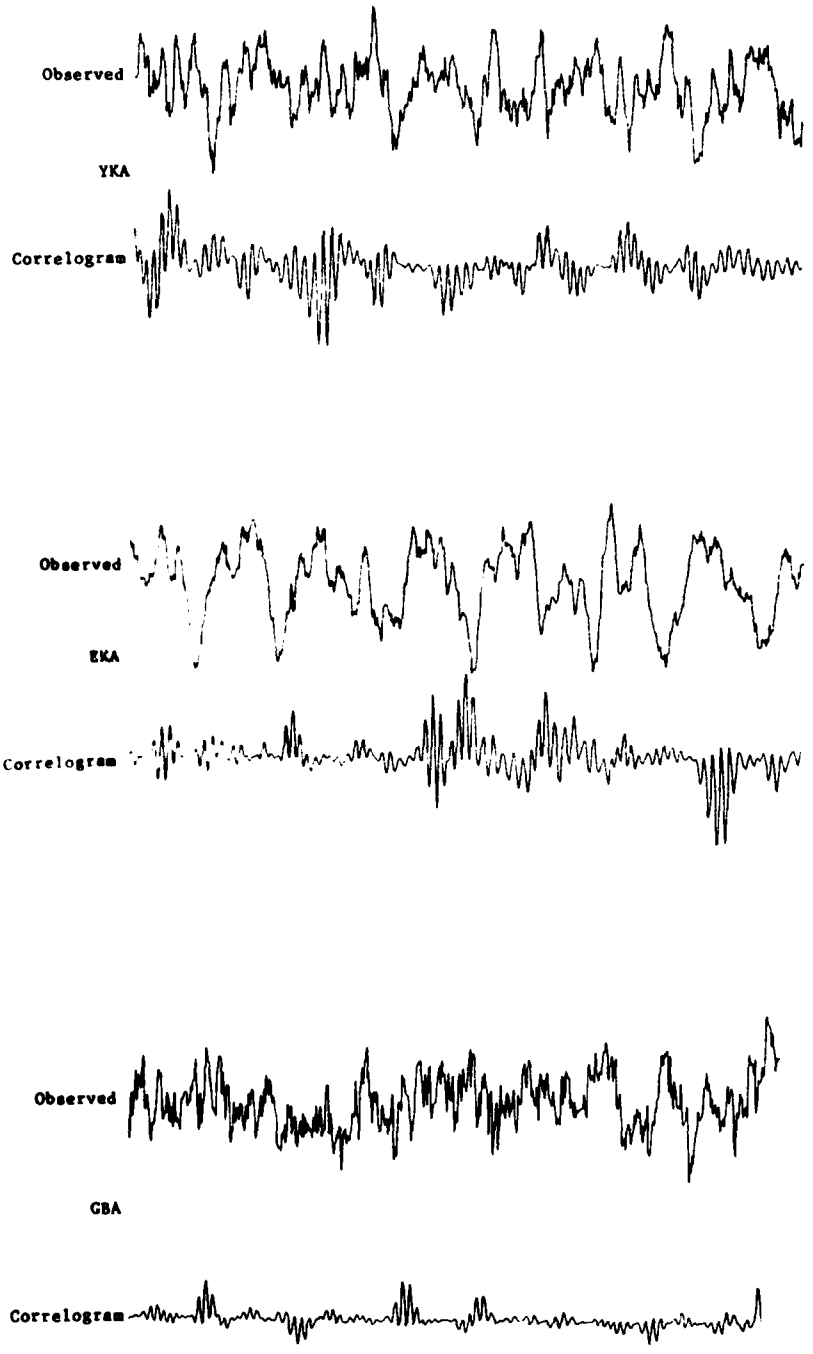

FIGURE 63

EVENT NO. 60 - CATEGORY 5

17 October 1976 03-25-33.1

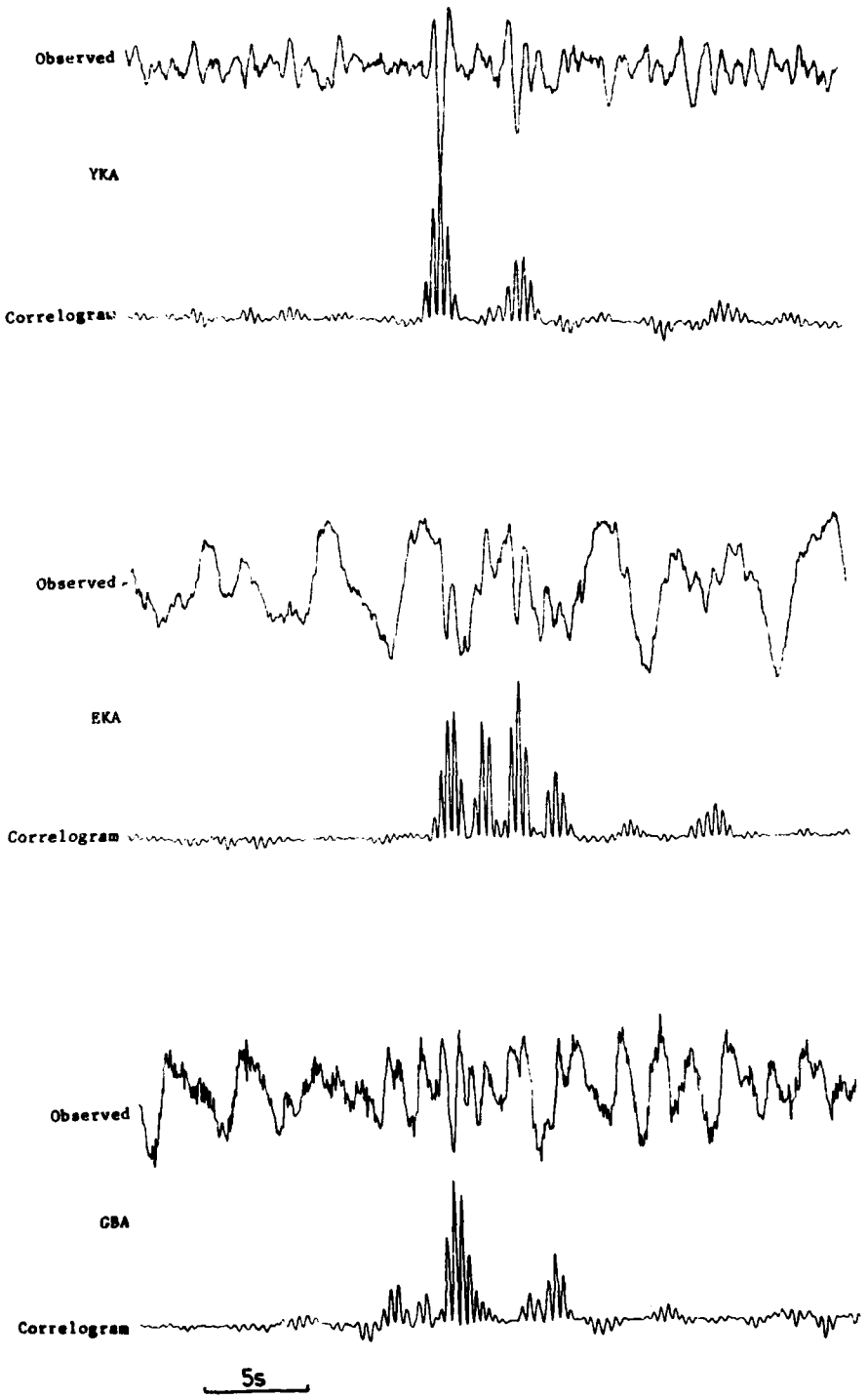

FIGURE 64

EVENT NO. 61 - CATEGORY 5

18 October 1976 21-01-48.2

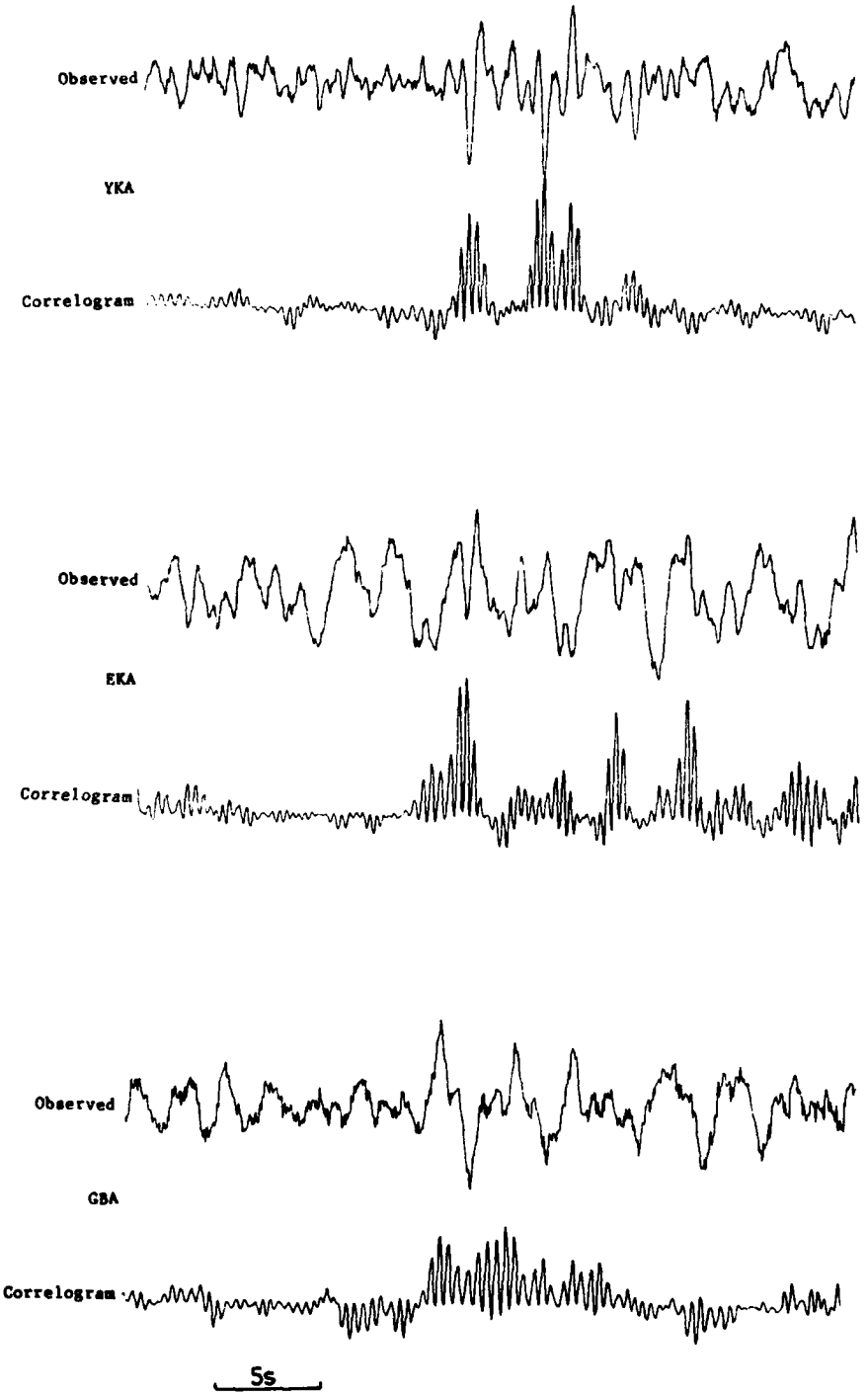

FIGURE 65

EVENT NO. 62 - CATEGORY 5

2 November 1976 22-19-33.3

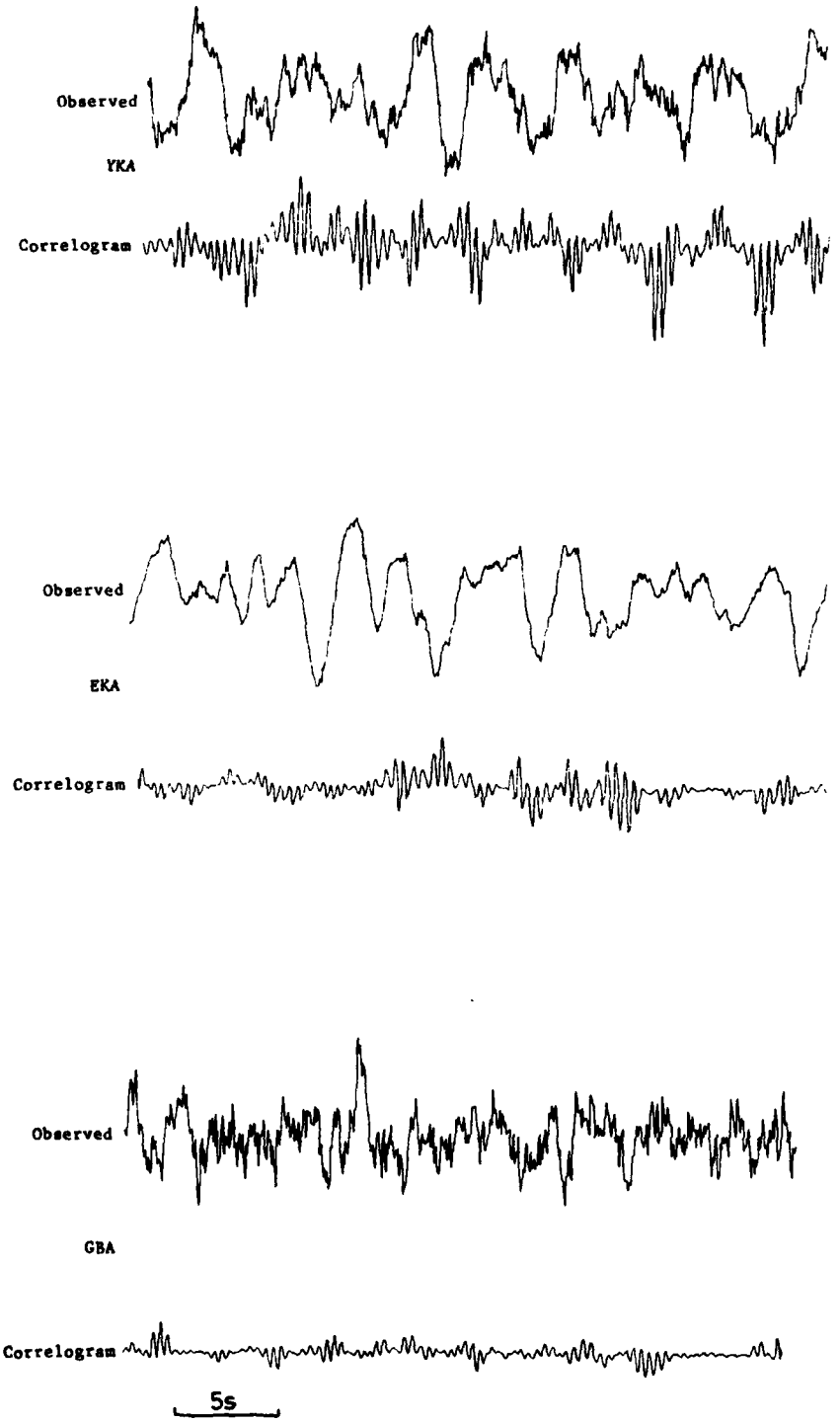

FIGURE 66

EVENT NO. 63 - CATEGORY 5

28 November 1976 20-39-39.0

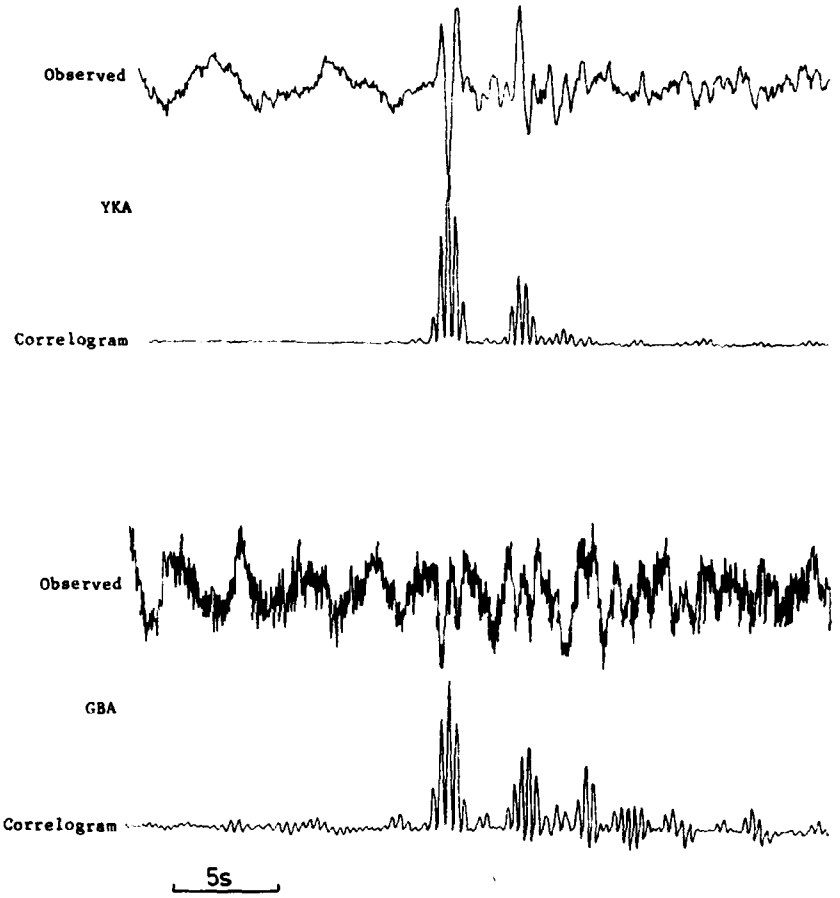

FIGURE 67

EVENT NO. 4 (CATEGORY 2)

8 April 1976 03-30-49.3 - YKA

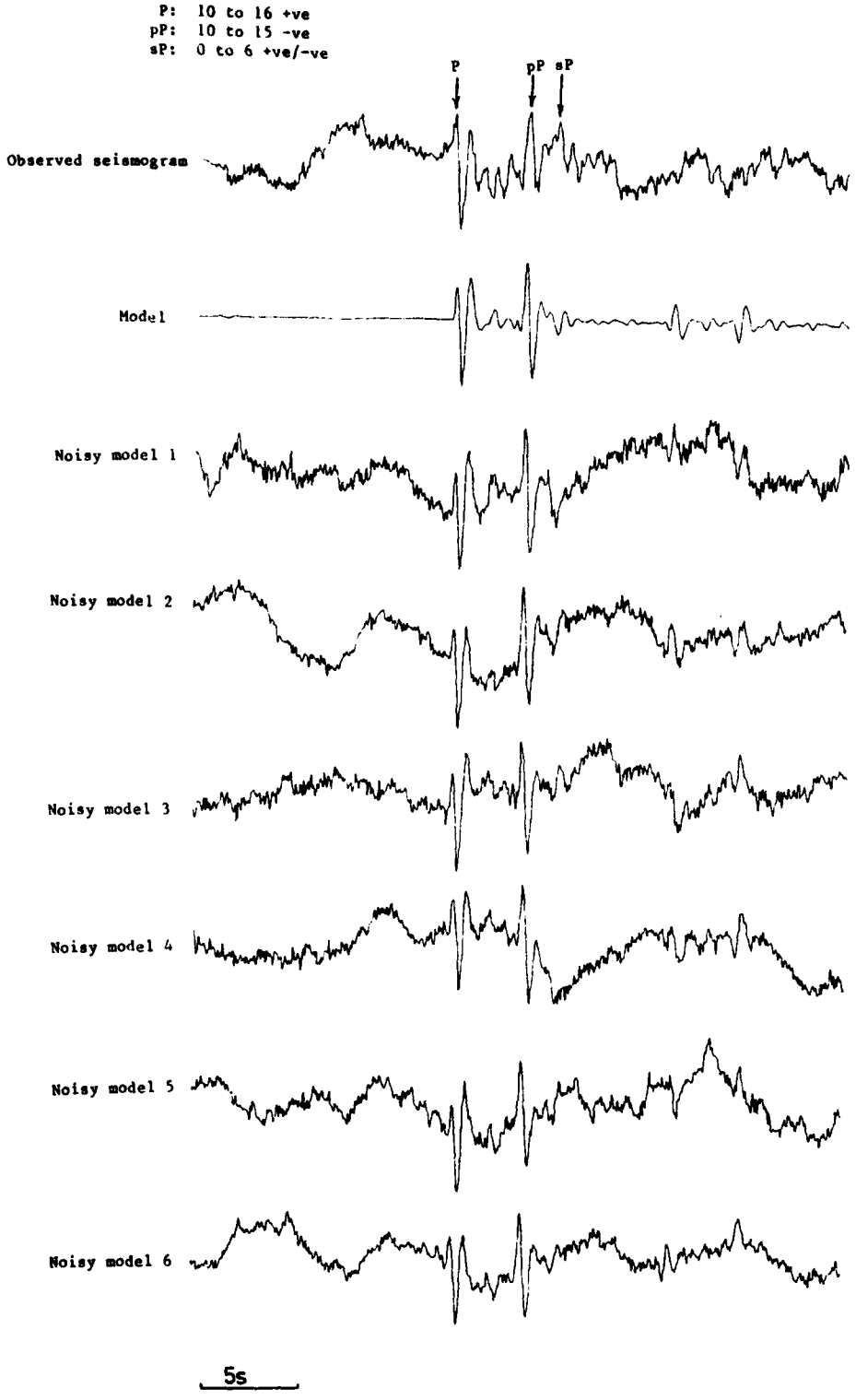

FIGURE 68

EVENT NO. 4 (CATEGORY 2)

8 April 1976 03-30-49.3 - EKA

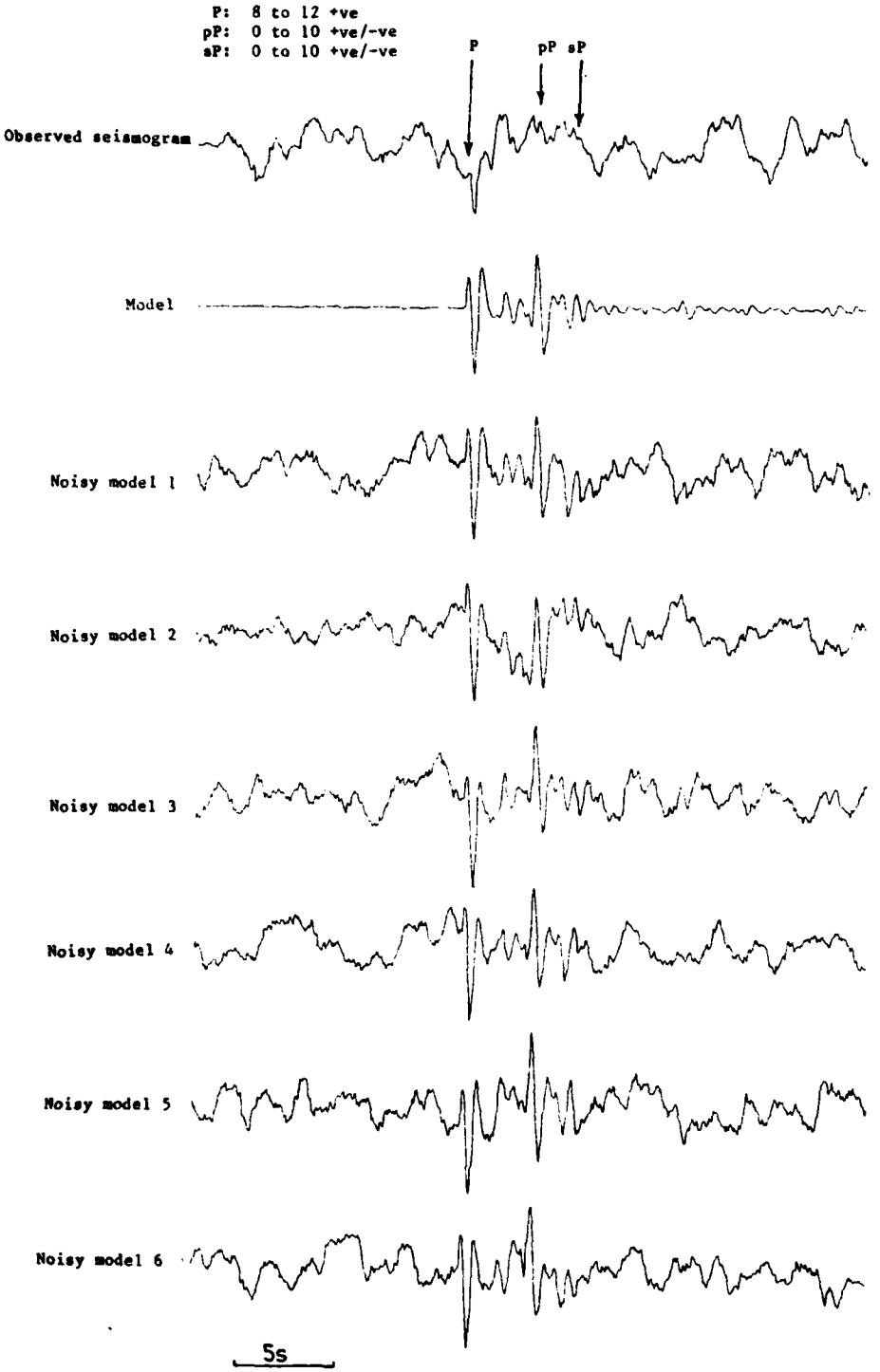

FIGURE 69

EVENT NO. 4 (CATEGORY 2)

8 April 1976 03-30-49.3 - GBA

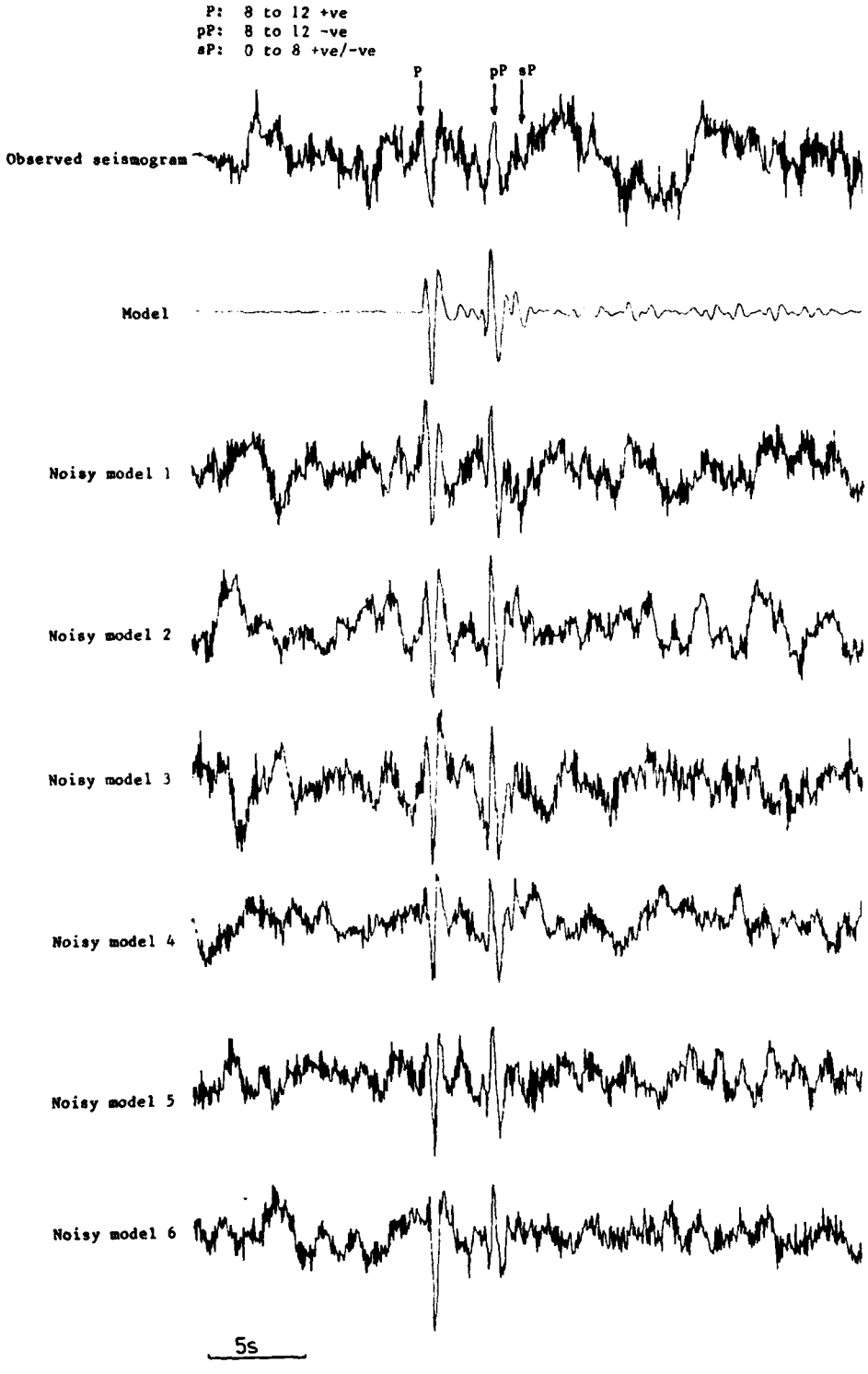

FIGURE 70

EVENT NO. 4 (CATEGORY 2)

8 April 1976 03-30-49.3 - WRA

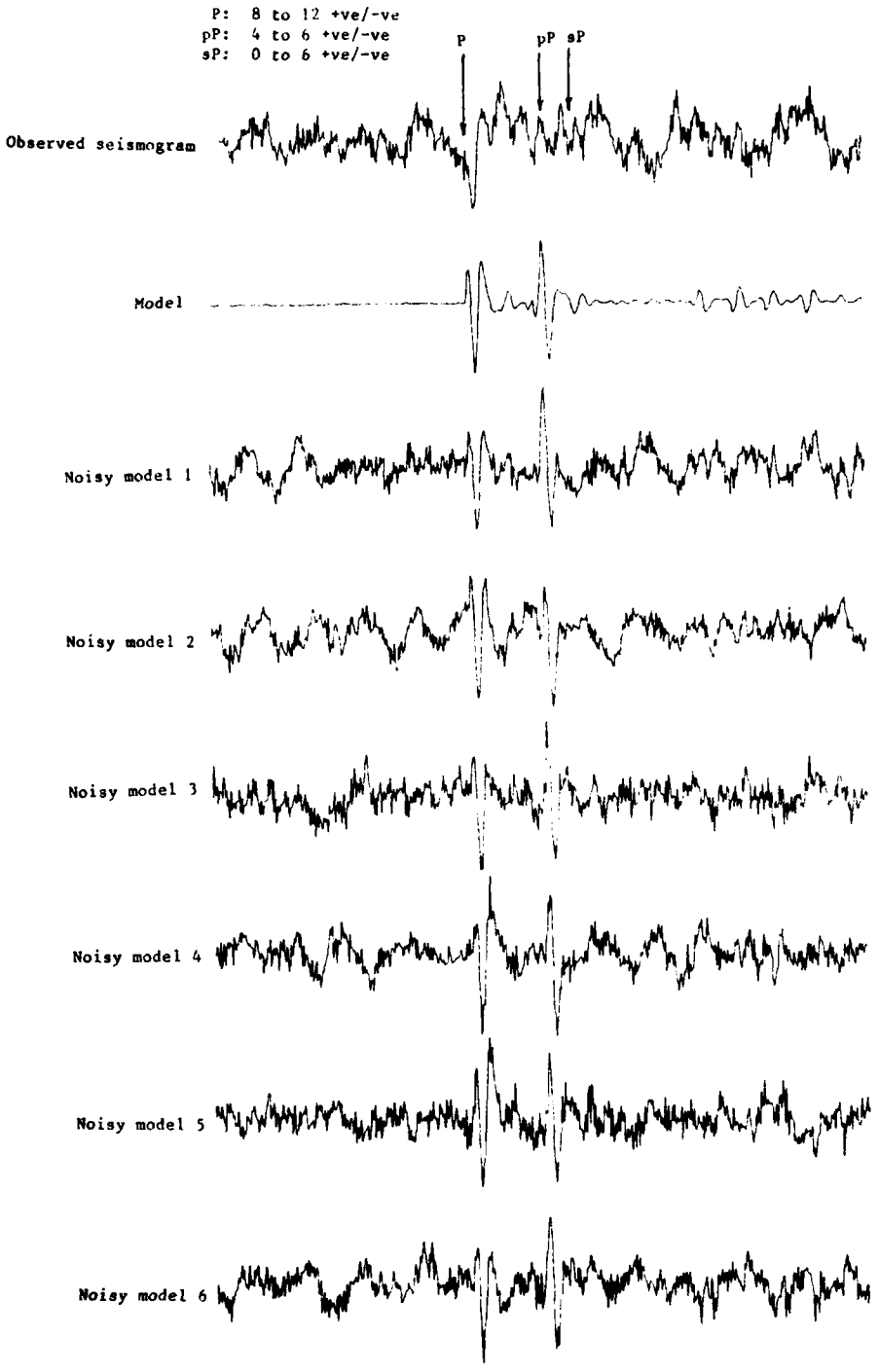

FIGURE 71

EVENT NO. 8 (CATEGORY 2)

8 April 1976 09-10-07.7 - YKA

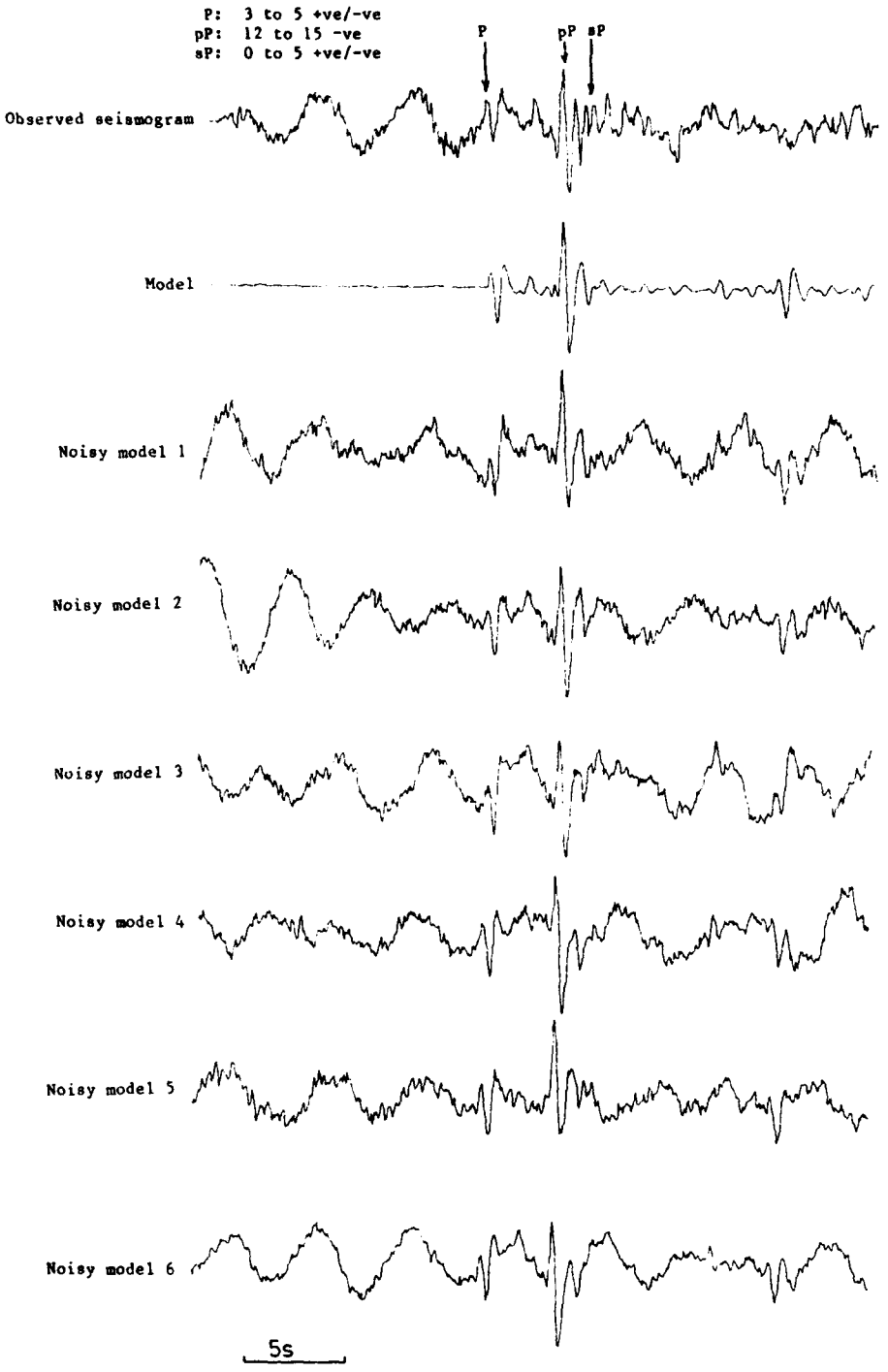

FIGURE 72

EVENT NO. 8 (CATEGORY 2)

8 April 1976 09-10-07.7 - EKA

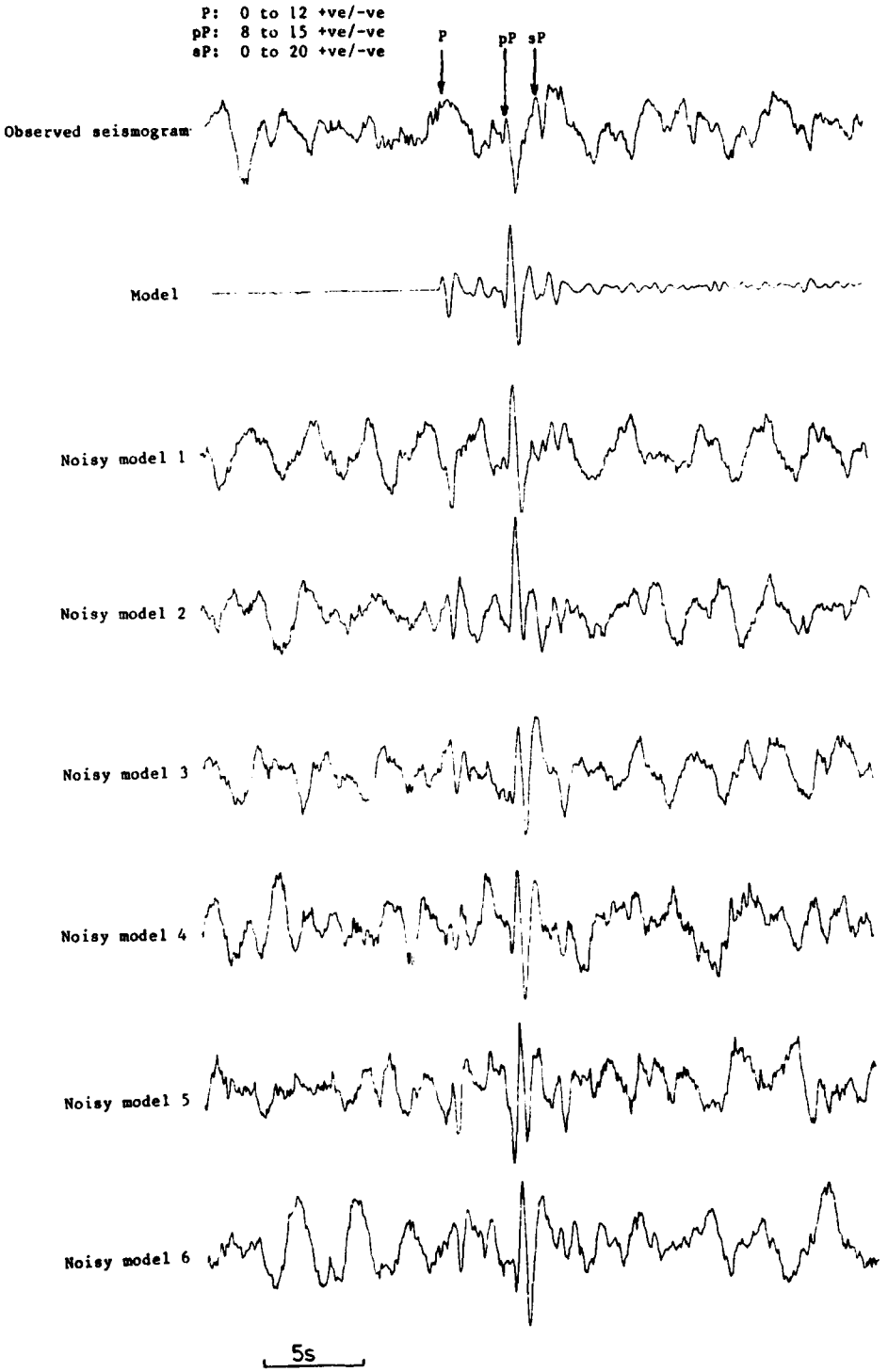

FIGURE 73

EVENT NO. 8 (CATEGORY 2)

8 April 1976 09-10-07.7 - GBA

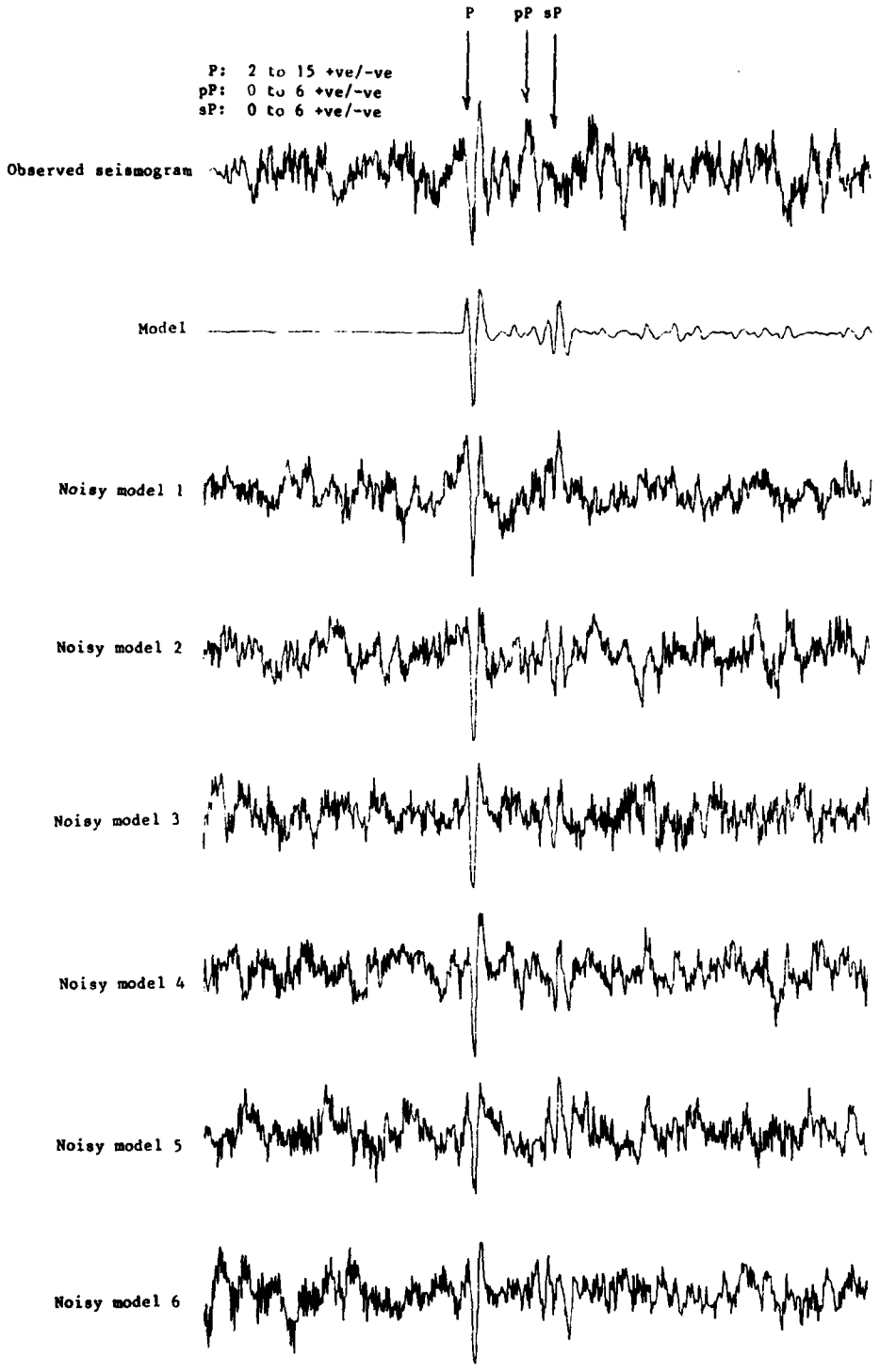

FIGURE 74

EVENT NO. 8 (CATEGORY 2)

8 April 1976 09-10-07.7 - WRA

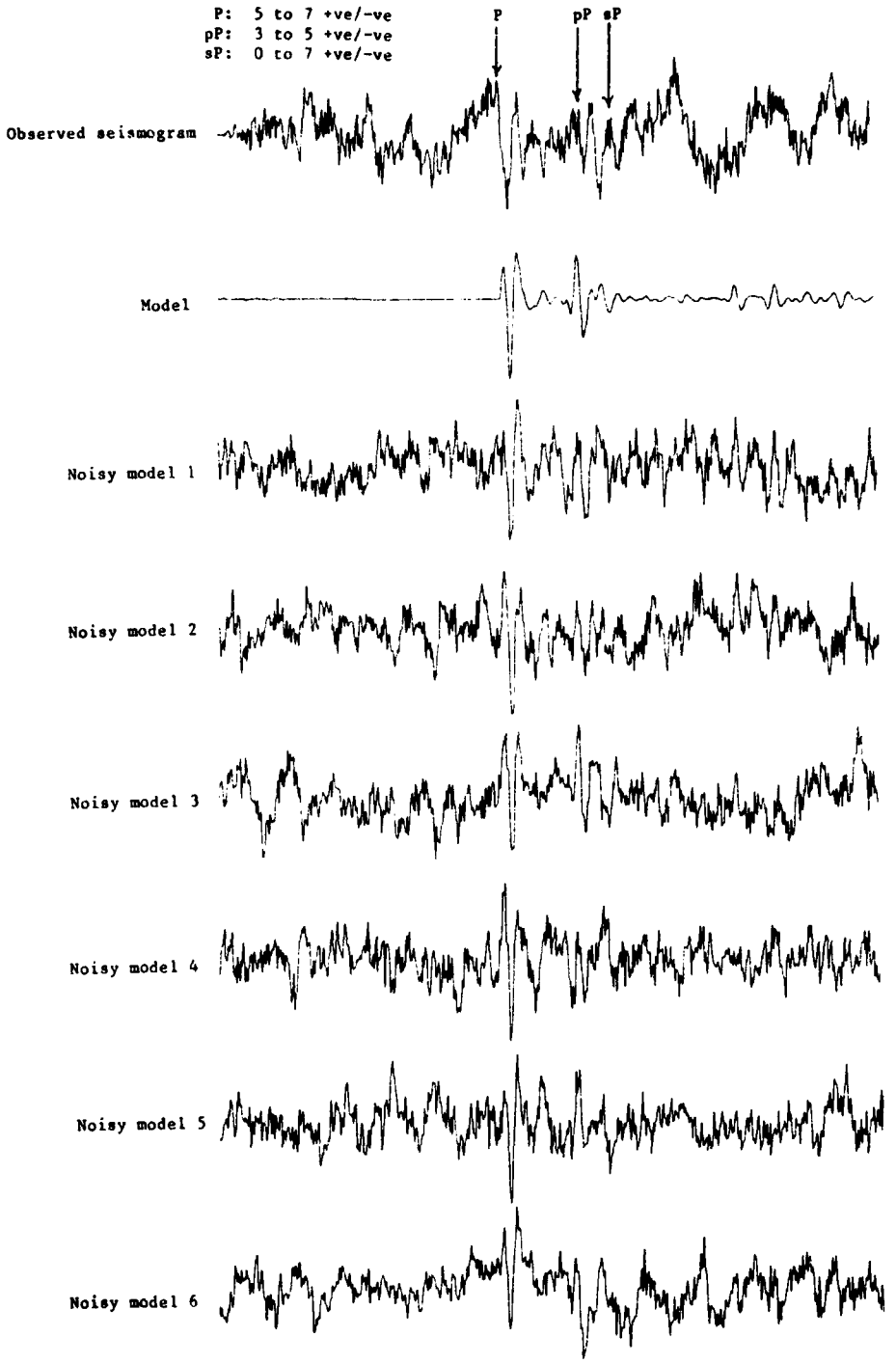

FIGURE 75

EVENT NO. 27 (CATEGORY 2)

23 April 1976 01-56-48.3 - YKA

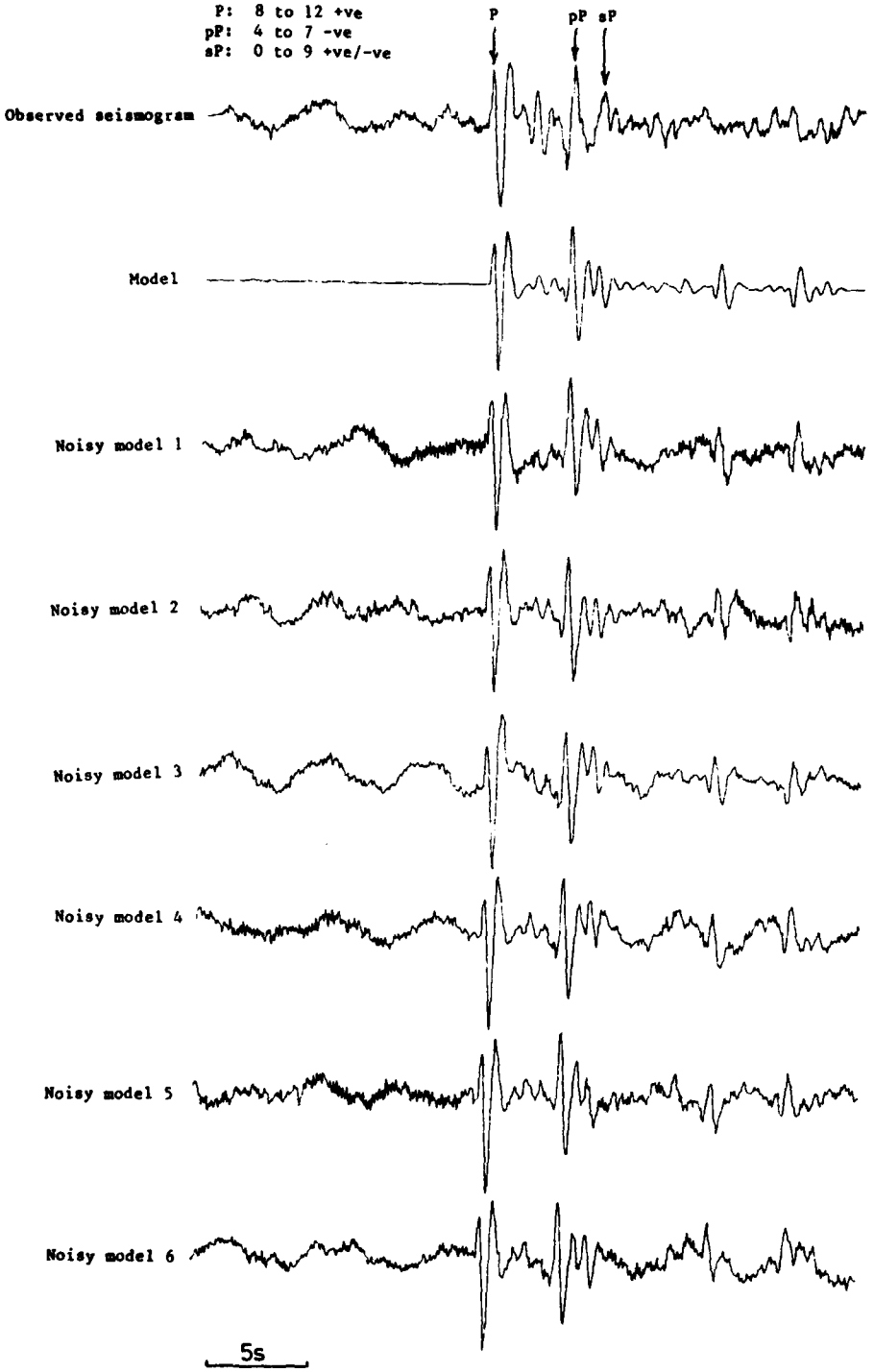

FIGURE 76

EVENT NO. 27 (CATEGORY 2)

23 April 1976 01-56-48.3 - EKA

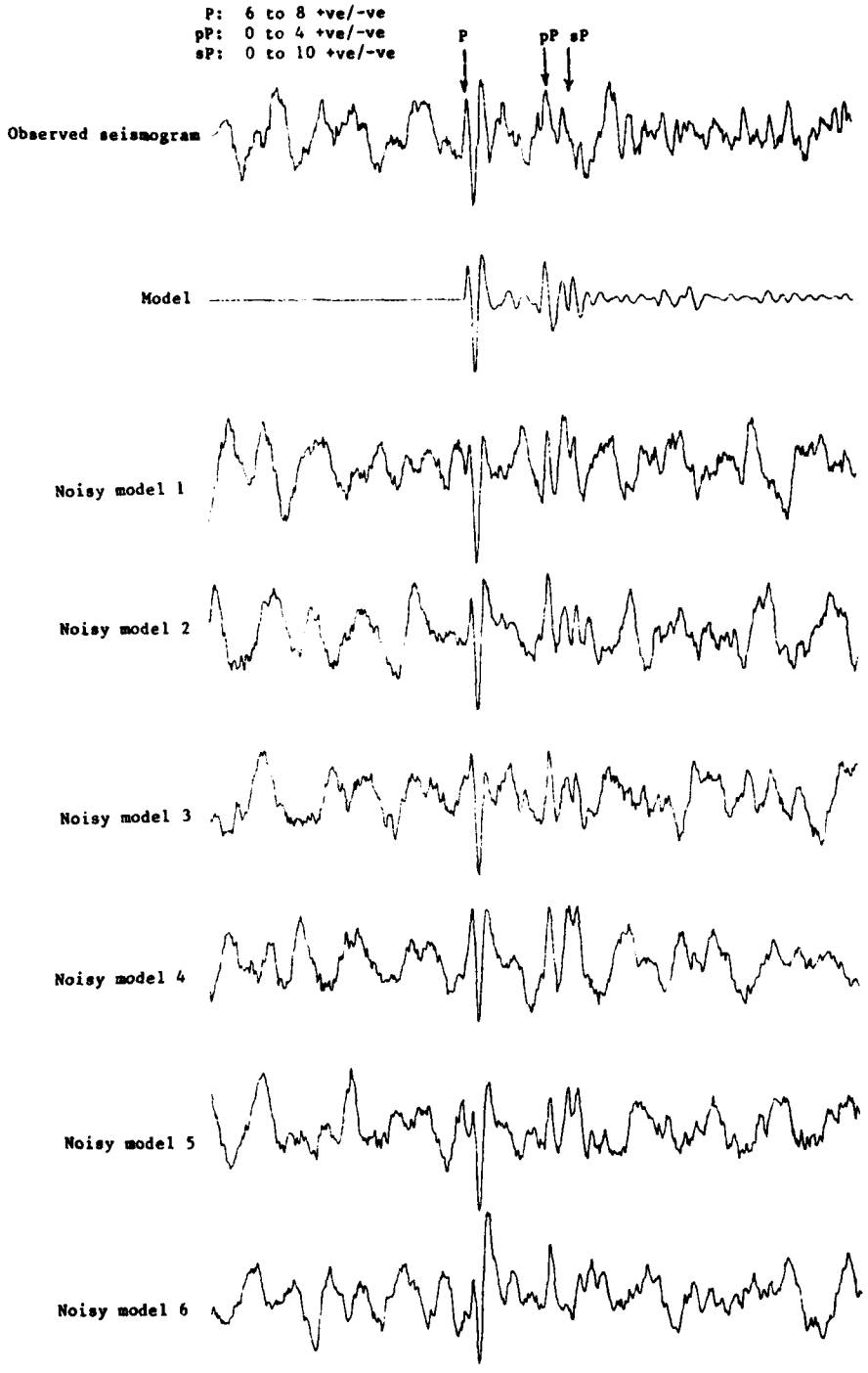

FIGURE 77

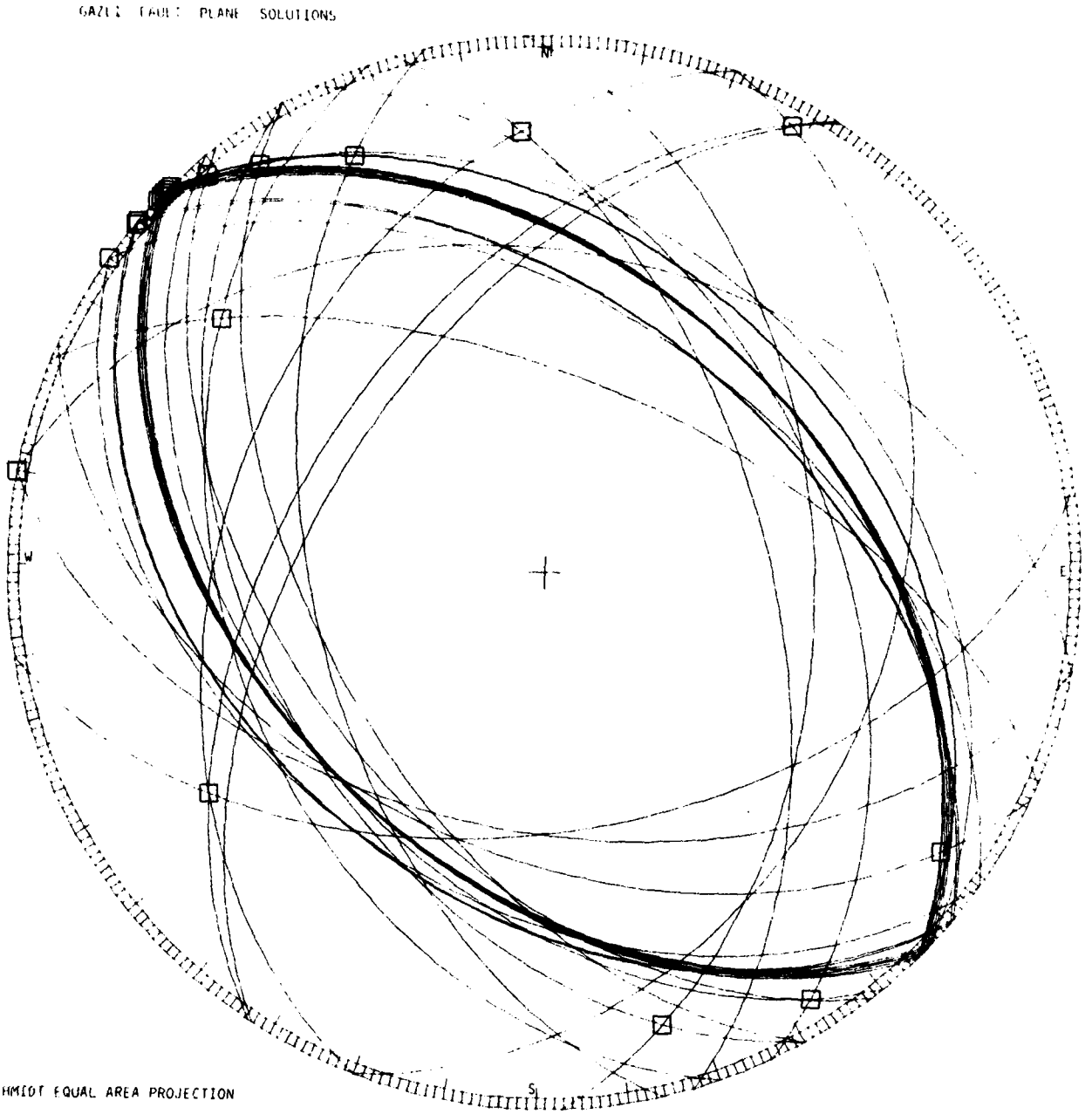

FIGURE 78. COMPOSITE PLOT OF FAULT PLANE SOLUTIONS USED FOR MODELLING EACH EVENT

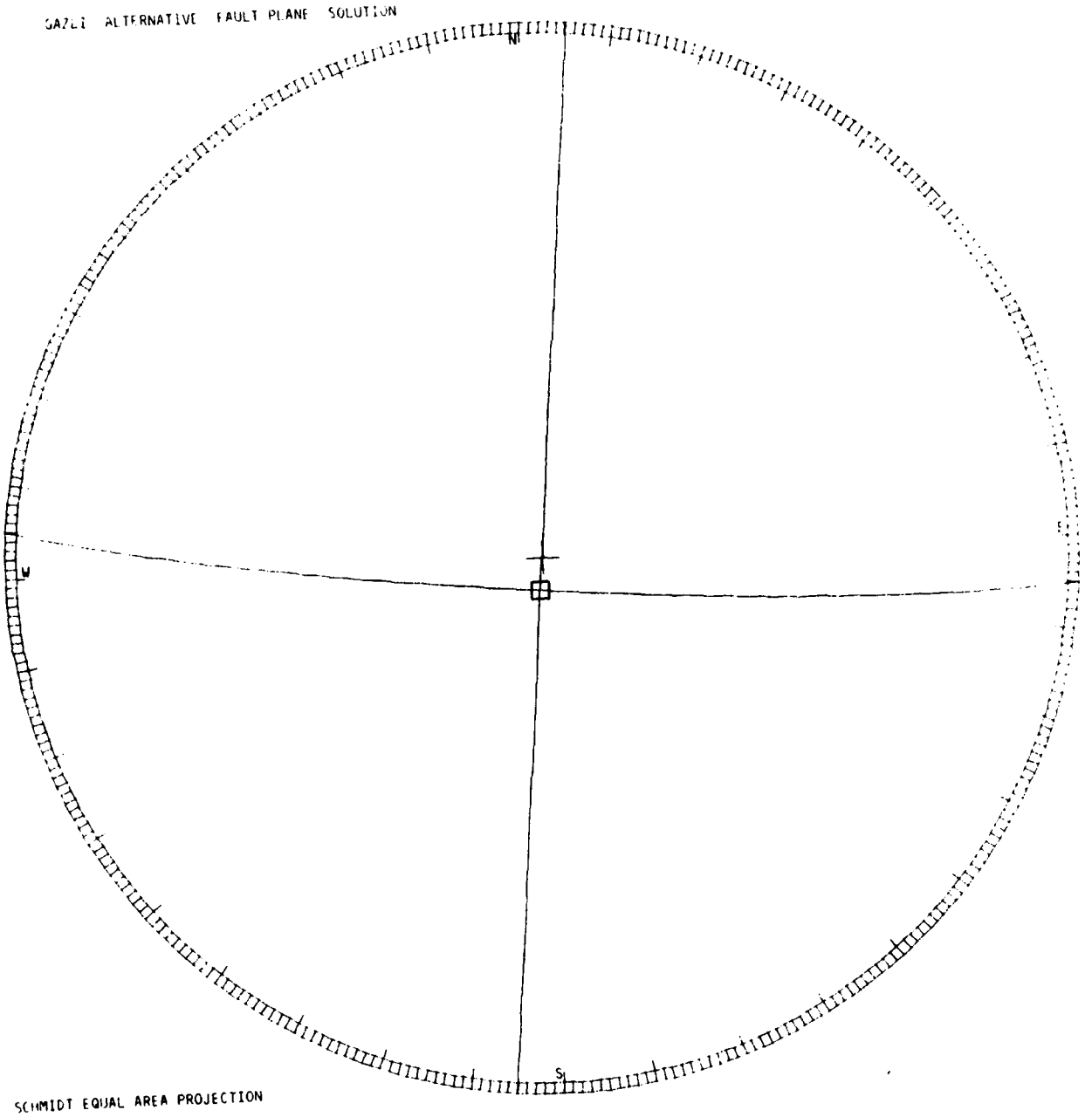

FIGURE 79. ORIENTATION USED FOR FIGURE 24

EVENT NO. 27: 23 April 1976 20-55-31.7
MAGNITUDE m_b (NEIS): 4.4

Although assigned to Category 2 the source orientation is less well constrained than others in Category 2, and the earthquake has not been modelled (see text).

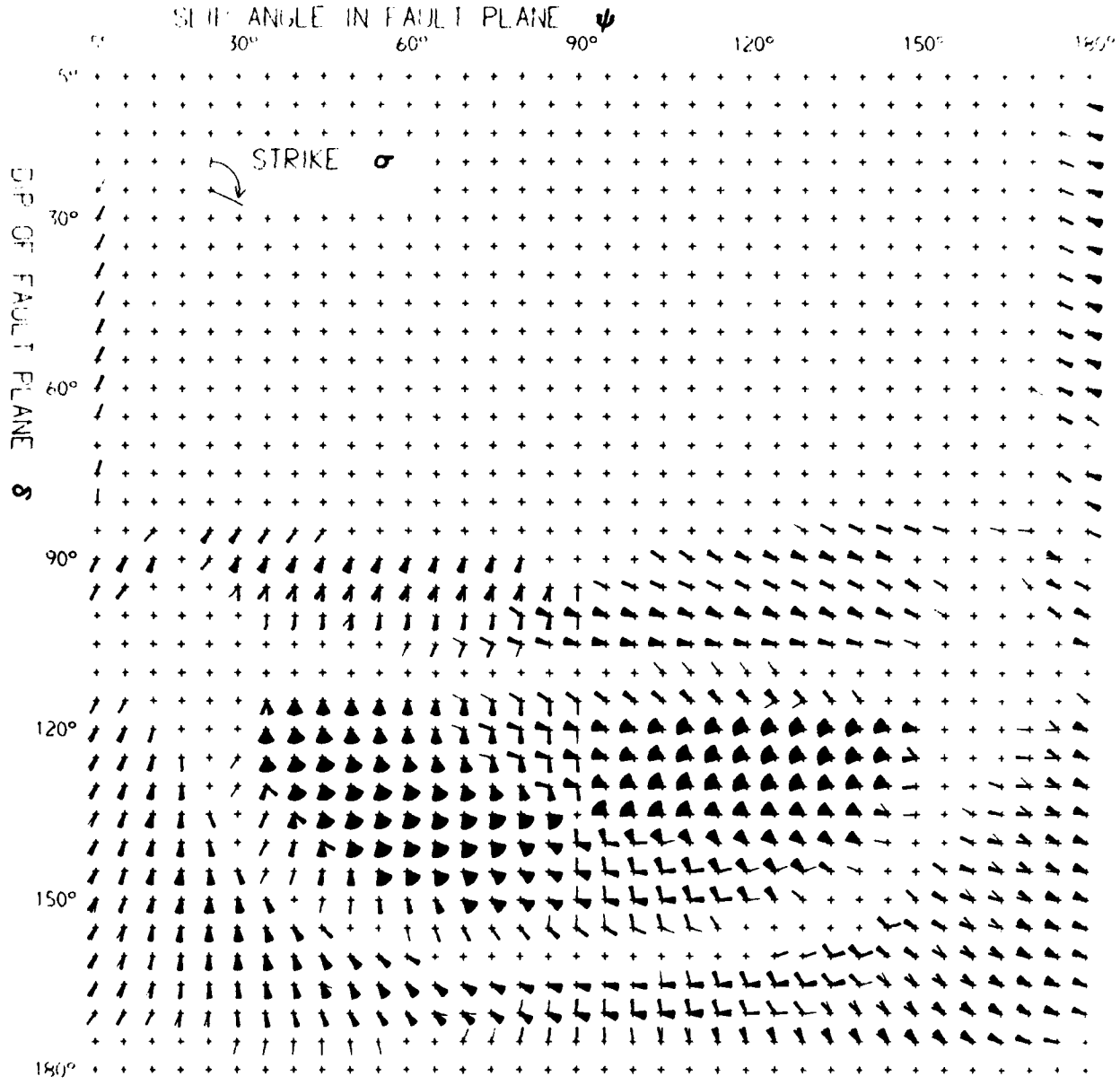

23 April 1976 20-55-31.7

(with no allowance for velocity structure)

Number of compatible orientations = 4216

FIGURE 80(a)

EVENT NO. 27 (CATEGORY 2)

23 April 1976 20-55-31.7

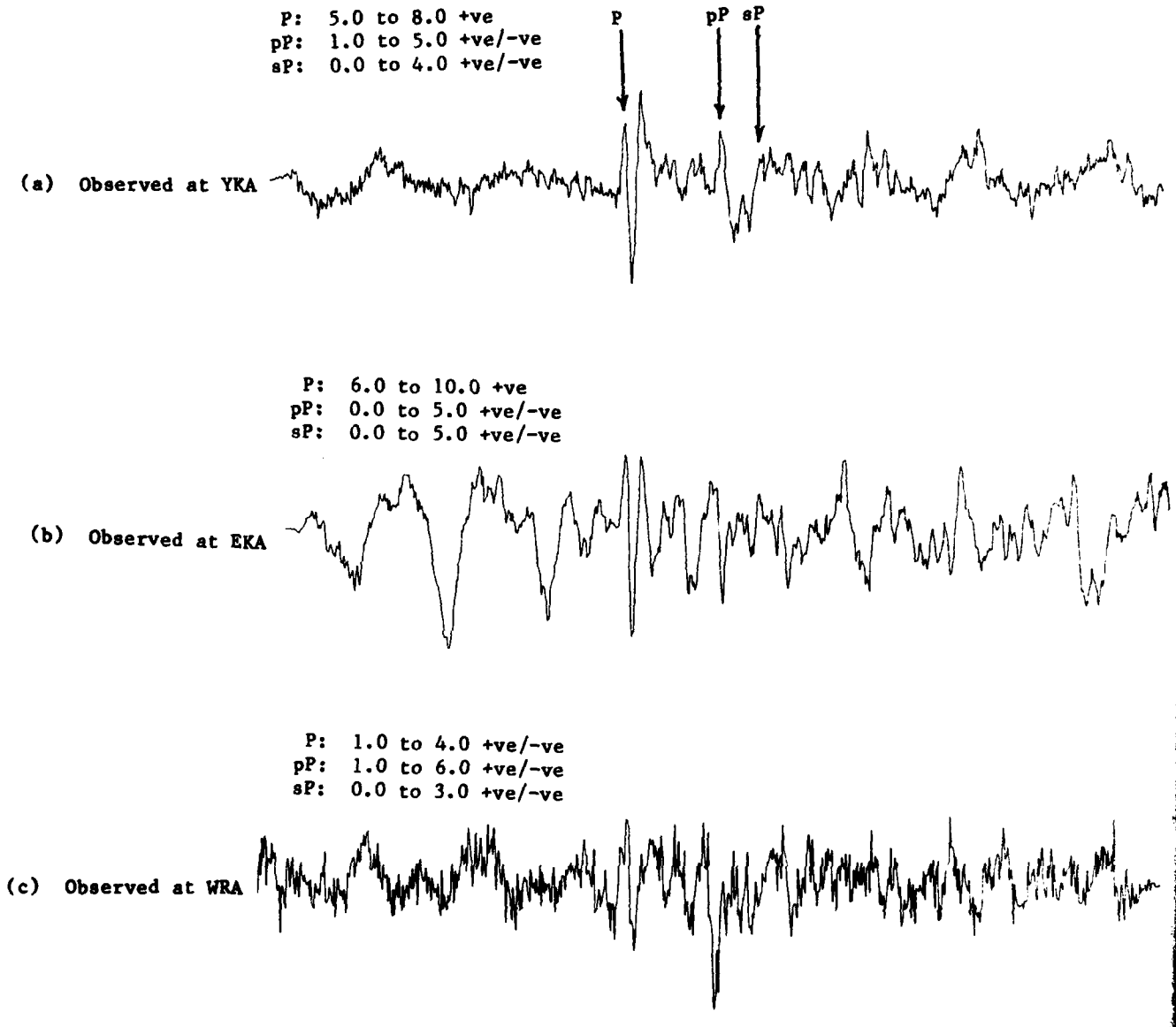

FIGURE 80(b)

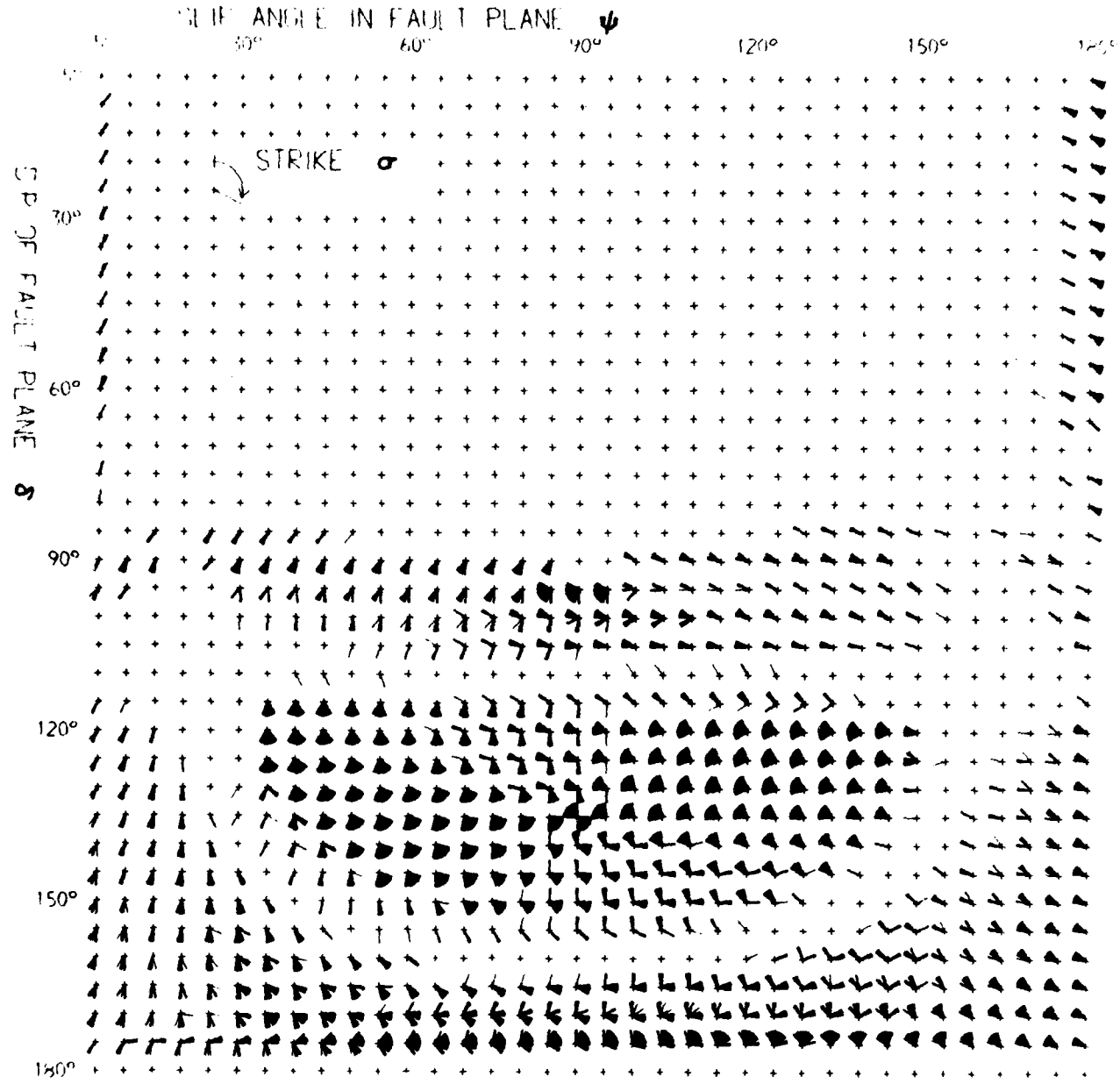

23 April 1976 20-55-31.7

(with allowance for velocity structure)

Number of compatible orientations = 5864

FIGURE 80(c)

EVENT NO. 49: 1 June 1976 07-31-59.2
MAGNITUDE m_b (NEIS): -

Although assigned to Category 2 the source orientation is less well constrained than others in Category 2, and the earthquake has not been modelled (see text).

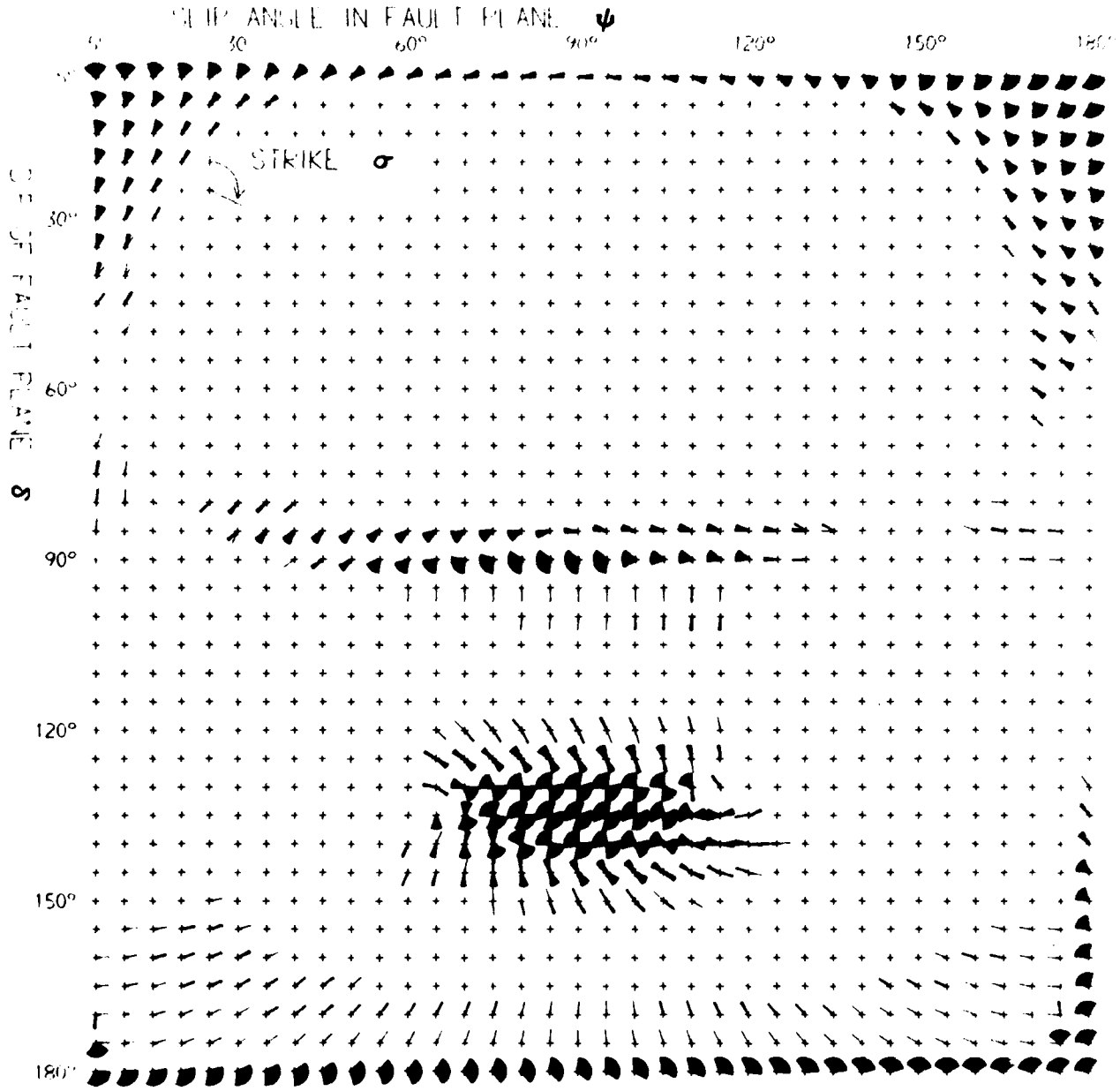

1 June 1976 07-31-59.2

(with no allowance for velocity structure)

Number of compatible orientations = 4363

FIGURE 81(a)

EVENT NO. 49 (CATEGORY 2)

1 June 1976 07-31-59.2

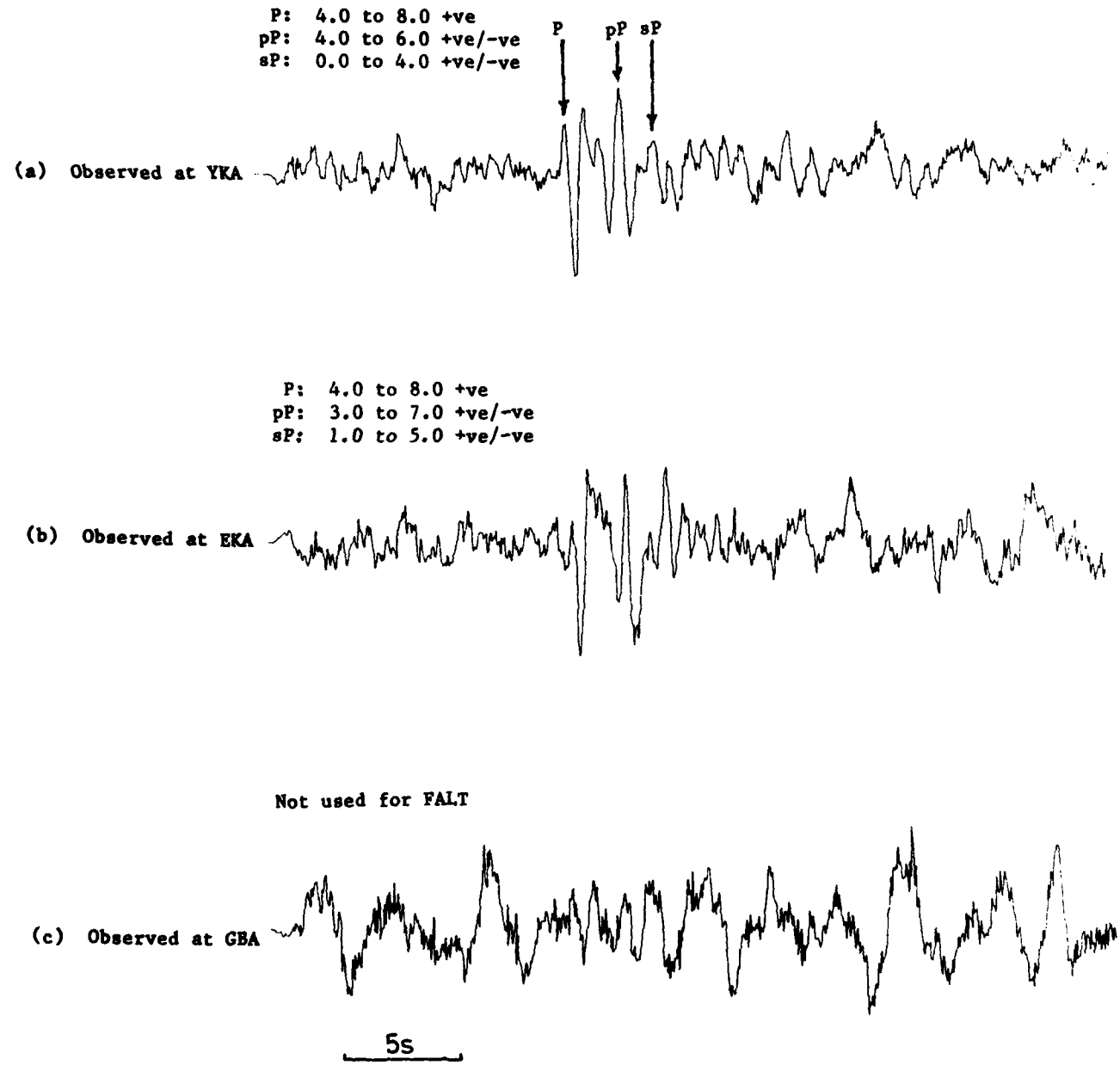

FIGURE 81(b)

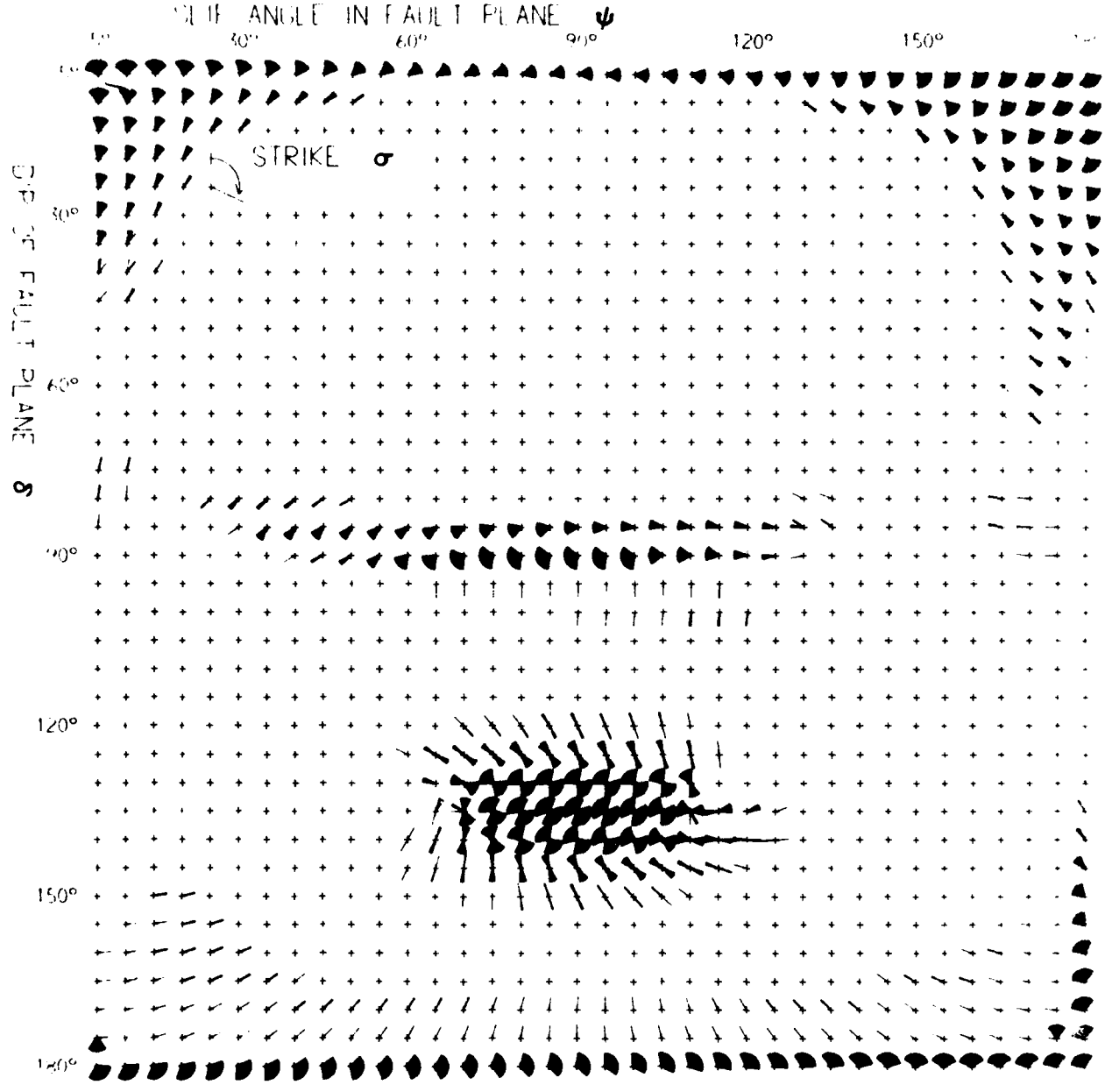

1 June 1976 07-31-59.2

(with allowance for velocity structure)

Number of compatible orientations = 4806

FIGURE 81(c)

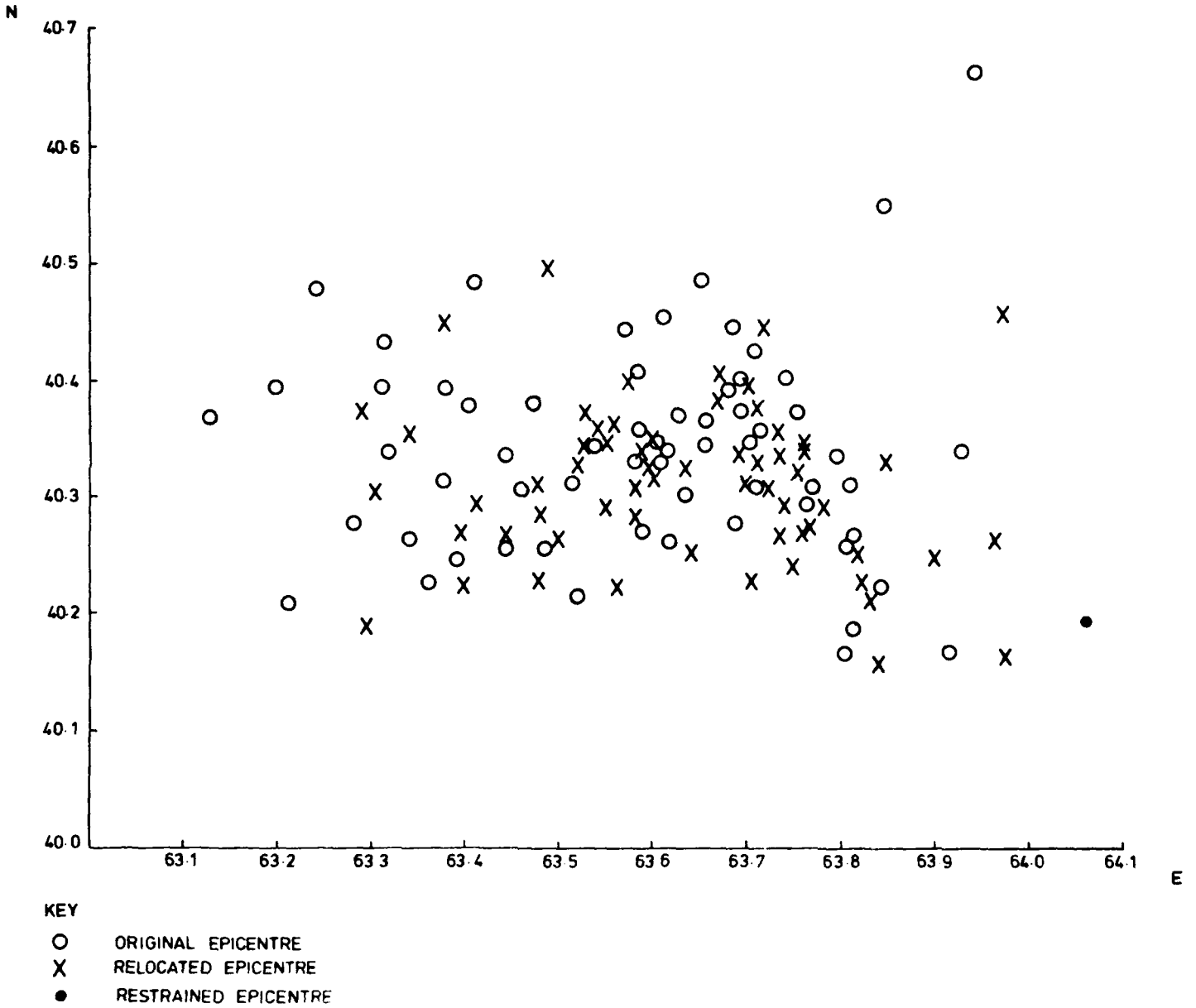

FIGURE 82. Joint Epicentre Determination Plot using NEIS Data as the Starting Approximations

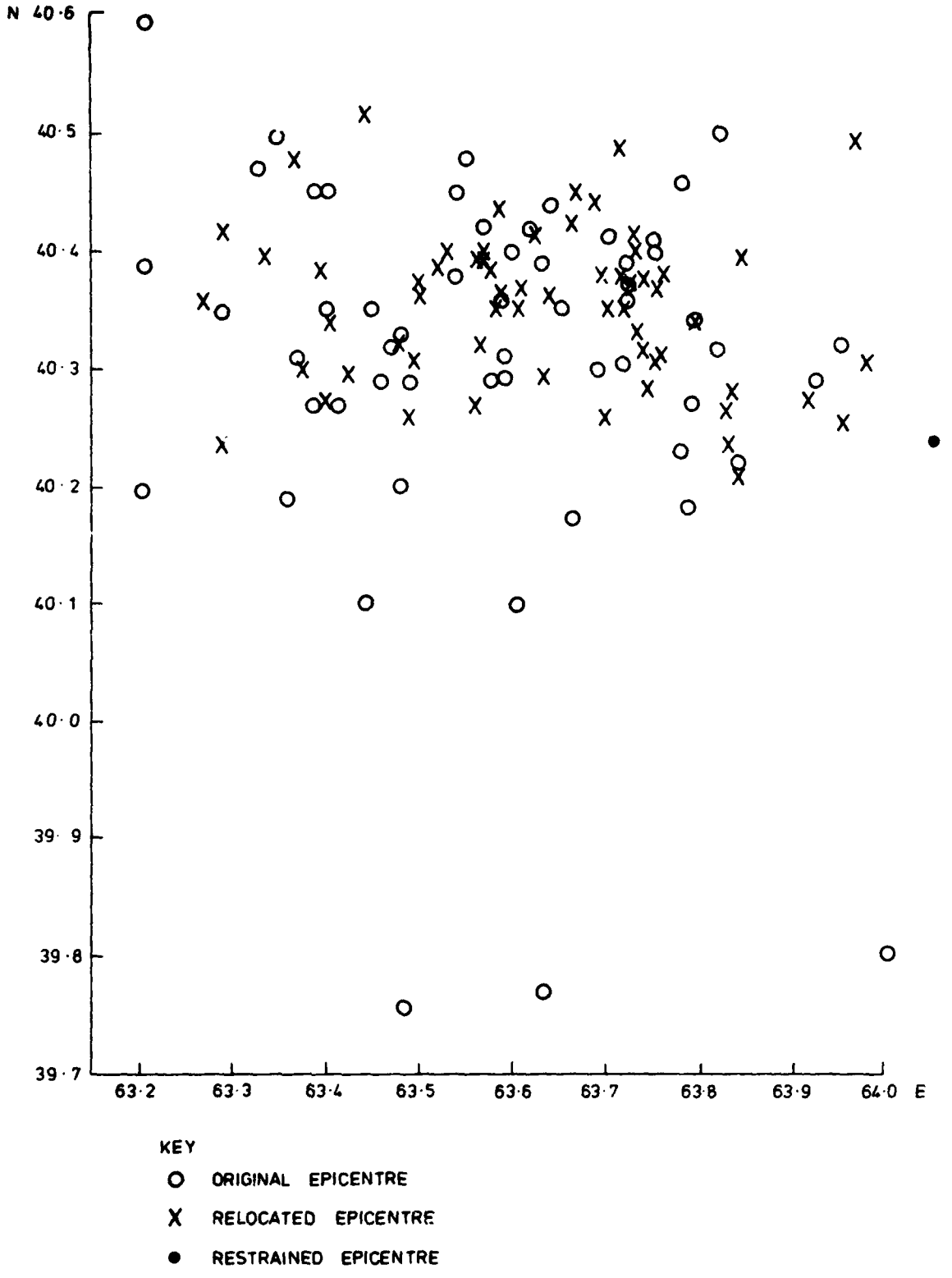

FIGURE 83 Joint Epicentre Determination Plot using ISC Data as the Starting Approximations

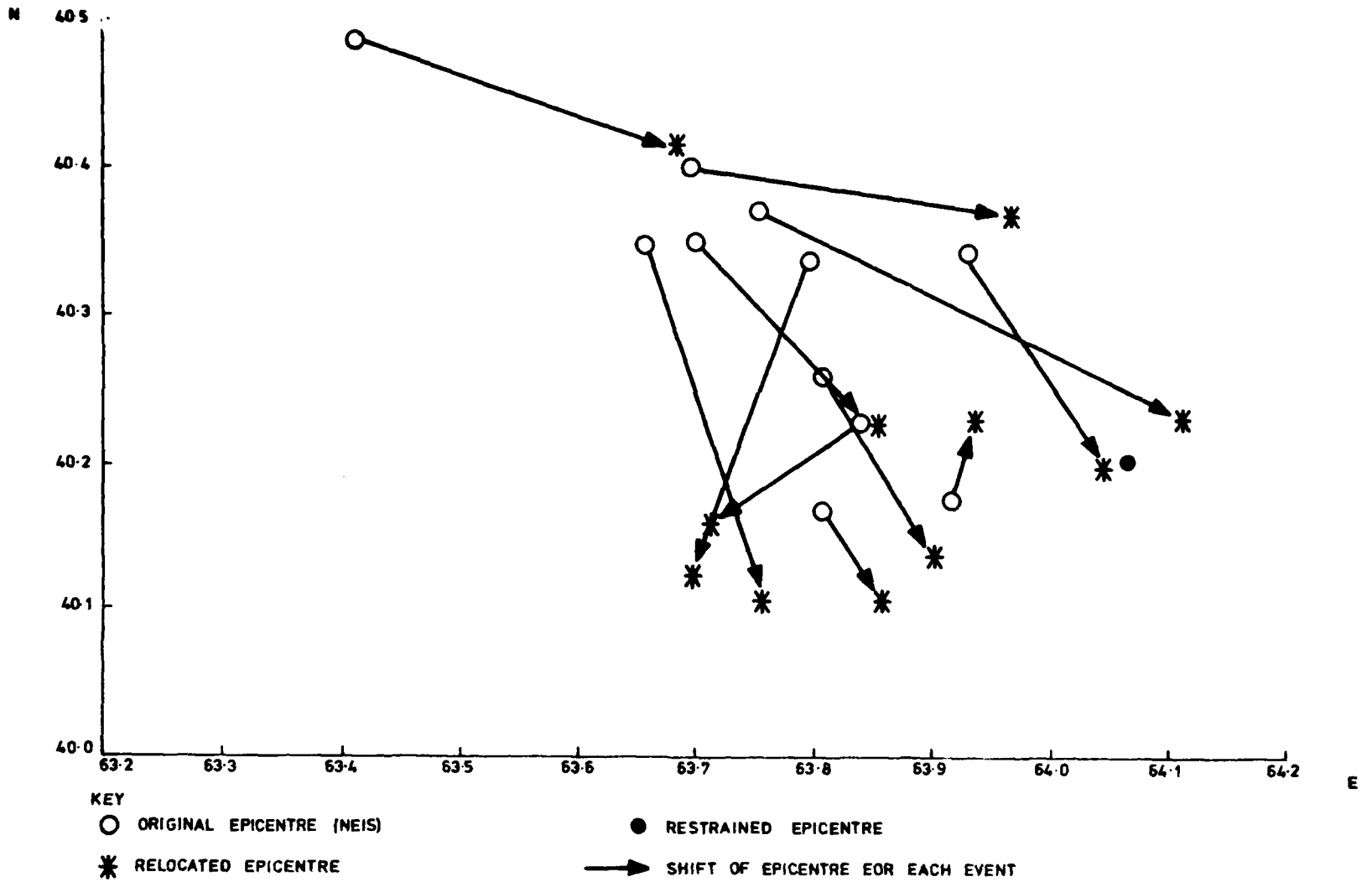

FIGURE 84. Joint Epicentre Determination Plot using Array Arrival Times only

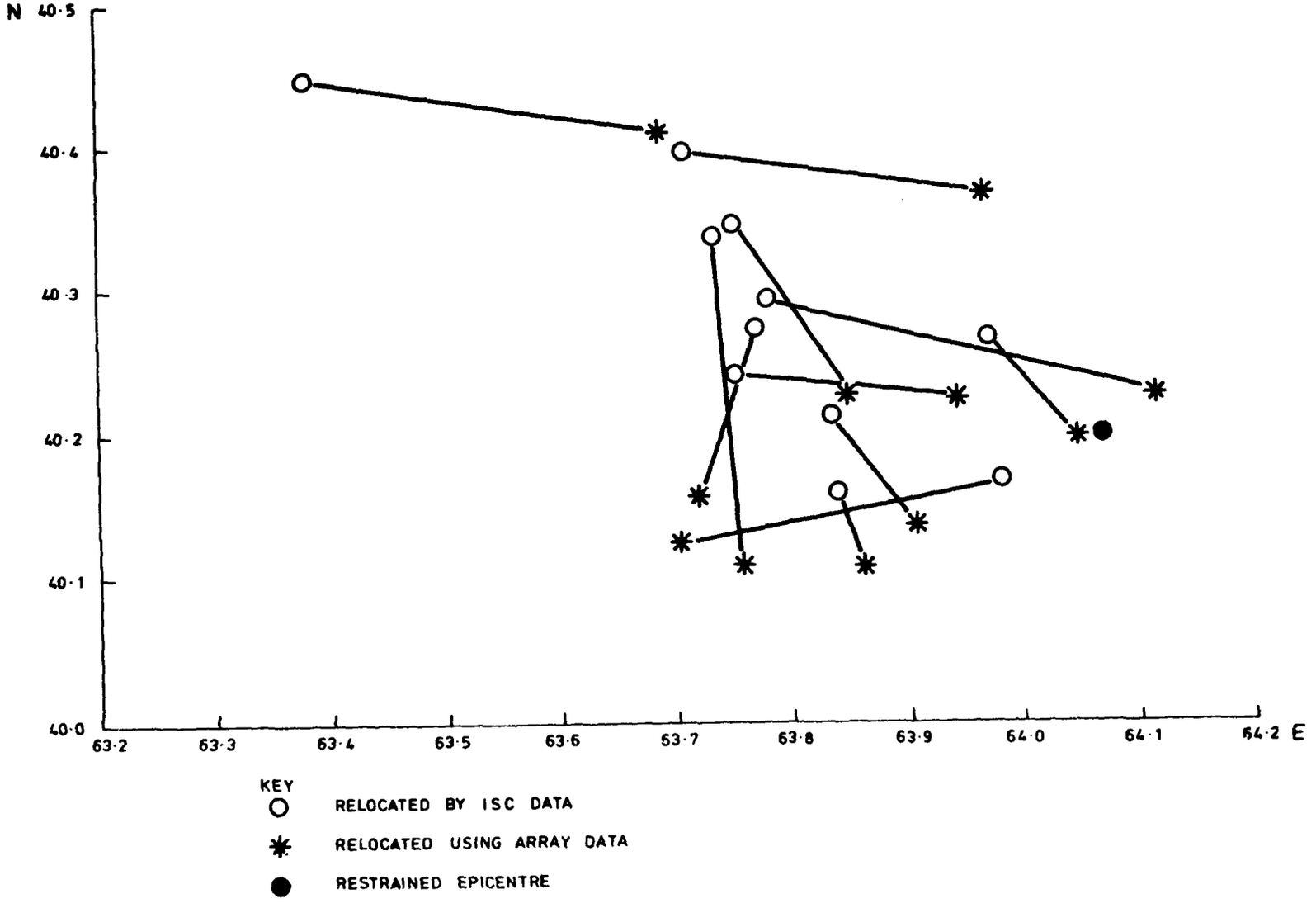

FIGURE 85. Plot of Relocated Epicentres Comparing Array Data Results and Results from ISC Station Data

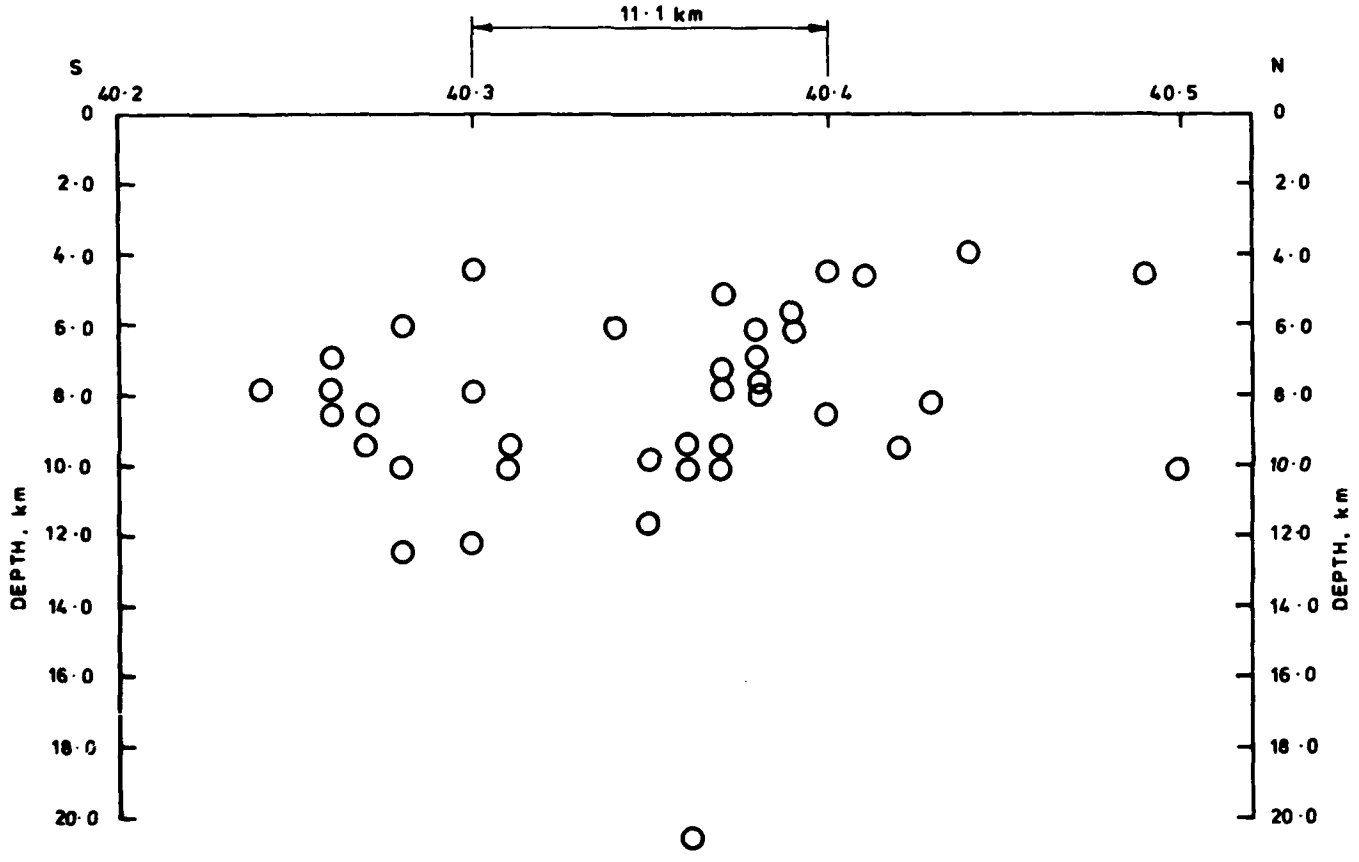

FIGURE 86 (a) Depth plot for Gazli Sequence (N/S SECTION)

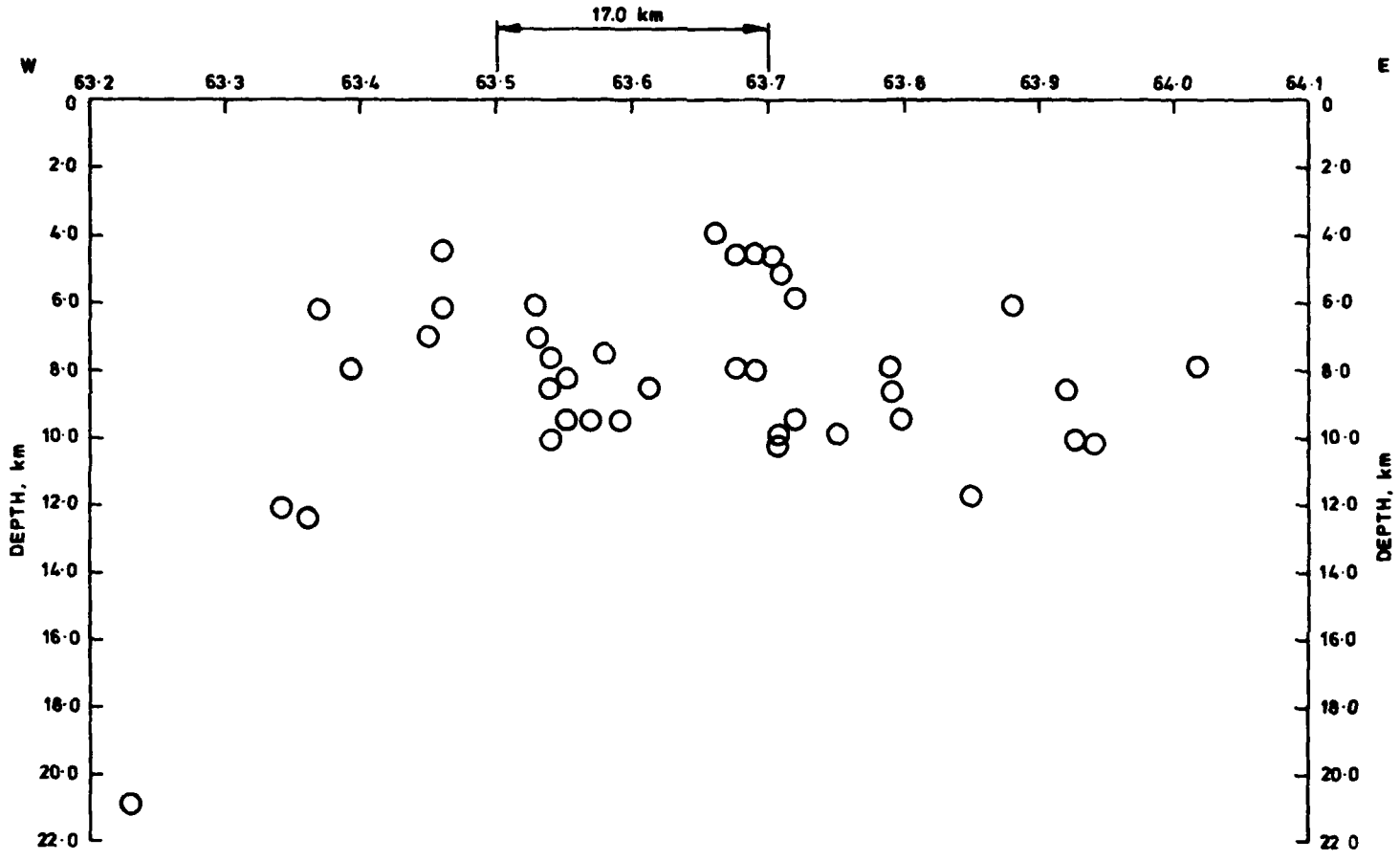

NOTE: 95% CONFIDENCE LIMITS FOR EPICENTRE LOCATIONS ARE ALL LESS THAN ± 10 km

FIGURE 86 (b) Depth Plot for Gazli Sequence. (E/W SECTION)

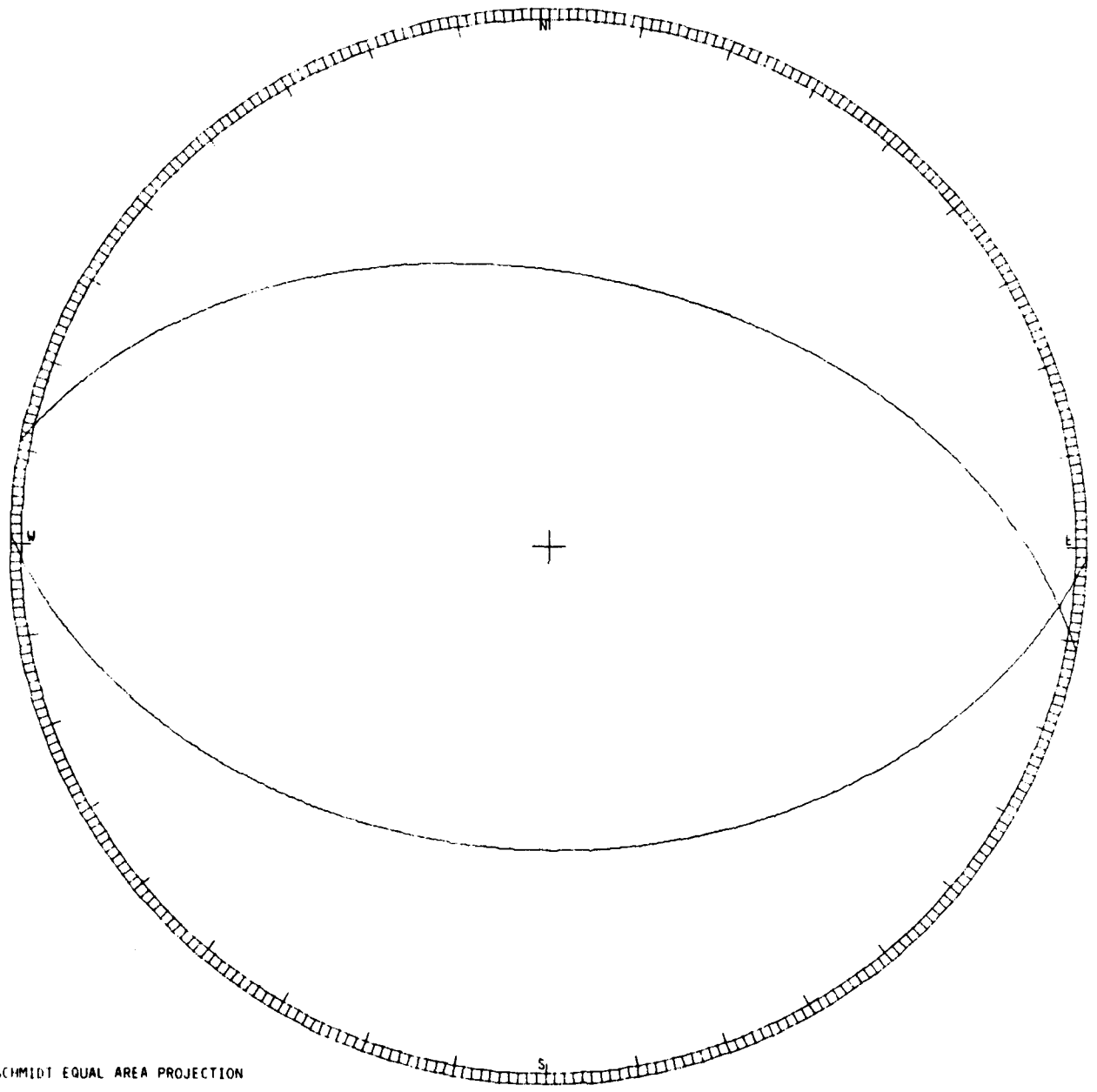

SCHMIDT EQUAL AREA PROJECTION

Nodal planes:-

(1) Strike = 91°, Dip = 43°

(2) Strike = 281°, Dip = 48°

FIGURE 87(a). SOURCE ORIENTATION OF 8 APRIL 1976 02-40-27.0 EARTHQUAKE (EVENT 1 OF TABLE 1) ACCORDING TO SYKES AND BURDICK (6)

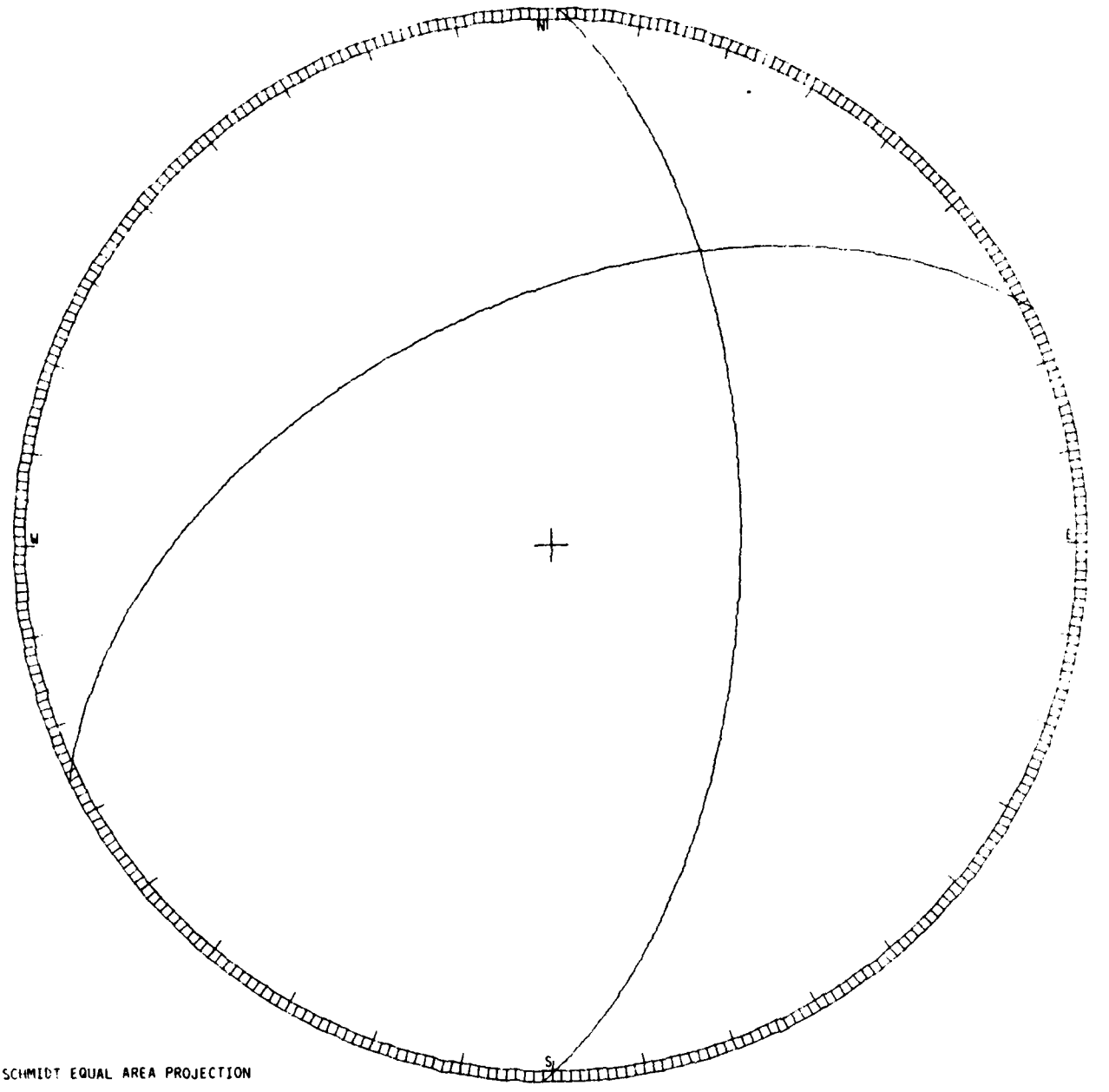

Nodal planes:-

(1) Strike = 1°, Dip = 61°

(2) Strike = 244°, Dip = 53°

FIGURE 87(b). SOURCE ORIENTATION OF 17 MAY 1976 02-58-40.6 EARTHQUAKE (EVENT 32 OF TABLE 1) ACCORDING TO SYKES AND BURDICK (6)

DOCUMENT CONTROL SHEET

Overall security classification of sheet ..... UNCLASSIFIED .....

(As far as possible this sheet should contain only unclassified information. If it is necessary to enter classified information, the box concerned must be marked to indicate the classification eg (R), (C) or (S)).

1. DRIC Reference (if known)	2. Originator's Reference	3. Agency Reference	4. Report Security Classification
-	AWRE REPORT NO. 027/80	-	UNLIMITED

5. Originator's Code (if known)	6. Originator (Corporate Author) Name and Location
-	Atomic Weapons Research Establishment, Aldermaston, Berkshire

5a. Sponsoring Agency's Code (if known)	6a. Sponsoring Agency (Contract Authority) Name and Location
-	-

7. Title
The 1976 Earthquake Sequence in Uzbekistan - Focal Mechanisms Determined Using the Relative Amplitude Method

7a. Title in Foreign Language (in the case of Translation)
-

7b. Presented at (for Conference Papers). Title, Place and Date of Conference
-

8. Author 1.Surname, Initials	9a. Author 2	9b. Authors 3, 4	10. Date	pp	ref
Pearce R G	Bainbridge Hilary	Key Pamela F Young J B	July 1980	171	13

11. Contract Number	12. Period	13. Project	14. Other References
-	-	-	-

15. Distribution Statement
No restriction

16. Descriptors (or Keywords) (TEST)

Earthquakes	Seismic epicenter	Seismic arrays	Teleseismic bodywaves
Discrimination	Fault plane	Seismic event	Uzbekistan
P-wave	Seismology		

Abstract

The relative amplitude method of determining earthquake source orientations is applied to short period teleseismic array observations of the 1976 Uzbekistan earthquake sequence. Many of these events are shown to be consistent with a double couple source, and the method provides well determined orientations for most events with magnitude m_b between 4.0 and 5.6. The value of the method both as a means of determining source orientations and as an earthquake/explosion discriminant is assessed.

Some Metric and SI Unit Conversion Factors

(Based on DEF STAN 00-11/2 "Metric Units for Use by the Ministry of Defence", DS Met 5501 "AWRE Metric Guide" and other British Standards)

Quantity	Unit	Symbol	Conversion
Basic Units			
Length	metre	m	1 m = 3.2808 ft 1 ft = 0.3048 m
Mass	kilogram	kg	1 kg = 2.2046 lb 1 lb = 0.45359237 kg 1 ton = 1016.05 kg
Derived Units			
Force	newton	N = kg m/s^2	1 N = 0.2248 lbf 1 lbf = 4.44822 N
Work, Energy, Quantity of Heat	joule	J = N m	1 J = 0.737562 ft lbf 1 J = 9.47817 × 10^{-4} Btu 1 J = 2.38846 × 10^{-4} kcal 1 ft lbf = 1.35582 J 1 Btu = 1055.06 J 1 kcal = 4186.8 J
Power	watt	W = J/s	1 W = 0.238846 cal/s 1 cal/s = 4.1868 W
Electric Charge	coulomb	C = A s	-
Electric Potential	volt	V = W/A = J/C	-
Electrical Capacitance	farad	F = A s/V = C/V	-
Electric Resistance	ohm	Ω = V/A	-
Conductance	siemen	S = 1 Ω^{-1}	-
Magnetic Flux	weber	Wb = V s	-
Magnetic Flux Density	tesla	T = Wb/m^2	-
Inductance	henry	H = V s/A = Wb/A	-
Complex Derived Units			
Angular Velocity	radian per second	rad/s	1 rad/s = 0.159155 rev/s 1 rev/s = 6.28319 rad/s
Acceleration	metre per square second	m/s^2	1 m/s^2 = 3.28084 ft/s^2 1 ft/s^2 = 0.3048 m/s^2
Angular Acceleration	radian per square second	rad/s^2	-
Pressure	newton per square metre	N/m^2 = Pa	1 N/m^2 = 145.038 × 10^{-6} lbf/in^2 1 lbf/in^2 = 6.89476 × 10^3 N/m^2
	bar	bar = 10^5 N/m^2	- 1 in. Hg = 3386.39 N/m^2
Torque	newton metre	N m	1 N m = 0.737562 lbf ft 1 lbf ft = 1.35582 N m
Surface Tension	newton per metre	N/m	1 N/m = 0.0685 lbf/ft 1 lbf/ft = 14.5939 N/m
Dynamic Viscosity	newton second per square metre	N s/m^2	1 N s/m^2 = 0.0208854 lbf s/ft^2 1 lbf s/ft^2 = 47.8803 N s/m^2
Kinematic Viscosity	square metre per second	m^2/s	1 m^2/s = 10.763^9 ft^2/s 1 ft^2/s = 0.0929 m^2/s
Thermal Conductivity	watt per metre kelvin	W/m K	-
Odd Units*			
Radioactivity	becquerel	Bq	1 Bq = 2.7027 × 10^{-11} Ci 1 Ci = 3.700 × 10^{10} Bq
Absorbed Dose	gray	Gy	1 Gy = 100 rad 1 rad = 0.01 Gy
Dose Equivalent	sievert	Sv	1 Sv = 100 rem 1 rem = 0.01 Sv
Exposure	coulomb per kilogram	C/kg	1 C/kg = 3876 R 1 R = 2.58 × 10^{-4} C/kg
Rate of Leak (Vacuum Systems)	millibar litre per second	mb l/s	1 mb = 0.750062 torr 1 torr = 1.33322 mb

*These terms are recognised terms within the metric system.